EUROPEAN ORGANIZATION FOR NUCLEAR RESEARCH

CERN-PH-EP/2006-042
LEPEWWG/2006-01
ALEPH 2006-001 PHYSICS 2006-001
DELPHI 2006-014 PHYS 948
L3 Note 2833
OPAL PR 419
hep-ex/0612034
14 December 2006

A Combination of Preliminary Electroweak Measurements and Constraints on the Standard Model

The LEP Collaborations[1] ALEPH, DELPHI, L3, OPAL, and the LEP Electroweak Working Group[2]

Prepared from Contributions of the LEP Experiments to the 2006 Summer Conferences.

Abstract

This note presents a combination of published and preliminary electroweak results from the four LEP collaborations ALEPH, DELPHI, L3 and OPAL based on electron-positron collision data taken at centre-of-mass energies above the Z-pole, 130 GeV to 209 GeV (LEP-II), as prepared for the 2006 summer conferences. Averages are derived for di-fermion cross sections and forward-backward asymmetries, photon-pair, W-pair, Z-pair, single-W and single-Z cross sections, electroweak gauge boson couplings, W mass and width and W decay branching ratios. An investigation of the interference of photon and Z-boson exchange is presented, and colour reconnection and Bose-Einstein correlation analyses in W-pair production are combined. The main changes with respect to the experimental results presented in 2005 are new preliminary combinations of final LEP-II results on the mass and width of the W boson.

Including the precision electroweak measurements performed at the Z pole published recently, the results are compared with precise electroweak measurements from other experiments, notably CDF and DØ at the Tevatron. Constraints on the input parameters of the Standard Model are derived from the results obtained in high-Q^2 interactions, and used to predict results in low-Q^2 experiments, such as atomic parity violation, Möller scattering, and neutrino-nucleon scattering.

[1] The LEP Collaborations each take responsibility for the preliminary results of their own experiment.

[2] WWW access at `http://www.cern.ch/LEPEWWG`

The members of the LEP Electroweak Working Group who contributed significantly to this note are:
J. Alcaraz, P. Azzurri, A. Bajo-Vaquero, E. Barberio, A. Blondel, D. Bourilkov, P. Checchia, R. Chierici, R. Clare, J. D'Hondt, B. de la Cruz, P. de Jong, G. Della Ricca, M. Dierckxsens, D. Duchesneau, G. Duckeck, M. Elsing, M.W. Grünewald, A. Gurtu, J.B. Hansen, R. Hawkings, St. Jezequel, R.W.L. Jones, T. Kawamoto, E. Lançon, W. Liebig, L. Malgeri, S. Mele, M.N. Minard, K. Mönig, C. Parkes, U. Parzefall, B. Pietrzyk, G. Quast, P. Renton, S. Riemann, K. Sachs, A. Straessner, D. Strom, R. Tenchini, F. Teubert, M.A. Thomson, S. Todorova-Nova, A. Valassi, A. Venturi, H. Voss, C.P. Ward, N.K. Watson, P.S. Wells, St. Wynhoff [†].

[†] deceased.

Chapter 1

Introduction

This article presents an updated summary of combined results on electroweak observables measured in high-energy electron-positron collisions. The results of the LEP experiments ALEPH, DELPHI, L3, OPAL and the SLD experiment at SLC based on data collected at the Z resonance and their combinations reported in previous summaries up to 2004 [1] have since then been finalised and are published [2]. All Z-pole results and observables derived thereof, in particular the various effective couplings of the neutral weak current, are reported in Reference 2 and are no longer described in this yearly update.

Since 1996 the electron-positron collider LEP has run at centre-of-mass energies above the Z pole, $\sqrt{s} \geq 130$ GeV (LEP-II), and mainly above the W-pair production threshold. In 2000, the final year of data taking at LEP, the maximum centre-of-mass energy of close to 209 GeV was attained, although most of the data taken in 2000 was collected at 205 and 207 GeV. By the end of LEP-II operations, a total integrated luminosity of approximately 700 pb^{-1} per experiment was recorded above the Z resonance.

The electroweak LEP-II measurements discussed here consist of di-fermion cross sections and forward-backward asymmetries; di-photon production, W-pair, Z-pair, single-W and single-Z production cross sections, and electroweak gauge boson self couplings. W boson properties, like mass, width and decay branching ratios are also measured. Studies on photon/Z interference in fermion-pair production as well as on colour reconnection and Bose-Einstein correlations in W-pair production are presented. The LEP-II combinations presented here supersede the previous analyses [3]. Most measurements are still preliminary. Note that in some cases some experiments have already published final results which are not yet included in the combinations presented here.

This note is organised as follows:

Chapter 2 Photon-pair production at energies above the Z;

Chapter 3 Fermion-pair production at energies above the Z;

Chapter 4 Photon/Z-boson interference;

Chapter 5 W and four-fermion production;

Chapter 6 Electroweak gauge boson self couplings;

Chapter 7 Colour reconnection in W-pair events;

Chapter 8 Bose-Einstein correlations in W-pair events;

Chapter 9 W-boson mass and width;

Chapter 10 Interpretation of all results, including final published Z-pole results [2] from LEP-I and SLD, as well as results from CDF and DØ, in terms of constraints on the Standard Model (SM);

Chapter 11 Conclusions including prospects for the future.

To allow a quick assessment, a box highlighting the updates is given at the beginning of each chapter.

Chapter 2

Photon-Pair Production at LEP-II

Updates with respect to summer 2005:
Unchanged w.r.t. summer 2002: ALEPH, L3 and OPAL have provided final results for the complete LEP-II dataset, DELPHI up to 1999 data and preliminary results for the 2000 data.
Note that some recent publications [4] are not yet included in this combination.

2.1 Introduction

The reaction $e^+e^- \to \gamma\gamma(\gamma)$ provides a clean test of QED at LEP energies and is well suited to detect the presence of non-standard physics. The differential QED cross-section at the Born level in the relativistic limit is given by [5,6]:

$$\left(\frac{d\sigma}{d\Omega}\right)_{\text{Born}} = \frac{\alpha^2}{s}\frac{1+\cos^2\theta}{1-\cos^2\theta}\,. \tag{2.1}$$

Since the two final state particles are identical the polar angle θ is defined such that $\cos\theta > 0$. Various models with deviations from this cross-section will be discussed in section 2.4. Results on the $\geq$2-photon final state using the high energy data collected by the four LEP collaborations are reported by the individual experiments [7]. Here the results of the LEP working group dedicated to the combination of the $e^+e^- \to \gamma\gamma(\gamma)$ measurements are reported. Results are given for the averaged total cross-section and for global fits to the differential cross-sections.

2.2 Event Selection

This channel is very clean and the event selection, which is similar for all experiments, is based on the presence of at least two energetic clusters in the electromagnetic calorimeters. A minimum energy is required, typically $(E_1+E_2)/\sqrt{s}$ larger than 0.3 to 0.6, where E_1 and E_2 are the energies of the two most energetic photons. In order to remove e^+e^- events, charged tracks are in general not allowed except when they can be associated to a photon conversion in one hemisphere.

The polar angle is defined in order to minimise effects due to initial state radiation as

$$\cos\theta = \left|\sin(\frac{\theta_1-\theta_2}{2})\right| \Big/ \sin(\frac{\theta_1+\theta_2}{2})\,,$$

where θ_1 and θ_2 are the polar angles of the two most energetic photons. The acceptance in polar angle is in the range of 0.90 to 0.96 on $|\cos\theta|$, depending on the experiment.

With these criteria, the selection efficiencies are in the range of 68% to 98% and the residual background (from e^+e^- events and from $e^+e^- \to \tau^+\tau^-$ with $\tau^\pm \to e^\pm\nu\bar{\nu}$) is very small, 0.1% to 1%. Detailed descriptions of the event selections performed by the four collaborations can be found in [7].

2.3 Total cross-section

The total cross-sections are combined using a χ^2 minimisation. For simplicity, given the different angular acceptances, the ratios of the measured cross-sections relative to the QED expectation, $r = \sigma_{\text{meas}}/\sigma_{\text{QED}}$, are averaged. Figure 2.1 shows the measured ratios $r_{i,k}$ of the experiments i at energies k with their statistical and systematic errors added in quadrature. There are no significant sources of experimental systematic errors that are correlated between experiments. The theoretical error on the QED prediction, which is fully correlated between energies and experiments is taken into account after the combination.

Denoting with Δ the vector of residuals between the measurements and the expected ratios, three different averages are performed:

1. per energy $k = 1,\ldots,7$: $\Delta_{i,k} = r_{i,k} - x_k$
2. per experiment $i = 1,\ldots,4$: $\Delta_{i,k} = r_{i,k} - y_i$
3. global value: $\Delta_{i,k} = r_{i,k} - z$

The seven fit parameters per energy x_k are shown in Figure 2.1 as LEP combined cross-sections. They are correlated with correlation coefficients ranging from 5% to 20%. The four fit-parameters per experiment y_i are uncorrelated between each other, the results are given in Table 2.1 together with the single global fit parameter z.

No significant deviations from the QED expectations are found. The global ratio is below unity by 1.8 standard deviations not accounting for the error on the radiative corrections. This theory error can be assumed to be about 10% of the applied radiative correction and hence depends on the selection. For this combination it is assumed to be 1% which is of same size as the experimental error (1.0%).

Experiment	cross-section ratio
ALEPH	0.953±0.024
DELPHI	0.976±0.032
L3	0.978±0.018
OPAL	0.999±0.016
global	0.982±0.010

Table 2.1: Cross-section ratios $r = \sigma_{\text{meas}}/\sigma_{\text{QED}}$ for the four LEP experiments averaged over all energies and the global average over all experiments and energies. The error includes the statistical and experimental systematic error but no error from theory.

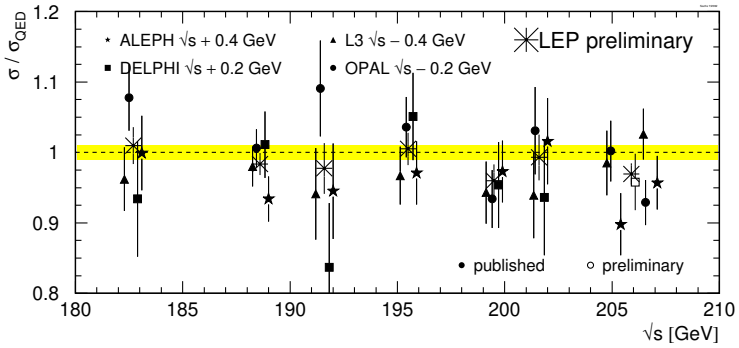

Figure 2.1: Cross-section ratios $r = \sigma_{\rm meas}/\sigma_{\rm QED}$ at different energies. The measurements of the single experiments are displaced by ± 200 or 400 MeV from the actual energy for clarity. Filled symbols indicate published results, open symbols stand for preliminary numbers. The average over the experiments at each energy is shown as a star. Measurements between 203 and 209 GeV are averaged to one energy point. The theoretical error is not included in the experimental errors but is represented as the shaded band.

	data used		sys. error [%]		$\lvert\cos\theta\rvert$
	published	preliminary	experimental	theory	
ALEPH	189 – 207	–	2	1	0.95
DELPHI	189 – 202	206	2.5	1	0.90
L3	183 – 207	–	2.1	1	0.96
OPAL	183 – 207	–	0.6 – 2.9	1	0.93

Table 2.2: The data samples used for the global fit to the differential cross-sections, the systematic errors, the assumed error on the theory and the polar angle acceptance for the LEP experiments.

2.4 Global fit to the differential cross-sections

The global fit is based on angular distributions at energies between 183 and 207 GeV from the individual experiments. As an example, angular distributions from each experiment are shown in Figure 2.2. Combined differential cross-sections are not available yet, since they need a common binning of the distributions. All four experiments give results including the whole year 2000 data-taking. Apart from the 2000 DELPHI data all inputs are final, as shown in Table 2.2. The systematic errors arise from the luminosity evaluation (including theory uncertainty on the small-angle Bhabha cross-section computation), from the selection efficiency and the background evaluations and from radiative corrections. The last contribution, owing to the fact that the available $e^+e^- \to \gamma\gamma(\gamma)$ cross-section calculation is based on $\mathcal{O}(\alpha^3)$ code, is assumed to be 1% and is considered correlated among energies and experiments.

Various model predictions are fitted to these angular distributions taking into account the experimental systematic error correlated between energies for each experiment and the error on the theory.

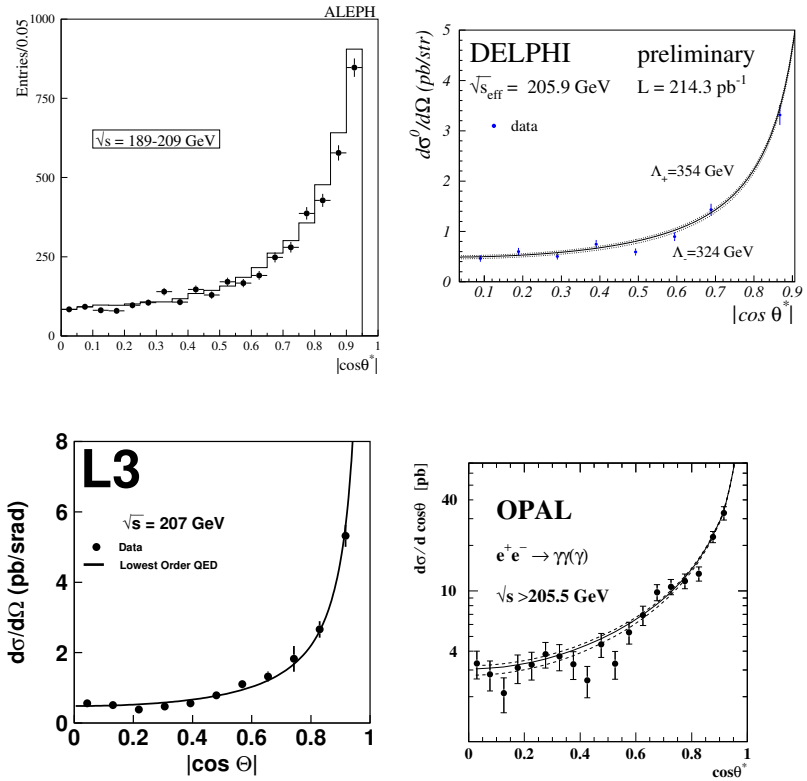

Figure 2.2: Examples for angular distributions of the four LEP experiments. Points are the data and the curves are the QED prediction (solid) and the individual fit results for $\Lambda_\pm$ (dashed). ALEPH shows the uncorrected number of observed events, the expectation is presented as histogram.

A binned log likelihood fit is performed with one free parameter for the model and five fit parameters used to keep the normalisation free within the systematic errors of the theory and the four experiments. Additional fit parameters are needed to accommodate the angular dependent systematic errors of OPAL.

The following models of new physics are considered. The simplest ansatz is a short-range exponential deviation from the Coulomb field parameterised by cut-off parameters $\Lambda_\pm$ [8,9]. This leads to a differential cross-section of the form

$$\left(\frac{d\sigma}{d\Omega}\right)_{\Lambda_\pm} = \left(\frac{d\sigma}{d\Omega}\right)_{\rm Born} \pm \frac{\alpha^2\pi s}{\Lambda_\pm^4}(1+\cos^2\theta)\ . \qquad (2.2)$$

New effects can also be introduced in effective Lagrangian theory [10]. Here dimension-6 terms lead to anomalous eeγ couplings. The resulting deviations in the differential cross-section are similar in form to those given in Equation 2.2, but with a slightly different definition of the parameter: $\Lambda_6^4 = \frac{2}{\alpha}\Lambda_\pm^4$. While for the ad hoc included cut-off parameters $\Lambda_\pm$ both signs are allowed the physics motivated parameter Λ_6 occurs only with the positive sign. Dimension 7 and 8 Lagrangians introduce ee$\gamma\gamma$ contact interactions and result in an angle-independent term added to the Born cross-section:

$$\left(\frac{d\sigma}{d\Omega}\right)_{\Lambda'} = \left(\frac{d\sigma}{d\Omega}\right)_{\text{Born}} + \frac{s^2}{16}\frac{1}{\Lambda'^6} \; . \tag{2.3}$$

The associated parameters are given by $\Lambda_7 = \Lambda'$ and $\Lambda_8^4 = m_e\Lambda'^3$ for dimension 7 and dimension 8 couplings, respectively. The subscript refers to the dimension of the Lagrangian.

Instead of an ordinary electron, an excited electron e^* with mass M_{e^*} could be exchanged in the t-channel [9, 11]. In the most general case $e^*e\gamma$ couplings would lead to a large anomalous magnetic moment of the electron [12]. This effect can be avoided by a chiral magnetic coupling of the form [13]:

$$\mathcal{L}_{e^*e\gamma} = \frac{1}{2\Lambda}\bar{e^*}\sigma^{\mu\nu}\left[gf\frac{\tau}{2}W_{\mu\nu} + g'f'\frac{Y}{2}B_{\mu\nu}\right]e_L + \text{h.c.} \; , \tag{2.4}$$

where τ are the Pauli matrices and Y is the hypercharge. The parameters of the model are the compositeness scale Λ and the weight factors f and f' associated to the gauge fields W and B with Standard Model couplings g and g'. For the process $e^+e^- \to \gamma\gamma(\gamma)$, the following cross-section results [14]:

$$\begin{aligned}\left(\frac{d\sigma}{d\Omega}\right)_{e^*} &= \left(\frac{d\sigma}{d\Omega}\right)_{\text{Born}} \\ &+ \frac{\alpha^2\pi}{2}\frac{f_\gamma^4}{\Lambda^4}M_{e^*}^2\left[\frac{p^4}{(p^2-M_{e^*}^2)^2} + \frac{q^4}{(q^2-M_{e^*}^2)^2} + \frac{\frac{1}{2}s^2\sin^2\theta}{(p^2-M_{e^*}^2)(q^2-M_{e^*}^2)}\right] \; ,\end{aligned} \tag{2.5}$$

with $f_\gamma = -\frac{1}{2}(f+f')$, $p^2 = -\frac{s}{2}(1-\cos\theta)$ and $q^2 = -\frac{s}{2}(1+\cos\theta)$. Effects vanish in the case of $f = -f'$. The cross-section does not depend on the sign of f_γ.

Theories of quantum gravity in extra spatial dimensions could solve the hierarchy problem because gravitons would be allowed to travel in more than 3+1 space-time dimensions [15]. While in these models the Planck mass M_D in $D = n+4$ dimensions is chosen to be of electroweak scale the usual Planck mass M_{Pl} in four dimensions would be

$$M_{\text{Pl}}^2 = R^n M_D^{n+2} \; , \tag{2.6}$$

where R is the compactification radius of the additional dimensions. Since gravitons couple to the energy-momentum tensor, their interaction with photons is as weak as with fermions. However, the huge number of Kaluza-Klein excitation modes in the extra dimensions may give rise to observable effects. These effects depend on the scale $M_s(\sim M_D)$ which may be as low as $\mathcal{O}(\text{TeV})$. Model dependencies are absorbed in the parameter λ which cannot be explicitly calculated without knowledge of the full theory, the sign is undetermined. The parameter λ is expected to be of $\mathcal{O}(1)$ and for this analysis it is assumed that $\lambda = \pm 1$. The expected differential cross-section is given by [15]:

$$\left(\frac{d\sigma}{d\Omega}\right)_{M_s} = \left(\frac{d\sigma}{d\Omega}\right)_{\text{Born}} - \alpha s\,\frac{\lambda}{M_s^4}\,(1+\cos^2\theta) + \frac{s^3}{8\pi}\,\frac{\lambda^2}{M_s^8}\,(1-\cos^4\theta) \; . \tag{2.7}$$

2.5 Fit Results

Where possible the fit parameters are chosen such that the likelihood function is approximately Gaussian. The preliminary results of the fits to the differential cross-sections are given in Table 2.3. No significant deviations with respect to the QED expectations are found (all the parameters are compatible with zero) and therefore 95% confidence level limits are obtained by renormalising the probability distribution of the fit parameter to the physically allowed region. The asymmetric limits $x_{95}^{\pm}$ on the fitting parameter are obtained by:

$$\frac{\int_0^{x_{95}^+}\Gamma(x,\mu,\sigma)dx}{\int_0^{\infty}\Gamma(x,\mu,\sigma)dx} = 0.95 \qquad \text{and} \qquad \frac{\int_{x_{95}^-}^0\Gamma(x,\mu,\sigma)dx}{\int_{-\infty}^0\Gamma(x,\mu,\sigma)dx} = 0.95 \; , \tag{2.8}$$

where Γ is a Gaussian with the central value and error of the fit result denoted by μ and σ, respectively. This is equivalent to the integration of a Gaussian probability function as a function of the fit parameter. The 95 % CL limits on the model parameters are derived from the limits on the fit parameters, e.g. the limit on Λ_+ is obtained as $[x_{95}^+(\Lambda_\pm^{-4})]^{-1/4}$.

The only model with more than one free model parameter is the search for excited electrons. In this case only one out of the two parameters f_γ and M_{e^*} is determined while the other is fixed. It is assumed that $\Lambda = M_{e^*}$. For limits on the coupling f_γ/Λ a scan over M_{e^*} is performed. The fit result at $M_{e^*} = 200$GeV is included in Table 2.3, limits for all masses are presented in Figure 2.3. For the determination of the excited electron mass the fit cannot be expressed in terms of a linear fit parameter. For $|f_\gamma| = 1$ the curve of the negative log likelihood, ΔLogL, as a function of M_{e^*} is shown in Figure 2.4. The value corresponding to $\Delta\text{LogL} = 1.92$ is $M_{e^*} = 248$ GeV.

Fit parameter	Fit result	95% CL limit [GeV]
$\Lambda_\pm^{-4}$	$\left(-12.5^{+25.1}_{-24.7}\right)\cdot 10^{-12}$ GeV^{-4}	$\Lambda_+ > 392$ $\Lambda_- > 364$
Λ_7^{-6}	$\left(-0.91^{+1.81}_{-1.78}\right)\cdot 10^{-18}$ GeV^{-6}	$\Lambda_7 > 831$
derived from Λ_+		$\Lambda_6 > 1595$
derived from Λ_7		$\Lambda_8 > 23.3$
λ/M_s^4	$\left(0.29^{+0.57}_{-0.58}\right)\cdot 10^{-12}$ GeV^{-4}	$\lambda = +1$: $M_s > 933$ $\lambda = -1$: $M_s > 1010$
$f_\gamma^4(M_{e^*} = 200\text{GeV})$	$0.037^{+0.202}_{-0.198}$	$f_\gamma/\Lambda < 3.9$ TeV^{-1}

Table 2.3: The preliminary combined fit parameters and the 95% confidence level limits for the four LEP experiments.

2.6 Conclusion

The LEP collaborations study the $e^+e^- \to \gamma\gamma(\gamma)$ channel up to the highest available centre-of-mass energies. The total cross-section results are combined in terms of the ratios with respect to the QED expectations. No deviations are found. The differential cross-sections are fit following different

parametrisations from models predicting deviations from QED. No evidence for deviations is found and therefore combined 95% confidence level limits are given.

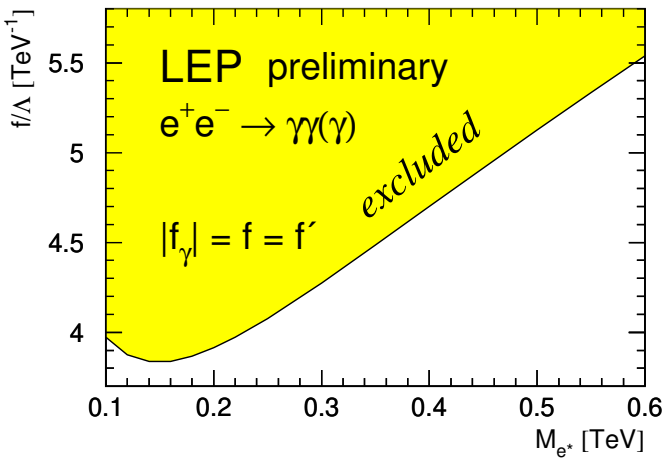

Figure 2.3: 95% CL limits on the coupling f_γ/Λ of an excited electron as a function of M_{e^*}. In the case of $f = f'$ it follows that $|f_\gamma| = f$. It is assumed that $\Lambda = M_{e^*}$.

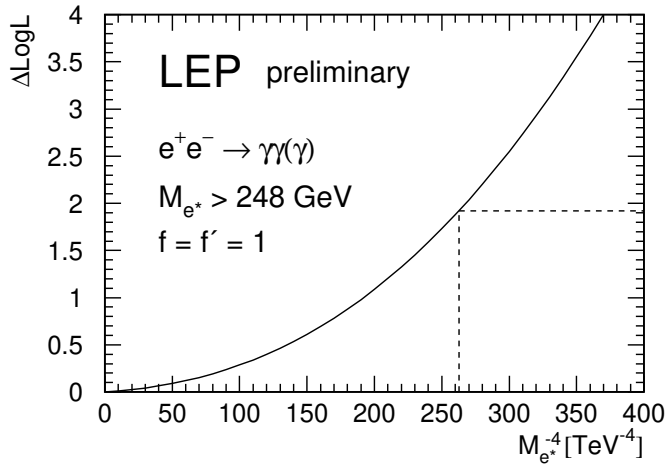

Figure 2.4: Log likelihood difference $\Delta\text{LogL} = -\ln\mathcal{L} + \ln\mathcal{L}_{\max}$ as a function of $M_{e^*}^{-4}$. The coupling is fixed at $f = f' = 1$. The value corresponding to $\Delta\text{LogL} = 1.92$ is $M_{e^*} = 248$ GeV.

Chapter 3

Fermion-Pair Production at LEP-II

Updates with respect to summer 2005:
Unchanged w.r.t. summer 2003: Results are preliminary.
Note that some recent publications [16–20] are not yet included in this combination.

3.1 Introduction

During the LEP-II program LEP delivered collisions at energies from ~ 130 GeV to ~ 209 GeV. The 4 LEP experiments have made measurements on the $e^+e^- \to f\bar{f}$ process over this range of energies, and a preliminary combination of these data is discussed in this note.

In the years 1995 through 1999 LEP delivered luminosity at a number of distinct centre-of-mass energy points. In 2000 most of the luminosity was delivered close to 2 distinct energies, but there was also a significant fraction of the luminosity delivered in, more-or-less, a continuum of energies. To facilitate the combination of the data, the 4 LEP experiments all divided the data they collected in 2000 into two energy bins: from 202.5 to 205.5 GeV; and 205.5 GeV and above. The nominal and actual centre-of-mass energies to which the LEP data are averaged for each year are given in Table 3.1.

A number of measurements on the process $e^+e^- \to f\bar{f}$ exist and are combined. The preliminary averages of cross-section and forward-backward asymmetry measurements are discussed in Section 3.2. The results presented in this section update those presented in [21]. Complete results of the combinations are available on the web page [22]. In Section 3.3 a preliminary average of the differential cross-sections measurements, $\frac{d\sigma}{d\cos\theta}$, for the channels $e^+e^- \to e^+e^-$, $e^+e^- \to \mu^+\mu^-$ and $e^+e^- \to \tau^+\tau^-$ is presented. In Section 3.4 a preliminary combination of the heavy flavour results R_b, R_c, $A_{FB}^{b\bar{b}}$ and $A_{FB}^{c\bar{c}}$ from LEP-II is presented. In Section 3.5 the combined results are interpreted in terms of contact interactions and the exchange of Z′ bosons, the exchange of leptoquarks or squarks and the exchange of gravitons in large extra dimensions. The results are summarised in section 3.6.

3.2 Averages for Cross-sections and Asymmetries

In this section the results of the preliminary combination of cross-sections and asymmetries are given. The individual experiments' analyses of cross-sections and forward-backward asymmetries are discussed in [23].

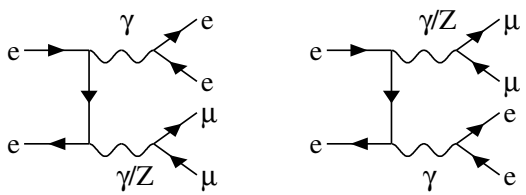

Figure 3.1: Diagrams leading to the production of initial state non-singlet electron-positron pairs in $e^+e^- \to \mu^+\mu^-$, which are considered as signal in the common signal definition.

Cross-section results are combined for the $e^+e^- \to q\overline{q}$, $e^+e^- \to \mu^+\mu^-$ and $e^+e^- \to \tau^+\tau^-$ channels, forward-backward asymmetry measurements are combined for the $\mu^+\mu^-$ and $\tau^+\tau^-$ final states. The averages are made for the samples of events with high effective centre-of-mass energies, $\sqrt{s'}$. Individual experiments have their own $f\overline{f}$ signal definitions; corrections are applied to bring the measurements to a common signal definitions:

- $\sqrt{s'}$ is taken to be the mass of the s-channel propagator, with the $f\overline{f}$ signal being defined by the cut $\sqrt{s'/s} > 0.85$.
- ISR-FSR photon interference is subtracted to render the propagator mass unambiguous.
- Results are given for the full 4π angular acceptance.
- Initial state non-singlet diagrams [24], see for example Figure 3.1, which lead to events containing additional fermions pairs are considered as part of the two fermion signal. In such events, the additional fermion pairs are typically lost down the beampipe of the experiments, such that the visible event topologies are usually similar to a difermion events with photons radiated from the initial state.

The corrected measurement of a cross-section or a forward backward asymmetry, M_{LEP}, corresponding to the common signal definition, is computed from the experimental measurement M_{exp},

$$M_{LEP} = M_{exp} + (P_{LEP} - P_{exp}), \tag{3.1}$$

where P_{exp} is the prediction for the measurement obtained for the experiments signal definition and P_{LEP} is the prediction for the common signal definition. The predictions are computed with ZFITTER [25].

In choosing a common signal definition there is a tension between the need to have a definition which is practical to implement in event generators and semi-analytical calculations, one which comes close to describing the underlying hard processes and one which most closely matches what is actually measured in experiments. Different signal definitions represent different balances between these needs. To illustrate how different choices would effect the quoted results a second signal definition is studied by calculating different predictions using ZFITTER:

- For dilepton events, $\sqrt{s'}$ is taken to be the bare invariant mass of the outgoing difermion pair (*i.e.*, the invariant mass excluding all radiated photons).

- For hadronic events, it is taken to be the mass of the s-channel propagator.
- In both cases, ISR-FSR photon interference is included and the signal is defined by the cut $\sqrt{s'/s} > 0.85$. When calculating the contribution to the hadronic cross-section due to ISR-FSR interference, since the propagator mass is ill-defined, it is replaced by the bare $q\overline{q}$ mass.

The definition of the hadronic cross-section is close to that used to define the signal for the heavy quark measurements given in Section 3.4.

Theoretical uncertainties associated with the Standard Model predictions for each of the measurements are not included during the averaging procedure, but must be included when assessing the compatibility of the data with theoretical predictions. The theoretical uncertainties on the Standard Model predictions amount to 0.26% on $\sigma(q\overline{q})$, 0.4% on $\sigma(\mu^+\mu^-)$ and $\sigma(\tau^+\tau^-)$, 2% on $\sigma(e^+e^-)$, and 0.004 on the leptonic forward-backward asymmetries [24].

The average is performed using the best linear unbiased estimator technique (BLUE) [26], which is equivalent to a χ^2 minimisation. All data from nominal centre-of-mass energies of 130–207 GeV are averaged at the same time.

Particular care is taken to ensure that the correlations between the hadronic cross-sections are reasonably estimated. The errors are broken down into 5 categories, with the ensuing correlations accounted for in the combinations:

1) The statistical uncertainty plus uncorrelated systematic uncertainties, combined in quadrature.
2) The systematic uncertainty for the final state X which is fully correlated between energy points for that experiment.
3) The systematic uncertainty for experiment Y which is fully correlated between different final states for this energy point.
4) The systematic uncertainty for the final state X which is fully correlated between energy points and between different experiments.
5) The systematic uncertainty which is fully correlated between energy points and between different experiments for all final states.

Uncertainties in the hadronic cross-sections arising from fragmentation models and modelling of ISR are treated as fully correlated between experiments. Despite some differences between the models used and the methods of evaluating the errors in the different experiments, there are significant common elements in the estimation of these sources of uncertainty.

New, preliminary, results from ALEPH are included in the average. The updated ALEPH measurements use a lower cut on the effective centre-of-mass energy, which makes the signal definition of ALEPH closer to the combined LEP signal definition.

Table 3.2 gives the averaged cross-sections and forward-backward asymmetries for all energies. The differences in the results obtained when using predictions of ZFITTER for the second signal definition are also given. The differences are significant when compared to the precision obtained from averaging together the measurements at all energies. The χ^2 per degree of freedom for the average of the LEP-II $f\overline{f}$ data is 160/180. Most correlations are rather small, with the largest components at any given pair of energies being between the hadronic cross-sections. The other off-diagonal terms in the correlation

matrix are smaller than 10%. The correlation matrix between the averaged hadronic cross-sections at different centre-of-mass energies is given in Table 3.3.

Figures 3.2 and 3.3 show the LEP averaged cross-sections and asymmetries, respectively, as a function of the centre-of-mass energy, together with the SM predictions. There is good agreement between the SM expectations and the measurements of the individual experiments and the combined averages. The cross-sections for hadronic final states at most of the energy points are somewhat above the SM expectations. Taking into account the correlations between the data points and also taking into account the theoretical error on the SM predictions, the ratio of the measured cross-sections to the SM expectations, averaged over all energies, is approximately a 1.7 standard deviation excess. It is concluded that there is no significant evidence in the results of the combinations for physics beyond the SM in the process $e^+e^- \to f\bar{f}$.

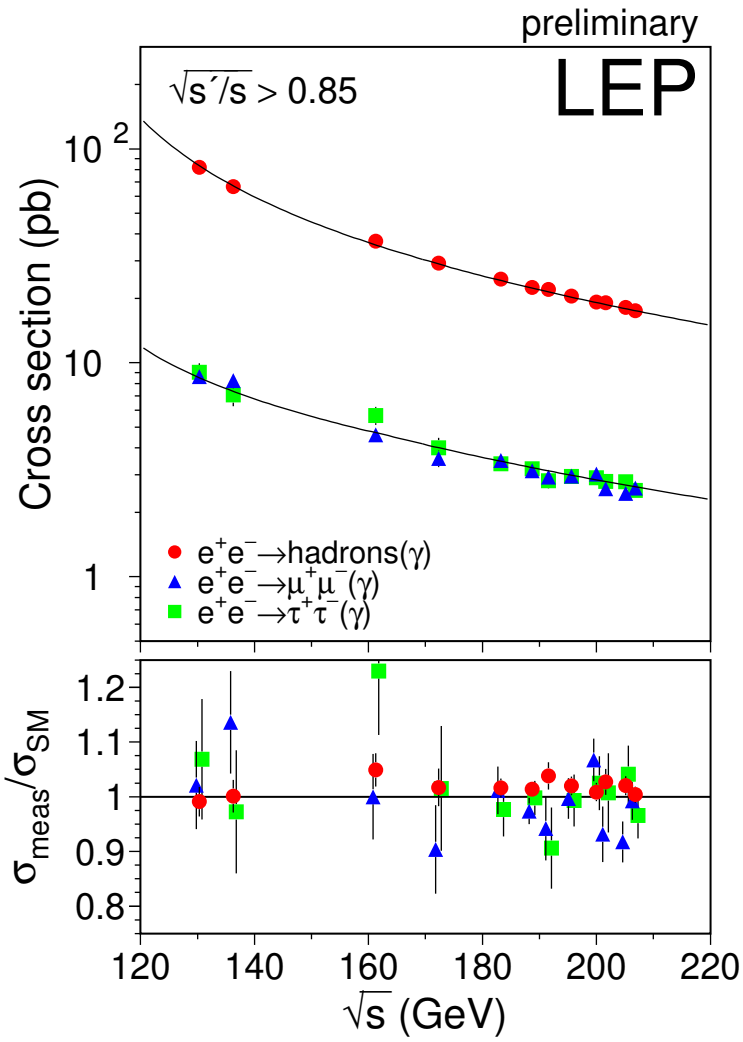

Figure 3.2: Preliminary combined LEP results on the cross-sections for $q\bar{q}$, $\mu^+\mu^-$ and $\tau^+\tau^-$ final states, as a function of centre-of-mass energy. The expectations of the SM, computed with ZFITTER [25], are shown as curves. The lower plot shows the ratio of the data divided by the SM.

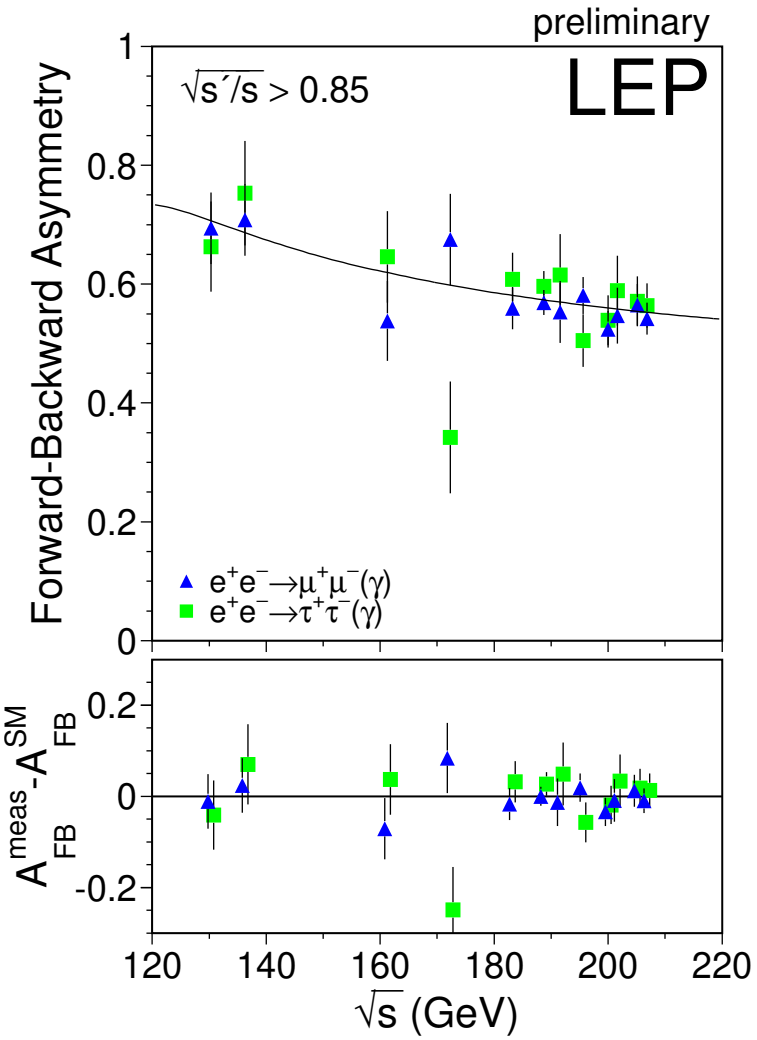

Figure 3.3: Preliminary combined LEP results on the forward-backward asymmetry for $\mu^+\mu^-$ and $\tau^+\tau^-$ final states as a function of centre-of-mass energy. The expectations of the SM computed with ZFITTER [25], are shown as curves. The lower plot shows differences between the data and the SM.

Year	Nominal Energy GeV	Actual Energy GeV	Luminosity pb^{-1}
1995	130	130.2	~ 3
	136	136.2	~ 3
	133*	133.2	~ 6
1996	161	161.3	~ 10
	172	172.1	~ 10
	167*	166.6	~ 20
1997	130	130.2	~ 2
	136	136.2	~ 2
	183	182.7	~ 50
1998	189	188.6	~ 170
1999	192	191.6	~ 30
	196	195.5	~ 80
	200	199.5	~ 80
	202	201.6	~ 40
2000	205	204.9	~ 80
	207	206.7	~ 140

Table 3.1: The nominal and actual centre-of-mass energies for data collected during LEP-II operation in each year. The approximate average luminosity analysed per experiment at each energy is also shown. Values marked with a * are average energies for 1995 and 1996 used for heavy flavour results. The data taken at nominal energies of 130 GeV and 136 GeV in 1995 and 1997 are combined by most experiments.

Table 3.2: Preliminary combined LEP results for $e^+e^- \to f\bar{f}$, with cross section quoted in units of picobarn. All the results correspond to the first signal definition. The Standard Model predictions are from ZFITTER [25]. The difference, Δ, in the predictions of ZFITTER for second definition relative to the first are given in the final column. The quoted uncertainties do not include the theoretical uncertainties discussed in the text.

$\sqrt{s}$ (GeV)	Quantity	Average value	SM	Δ
130	$\sigma(q\bar{q})$	82.1±2.2	82.8	-0.3
130	$\sigma(\mu^+\mu^-)$	8.62±0.68	8.44	-0.33
130	$\sigma(\tau^+\tau^-)$	9.02±0.93	8.44	-0.11
130	$A_{FB}(\mu^+\mu^-)$	0.694±0.060	0.705	0.012
130	$A_{FB}(\tau^+\tau^-)$	0.663±0.076	0.704	0.012
136	$\sigma(q\bar{q})$	66.7±2.0	66.6	-0.2
136	$\sigma(\mu^+\mu^-)$	8.27±0.67	7.28	-0.28
136	$\sigma(\tau^+\tau^-)$	7.078±0.820	7.279	-0.091
136	$A_{FB}(\mu^+\mu^-)$	0.708±0.060	0.684	0.013
136	$A_{FB}(\tau^+\tau^-)$	0.753±0.088	0.683	0.014
161	$\sigma(q\bar{q})$	37.0±1.1	35.2	-0.1
161	$\sigma(\mu^+\mu^-)$	4.61±0.36	4.61	-0.18
161	$\sigma(\tau^+\tau^-)$	5.67±0.54	4.61	-0.06
161	$A_{FB}(\mu^+\mu^-)$	0.538±0.067	0.609	0.017
161	$A_{FB}(\tau^+\tau^-)$	0.646±0.077	0.609	0.016
172	$\sigma(q\bar{q})$	29.23±0.99	28.74	-0.12
172	$\sigma(\mu^+\mu^-)$	3.57±0.32	3.95	-0.16
172	$\sigma(\tau^+\tau^-)$	4.01±0.45	3.95	-0.05
172	$A_{FB}(\mu^+\mu^-)$	0.675±0.077	0.591	0.018
172	$A_{FB}(\tau^+\tau^-)$	0.342±0.094	0.591	0.017
183	$\sigma(q\bar{q})$	24.59±0.42	24.20	-0.11
183	$\sigma(\mu^+\mu^-)$	3.49±0.15	3.45	-0.14
183	$\sigma(\tau^+\tau^-)$	3.37±0.17	3.45	-0.05
183	$A_{FB}(\mu^+\mu^-)$	0.559±0.035	0.576	0.018
183	$A_{FB}(\tau^+\tau^-)$	0.608±0.045	0.576	0.018
189	$\sigma(q\bar{q})$	22.47±0.24	22.156	-0.101
189	$\sigma(\mu^+\mu^-)$	3.123±0.076	3.207	-0.131
189	$\sigma(\tau^+\tau^-)$	3.20±0.10	3.20	-0.048
189	$A_{FB}(\mu^+\mu^-)$	0.569±0.021	0.569	0.019
189	$A_{FB}(\tau^+\tau^-)$	0.596±0.026	0.569	0.018
192	$\sigma(q\bar{q})$	22.05±0.53	21.24	-0.10
192	$\sigma(\mu^+\mu^-)$	2.92±0.18	3.10	-0.13
192	$\sigma(\tau^+\tau^-)$	2.81±0.23	3.10	-0.05
192	$A_{FB}(\mu^+\mu^-)$	0.553±0.051	0.566	0.019
192	$A_{FB}(\tau^+\tau^-)$	0.615±0.069	0.566	0.019
196	$\sigma(q\bar{q})$	20.53±0.34	20.13	-0.09
196	$\sigma(\mu^+\mu^-)$	2.94±0.11	2.96	-0.12
196	$\sigma(\tau^+\tau^-)$	2.94±0.14	2.96	-0.05
196	$A_{FB}(\mu^+\mu^-)$	0.581±0.031	0.562	0.019
196	$A_{FB}(\tau^+\tau^-)$	0.505±0.044	0.562	0.019
200	$\sigma(q\bar{q})$	19.25±0.32	19.09	-0.09
200	$\sigma(\mu^+\mu^-)$	3.02±0.11	2.83	-0.12
200	$\sigma(\tau^+\tau^-)$	2.90±0.14	2.83	-0.04
200	$A_{FB}(\mu^+\mu^-)$	0.524±0.031	0.558	0.019
200	$A_{FB}(\tau^+\tau^-)$	0.539±0.042	0.558	0.019
202	$\sigma(q\bar{q})$	19.07±0.44	18.57	-0.09
202	$\sigma(\mu^+\mu^-)$	2.58±0.14	2.77	-0.12
202	$\sigma(\tau^+\tau^-)$	2.79±0.20	2.77	-0.04
202	$A_{FB}(\mu^+\mu^-)$	0.547±0.047	0.556	0.020
202	$A_{FB}(\tau^+\tau^-)$	0.589±0.059	0.556	0.019
205	$\sigma(q\bar{q})$	18.17±0.31	17.81	-0.09
205	$\sigma(\mu^+\mu^-)$	2.45±0.10	2.67	-0.11
205	$\sigma(\tau^+\tau^-)$	2.78±0.14	2.67	-0.042
205	$A_{FB}(\mu^+\mu^-)$	0.565±0.035	0.553	0.020
205	$A_{FB}(\tau^+\tau^-)$	0.571±0.042	0.553	0.019
207	$\sigma(q\bar{q})$	17.49±0.26	17.42	-0.08
207	$\sigma(\mu^+\mu^-)$	2.595±0.088	2.623	-0.111
207	$\sigma(\tau^+\tau^-)$	2.53±0.11	2.62	-0.04
207	$A_{FB}(\mu^+\mu^-)$	0.542±0.027	0.552	0.020
207	$A_{FB}(\tau^+\tau^-)$	0.564±0.037	0.551	0.019

Table 3.3: The correlation coefficients between averaged hadronic cross-sections at different energies.

$\sqrt{s}$ (GeV)	130	136	161	172	183	189	192	196	200	202	205	207
130	1.000	0.071	0.080	0.072	0.114	0.146	0.077	0.105	0.120	0.086	0.117	0.138
136	0.071	1.000	0.075	0.067	0.106	0.135	0.071	0.097	0.110	0.079	0.109	0.128
161	0.080	0.075	1.000	0.077	0.120	0.153	0.080	0.110	0.125	0.090	0.124	0.145
172	0.072	0.067	0.077	1.000	0.108	0.137	0.072	0.099	0.112	0.081	0.111	0.130
183	0.114	0.106	0.120	0.108	1.000	0.223	0.117	0.158	0.182	0.129	0.176	0.208
189	0.146	0.135	0.153	0.137	0.223	1.000	0.151	0.206	0.235	0.168	0.226	0.268
192	0.077	0.071	0.080	0.072	0.117	0.151	1.000	0.109	0.126	0.090	0.118	0.138
196	0.105	0.097	0.110	0.099	0.158	0.206	0.109	1.000	0.169	0.122	0.162	0.190
200	0.120	0.110	0.125	0.112	0.182	0.235	0.126	0.169	1.000	0.140	0.184	0.215
202	0.086	0.079	0.090	0.081	0.129	0.168	0.090	0.122	0.140	1.000	0.132	0.153
205	0.117	0.109	0.124	0.111	0.176	0.226	0.118	0.162	0.184	0.132	1.000	0.213
207	0.138	0.128	0.145	0.130	0.208	0.268	0.138	0.190	0.215	0.153	0.213	1.000

3.3 Averages for Differential Cross-sections

3.3.1 e^+e^- final state

The LEP experiments have measured the differential cross-section, $\frac{d\sigma}{d\cos\theta}$, for the $e^+e^- \to e^+e^-$ channel.A preliminary combination of these results is made by performing a χ^2 fit to the measured differential cross-sections, using the statistical errors as given by the experiments. In contrast to the muon and tau channels (Section 3.3.2) the higher statistics makes the use of expected statistical errors unnecessary. The combination includes data from 189 GeV to 207 GeV from all experiments but DELPHI. The data used in the combination are summarised in Table 3.4.

Each experiment's data are binned according to an agreed common definition, which takes into account the large forward peak of Bhabha scattering:

- 10 bins for $\cos\theta$ between 0.0 and 0.90 and
- 5 bins for $\cos\theta$ between -0.90 and 0.0

at each energy. The scattering angle, θ, is the angle of the negative lepton with respect to the incoming electron direction in the lab coordinate system. The outer acceptances of the most forward and most backward bins for which the experiments present their data are different. The ranges in $\cos\theta$ of the individual experiments and the average are given in Table 3.5. Except for the binning, each experiment uses their own signal definition, for example different experiments have different acollinearity cuts to select events. The signal definition used for the LEP average corresponds to an acollinearity cut of 10°. The experimental measurements are corrected to the common signal definition following the procedure described in Section 3.2. The theoretical predictions are taken from the Monte Carlo event generator BHWIDE [27].

Correlated systematic errors between different experiments, energies and bins at the same energy, arising from uncertainties on the overall normalisation, and from migration of events between forward and backward bins with the same absolute value of $\cos\theta$ due to uncertainties in the corrections for charge confusion, were considered in the averaging procedure.

An average for all energies between 189–207 GeV is performed. The results of the averages are shown in Figure 3.4. The χ^2 per degree of freedom for the average is 190.8/189.

The correlations between bins in the average are well below 5% of the total error on the averages in each bin for most of the cases, and exceed 10% for the most forward bin for the energy points with the highest accumulated statistics. The agreement between the averaged data and the predictions from the Monte Carlo generator BHWIDE is good.

3.3.2 $\mu^+\mu^-$and $\tau^+\tau^-$ final states

The LEP experiments have measured the differential cross-section, $\frac{d\sigma}{d\cos\theta}$, for the $e^+e^- \to \mu^+\mu^-$ and $e^+e^- \to \tau^+\tau^-$ channels for samples of events with high effective centre-of-mass energy, $\sqrt{s'/s} > 0.85$. A preliminary combination of these results is made using the BLUE technique. The statistical error associated with each measurement is taken as the expected statistical error on the differential cross-section, computed from the expected number of events in each bin for each experiment. Using a

Monte Carlo simulation it has been shown that this method provides a good approximation to the exact likelihood method based on Poisson statistics [28].

The combination includes data from 183 GeV to 207 GeV, but not all experiments provided data at all energies. The data used in the combination are summarised in Table 3.6.

Each experiment's data are binned in 10 bins of $\cos\theta$ at each energy, using their own signal definition. The scattering angle, θ, is the angle of the negative lepton with respect to the incoming electron direction in the lab coordinate system. The outer acceptances of the most forward and most backward bins for which the four experiments present their data are different. This was accounted for as part of the correction to a common signal definition. The ranges in $\cos\theta$ for the measurements of the individual experiments and the average are given in Table 3.7. The signal definition used corresponded to the first definition given in Section 3.2.

Correlated systematic errors between different experiments, channels and energies, arising from uncertainties on the overall normalisation are considered in the averaging procedure. All data from all energies are combined in a single fit to obtain averages at each centre-of-mass energy yielding the full covariance matrix between the different measurements at all energies.

The results of the averages are shown in Figures 3.5 and 3.6. The correlations between bins in the average are less that 2% of the total error on the averages in each bin. Overall the agreement between the averaged data and the predictions is reasonable, with a χ^2 of 200 for 160 degrees of freedom. At 202 GeV the measured differential cross-sections in the most backward bins, $-1.00 < \cos\theta < 0.8$, for both muon and tau final states are above the predictions. The data at 202 GeV suffer from rather low delivered luminosity, with less than 4 events expected in each experiment in each channel in this backward $\cos\theta$ bin. The agreement between the data and the predictions in the same $\cos\theta$ bin is more consistent at higher energies.

	$e^+e^- \to e^+e^-$			
$\sqrt{s}$(GeV)	A	D	L	O
189	P	-	P	F
192–202	P	-	P	P
205–207	P	-	P	P

Table 3.4: Differential cross-section data provided by the LEP collaborations (ALEPH, DELPHI, L3 and OPAL) for $e^+e^- \to e^+e^-$. Data indicated with F are final, published data. Data marked with P are preliminary. Data marked with a - were not available for combination.

Experiment	$\cos\theta_{min}$	$\cos\theta_{max}$
ALEPH ($\sqrt{s'/s} > 0.85$)	-0.90	0.90
L3 (acol. $<$ 25°)	-0.72	0.72
OPAL (acol. $<$ 10°)	-0.90	0.90
Average (acol. $<$ 10°)	-0.90	0.90

Table 3.5: The acceptances for which experimental data are presented for the $e^+e^- \to e^+e^-$ channel and the acceptance for the LEP average.

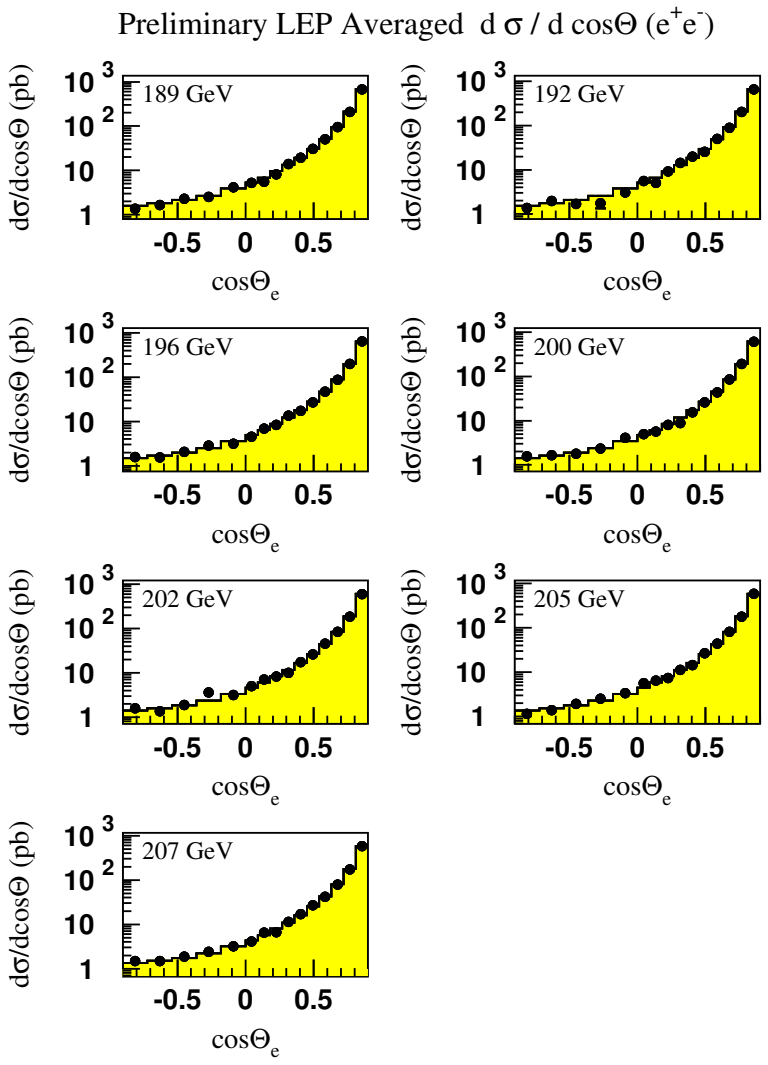

Figure 3.4: LEP averaged differential cross-sections for $e^+e^- \to e^+e^-$ at energies of 189–207 GeV. The SM predictions, shown as solid histograms, are computed with BHWIDE [27].

	$e^+e^- \to \mu^+\mu^-$				$e^+e^- \to \tau^+\tau^-$			
$\sqrt{s}$(GeV)	A	D	L	O	A	D	L	O
183	-	F	-	F	-	F	-	F
189	P	F	F	F	P	F	F	F
192–202	P	P	P	P	P	P	-	P
205–207	P	P	P	P	P	P	-	P

Table 3.6: Differential cross-section data provided by the LEP collaborations (ALEPH, DELPHI, L3 and OPAL) for $e^+e^- \to \mu^+\mu^-$ and $e^+e^- \to \tau^+\tau^-$ combination at different centre-of-mass energies. Data indicated with F are final, published data. Data marked with P are preliminary. Data marked with a - were not available for combination.

Experiment	$\cos\theta_{min}$	$\cos\theta_{max}$
ALEPH	−0.95	0.95
DELPHI ($e^+e^- \to \mu^+\mu^-$ 183)	−0.94	0.94
DELPHI ($e^+e^- \to \mu^+\mu^-$ 189–207)	−0.97	0.97
DELPHI ($e^+e^- \to \tau^+\tau^-$)	−0.96	0.96
L3	−0.90	0.90
OPAL	−1.00	1.00
Average	−1.00	1.00

Table 3.7: The acceptances for which experimental data are presented and the acceptance for the LEP average. For DELPHI the acceptance is shown for the different channels and for the muons for different centre of mass energies. For all other experiments the acceptance is the same for muon and tau-lepton channels and for all energies provided.

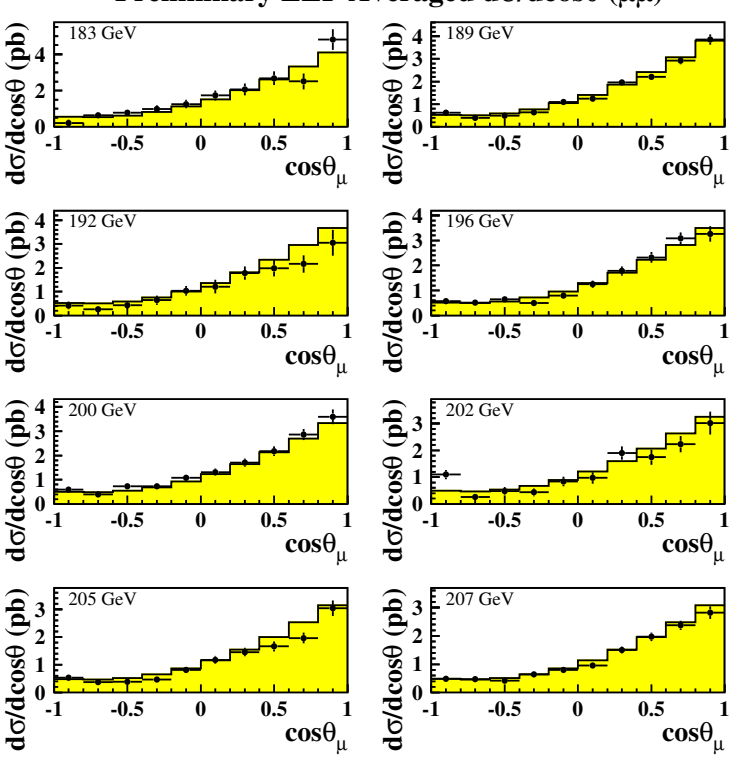

Figure 3.5: LEP averaged differential cross-sections for $e^+e^- \to \mu^+\mu^-$ at energies of 183–207 GeV. The SM predictions, shown as solid histograms, are computed with ZFITTER [25].

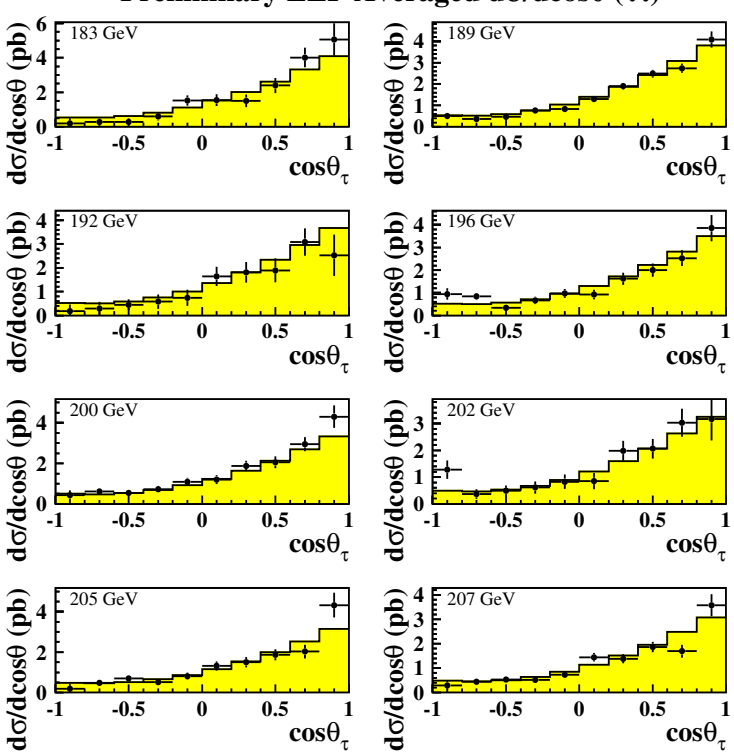

Figure 3.6: LEP averaged differential cross-sections for $e^+e^- \to \tau^+\tau^-$ at energies of 183–207 GeV. The SM predictions, shown as solid histograms, are computed with ZFITTER [25].

3.4 Averages for Heavy Flavour Measurements

This section presents a preliminary combination of both published [29] and preliminary [30] measurements of the ratios cross section ratios R_q defined as $\frac{\sigma_{q\bar{q}}}{\sigma_{had}}$ for b and c production, R_b and R_c, and the forward-backward asymmetries, $A_{FB}^{b\bar{b}}$ and $A_{FB}^{c\bar{c}}$, from the LEP collaborations at centre-of-mass energies in the range of 130 GeV to 207 GeV. Table 3.8 summarises all the inputs that have been combined so far.

A common signal definition is defined for all the measurements, requiring:

- an effective centre-of-mass energy $\sqrt{s'} > 0.85\sqrt{s}$
- no subtraction of ISR and FSR photon interference contribution and
- extrapolation to full angular acceptance.

Systematic errors are divided into three categories: uncorrelated errors, errors correlated between the measurements of each experiment, and errors common to all experiments.

Due to the fact that R_c measurements are only provided by a single experiment and are strongly correlated with R_b measurements, it was decided to fit the b sector and c sector separately, the other flavour's measurements being fixed to their Standard Model predictions. In addition, these fitted values are used to set limits upon physics beyond the Standard Model, such as contact term interactions, in which only one quark flavour is assumed to be effected by the new physics during each fit, therefore this averaging method is consistent with the interpretations.

Full details concerning the combination procedure can be found in [31].

The results of the combination are presented in Table 3.9 and Table 3.10 and in Figures 3.7 and 3.8. The results for both b and c sector are in agreement with the Standard Model predictions of ZFITTER. The averaged discrepancies with respect to the Standard Model predictions is -2.08 σ for R_b, +0.30 σ for R_c, -1.56 σ for $A_{FB}^{b\bar{b}}$ and -0.24 σ for $A_{FB}^{c\bar{c}}$. A list of the error contributions from the combination at 189 GeV is shown in Table 3.11.

$\sqrt{s}$ (GeV)	R_b				R_c				$A_{FB}^{b\bar{b}}$				$A_{FB}^{c\bar{c}}$			
	A	D	L	O	A	D	L	O	A	D	L	O	A	D	L	O
133	F	F	F	F	-	-	-	-	-	F	-	F	-	F	-	F
167	F	F	F	F	-	-	-	-	-	F	-	F	-	F	-	F
183	F	P	F	F	F	-	-	-	F	-	-	F	P	-	-	F
189	P	P	F	F	P	-	-	-	P	P	F	F	P	-	-	F
192 to 202	P	P	P	-	P*	-	-	-	P	P	-	-	-	-	-	-
205 and 207	-	P	P	-	P	-	-	-	P	P	-	-	-	-	-	-

Table 3.8: Data provided by the ALEPH, DELPHI, L3, OPAL collaborations for combination at different centre-of-mass energies. Data indicated with F are final, published data. Data marked with P are preliminary and for data marked with P*, not all energies are supplied. Data marked with a - were not supplied for combination.

$\sqrt{s}$ (GeV)	R_b	$A_{FB}^{b\bar{b}}$
133	0.1822 ± 0.0132 (0.1867)	0.367 ± 0.251 (0.504)
167	0.1494 ± 0.0127 (0.1727)	0.624 ± 0.254 (0.572)
183	0.1646 ± 0.0094 (0.1692)	0.515 ± 0.149 (0.588)
189	0.1565 ± 0.0061 (0.1681)	0.529 ± 0.089 (0.593)
192	0.1551 ± 0.0149 (0.1676)	0.424 ± 0.267 (0.595)
196	0.1556 ± 0.0097 (0.1670)	0.535 ± 0.151 (0.598)
200	0.1683 ± 0.0099 (0.1664)	0.596 ± 0.149 (0.600)
202	0.1646 ± 0.0144 (0.1661)	0.607 ± 0.241 (0.601)
205	0.1606 ± 0.0126 (0.1657)	0.715 ± 0.214 (0.603)
207	0.1694 ± 0.0107 (0.1654)	0.175 ± 0.156 (0.604)

Table 3.9: Combined results on R_b and $A_{FB}^{b\bar{b}}$. Quoted errors represent the statistical and systematic errors added in quadrature. For comparison, the Standard Model predictions computed with ZFITTER [32] are given in parentheses.

$\sqrt{s}$ (GeV)	R_c	$A_{FB}^{c\bar{c}}$
133	-	0.630 ± 0.313 (0.684)
167	-	0.980 ± 0.343 (0.677)
183	0.2628 ± 0.0397 (0.2472)	0.717 ± 0.201 (0.663)
189	0.2298 ± 0.0213 (0.2490)	0.542 ± 0.143 (0.656)
196	0.2734 ± 0.0387 (0.2508)	-
200	0.2535 ± 0.0360 (0.2518)	-
205	0.2816 ± 0.0394 (0.2530)	-
207	0.2890 ± 0.0350 (0.2533)	-

Table 3.10: Combined results on R_c and $A_{FB}^{c\bar{c}}$. Quoted errors represent the statistical and systematic errors added in quadrature. For comparison, the Standard Model predictions computed with ZFITTER [32] are given in parentheses.

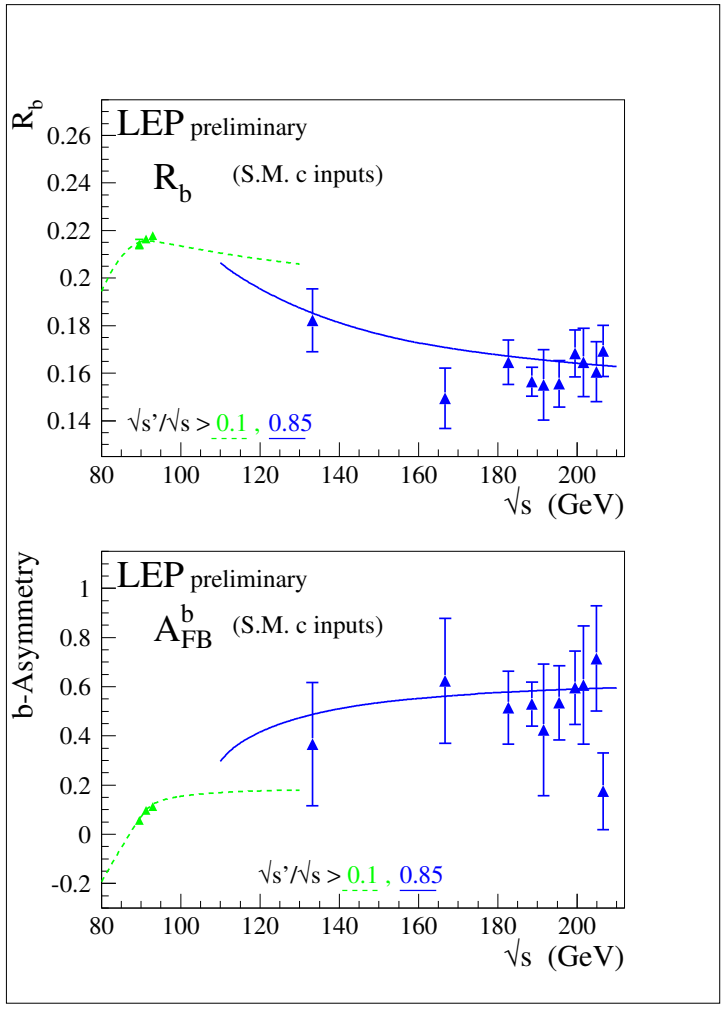

Figure 3.7: Preliminary combined LEP measurements of R_b and $A_{FB}^{b\bar{b}}$. Solid lines represent the Standard Model prediction for the high $\sqrt{s'}$ selection used at LEP-II and dotted lines the inclusive prediction used at LEP-I. Both are computed with ZFITTER[32]. The LEP-I measurements have been taken from [33].

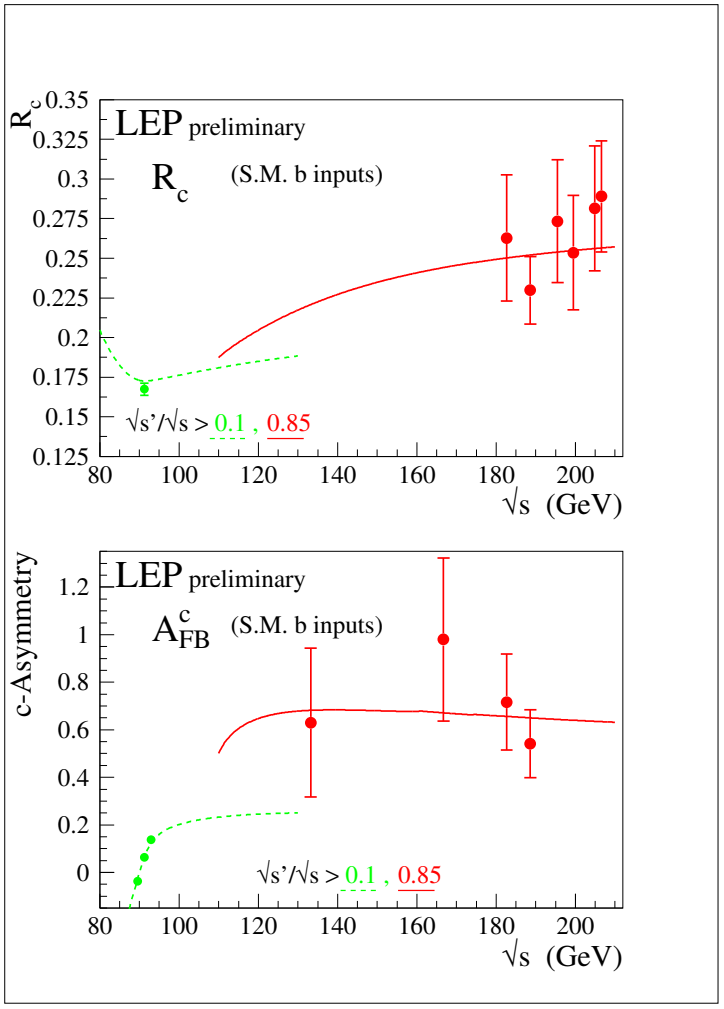

Figure 3.8: Preliminary combined LEP measurements of R_c and $A_{FB}^{c\bar{c}}$. Solid lines represent the Standard Model prediction for the high $\sqrt{s'}$ selection used at LEP-II and dotted lines the inclusive prediction used at LEP-I. Both are computed with ZFITTER [32]. The LEP-I measurements have been taken from [33].

Error list	R_b (189 GeV)	$A_{FB}^{b\bar{b}}$ (189 GeV)	R_c (189 GeV)	$A_{FB}^{c\bar{c}}$ (189 GeV)
statistics	0.0057	0.084	0.0169	0.119
internal syst	0.0020	0.025	0.0109	0.042
common syst	0.0007	0.011	0.0072	0.069
total syst	0.0021	0.027	0.0130	0.081
total error	0.0061	0.089	0.0213	0.143

Table 3.11: Error breakdown at 189 GeV.

3.5 Interpretation

The combined measurements presented above are interpreted in a variety of models. The cross-section and asymmetry results are used to place limits on contact interactions between leptons and quarks and, using the results on heavy flavour production, on contact interaction between electrons and b and c quarks specifically. Limits on the mass of a possible additional heavy neutral boson, Z′, are obtained for a variety of models. Using the combined differential cross-sections for e^+e^- final states, limits on contact interactions in the $e^+e^- \to e^+e^-$ channel and limits on the scale of gravity in models with large extra-dimensions are presented. Limits are also derived on the masses of leptoquarks - assuming a coupling of electromagnetic strength. In all cases the Born level predictions for the physics beyond the Standard Model have been corrected to take into account QED radiation.

3.5.1 Contact Interactions

The averages of cross-sections and forward-backward asymmetries for muon-pair and tau-lepton pair and the cross-sections for $q\bar{q}$ final states are used to search for contact interactions between fermions.

Following [34], contact interactions are parameterised by an effective Lagrangian, $\mathcal{L}_{\text{eff}}$, which is added to the Standard Model Lagrangian and has the form:

$$\mathcal{L}_{\text{eff}} = \frac{g^2}{(1+\delta)\Lambda^2} \sum_{i,j=L,R} \eta_{ij} \overline{e}_i \gamma_\mu e_i \overline{f}_j \gamma^\mu f_j, \tag{3.2}$$

where $g^2/4\pi$ is taken to be 1 by convention, $\delta = 1(0)$ for $f = e$ ($f \neq e$), $\eta_{ij} = \pm 1$ or 0 for different interaction types, Λ is the scale of the contact interactions, e_i and f_j are left or right-handed spinors. By assuming different helicity coupling between the initial state and final state currents, a set of different models can be defined from this Lagrangian [35], with either constructive (+) or destructive (−) interference between the Standard Model process and the contact interactions. The models and corresponding choices of η_{ij} are given in Table 3.12. The models $LL^\pm$, $RR^\pm$, $VV^\pm$, $AA^\pm$, $LR^\pm$, $RL^\pm$, $V0^\pm$, $A0^\pm$ are considered here since these models lead to large deviations in $e^+e^- \to f\overline{f}$ at LEP-II. The corresponding energies scales for the models with constructive or destructive interference are denoted by Λ^+ and Λ^- respectively.

For leptonic final states 4 different fits are made

- individual fits to contact interactions in $e^+e^- \to \mu^+\mu^-$ and $e^+e^- \to \tau^+\tau^-$ using the measured cross-sections and asymmetries,
- fits to $e^+e^- \to \ell^+\ell^-$ (simultaneous fits to $e^+e^- \to \mu^+\mu^-$ and $e^+e^- \to \tau^+\tau^-$) again using the measured cross-sections and asymmetries,

- fits to $e^+e^- \to e^+e^-$, using the measured differential cross-sections.

For the inclusive hadronic final states three different model assumptions are used to fit the total hadronic cross-section

- the contact interactions affect only one quark flavour of up-type using the measured hadronic cross-sections,
- the contact interactions affect only one quark flavour of down-type using the measured hadronic cross-sections,
- the contact interactions contribute to all quark final states with the same strength.

Limits on contact interactions between electrons and b and c quarks are obtained using all the heavy flavour LEP-II combined results from 133 GeV to 207 GeV given in Tables 3.9 and 3.10. For the purpose of fitting contact interaction models to the data, R_b and R_c are converted to cross-sections $\sigma_{b\bar{b}}$ and $\sigma_{c\bar{c}}$ using the averaged $q\bar{q}$ cross-section of section 3.2 corresponding to the second signal definition. In the calculation of errors, the correlations between R_b, R_c and $\sigma_{q\bar{q}}$ are assumed to be negligible. These results are of particular interest since they are inaccessible to $p\bar{p}$ or ep colliders.

For the purpose of fitting contact interaction models to the data, the parameter $\epsilon = 1/\Lambda^2$ is used, with $\epsilon = 0$ in the limit that there are no contact interactions. This parameter is allowed to take both positive and negative values in the fits. Theoretical uncertainties on the Standard Model predictions are taken from [24].

The values of ϵ extracted for each model are all compatible with the Standard Model expectation $\epsilon = 0$, at the two standard deviation level. As expected, the errors on ϵ are typically a factor of two smaller than those obtained from a single LEP experiment with the same data set. The fitted values of ϵ are converted into 95% confidence level lower limits on Λ. The limits are obtained by integrating the likelihood function in ϵ over the physically allowed values[1], $\epsilon \geq 0$ for each Λ^+ limit and $\epsilon \leq 0$ for Λ^- limits.

The fitted values of ϵ and their 68% confidence level uncertainties together with the 95% confidence level lower limit on Λ are shown in Table 3.13 for the fits to $e^+e^- \to \ell^+\ell^-$ ($\ell \neq e$), $e^+e^- \to e^+e^-$, inclusive $e^+e^- \to q\bar{q}$, $e^+e^- \to b\bar{b}$ and $e^+e^- \to c\bar{c}$. Table 3.14 shows only the limits obtained on the scale Λ for other fits. The limits are shown graphically in Figure 3.9.

For the VV model with positive interference and assuming electromagnetic coupling strength instead of $g^2/4\pi = 1$, the scale Λ obtained in the $e^+e^- \to e^+e^-$ channel is converted to an upper limit on the electron size:

$$r_e < 1.4 \times 10^{-19} \text{m} \tag{3.3}$$

Models with stronger couplings will make this upper limit even tighter.

[1] To be able to obtain confidence limits from the likelihood function in ϵ it is necessary to convert the likelihood to a probability density function for ϵ; this is done by multiplying by a prior probability function. Simply integrating the likelihood over ϵ is equivalent to multiplying by a uniform prior probability function in ϵ.

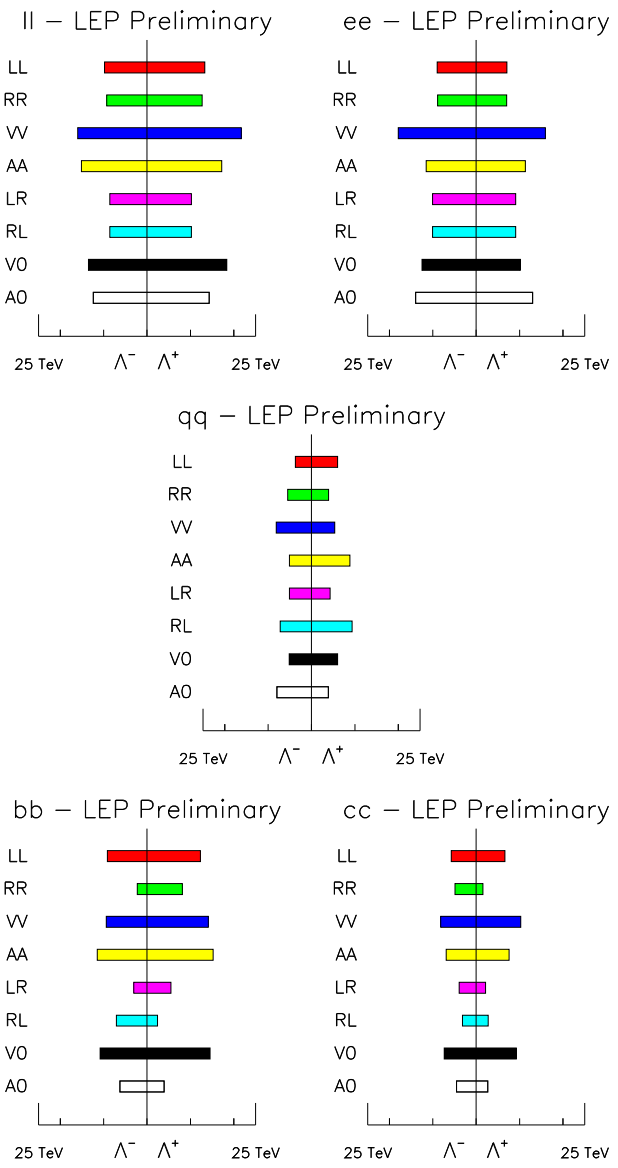

Figure 3.9: The limits on Λ for $e^+e^- \to \ell^+\ell^-$ assuming universality in the contact interactions between $e^+e^- \to \ell^+\ell^-$ ($\ell \neq e$), for $e^+e^- \to e^+e^-$, for $e^+e^- \to q\overline{q}$ assuming equal strength contact interactions for quarks and for $e^+e^- \to b\overline{b}$ and $e^+e^- \to c\overline{c}$.

Model	η_{LL}	η_{RR}	η_{LR}	η_{RL}
$LL^{\pm}$	±1	0	0	0
$RR^{\pm}$	0	±1	0	0
$VV^{\pm}$	±1	±1	±1	±1
$AA^{\pm}$	±1	±1	∓1	∓1
$LR^{\pm}$	0	0	±1	0
$RL^{\pm}$	0	0	0	±1
$V0^{\pm}$	±1	±1	0	0
$A0^{\pm}$	0	0	±1	±1

Table 3.12: Choices of η_{ij} for different contact interaction models

.

3.5.2 Models with Z′ Bosons

The combined hadronic and leptonic cross-sections and the leptonic forward-backward asymmetries are used to fit the data to models including an additional, heavy, neutral boson, Z′.

Fits are made to $M_{Z'}$, the mass of a Z′ for models resulting from an E_6 GUT and L-R symmetric models [36] and for the Sequential Standard Model (SSM) [37], which proposes the existence of a Z′ with exactly the same coupling to fermions as the standard Z. LEP-II data alone does not significantly constrain the mixing angle between the Z and Z′ fields, $\Theta_{ZZ'}$. However results from a single experiment, in which LEP-I data is used in the fit, show that the mixing is consistent with zero (see for example [38]). So for these fits $\Theta_{ZZ'}$ was fixed to zero.

No significant evidence is found for the existence of a Z′ boson in any of the models. The procedure to find limits on the Z′ mass corresponds to that in case of contact interactions: for large masses the exchange of a Z′ can be approximated by contact terms, $\Lambda \propto M_{Z'}$. The lower limits on the Z′ mass are shown in Figure 3.10 varying the parameters θ_6 for the E_6 models and α_{LR} for the left-right models. The results for the specific models χ, ψ ,η ($\theta_6 = 0,\ \pi/2,\ -\arctan\sqrt{5/3}$), L-R ($\alpha_{LR}$=1.53) and SSM are shown in Table 3.15.

3.5.3 Leptoquarks and R-parity violating squarks

Leptoquarks (LQ) would mediate quark-lepton transitions. Following the notations in Reference [39, 40], scalar leptoquarks, S_I, and vector leptoquarks,V_I are indicated based on spin and isospin I. Leptoquarks with the same Isospin but with different hypercharges are distinguished by an additional tilde. See Reference 40 for further details. They carry fermion numbers, $F = L + 3B$. It is assumed that leptoquark couplings to quark-lepton pairs preserve baryon- and lepton-number. The couplings g_L, g_R, are labelled according to the chirality of the lepton.

$\tilde{S}_{1/2}$(L) and S_0(L) leptoquarks are equivalent to up-type anti-squarks and down-type squarks, respectively. Limits in terms of the leptoquark coupling are then exactly equivalent to limits on λ_{1jk} in the Lagrangian $\lambda_{1jk}L_1Q_j\bar{D}_k$.

At LEP, the exchange of a leptoquark can modify the hadronic cross-sections and asymmetries, as described at the Born level by the equations given in Reference 40. Using the LEP combined measurements of hadronic cross-sections, and the measurements of heavy quark production, R_b, R_c,

$e^+e^- \to \ell^+\ell^-$			
Model	ϵ (TeV^{-2})	Λ^- (TeV)	Λ^+ (TeV)
LL	$-0.0044^{+0.0035}_{-0.0035}$	9.8	13.3
RR	$-0.0049^{+0.0039}_{-0.0039}$	9.3	12.7
VV	$-0.0016^{+0.0013}_{-0.0014}$	16.0	21.7
AA	$-0.0013^{+0.0017}_{-0.0017}$	15.1	17.2
LR	$-0.0036^{+0.0052}_{-0.0054}$	8.6	10.2
RL	$-0.0036^{+0.0052}_{-0.0054}$	8.6	10.2
V0	$-0.0023^{+0.0018}_{-0.0018}$	13.5	18.4
A0	$-0.0018^{+0.0026}_{-0.0026}$	12.4	14.3

$e^+e^- \to e^+e^-$			
Model	ϵ (TeV^{-2})	Λ^- (TeV)	Λ^+ (TeV)
LL	$0.0049^{+0.0084}_{-0.0084}$	9.0	7.1
RR	$0.0056^{+0.0082}_{-0.0092}$	8.9	7.0
VV	$0.0004^{+0.0022}_{-0.0016}$	18.0	15.9
AA	$0.0009^{+0.0041}_{-0.0039}$	11.5	11.3
LR	$0.0008^{+0.0064}_{-0.0052}$	10.0	9.1
RL	$0.0008^{+0.0064}_{-0.0052}$	10.0	9.1
V0	$0.0028^{+0.0038}_{-0.0045}$	12.5	10.2
A0	$-0.0008^{+0.0028}_{-0.0030}$	14.0	13.0

$e^+e^- \to q\overline{q}$			
Model	ϵ (TeV^{-2})	Λ^- (TeV)	Λ^+ (TeV)
LL	$0.0152^{+0.0064}_{-0.0076}$	3.7	6.0
RR	$-0.0208^{+0.0103}_{-0.0082}$	5.5	3.9
VV	$-0.0096^{+0.0051}_{-0.0037}$	8.1	5.3
AA	$0.0068^{+0.0033}_{-0.0034}$	5.1	8.8
LR	$-0.0308^{+0.0172}_{-0.0055}$	5.1	4.3
RL	$-0.0108^{+0.0057}_{-0.0054}$	7.2	9.3
V0	$0.0174^{+0.0057}_{-0.0074}$	5.1	6.0
A0	$-0.0092^{+0.0049}_{-0.0041}$	8.0	3.9

$e^+e^- \to b\overline{b}$			
Model	ϵ (TeV^{-2})	Λ^- (TeV)	Λ^+ (TeV)
LL	$-0.0038^{+0.0044}_{-0.0047}$	9.1	12.3
RR	$-0.1729^{+0.1584}_{-0.0162}$	2.2	8.1
VV	$-0.0040^{+0.0039}_{-0.0041}$	9.4	14.1
AA	$-0.0022^{+0.0029}_{-0.0031}$	11.5	15.3
LR	$-0.0620^{+0.0692}_{-0.0313}$	3.1	5.5
RL	$0.0180^{+0.1442}_{-0.0249}$	7.0	2.4
V0	$-0.0028^{+0.0032}_{-0.0033}$	10.8	14.5
A0	$0.0375^{+0.0193}_{-0.0379}$	6.3	3.9

$e^+e^- \to c\overline{c}$			
Model	ϵ (TeV^{-2})	Λ^- (TeV)	Λ^+ (TeV)
LL	$-0.0091^{+0.0126}_{-0.0126}$	5.7	6.6
RR	$0.3544^{+0.0476}_{-0.3746}$	4.9	1.5
VV	$-0.0047^{+0.0057}_{-0.0060}$	8.2	10.3
AA	$-0.0059^{+0.0095}_{-0.0090}$	6.9	7.6
LR	$0.1386^{+0.0555}_{-0.1649}$	3.9	2.1
RL	$0.0106^{+0.0848}_{-0.0757}$	3.1	2.8
V0	$-0.0058^{+0.0075}_{-0.0071}$	7.4	9.2
A0	$0.0662^{+0.0564}_{-0.0905}$	4.5	2.7

Table 3.13: The fitted values of ϵ and the derived 95% confidence level lower limits on the parameter Λ of contact interaction derived from fits to lepton-pair cross-sections and asymmetries and from fits to hadronic cross-sections. The limits Λ_+ and Λ_- given in TeV correspond to the upper and lower signs of the parameters η_{ij} in Table 3.12. For $\ell^+\ell^-$ ($\ell \neq e$) the couplings to $\mu^+\mu^-$ and $\tau^+\tau^-$ are a assumed to be universal and for inclusive $q\overline{q}$ final states all quarks are assumed to experience contact interactions with the same strength.

leptons				
	$\mu^+\mu^-$		$\tau^+\tau^-$	
Model	Λ_-	Λ_+	Λ_-	Λ_+
LL	8.5	12.5	9.1	8.6
RR	8.1	11.9	8.7	8.2
VV	14.3	19.7	14.2	14.5
AA	12.7	16.4	14.0	11.3
LR	7.9	8.9	2.2	7.9
RL	7.9	8.9	2.2	7.9
V0	11.7	17.2	12.7	11.8
A0	11.5	12.4	9.8	10.8

hadrons				
	up-type		down-type	
Model	Λ_-	Λ_+	Λ_-	Λ_+
LL	6.7	10.2	10.6	6.0
RR	5.7	8.3	2.2	4.3
VV	9.6	14.3	11.4	7.0
AA	8.0	11.5	13.3	7.7
LR	4.2	2.3	2.7	3.5
RL	3.5	2.8	4.2	2.4
V0	8.7	13.4	12.5	7.1
A0	4.9	2.8	4.2	3.3

Table 3.14: The 95% confidence level lower limits on the parameter Λ of contact interaction derived from fits to lepton-pair cross-sections and asymmetries and from fits to hadronic cross-sections. The limits Λ_+ and Λ_- given in TeV correspond to the upper and lower signs of the parameters η_{ij} in Table 3.12. For hadrons the limits for up-type and down-type quarks are derived assuming a single up or down type quark undergoes contact interactions.

Z′ model	χ	ψ	η	L-R	SSM
$M^{limit}_{Z'}$ (GeV/c^2)	673	481	434	804	1787

Table 3.15: The 95% confidence level lower limits on the Z′ mass for χ, ψ, η, L-R and SSM models.

$A^{b\overline{b}}_{FB}$ and $A^{c\overline{c}}_{FB}$, upper limits can be set on the leptoquark's coupling g as a function of its mass M_{LQ} for leptoquarks coupling electrons to first, second and third generation quarks. For convenience, one type of leptoquark is assumed to be much lighter than the others. Furthermore, experimental constraints on the product $g_L g_R$ allow the study leptoquarks assuming either only $g_L \neq 0$ or $g_R \neq 0$. Limits are then denoted by either (L) for leptoquarks coupling to left handed leptons or (R) for leptoquarks coupling to right handed leptons.

In the processes $e^+e^- \to u\overline{u}$ and $e^+e^- \to d\overline{d}$ first generation leptoquarks could be exchanged in u- or t-channel (F=2 or F=0) which would lead to a change of the hadronic cross-section. In the processes $e^+e^- \to c\overline{c}$ and $e^+e^- \to b\overline{b}$ the exchange of leptoquarks with cross-generational couplings can alter

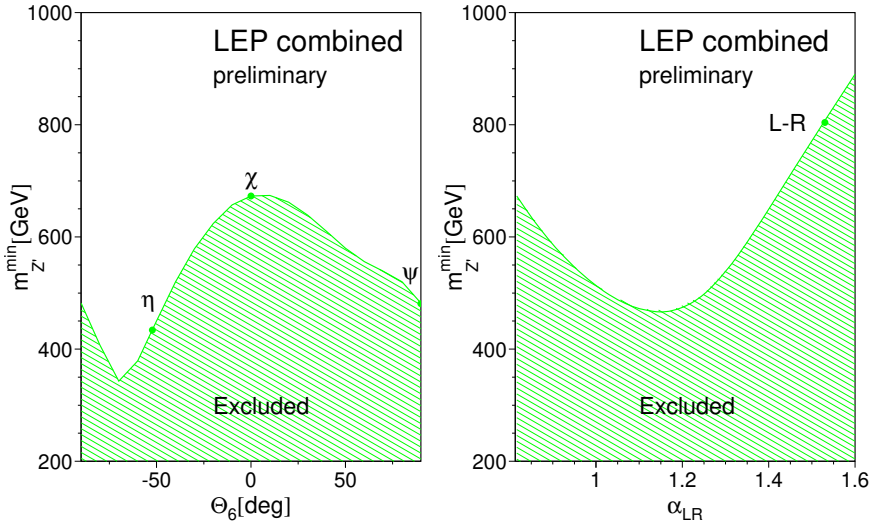

Figure 3.10: The 95% confidence level limits on $M_{Z'}$ as a function of the model parameter θ_6 for E_6 models and α_{LR} for left-right models. The Z-Z′ mixing is fixed, $\Theta_{ZZ'} = 0$.

the $q\bar{q}$ angular distribution, especially at low polar angle. The reported measurements on heavy quark production have been extrapolated to 4π acceptance, using SM predictions, from the measurements performed in restricted angular ranges, corresponding to the acceptance of the vertex-detector in each experiment. Therefore, when fitting limits on leptoquarks' coupling to the 2nd or 3rd generation of quarks, the LEP combined results for b and c sector are extrapolated back to an angular range of $|\cos\theta| < 0.85$ using ZFITTER predictions.

The following measurements are used to constrain different types of leptoquarks

- For leptoquarks coupling electrons to 1^{st} generation quarks, all LEP combined hadronic cross-sections at centre-of-mass energies from 130 GeV to 207 GeV are used
- For leptoquarks coupling electrons to 2^{nd} generation quarks, $\sigma_{c\bar{c}}$ is calculated from R_c and the hadronic cross-section at the energy points where R_c is measured. The measurements of $\sigma_{c\bar{c}}$ and $A_{FB}^{c\bar{c}}$ are then extrapolated back to $|\cos\theta| < 0.85$. Since measurements in the c-sector are scarce and originate from, at most, 2 experiments, hadronic cross-sections, extrapolated down to $|\cos\theta| < 0.85$ are also used in the fit, with an average 10% correlated errors.
- For leptoquarks coupling electrons to 3^{rd} generation quarks, only $\sigma_{b\bar{b}}$ and $A_{FB}^{b\bar{b}}$, extrapolated back to a $|\cos\theta| < 0.85$ are used.

The 95% confidence level lower limits on masses M_{LQ} are derived assuming a coupling of electromagnetic strength, $g = \sqrt{4\pi\alpha_{em}}$, where α_{em} is the fine structure constant. The results are summarised

Limit on scalar LQ mass (GeV/c^2)							
	S_0(L)	S_0(R)	$\tilde{S}_0$(R)	$S_{\frac{1}{2}}$(L)	$S_{\frac{1}{2}}$(R)	$\tilde{S}_{\frac{1}{2}}$(L)	S_1(L)
LQ_{1st}	655	520	202	178	232	-	361
LQ_{2nd}	539	430	285	269	309	-	478
LQ_{3rd}	NA	NA	465	NA	389	107	1050

Limit on vector LQ mass (GeV/c^2)							
	V_0(L)	V_0(R)	$\tilde{V}_0$(R)	$V_{\frac{1}{2}}$(L)	$V_{\frac{1}{2}}$(R)	$\tilde{V}_{\frac{1}{2}}$(L)	V_1(L)
LQ_{1st}	917	165	489	303	227	176	659
LQ_{2nd}	692	183	630	357	256	187	873
LQ_{3rd}	829	170	NA	451	183	NA	829

Table 3.16: 95% confidence level lower limits on the LQ mass for leptoquarks coupling between electrons and the first, second and third generation of quarks. A dash indicates that no limit can be set and N.A denotes leptoquarks coupling only to top quarks and hence not visible at LEP.

in Table 3.16. These results complement the leptoquark searches at HERA [41, 42] and the Tevatron [43]. Figures 3.11 and 3.12 give the 95% confidence level limits on the coupling as a function of the leptoquark mass for leptoquarks coupling electrons to the second and third generations of quarks.

3.5.4 Low Scale Gravity in Large Extra Dimensions

The averaged differential cross-sections for $e^+e^- \to e^+e^-$ are used to search for the effects of graviton exchange in large extra dimensions.

A new approach to the solution of the hierarchy problem has been proposed in [44–48], which brings close the electroweak scale $m_{EW} \sim 1$ TeV and the Planck scale $M_{Pl} = \frac{1}{\sqrt{G_N}} \sim 10^{15}$ TeV. In this framework the effective 4 dimensional M_{Pl} is connected to a new $M_{Pl(4+n)}$ scale in a (4+n) dimensional theory:

$$M_{Pl}^2 \sim M_{Pl(4+n)}^{2+n} R^n, \tag{3.4}$$

where there are n extra compact spatial dimensions of radius $\sim$ R.

In the production of fermion- or boson-pairs in e^+e^- collisions this class of models can be manifested through virtual effects due to the exchange of gravitons (Kaluza-Klein excitations). As discussed in [49–53], the exchange of spin-2 gravitons modifies in a unique way the differential cross-sections for fermion pairs, providing clear signatures. These models introduce an effective scale (ultraviolet cut-off). Adopting the notation from [49] the gravitational mass scale is called M_H. The cut-off scale is supposed to be of the order of the fundamental gravity scale in 4+n dimensions.

The parameter ε_H is defined as

$$\varepsilon_H = \frac{\lambda}{M_H^4}, \tag{3.5}$$

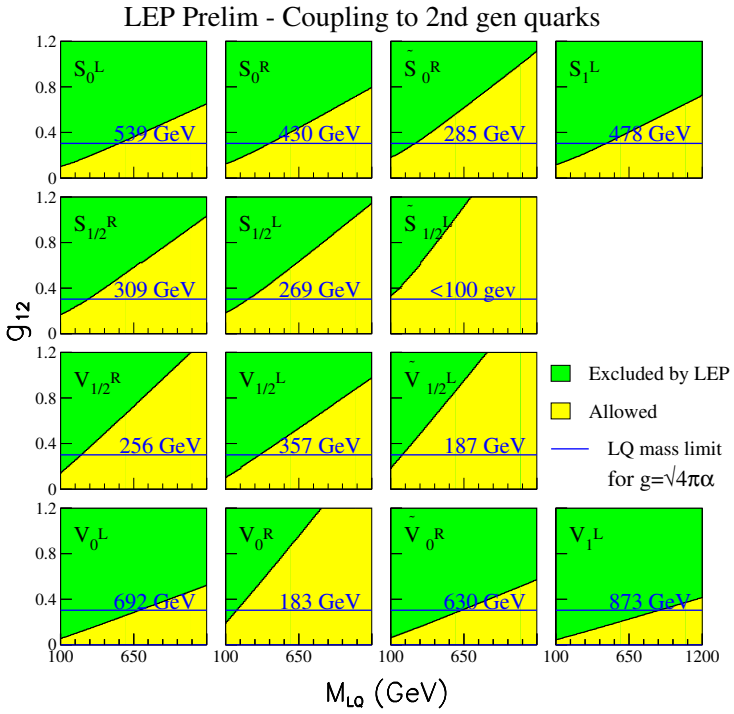

Figure 3.11: 95% confidence level limit on the coupling of leptoquarks to 2nd generation of quarks.

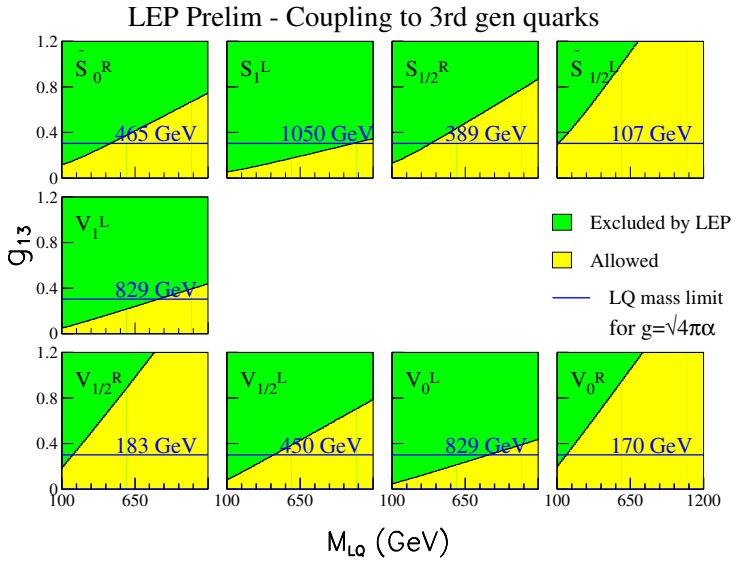

Figure 3.12: 95% confidence level limit on the coupling of leptoquarks to 3rd generation of quarks.

where the coefficient λ is of $\mathcal{O}(1)$ and can not be calculated explicitly without knowledge of the full quantum gravity theory. In the following analysis we will assume that $\lambda = \pm 1$ in order to study both the cases of positive and negative interference. To compute the deviations from the Standard Model due to virtual graviton exchange the calculations [50,51] were used.

Theoretical uncertainties on the Standard Model predictions are taken from [24]. The full correlation matrix of the differential cross-sections, obtained in our averaging procedure, is used in the fits. This is an improvement compared to previous combined analyses of published or preliminary LEP data on Bhabha scattering, performed before this detailed information was available (see e.g. [54–56]).

The extracted value of ε_H is compatible with the Standard Model expectation $\varepsilon_H = 0$. The errors on ε_H are ~ 1.5 smaller than those obtained from a single LEP experiment with the same data set. The fitted value of ε_H is converted into 95% confidence level lower limits on M_H by integrating the likelihood function over the physically allowed values, $\varepsilon_H \geq 0$ for $\lambda = +1$ and $\varepsilon_H \leq 0$ for $\lambda = -1$

giving:

$$M_H > 1.20 \text{ TeV} \qquad \text{for } \lambda = +1\,, \tag{3.6}$$
$$M_H > 1.09 \text{ TeV} \qquad \text{for } \lambda = -1\,. \tag{3.7}$$

An example of our analysis for the highest energy point is shown in Figure 3.13.

The interference of virtual graviton exchange amplitudes with both t-channel and s-channel Bhabha scattering amplitudes makes this the most sensitive search channel at LEP. The results obtained here would not be strictly valid if the luminosity measurements of the LEP experiments, based on the very same process, are also significantly affected by graviton exchange. As shown in [54], the effect on the cross-section in the luminosity angular range is so small that it can safely be neglected in this analysis.

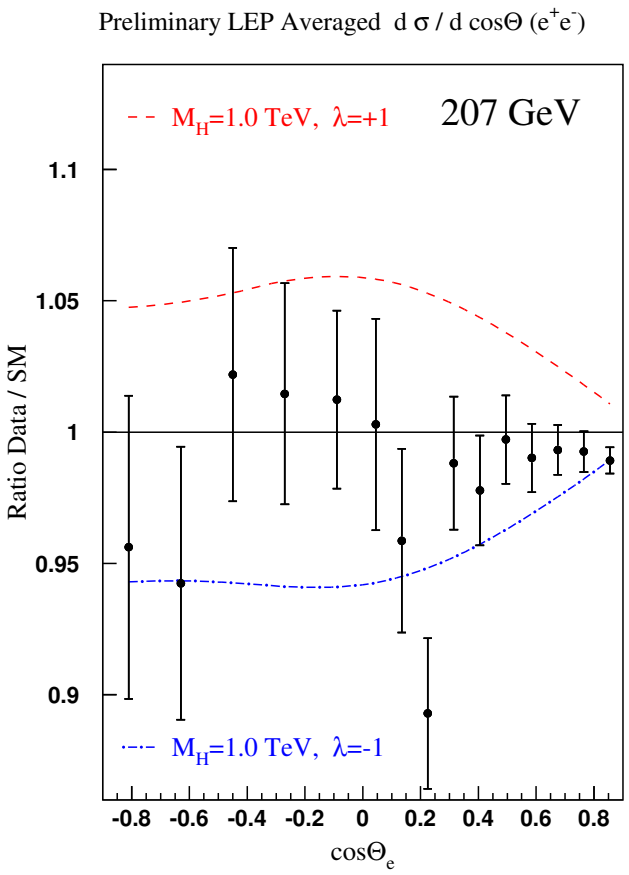

Figure 3.13: Ratio of the LEP averaged differential cross-section for $e^+e^- \to e^+e^-$ at energy of 207 GeV compared to the SM prediction. The effects expected from virtual graviton exchange are also shown.

3.6 Summary

A preliminary combination of the LEP-II $e^+e^- \to f\bar{f}$ cross-sections (for hadron, muon and tau-lepton final states) and forward-backward asymmetries (for muon and tau final states) from LEP running at energies from 130 GeV to 207 GeV has been made. The results from the four LEP experiments are in good agreement with each other. The averages for all energies are shown given in Table 3.2. Overall the data agree with the Standard Model predictions of ZFITTER, although the combined hadronic cross-sections are on average 1.7 standard deviations above the predictions. Further information is available at [22].

Preliminary differential cross-sections, $\frac{d\sigma}{d\cos\theta}$, for $e^+e^- \to e^+e^-$, $e^+e^- \to \mu^+\mu^-$ and $e^+e^- \to \tau^+\tau^-$ were combined. Results are shown in Figures 3.4, 3.5 and 3.6.

A preliminary average of results on heavy flavour production at LEP-II has also been made for measurements of R_b, R_c, $A_{FB}^{b\bar{b}}$ and $A_{FB}^{c\bar{c}}$, using results from LEP centre-of-mass energies from 130 to 207 GeV. Results are given in Tables 3.9 and 3.10 and shown graphically in Figures 3.7 and 3.8. The results are in good agreement with the predictions of the SM.

The preliminary averaged cross-section and forward-backward asymmetry results together with the combined results on heavy flavour production have been interpreted in a variety of models. Limits on the scale of contact interactions between leptons and quarks and in $e^+e^- \to e^+e^-$ and also between electrons and specifically $b\bar{b}$ and $c\bar{c}$ final states have been determined. A full set of limits are given in Tables 3.13 and 3.14. The LEP-II averaged cross-sections have been used to obtain lower limits on the mass of a possible Z′ boson in different models. Limits range from 340 to 1787 GeV/c^2 depending on the model. Limits on the masses of leptoquarks have been derived from the hadronic cross-sections. The limits range from 101 to 1036 GeV/c^2 depending on the type of leptoquark. Limits on the scale of gravity in models with large extra dimensions have been obtained from combined differential cross-sections for $e^+e^- \to e^+e^-$; for positive interference between the new physics and the Standard model the limit is 1.20 TeV and for negative interference 1.09 TeV.

Chapter 4

Investigation of the Photon/Z-Boson Interference

Updates with respect to summer 2005:
Unchanged w.r.t. summer 2002: Results are preliminary.
Note that some recent publications [16–20] are not yet included in this combination.

4.1 Introduction

The S-Matrix ansatz provides a coherent way of describing LEP measurements of the cross-section and forward-backward asymmetries in s-channel $e^+e^- \to f\bar{f}$ processes at centre-of-mass energies around the Z resonance, from the LEP-I program, and the measurements at centre-of-mass energies from 130 – 207 GeV from the LEP-II program.

Compared with the standard 5 and 9 parameter descriptions of the measurements at the Z [57], the S-Matrix formalism includes an extra 3 parameters (assuming lepton universality) or 7 parameters (without lepton universality) which explicitly determine the contributions to the cross-sections and forward-backward asymmetries of the interference between the exchange of a Z and a photon. The LEP-I data alone cannot tightly constrain these interference terms, in particular the interference term for hadronic cross-sections, since their contributions are small around the Z resonance and change sign at the pole. Due to strong correlations between the size of the hadronic interference term and the mass of the Z, this leads to a larger error on the fitted mass of the Z compared to the standard 5 and 9 parameter fits, where the hadronic interference term is fixed to the value predicted in the Standard Model. Including the LEP-II data leads to a significant improvement in the constraints on the interference terms and a corresponding reduction in the uncertainty on the mass of the Z. This results in a measurement of m_Z which is almost as sensitive as the standard results, but without constraining the interference to the Standard Model prediction.

This chapter describes the first, preliminary, combination of data from the full data sets of the 4 LEP experiments, to obtain a LEP combined results on the parameters of the S-Matrix ansatz. These results update those of a previous combination [58] which was based on preliminary LEP-I data and only partial statistics from the full LEP-II data set.

Different strategies are used to combine the LEP-I and LEP-II data. For LEP-I data, an average of the individual experiment's results on the S-Matrix parameters is made. This approach is rather

similar to the method used to combine the results of the 5 and 9 parameter fits. To include LEP-II data, a fit is made to LEP combined measurements of cross-sections and asymmetries above the Z, taking into account the results of the LEP-I combination of S-Matrix parameters.

In Section 4.2 the parameters of the S-Matrix ansatz are explained. In Sections 4.3.1 and 4.3.2 the average of the LEP-I data and the inclusion of the LEP-II data are described. The results are discussed in Section 4.3.3 and conclusions are drawn in Section 4.4.

4.2 The S-Matrix Ansatz

The S-matrix ansatz [59] is a rigorous approach to describe the cross-sections and forward-backward asymmetries in the s-channel e^+e^- annihilations under the assumption that the processes can be parameterised as the exchange of a massless and a massive vector boson, in which the couplings of the bosons including their interference are treated as free parameters.

In this model, the cross-sections can be parametrised as follows:

$$\sigma^0_{tot,f}(s) = \frac{4}{3}\pi\alpha^2 \left[\frac{g_f^{tot}}{s} + \frac{j_f^{tot}(s-\overline{m}_Z^2) + r_f^{tot}\, s}{(s-\overline{m}_Z^2)^2 + \overline{m}_Z^2\overline{\Gamma}_Z^2} \right] \quad \text{with f} = \text{had}, e, \mu, \tau\,, \tag{4.1}$$

while the forward-backward asymmetries are given by:

$$A^0_{fb,f}(s) = \pi\alpha^2 \left[\frac{g_f^{fb}}{s} + \frac{j_f^{fb}(s-\overline{m}_Z^2) + r_f^{fb}\, s}{(s-\overline{m}_Z^2)^2 + \overline{m}_Z^2\overline{\Gamma}_Z^2} \right] / \sigma^0_{tot,f}(s)\,, \tag{4.2}$$

where $\sqrt{s}$ is the centre-of-mass energy. The parameters r_f and j_f scale the Z exchange and the $Z-\gamma$ interference contributions to the total cross-section and forward-backward asymmetries. The contribution g_f of the pure γ exchange was fixed to the value predicted by QED in all fits. Neither the hadronic charge asymmetry, nor the flavour tagged quark forward-backward asymmetries are considered here, which leaves 16 free parameters to described the LEP data: 14 r_f and j_f parameters and the mass and width of the massive Z resonance. Applying the constraint of lepton universality reduces this to 8 parameters.

In the Standard Model the Z exchange term, the $Z-\gamma$ interference term and the photon exchange term are given in terms of the fermion charges and their effective vector and axial couplings to the Z by:

$$\begin{aligned}
r_f^{\text{tot}} &= \kappa^2 \left[g_{Ae}^2 + g_{Ve}^2 \right] \left[g_{Af}^2 + g_{Vf}^2 \right] - 2\kappa\, g_{Ve}\, g_{Vf} C_{Im} \\
j_f^{\text{tot}} &= 2\kappa\, g_{Ve}\, g_{Vf}\, (C_{Re} + C_{Im}) \\
g_f^{\text{tot}} &= Q_e^2 Q_f^2\, |F_A(m_Z)|^2 \\
r_f^{\text{fb}} &= 4\kappa^2 g_{Ae}\, g_{Ve}\, g_{Af}\, g_{Vf} - 2\kappa\, g_{Ae}\, g_{Af} C_{Im} \\
j_f^{\text{fb}} &= 2\kappa\, g_{Ae}\, g_{Af}\, (C_{Re} + C_{Im}) \\
g_f^{\text{fb}} &= 0\,,
\end{aligned} \tag{4.3}$$

with the following definitions:

$$\begin{aligned}
\kappa &= \frac{G_F m_{\rm Z}^2}{2\sqrt{2}\,\pi\alpha} \approx 1.50 \\
C_{Im} &= \frac{\Gamma_{\rm Z}}{m_{\rm Z}}\, Q_{\rm e} Q_{\rm f}\, {\rm Im}\left\{F_A(m_{\rm Z})\right\} \\
C_{Re} &= Q_{\rm e} Q_{\rm f}\, {\rm Re}\left\{F_A(m_{\rm Z})\right\} \\
F_A(m_{\rm Z}) &= \frac{\alpha(m_{\rm Z})}{\alpha}\,,
\end{aligned} \tag{4.4}$$

where $\alpha(m_{\rm Z})$ is the complex fine-structure constant, and $\alpha \equiv \alpha(0)$. The photonic virtual and bremsstrahlung corrections are included through the convolution of Equations 4.1 and 4.2 with radiator functions as in the 5 and 9 parameter fits. The expressions of the S-Matrix parameters in terms of the effective vector and axial-vector couplings given above neglect the imaginary parts of the effective couplings.

The usual definitions of the mass $m_{\rm Z}$ and width $\Gamma_{\rm Z}$ of a Breit-Wigner resonance are used, the width being s-dependent, such that:

$$\begin{aligned}
m_{\rm Z} &\equiv \overline{m}_{\rm Z}\sqrt{1+\overline{\Gamma}_{\rm Z}^2/\overline{m}_{\rm Z}^2} &\approx \overline{m}_{\rm Z}{+}34.20\ {\rm MeV}/c^2 \\
\Gamma_{\rm Z} &\equiv \overline{\Gamma}_{\rm Z}\sqrt{1+\overline{\Gamma}_{\rm Z}^2/\overline{m}_{\rm Z}^2} &\approx \overline{\Gamma}_{\rm Z} + \ 0.94\ {\rm MeV}\,.
\end{aligned} \tag{4.5}$$

In the following fits, the predictions from the S-Matrix ansatz and the QED convolution for cross-sections and asymmetries are made using SMATASY [60], which in turn uses ZFITTER [61] to calculate the QED convolution of the electroweak kernel. In case of the e^+e^- final state, t-channel and s/t interference contributions are added to the s-channel ansatz.

4.3 LEP combination

In the following sections the combinations of the results from the individual LEP experiments are described: firstly the LEP-I combination, then the combination of both LEP-I and LEP-II data. The results from these combinations are compared in Section 4.3.3. Although all 16 parameters are averaged during the combination, only results for the parameters $m_{\rm Z}$ and $j_{\rm had}^{\rm tot}$ are reported here. Systematic studies specific to the other parameters are ongoing.

4.3.1 LEP-I combination

Individual LEP experiments have their own determinations of the 16 S-Matrix parameters [62–65] from LEP-I data alone, using the full LEP-I data sets.

These results are averaged using a multi-parameter BLUE technique based on an extension of Reference 26. Sources of systematic uncertainty correlated between the experiments have been investigated, using techniques described in [57] and are accounted for in the averaging procedure and benefiting from the experience gained in those combinations.

	$m_{\rm Z}$ [GeV]	$j_{\rm had}^{\rm tot}$	correlation
LEP-I only	91.1925±0.0059	-0.084±0.324	-0.935
LEP-I & LEP-II	91.1869±0.0023	0.277±0.065	-0.461

Table 4.1: Averaged LEP-I and LEP-II S-Matrix results for $m_{\rm Z}$ and $j_{\rm had}^{\rm tot}$.

The parameters $m_{\rm Z}$ and $j_{\rm had}^{\rm tot}$ are the most sensitive of all 16 S-matrix parameters to the inclusion of the LEP-II data, and are also the most interesting ones in the context of the 5 and 9 parameter fits. For these parameters the most significant source of systematic error which is correlated between experiments comes from the uncertainty on the e^+e^- collision energy as determined by models of the LEP RF system and calibrations using the resonant depolarisation technique. These errors amount to ± 3 MeV on $m_{\rm Z}$ and ± 0.16 on $j_{\rm had}^{\rm tot}$ with a correlation coefficient of -0.86. The LEP averaged values of $m_{\rm Z}$ and $j_{\rm had}^{\rm tot}$ are given in Table 4.1, together with their correlation coefficient. The χ^2/D.O.F. for the average of all 16 parameters is 62.0/48, corresponding to a probability of 8%, which is acceptable.

4.3.2 LEP-I and LEP-II combination

Some experiments have determined S-Matrix parameters using their LEP-I and LEP-II measured cross-sections and forward-backward asymmetries [62,63,66,67]. To do a full LEP combination would require each experiment to provide S-Matrix results and would require an analysis of the correlated systematic errors on each measured parameter.

However, preliminary combinations of the measurements of forward-backward asymmetries and cross-sections from all 4 LEP experiments, for the full LEP-II period, have already been made [61] and correlations between these measurements have been estimated. The combination procedure averages measurements of cross-sections and asymmetry for those events with reduced centre-of-mass energies, $\sqrt{s'}$, close to the actual centre-of-mass energy of the e^+e^- beams, $\sqrt{s}$, removing those events which are less sensitive to the $Z-\gamma$ interference where, predominantly, initial state radiation reduces the centre-of-mass energy to close to the mass of the Z. The only significant correlations are those between hadronic cross-section measurements at different energies, which are around 20–40%, depending on energies.

The predictions from SMATASY are fitted to the combined LEP-II cross-section and forward-backward asymmetry measurements [61]. The signal definition 1 of Reference 61 is used for the data and for the predictions of SMATASY. Theoretical uncertainties on the S-Matrix predictions for the LEP-II results and on the corrections of the LEP-II data to the common signal defintion are taken to be the same as for the Standard Model predictions of ZFITTER [61] which are dominated by uncertainties in the QED convolution. These amount to a relative uncertainty of 0.26% on the hadronic cross-sections, fully correlated between all LEP-II energies.

The fit also uses as inputs the averaged LEP-I S-Matrix parameters and covariance matrix. These inputs effectively constrain those parameters, such as $m_{\rm Z}$, which are not accurately determined by LEP-II data. There are no significant correlations between the LEP-I and LEP-II inputs.

The LEP averaged values of $m_{\rm Z}$ and $j_{\rm had}^{\rm tot}$ for both LEP-I and LEP-II data are given in Table 4.1, together with their correlation coefficient. The χ^2/D.O.F. for the average of all 16 parameters is 64.4/60, corresponding to a probability of 33%, which is good.

4.3.3 Discussion

In the LEP-I combination the measured values of the Z boson mass $m_Z = 91.1925 \pm 0.0059$ GeV agrees well with the results of the standard 9 parameter fit (91.1876 ± 0.0021 GeV) albeit with a significantly larger error, resulting from the correlation with the large uncertainty on j^{tot}_{had} which is then the dominant source of uncertainty on m_Z in the S-Matrix fits. The measured value of $j^{tot}_{had} = -0.084 \pm 0.324$, also agrees with the prediction of the Standard Model ($0.2201^{+0.0032}_{-0.0137}$).

Including the LEP-II data brings a significant improvement in the uncertainty on the size of the interference between Z and photon exchange compared to LEP-I data alone. The measured value $j^{tot}_{had} = 0.277 \pm 0.065$, agrees well with the values predicted from the Standard Model. Correspondingly, the uncertainty on the the mass of the Z in this ansatz, 2.3 MeV, is close to the precision obtained from LEP-I data alone using the standard 9 parameter fit, 2.1 MeV. The slightly larger error is due to the uncertainty on j^{tot}_{had} which amounts to 0.9 MeV. The measured value, $m_Z = 91.1869 \pm 0.0023$ GeV, agrees with that obtained from the standard 9 parameter fits. The results are summarised in Figure 4.1.

The good agreement found between the values of m_Z and j^{tot}_{had} and their expectations provide a validation of the approach taken in the standard 5 and 9 parameter fits, in which the size of the interference between Z boson and photon exchange in the hadronic cross-sections was fixed to the Standard Model expectation.

The precision on j^{tot}_{had} is slightly better than that obtained by the VENUS collaboration [68] of ± 0.08, which was obtained using preliminary results from LEP-I and their own measurements of the hadronic cross-section below the Z resonance. The measurement of the hadronic cross-sections from VENUS [68] and TOPAZ [69] could be included in the future to give a further reduction in the uncertainty on j^{tot}_{had}.

Work is in progress to understand those sources of systematic error, correlated between experiments, which are significant for the remaining S-Matrix parameter that have not been presented here. In particular, for j^{tot}_e and j^{fb}_e, it is important to understand the errors resulting from t-channel contributions to the $e^+e^- \to e^+e^-$ process. These errors have only limited impact on the standard 5 and 9 parameter fits.

4.4 Conclusion

Results for the S-Matrix parameter m_Z and j^{tot}_{had} have been presented for LEP-I data alone and for a fit using the full data sets for LEP-I and LEP-II from all 4 LEP experiments. Inclusion of LEP-II data brings a significant improvement in the determination of j^{tot}_{had}, the fitted value 0.277 ± 0.065, agrees well with the values predicted from the Standard Model. As a result in the improvement of the uncertainty in j^{tot}_{had}, the uncertainty on the fitted value of m_Z approaches that of the standard 5 and 9 parameter fits and the measured value $m_Z = 91.1869 \pm 0.0023$ GeV is compatible with that from the standard fits.

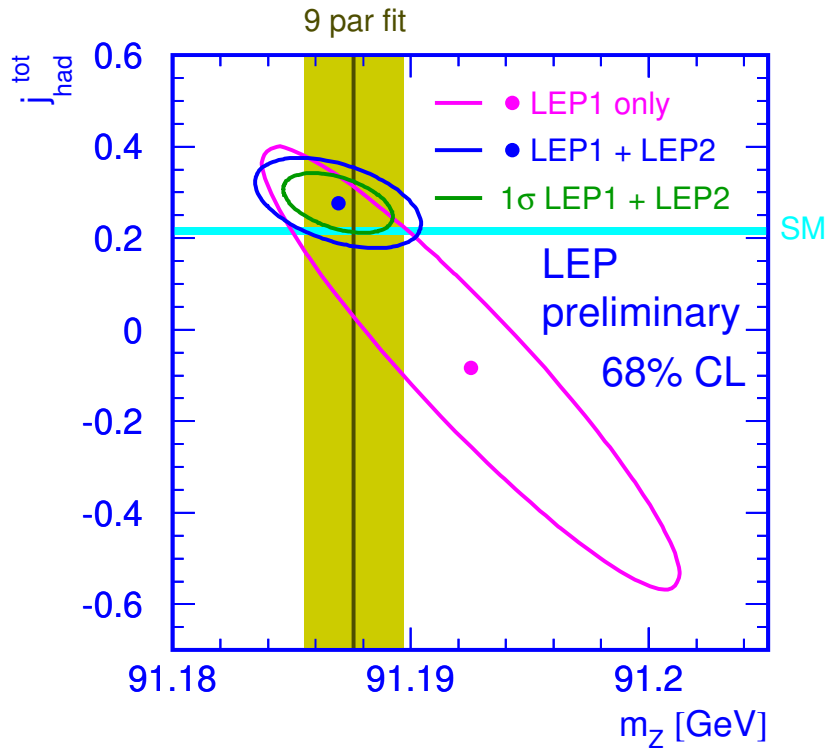

Figure 4.1: Error ellipses for m_Z and j^{tot}_{had} for LEP-I (at 39% and 68%) and the combination of LEP-I and LEP-II (at 68%).

Chapter 5

W and Four-Fermion Production at LEP-II

Updates with respect to summer 2005:
Unchanged w.r.t. summer 2005. Results are preliminary.
Note that some recent publications [70] are not yet included in this combination.

5.1 Introduction

This chapter summarises the present status of the combination of published and preliminary results of the four LEP experiments on four-fermion cross-sections for the Summer 2005 Conferences. If not stated otherwise, all presented results use the full LEP-II data sample at centre–of–mass energies up to 209 GeV, supersede the results presented at the Summer 2004 Conferences [71] and have to be considered as preliminary.

The centre–of–mass energies and the corresponding integrated luminosities are provided by the experiments and are the same used for previous conferences. The LEP energy value in each point (or group of points) is the luminosity-weighted average of those values.

Cross-section results from different experiments are combined by χ^2 minimisation using the Best Linear Unbiased Estimate method described in Ref. [26], properly taking into account the correlations between the systematic uncertainties.

The detailed inputs from the experiments and the resulting LEP combined values, with the full breakdown of systematic errors is described in Appendix A. Experimental results are compared with recent theoretical predictions, many of which were developed in the framework of the LEP-II Monte Carlo workshop [72].

5.2 W-pair production cross-section

ALEPH, DELPHI and L3 have presented final results on the W-pair (CC03 [72]) production cross-section and W branching ratios for all LEP-II centre–of–mass energies [73–77]. OPAL has final results from 161 to 189 GeV [73,74,78] and preliminary measurements at $\sqrt{s} = 192$–207 GeV [79].

With respect to the Summer 2004 Conferences, new final results from ALEPH are now included in the LEP averages. The difference in the combined results is marginal with respect to last summer. The same grouping of the systematic errors consolidated in previous combinations [71] was used.

The detailed inputs used for the combinations are given in Appendix A.

The measured statistical errors are used for the combination; after building the full 32×32 covariance matrix for the measurements, the χ^2 minimisation fit is performed by matrix algebra, as described in Ref. [80], and is cross-checked using Minuit [81].

The results from each experiment for the W-pair production cross-section are shown in Table 5.1, together with the LEP combination at each energy. All measurements assume Standard Model values for the W decay branching fractions. The results for centre–of–mass energies between 183 and 207 GeV, for which new LEP averages have been computed, supersede the ones presented in [71]. For completeness, the measurements at 161 and 172 GeV are also listed in the table.

$\sqrt{s}$	WW cross-section (pb)					χ^2/d.o.f.
(GeV)	ALEPH	DELPHI	L3	OPAL	LEP	
161.3	4.23 ± 0.75*	$3.67 \pm^{0.99}_{0.87}$ *	$2.89 \pm^{0.82}_{0.71}$ *	$3.62 \pm^{0.94}_{0.84}$ *	3.69 ± 0.45 *	} 1.3 / 3
172.1	11.7 ± 1.3 *	11.6 ± 1.4 *	12.3 ± 1.4 *	12.3 ± 1.3 *	12.0 ± 0.7 *	} 0.22/ 3
182.7	15.86 ± 0.63*	16.07 ± 0.70*	16.53 ± 0.72*	15.43 ± 0.66*	15.88 ± 0.35 *	}
188.6	15.78 ± 0.36*	16.09 ± 0.42*	16.17 ± 0.41*	16.30 ± 0.39*	16.03 ± 0.21 *	}
191.6	17.10 ± 0.90 *	16.64 ± 1.00*	16.11 ± 0.92 *	16.60 ± 0.99	16.56 ± 0.48	}
195.5	16.60 ± 0.54 *	17.04 ± 0.60*	16.22 ± 0.57 *	18.59 ± 0.75	16.90 ± 0.31	}
199.5	16.93 ± 0.52 *	17.39 ± 0.57*	16.49 ± 0.58 *	16.32 ± 0.67	16.76 ± 0.30	} 26.6/24
201.6	16.63 ± 0.71 *	17.37 ± 0.82*	16.01 ± 0.84 *	18.48 ± 0.92	16.99 ± 0.41	}
204.9	16.84 ± 0.54 *	17.56 ± 0.59*	17.00 ± 0.60 *	15.97 ± 0.64	16.79 ± 0.31	}
206.6	17.42 ± 0.43 *	16.35 ± 0.47*	17.33 ± 0.47 *	17.77 ± 0.57	17.15 ± 0.25	}

Table 5.1: W-pair production cross-section from the four LEP experiments and combined values at all recorded centre–of–mass energies. All results are preliminary, with the exception of those indicated by *. The measurements between 183 and 207 GeV have been combined in one global fit, taking into account inter-experiment as well as inter-energy correlations of systematic errors. The results for the combined LEP W-pair production cross-section at 161 and 172 GeV are taken from [82, 83] respectively.

Figure 5.1 shows the combined LEP W-pair cross-section measured as a function of the centre–of–mass energy. The experimental points are compared with the theoretical calculations from YFSWW [84] and RACOONWW [85] between 155 and 215 GeV for $m_{\mathrm{W}} = 80.35$ GeV. The two codes have been extensively compared and agree at a level better than 0.5% at the LEP-II energies [72]. The calculations above 170 GeV, based for the two programs on the so-called leading pole (LPA) or double pole approximations (DPA) [86], have theoretical uncertainties decreasing from 0.7% at 170 GeV to about 0.4% at centre–of–mass energies larger than 200 GeV, while in the threshold region, where the codes are run in Improved Born Approximation, a larger theoretical uncertainty of 2% is assigned [87]. This theoretical uncertainty is represented by the blue band in Figure 5.1. An error of 50 MeV on the W mass would translate into additional errors of 0.1% (3.0%) on the cross-section predictions at 200 GeV (161 GeV, respectively). All results, up to the highest centre–of–mass energies, are in agreement with the considered theoretical predictions.

The agreement between the measured W-pair cross-section, $\sigma_{\rm WW}^{\rm meas}$, and its expectation according to a given theoretical model, $\sigma_{\rm WW}^{\rm theo}$, can be expressed quantitatively in terms of their ratio

$$\mathcal{R}_{\rm WW} = \frac{\sigma_{\rm WW}^{\rm meas}}{\sigma_{\rm WW}^{\rm theo}}, \tag{5.1}$$

averaged over the measurements performed by the four experiments at different energies in the LEP-II region. The above procedure has been used to compare the measurements at the eight energies between 183 and 207 GeV to the predictions of GENTLE [88], KORALW [89], YFSWW [84] and RACOONWW [85]. The measurements at 161 and 172 GeV have not been used in the combination because they were performed using data samples of low statistics and because of the high sensitivity of the cross-section to the value of the W mass at these energies.

The combination of the ratio $\mathcal{R}_{\rm WW}$ is performed using as input from the four experiments the 32 cross-sections measured at each of the eight energies. These are then converted into 32 ratios by dividing them by the considered theoretical predictions, listed in Appendix A. The full 32×32 covariance matrix for the ratios is built taking into account the same sources of systematic errors used for the combination of the W-pair cross-sections at these energies.

The small statistical errors on the theoretical predictions at the various energies, taken as fully correlated for the four experiments and uncorrelated between different energies, are also translated into errors on the individual measurements of $\mathcal{R}_{\rm WW}$. The theoretical errors on the predictions, due to the physical and technical precision of the generators used, are not propagated to the individual ratios but are used when comparing the combined values of $\mathcal{R}_{\rm WW}$ to unity. For each of the four models considered, two fits are performed: in the first, eight values of $\mathcal{R}_{\rm WW}$ at the different energies are extracted, averaged over the four experiments; in the second, only one value of $\mathcal{R}_{\rm WW}$ is determined, representing the global agreement of measured and predicted cross-sections over the whole energy range.

$\sqrt{s}$(GeV)	$\mathcal{R}_{\rm WW}^{\rm YFSWW}$	$\mathcal{R}_{\rm WW}^{\rm RACOONWW}$
182.7	1.034 ± 0.023	1.033 ± 0.023
188.6	0.986 ± 0.013	0.987 ± 0.013
191.6	1.000 ± 0.029	1.003 ± 0.029
195.5	1.003 ± 0.019	1.006 ± 0.019
199.5	0.985 ± 0.018	0.987 ± 0.018
201.6	0.995 ± 0.024	0.998 ± 0.024
204.9	0.980 ± 0.018	0.983 ± 0.018
206.6	1.000 ± 0.015	1.004 ± 0.015
χ^2/d.o.f	26.6/24	26.6/24
Average	0.994 ± 0.009	0.996 ± 0.009
χ^2/d.o.f	32.2/31	32.0/31

Table 5.2: Ratios of LEP combined W-pair cross-section measurements to the expectations according to YFSWW [84] and RACOONWW [85]. For each of the two models, two fits are performed, one to the LEP combined values of $\mathcal{R}_{\rm WW}$ at the eight energies between 183 and 207 GeV, and another to the LEP combined average of $\mathcal{R}_{\rm WW}$ over all energies. The results of the fits are given in the table together with the resulting χ^2. Both fits take into account inter-experiment as well as inter-energy correlations of systematic errors.

The results of the two fits to $\mathcal{R}_{\rm WW}$ for YFSWW and RACOONWW are given in Table 5.2. As already qualitatively noted from Figure 5.1, the LEP measurements of the W-pair cross-section

above threshold are in very good agreement to the predictions and can test the theory at the level of better than 1%. In contrast, the predictions from GENTLE and KORALW are about 3% too high with respect to the measurements; the equivalent values of $\mathcal{R}_{\rm WW}$ in those cases are, respectively, 0.969 ± 0.009 and 0.975 ± 0.009.

The main differences between these two sets of predictions come from non-leading $\mathcal{O}(\alpha)$ electroweak radiative corrections to the W-pair production process and non-factorisable corrections, which are included (in the LPA/DPA approximation [86]) in both YFSWW and RACOONWW, but not in GENTLE and KORALW. The data clearly prefer the computations which more precisely include $\mathcal{O}(\alpha)$ radiative corrections.

The results of the fits for YFSWW and RACOONWWare also shown in Figure 5.2, where relative errors of 0.5% on the cross-section predictions have been assumed. For simplicity in the figure the energy dependence of the theory error on the W-pair cross-section has been neglected.

5.3 W branching ratios and $|V_{cs}|$

From the partial cross-sections WW→ 4f measured by the four experiments at all energies above 161 GeV, the W decay branching fractions $\mathcal{B}(W \to f\bar{f}')$ are determined, with and without the assumption of lepton universality.

The two combinations use as inputs from the experiments the three leptonic branching fractions, with their systematic and observed statistical errors and their correlation matrices. In the fit with lepton universality, the branching fraction to hadrons is determined from that to leptons by constraining the sum to unity. The part of the systematic error correlated between experiments is properly accounted for when building the full covariance matrix.

The detailed inputs used for the combinations are given in Appendix A. The results from each experiment are given in Table 5.3 together with the result of the LEP combination. The same results are shown in Figure 5.3.

	Lepton non–universality			Lepton universality
Experiment	$\mathcal{B}(W \to e\overline{\nu}_e)$ [%]	$\mathcal{B}(W \to \mu\overline{\nu}_\mu)$ [%]	$\mathcal{B}(W \to \tau\overline{\nu}_\tau)$ [%]	$\mathcal{B}$(W → hadrons) [%]
ALEPH	$10.78 \pm 0.29^*$	$10.87 \pm 0.26^*$	$11.25 \pm 0.38^*$	$67.13 \pm 0.40^*$
DELPHI	$10.55 \pm 0.34^*$	$10.65 \pm 0.27^*$	$11.46 \pm 0.43^*$	$67.45 \pm 0.48^*$
L3	$10.78 \pm 0.32^*$	$10.03 \pm 0.31^*$	$11.89 \pm 0.45^*$	$67.50 \pm 0.52^*$
OPAL	10.40 ± 0.35	10.61 ± 0.35	11.18 ± 0.48	67.91 ± 0.61
LEP	10.65 ± 0.17	10.59 ± 0.15	11.44 ± 0.22	67.48 ± 0.28
χ^2/d.o.f.	6.3/9			15.4/11

Table 5.3: Summary of W branching fractions derived from W-pair production cross sections measurements up to 207 GeV centre–of–mass energy. All results are preliminary with the exception of those indicated by *.

The results of the fit which does not make use of the lepton universality assumption show a

negative correlation of 19.5% (13.2%) between the $W \to \tau\overline{\nu}_\tau$ and $W \to e\overline{\nu}_e$ ($W \to \mu\overline{\nu}_\mu$) branching fractions, while between the electron and muon decay channels there is a positive correlation of 11.0%.

From the results on the leptonic branching ratios an excess of the branching ratio $W \to \tau\overline{\nu}_\tau$ with respect to the other leptons is evident. The excess can be quantified with the two-by-two comparison of these branching fractions, which represents a test of lepton universality in the decay of on–shell W bosons at the level of 2.9%:

$$\begin{aligned}
\mathcal{B}(W \to \mu\overline{\nu}_\mu) \,/\, \mathcal{B}(W \to e\overline{\nu}_e) &= 0.994 \pm 0.020\,, \\
\mathcal{B}(W \to \tau\overline{\nu}_\tau) \,/\, \mathcal{B}(W \to e\overline{\nu}_e) &= 1.074 \pm 0.029\,, \\
\mathcal{B}(W \to \tau\overline{\nu}_\tau) \,/\, \mathcal{B}(W \to \mu\overline{\nu}_\mu) &= 1.080 \pm 0.028\,.
\end{aligned}$$

The branching fractions in taus with respect to electrons and muons differ by more than two standard deviations, where the correlations have been taken into account. The branching fractions of W into electrons and into muons perfectly agree.

Assuming only partial lepton universality the ratio between the tau fractions and the average of electrons and muons can also be computed:

$$2\mathcal{B}(W \to \tau\overline{\nu}_\tau) \,/\, (\mathcal{B}(W \to e\overline{\nu}_e) + \mathcal{B}(W \to \mu\overline{\nu}_\mu)) = 1.077 \pm 0.026$$

resulting in a poor agreement at the level of 2.8 standard deviations, with all correlations included.

If complete lepton universality is assumed, the measured hadronic branching fraction can be determined, yielding $67.48 \pm 0.18(\text{stat.}) \pm 0.21(\text{syst.})\%$, whereas for the leptonic one gets $10.84 \pm 0.06(\text{stat.}) \pm 0.07(\text{syst.})\%$. These results are consistent with their Standard Model expectations, of 67.51% and 10.83% respectively. The systematic error receives equal contributions from the correlated and uncorrelated sources.

Within the Standard Model, the branching fractions of the W boson depend on the six matrix elements $|V_{qq'}|$ of the Cabibbo–Kobayashi–Maskawa (CKM) quark mixing matrix not involving the top quark. In terms of these matrix elements, the leptonic branching fraction of the W boson $\mathcal{B}(W \to \ell\overline{\nu}_\ell)$ is given by

$$\frac{1}{\mathcal{B}(W \to \ell\overline{\nu}_\ell)} = 3\left\{1 + \left[1 + \frac{\alpha_s(M_W^2)}{\pi}\right] \sum_{\substack{i=(u,c),\\ j=(d,s,b)}} |V_{ij}|^2\right\},$$

where $\alpha_s(M_W^2)$ is the strong coupling constant. Taking $\alpha_s(M_W^2) = 0.119 \pm 0.002$ [90], and using the experimental knowledge of the sum $|V_{ud}|^2 + |V_{us}|^2 + |V_{ub}|^2 + |V_{cd}|^2 + |V_{cb}|^2 = 1.0476 \pm 0.0074$ [90], the above result can be interpreted as a measurement of $|V_{cs}|$ which is the least well determined of these matrix elements:

$$|V_{cs}| = 0.976 \pm 0.014.$$

The error includes a ± 0.0006 contribution from the uncertainty on α_s and a ± 0.004 contribution from the uncertainties on the other CKM matrix elements, the largest of which is that on $|V_{cd}|$. These contributions are negligible in the error on this determination of $|V_{cs}|$, which is dominated by the ± 0.013 experimental error from the measurement of the W branching fractions. The value of $|V_{cs}|$ is in agreement with unity.

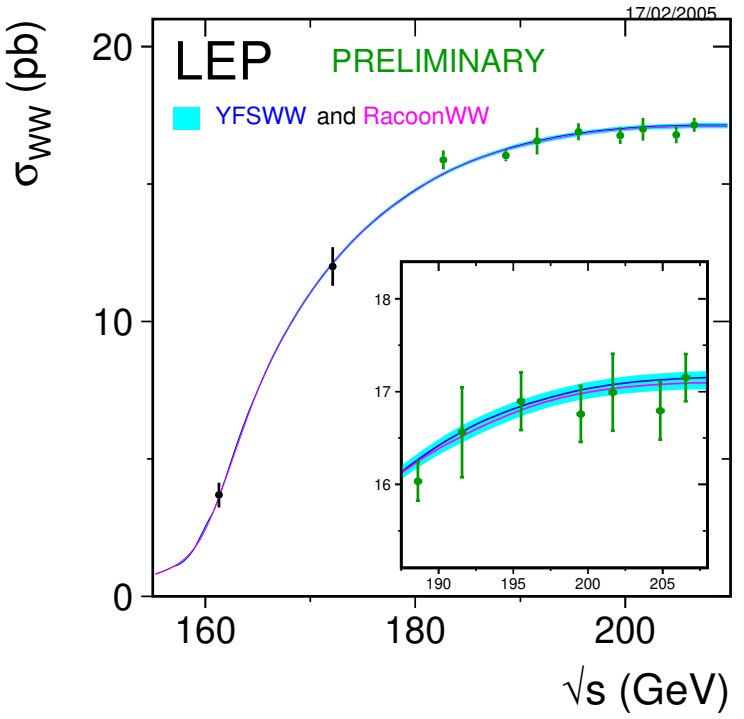

Figure 5.1: Measurements of the W-pair production cross-section, compared to the predictions of RACOONWW [85] and YFSWW [84]. The shaded area represents the uncertainty on the theoretical predictions, estimated in $\pm 2\%$ for $\sqrt{s} < 170$ GeV and ranging from 0.7 to 0.4% above 170 GeV.

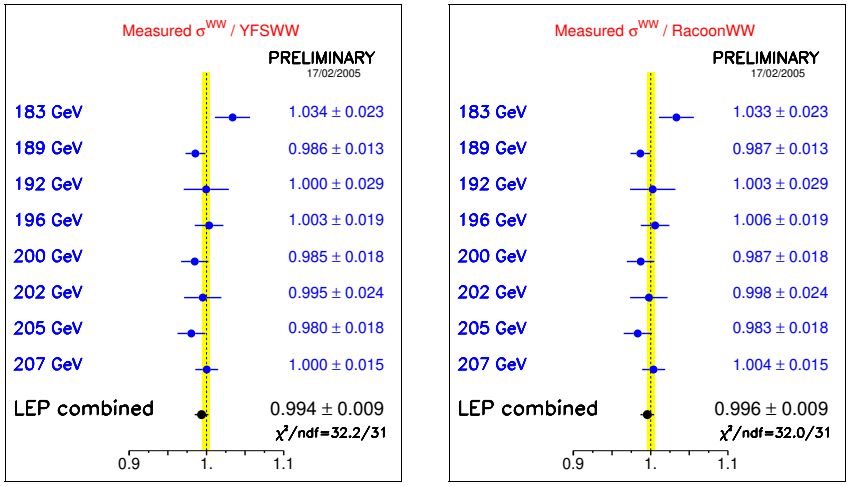

Figure 5.2: Ratios of LEP combined W-pair cross-section measurements to the expectations according to YFSWW [84] and RACOONWW [85] The yellow bands represent constant relative errors of 0.5% on the two cross-section predictions.

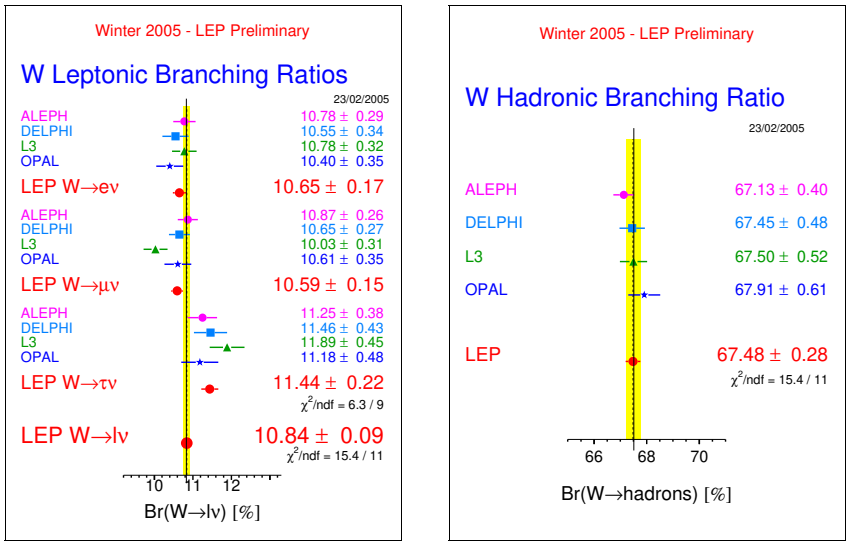

Figure 5.3: Leptonic and hadronic W branching fractions, as measured by the experiments, and the LEP combined values according to the procedures described in the text.

5.4 Combination of the $\cos\theta_{W^-}$ distribution

5.4.1 Introduction and definitions

In addition to measuring the total W^+W^- cross-section, the LEP experiments produce results for the differential cross-section, $d(\sigma_{WW})/d(\cos\theta_W)$ ($\cos\theta_W$ is the polar angle of the produced W^- with respect to the e^- beam direction). The LEP combination of these measurements will allow future theoretical models which predict deviations in this distribution to be tested against the LEP data in a direct and as much as possible model independent manner. To reconstruct the $\cos\theta_W$ distribution it is necessary to identify the charges of the decaying W bosons. This can only be performed without significant ambiguity when one of W-boson decays via $W \to e\nu$ or $W \to \mu\nu$ (in which case the lepton provides the charge tag). Consequently, the combination of the differential cross-section measurements is performed for the $q\bar{q}e\nu$ and $q\bar{q}\mu\nu$ channels combined. Selected $q\bar{q}\tau\nu$ events are not considered due to the larger backgrounds and difficulties in determining the tau lepton charge.

The measured $q\bar{q}e\nu$ and $q\bar{q}\mu\nu$ differential cross-sections are corrected to correspond to the CC03 set of diagrams with the additional constraint that the charged lepton is more than 20° away from the e^+e^- beam direction, $|\theta_{\ell^\pm}| > 20°$. This angular requirement corresponds closely to the experimental acceptance of the four LEP experiments and also greatly reduces the difference between the full $4f$ cross-section and the CC03 cross-section by reducing the contribution of t-channel diagrams in the $q\bar{q}e\nu$ final state[1]. The anlge $\cos\theta_W$ is reconstructed from the four-momenta of the fermions from the W^- decay using the ECALO5 photon recombination scheme [72].

5.4.2 LEP combination method

The LEP combination is performed in ten bins of $\cos\theta_W$. Because the differential cross-section distribution evolves with $\sqrt{s}$, reflecting the changing relative $s-$ and $t-$ channel contributions, the LEP data are divided into four $\sqrt{s}$ ranges: $180.0 < \sqrt{s} \leq 184.0$; $184.0 < \sqrt{s} \leq 194.0$; $194.0 < \sqrt{s} \leq 204.0$; and $204.0 < \sqrt{s} \leq 210.0$. It has been verified for each $\sqrt{s}$ range that the differences in the differential cross-sections at the mean value of $\sqrt{s}$ compared to the luminosity weighted sum of the differential cross-sections reflecting the actual distribution of the data across $\sqrt{s}$ are negligible compared to the statistical errors.

The experimental resolution in LEP on the reconstructed minus generated value of $\cos\theta_W$ is typically 0.15-0.2 and, as a result, there is a significant migration between generated and reconstructed bins of $\cos\theta_W$. The effects of bin-to-bin migration are not explicitely unfolded, instead each experiment obtains the cross-section in i^{th} bin of the differential distribution, σ_i, from

$$\sigma_i = \frac{N_i - b_i}{\epsilon_i \mathcal{L}}, \tag{5.2}$$

where:

N_i is the observed number of $q\bar{q}e\nu/q\bar{q}\mu\nu$ events reconstructed in the ith bin of the $\cos\theta_W$ distribution.

[1] With this requirement the difference between the total CC20 and CC03 $q\bar{q}e\nu$ cross-sections is approximately 3.5 %, as opposed to 24.0 % without the lepton angle requirement. For the $q\bar{q}\mu\nu$ channel the differences between the CC10 and CC03 cross-sections are less than 1 % in both cases.

b_i is the expected number of background events in bin i. The contribution from four-fermion background is treated as in each of the experiments W^+W^- cross-section analyses.

ϵ_i is the Monte Carlo efficiency in bin i, defined as $\epsilon_i = S_i/G_i$ where S_i is the number of selected CC03 MC $q\overline{q}\ell\overline{\nu}_\ell$ events reconstructed in bin i and G_i is the number of MC CC03 $q\overline{q}e\nu/q\overline{q}\mu\nu$ events with generated $\cos\theta_W$ (calculated using the ECALO5 recombination scheme) lying in the ith bin ($|\theta_{\ell^\pm}| > 20°$). Selected $q\overline{q}\tau\nu$ events are included in the numerator of the efficiency.

This bin-by-bin efficiency correction method has the advantages of simplicity and that the resulting σ_i are uncorrelated. The main disadvantage of this procedure is that bin-by-bin migrations between generated and reconstructed $\cos\theta_W$ are corrected purely on the basis of the Standard Model expectation. If the data deviate from it the resulting differential cross-section may be therefore biased toward the Standard Model expectation. However, the validity of the simple correction procedure has been tested by considering a range of deviations from the SM. Specifically the SM $\cos\theta_W$ distribution was reweighted by $1 + 0.10\,(\cos\theta_W - 1.0)$, $1 - 0.20\cos^2\theta_{W^-}$, $1 + 0.20\cos^2\theta_{W^-}$ and $1 - 0.40\cos^8\theta_{W^-}$ and data samples generated corresponding to the combined LEP luminosity. These reweighting functions represent deviations which are large compared to the statistics of the combined LEP measurements. The bin-by-bin correction method was found to result in good χ^2 distributions when the extracted $\cos\theta_W$ distributions were compared with the underlying generated distribution (*e.g.* the worst case gave a mean χ^2 of 11.3 for the 10 degrees of freedom corresponding to the ten $\cos\theta_W$ bins).

For the LEP combination the systematic uncertainties on measured differential cross-sections are broken down into two terms: errors which are 100 % correlated between bins and experiments and errors which are correlated between bins but uncorrelated between experiments. This procedure reflects the the fact that the dominant systematic errors affect the overall normalisation of the measured distributions rather than the shape.

5.4.3 Results

For the Winter Conferences 2005 the combination of the W angular distribution has been performed using final numbers by ALEPH [75], DELPHI [76] and L3 [77]. The detailed inputs by the experiments are reported in the appendix A, whereas Table 5.4 presents the combined LEP results according to the above described procedure. In the table the error breakdown bin by bin is also reported.

The result is also presented in Figure 5.4, where the combined data are superimposed to the four-fermion theory predictions from YFSWW and from RACOONWW that provide undistinguishable results on the plot scale.

$\sqrt{s}$ interval (GeV)			Total luminosity (pb^{-1})			Lumi weighted $\sqrt{s}$ (GeV)				
180-184			163.90			182.66				
$\cos\theta_{W^-}$ bin i	1	2	3	4	5	6	7	8	9	10
σ_i (pb)	0.515	0.633	0.772	1.295	1.370	2.090	2.659	2.489	4.406	5.619
$\delta\sigma_i$ (pb)	0.131	0.139	0.155	0.250	0.217	0.288	0.328	0.287	0.451	0.512
$\delta\sigma_i$(stat) (pb)	0.129	0.137	0.153	0.249	0.215	0.285	0.325	0.283	0.447	0.508
$\delta\sigma_i$(syst) (pb)	0.019	0.018	0.020	0.024	0.027	0.045	0.043	0.050	0.062	0.067
$\sqrt{s}$ interval (GeV)			Total luminosity (pb^{-1})			Lumi weighted $\sqrt{s}$ (GeV)				
184-194			587.95			189.09				
$\cos\theta_{W^-}$ bin i	1	2	3	4	5	6	7	8	9	10
σ_i (pb)	0.748	0.811	1.012	1.091	1.314	1.735	2.225	2.877	4.161	5.748
$\delta\sigma_i$ (pb)	0.087	0.090	0.101	0.102	0.112	0.149	0.171	0.180	0.213	0.256
$\delta\sigma_i$(stat) (pb)	0.085	0.089	0.099	0.099	0.109	0.144	0.167	0.174	0.203	0.243
$\delta\sigma_i$(syst) (pb)	0.017	0.017	0.021	0.024	0.026	0.037	0.036	0.047	0.063	0.078
$\sqrt{s}$ interval (GeV)			Total luminosity (pb^{-1})			Lumi weighted $\sqrt{s}$ (GeV)				
194-204			605.05			198.38				
σ_i (pb)	0.685	0.623	1.043	0.982	1.178	1.598	2.155	3.026	4.080	6.379
$\delta\sigma_i$ (pb)	0.091	0.072	0.099	0.096	0.108	0.134	0.149	0.190	0.213	0.262
$\delta\sigma_i$(stat) (pb)	0.090	0.071	0.098	0.094	0.106	0.129	0.145	0.185	0.203	0.248
$\delta\sigma_i$(syst) (pb)	0.013	0.014	0.017	0.021	0.022	0.034	0.034	0.042	0.062	0.084
$\cos\theta_{W^-}$ bin i	1	2	3	4	5	6	7	8	9	10
$\sqrt{s}$ interval (GeV)			Total luminosity (pb^{-1})			Lumi weighted $\sqrt{s}$ (GeV)				
204-210			630.51			205.92				
$\cos\theta_{W^-}$ bin i	1	2	3	4	5	6	7	8	9	10
σ_i (pb)	0.495	0.601	0.726	1.084	1.293	1.603	2.291	2.764	4.443	7.760
$\delta\sigma_i$ (pb)	0.065	0.076	0.084	0.115	0.112	0.136	0.172	0.166	0.217	0.307
$\delta\sigma_i$(stat) (pb)	0.064	0.075	0.083	0.113	0.109	0.130	0.169	0.160	0.206	0.291
$\delta\sigma_i$(syst) (pb)	0.013	0.013	0.015	0.022	0.024	0.037	0.033	0.045	0.070	0.098

Table 5.4: Combined W^- differential angular cross-section in the 10 angular bins for the four chosen energy intervals. For each energy range, the sum of the measured integrated luminosities and the luminosity weighted centre-of-mass energy is reported. The results per angular bin in each of the energy interval are then presented: σ_i indicates the average of $d[\sigma_{WW}(BR_{e\nu}+BR_{\mu\nu})]/d\cos\theta_{W^-}$ in the i-th bin of $\cos\theta_{W^-}$ with width 0.2. The values, in each bin, of the total, statistical and systematic errors are reported as well. All values are expressed in pb

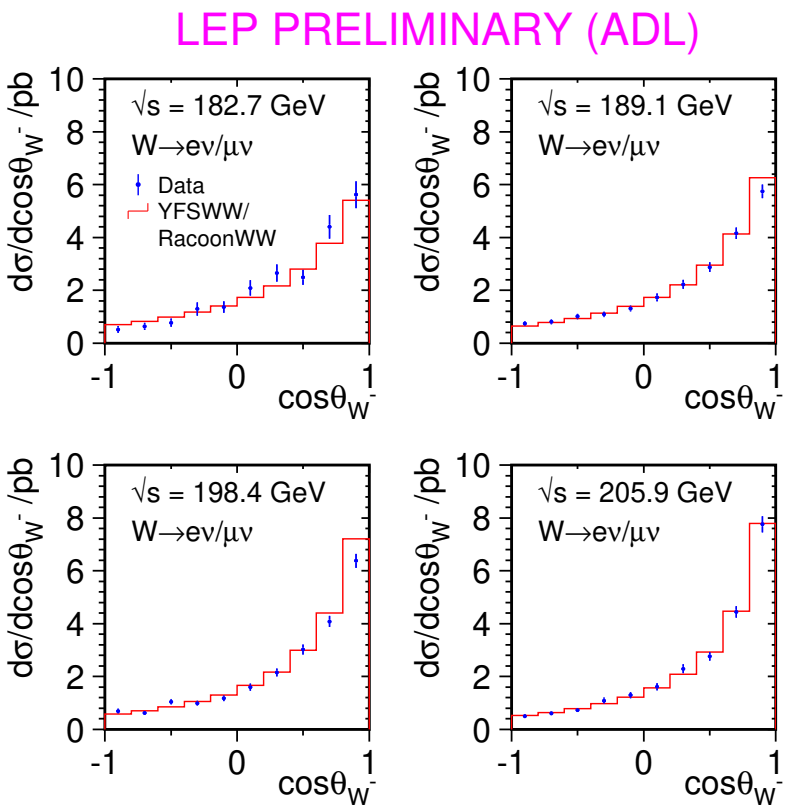

Figure 5.4: LEP combined $d[\sigma_{WW}(BR_{e\nu}+BR_{\mu\nu})]/d\cos\theta_{W^-}$ distributions for the four chosen energy intervals. The combined values (points) are superimposed with the four-fermion predictions from KandY [91].

5.5 Single-W production cross-section

The LEP combination of the single-W production cross-section has been updated using the final DELPHI [92] results, and supersede the last combination presented at the 2004 Summer Conferences [71].

Single-W production at LEP-II is defined as the complete t-channel subset of Feynman diagrams contributing to $e\nu_e f\bar{f}'$ final states, with additional cuts on kinematic variables to exclude the regions of phase space dominated by multiperipheral diagrams, where the cross-section calculation is affected by large uncertainties. The kinematic cuts used in the signal definitions are: $m_{q\bar{q}} > 45$ GeV/c^2 for the $e\nu_e q\bar{q}$ final states, $E_\ell > 20$ GeV for the $e\nu_e \ell\bar{\nu}_\ell$ final states with $\ell = \mu$ or τ, and finally $|\cos\theta_{e^-}| > 0.95$, $|\cos\theta_{e^+}| < 0.95$ and $E_{e^+} > 20$ GeV (or the charge conjugate cuts) for the $e\nu_e e\nu_e$ final states.

In the LEP combination the correlation of the systematic errors in energy and among experiments is properly taken into account. The expected statistical errors have been used for all measurements, given the limited statistical precision of the single-W cross-section measurements.

The total and the hadronic single-W cross-sections, less contamined by $\gamma\gamma$ interaction contributions, are combined independently; the inputs by the four LEP experiments between 183 and 207 GeV are listed in Tables 5.5 and 5.6, and the corresponding LEP combined values presented.

$\sqrt{s}$	Single-W hadronic cross-section (pb)					
(GeV)	ALEPH	DELPHI	L3	OPAL	LEP	χ^2/d.o.f.
182.7	$0.44 \pm 0.24 \pm 0.29$*	$0.11 \pm 0.14 \pm 0.31$*	$0.58 \pm 0.20 \pm 0.23$ *	—	0.42 ± 0.15	13.3/16
188.6	$0.33 \pm 0.15 \pm 0.16$*	$0.57 \pm 0.20 \pm 0.21$*	$0.52 \pm 0.13 \pm 0.14$ *	$0.53 \pm 0.13 \pm 0.14$	0.48 ± 0.08	
191.6	$0.52 \pm 0.40 \pm 0.52$*	$0.30 \pm 0.31 \pm 0.48$*	$0.84 \pm 0.37 \pm 0.44$ *	—	0.56 ± 0.25	
195.5	$0.61 \pm 0.25 \pm 0.28$*	$0.50 \pm 0.27 \pm 0.30$*	$0.66 \pm 0.23 \pm 0.25$ *	—	0.60 ± 0.14	
199.5	$1.06 \pm 0.27 \pm 0.30$*	$0.57 \pm 0.26 \pm 0.28$*	$0.37 \pm 0.20 \pm 0.22$ *	—	0.65 ± 0.14	
201.6	$0.72 \pm 0.33 \pm 0.39$*	$0.67 \pm 0.36 \pm 0.40$*	$1.10 \pm 0.35 \pm 0.40$ *	—	0.82 ± 0.20	
204.9	$0.34 \pm 0.21 \pm 0.24$*	$0.99 \pm 0.31 \pm 0.33$*	$0.42 \pm 0.21 \pm 0.25$ *	—	0.54 ± 0.15	
206.6	$0.64 \pm 0.19 \pm 0.21$*	$0.81 \pm 0.22 \pm 0.23$*	$0.66 \pm 0.18 \pm 0.20$ *	—	0.69 ± 0.12	

Table 5.5: Single-W production cross-section from the four LEP experiments and combined values for the eight energies between 183 and 207 GeV, in the hadronic decay channel of the W boson. All results are preliminary with the exception of those indicated by *.

The LEP measurements of the single-W cross-section are shown, as a function of the LEP centre–of–mass energy, in Figure 5.5 for the hadronic decays and in Figure 5.6 for all decays of the W boson. In the two figures, the measurements are compared with the expected values from WPHACT [94] and `grc4f` [95]. WTO [93], which includes fermion-loop corrections for the hadronic final states, is also used in Figure 5.5. As discussed more in detail in [96] and [72], the theoretical predictions are scaled upward to correct for the implementation of QED radiative corrections at the wrong energy scale s. The full correction factor of 4%, derived [72] by the comparison to the theoretical predictions from SWAP [97], is conservatively taken as a systematic error. This uncertainty dominates the $\pm 5\%$ theoretical error currently assigned to these predictions [72, 96], represented by the shaded area in Figures 5.5 and 5.6. All results, up to the highest centre–of–mass energies, are in agreement with the theoretical predictions.

The agreement can also be appreciated in Table 5.7, where the values of the ratio between mea-

$\sqrt{s}$	Single-W total cross-section (pb)					χ^2/d.o.f.
(GeV)	ALEPH	DELPHI	L3	OPAL	LEP	
182.7	$0.60 \pm^{0.32*}_{0.26}$	$0.69 \pm^{0.42*}_{0.25}$	$0.80 \pm^{0.28*}_{0.25}$	—	0.70 ± 0.17	8.1/16
188.6	$0.55 \pm^{0.18*}_{0.16}$	$0.75 \pm^{0.23*}_{0.22}$	$0.69 \pm^{0.16*}_{0.15}$	$0.67 \pm^{0.17}_{0.15}$	0.66 ± 0.09	
191.6	$0.89 \pm^{0.58*}_{0.44}$	$0.40 \pm^{0.55*}_{0.33}$	$1.11 \pm^{0.48*}_{0.41}$	—	0.81 ± 0.28	
195.5	$0.87 \pm^{0.31*}_{0.27}$	$0.68 \pm^{0.34*}_{0.38}$	$0.97 \pm^{0.27*}_{0.25}$	—	0.85 ± 0.16	
199.5	$1.31 \pm^{0.32*}_{0.29}$	$0.95 \pm^{0.34*}_{0.30}$	$0.88 \pm^{0.26*}_{0.24}$	—	1.05 ± 0.16	
201.6	$0.80 \pm^{0.42*}_{0.35}$	$1.24 \pm^{0.52*}_{0.43}$	$1.50 \pm^{0.45*}_{0.40}$	—	1.17 ± 0.23	
204.9	$0.65 \pm^{0.27*}_{0.23}$	$1.06 \pm^{0.37*}_{0.32}$	$0.78 \pm^{0.29*}_{0.25}$	—	0.80 ± 0.17	
206.6	$0.81 \pm^{0.22*}_{0.20}$	$1.14 \pm^{0.28*}_{0.25}$	$1.08 \pm^{0.21*}_{0.20}$	—	1.00 ± 0.14	

Table 5.6: Single-W total production cross-section from the four LEP experiments and combined values for the eight energies between 183 and 207 GeV. All results are preliminary with the exception of those indicated by *.

sured and expected cross-section values according to the computations by `grc4f` and WPHACT are reported. The combination is performed accounting for the energy and experiment correlations of the systematic sources. The results are also presented in Figure 5.7.

$\sqrt{s}$(GeV)	$\mathcal{R}^{\texttt{grc4f}}_{\mathrm{We}\nu}$	$\mathcal{R}^{\mathrm{WPHACT}}_{\mathrm{We}\nu}$
182.7	1.122 ± 0.272	1.157 ± 0.281
188.6	0.942 ± 0.130	0.971 ± 0.134
191.6	1.094 ± 0.373	1.128 ± 0.385
195.5	1.081 ± 0.203	1.115 ± 0.210
199.5	1.242 ± 0.187	1.280 ± 0.193
201.6	1.340 ± 0.261	1.380 ± 0.269
204.9	0.873 ± 0.189	0.899 ± 0.195
206.6	1.058 ± 0.143	1.089 ± 0.148
χ^2/d.o.f	8.1/16	8.1/16
Average	1.051 ± 0.075	1.083 ± 0.078
χ^2/d.o.f	12.2/24	12.2/24

Table 5.7: Ratios of LEP combined total single-W cross-section measurements to the expectations according to `grc4f` [95] and WPHACT [94]. The resulting averages over energies are also given. The averages take into account inter-experiment as well as inter-energy correlations of systematic errors.

The theory predictions and the details of the experimental inputs and the LEP combined values of the single-W cross-sections and the ratios to theory are reported in Appendix A.

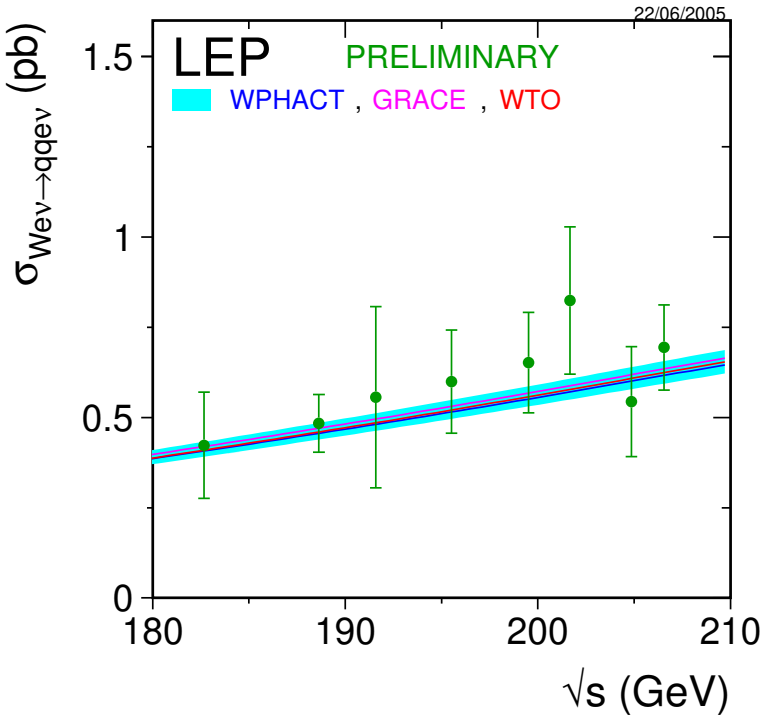

Figure 5.5: Measurements of the single-W production cross-section in the hadronic decay channel of the W boson, compared to the predictions of WTO [93], WPHACT [94] and `grc4f` [95] . The shaded area represents the ±5% uncertainty on the predictions.

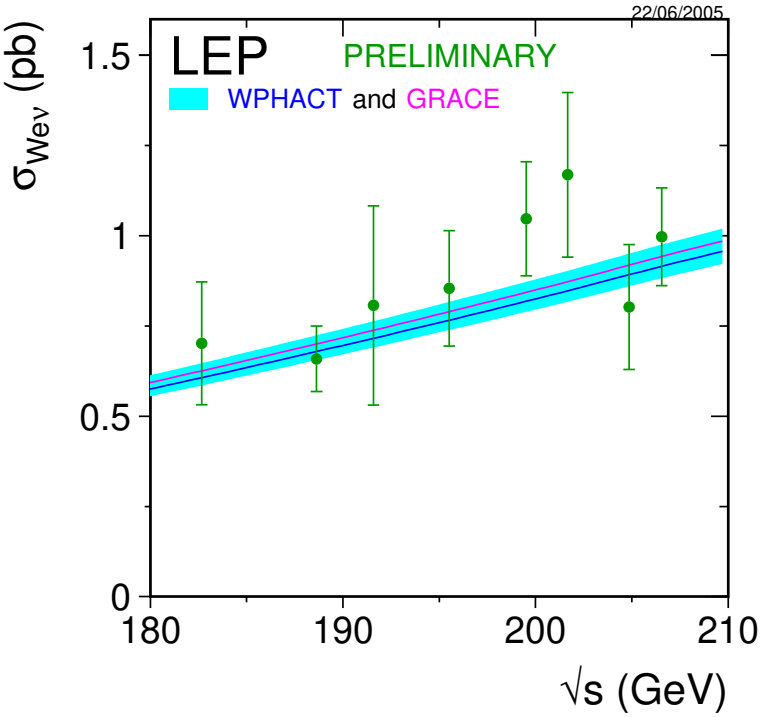

Figure 5.6: Measurements of the single-W total production cross-section, compared to the predictions of WPHACT and `grc4f`. The shaded area represents the ±5% uncertainty on the predictions.

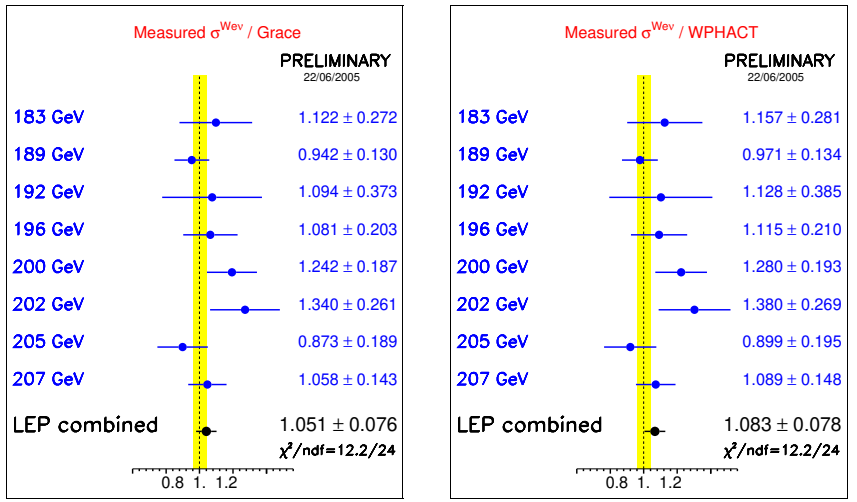

Figure 5.7: Ratios of LEP combined total single-W cross-section measurements to the expectations according to `grc4f` [95] and WPHACT [94]. The yellow bands represent constant relative errors of 5% on the two cross-section predictions.

5.6 Z-pair production cross-section

The Z-pair production cross-section is defined as the NC02 [72] contribution to four-fermion cross-section. Final results from DELPHI, L3 and OPAL at all centre–of–mass energies are available [98–100]. ALEPH published final results at 183 and 189 GeV [101] and contributed preliminary results for all other energies up to 207 GeV [102].

The combination of results is performed with the same technique used for the WW cross-section. The symmetrized expected statistical error of each analysis is used, to avoid biases due to the limited number of selected events. All the cross-sections used for the combination and presented in Table 5.8 are determined by the experiments using the frequentist approach, i.e. without assuming any prior for the value of the cross-section itself.

$\sqrt{s}$	ZZ cross-section (pb)					
(GeV)	ALEPH	DELPHI	L3	OPAL	LEP	χ^2/d.o.f.
182.7	$0.11\ ^{+\ 0.16}_{-\ 0.12}$ *	$0.35\ ^{+\ 0.20}_{-\ 0.15}$ *	0.31 ± 0.17*	$0.12\ ^{+\ 0.20}_{-\ 0.18}$ *	0.22 ± 0.08 *	16.1/24
188.6	$0.67\ ^{+\ 0.14}_{-\ 0.13}$ *	$0.52\ ^{+\ 0.12}_{-\ 0.11}$ *	0.73 ± 0.15 *	$0.80\ ^{+\ 0.15}_{-\ 0.14}$ *	0.66 ± 0.07 *	
191.6	$0.53\ ^{+\ 0.34}_{-\ 0.27}$	$0.63\ ^{+\ 0.36}_{-\ 0.30}$*	0.29 ± 0.22*	$1.29\ ^{+\ 0.48}_{-\ 0.41}$*	0.65 ± 0.17	
195.5	$0.69\ ^{+\ 0.23}_{-\ 0.20}$	$1.05\ ^{+\ 0.25}_{-\ 0.22}$*	1.18 ± 0.26*	$1.13\ ^{+\ 0.27}_{-\ 0.25}$*	0.99 ± 0.12	
199.5	$0.70\ ^{+\ 0.22}_{-\ 0.20}$	$0.75\ ^{+\ 0.20}_{-\ 0.18}$*	1.25 ± 0.27*	$1.05\ ^{+\ 0.26}_{-\ 0.23}$*	0.90 ± 0.12	
201.6	$0.70\ ^{+\ 0.33}_{-\ 0.28}$	$0.85\ ^{+\ 0.33}_{-\ 0.28}$*	0.95 ± 0.39*	$0.79\ ^{+\ 0.36}_{-\ 0.30}$*	0.81 ± 0.17	
204.9	$1.21\ ^{+\ 0.26}_{-\ 0.23}$	$1.03\ ^{+\ 0.23}_{-\ 0.20}$*	$0.77\ ^{+\ 0.21}_{-\ 0.19}$*	$1.07\ ^{+\ 0.28}_{-\ 0.25}$*	0.98 ± 0.13	
206.6	$1.01\ ^{+\ 0.19}_{-\ 0.17}$	$0.96\ ^{+\ 0.16}_{-\ 0.15}$*	$1.09\ ^{+\ 0.18}_{-\ 0.17}$*	$0.97\ ^{+\ 0.20}_{-\ 0.19}$*	0.99 ± 0.09	

Table 5.8: Z-pair production cross-sections from the four LEP experiments and combined values for the eight energies between 183 and 207 GeV. All results are preliminary with the exception of those indicated by *.

$\sqrt{s}$(GeV)	$\mathcal{R}_{ZZ}^{ZZTO}$	$\mathcal{R}_{ZZ}^{YFSZZ}$
182.7	0.857 ± 0.320	0.857 ± 0.320
188.6	1.017 ± 0.113	1.007 ± 0.111
191.6	0.831 ± 0.225	0.826 ± 0.224
195.5	1.100 ± 0.133	1.100 ± 0.133
199.5	0.915 ± 0.125	0.912 ± 0.124
201.6	0.799 ± 0.174	0.795 ± 0.173
204.9	0.937 ± 0.121	0.931 ± 0.120
206.6	0.937 ± 0.091	0.928 ± 0.090
χ^2/d.o.f	16.1/24	16.1/24
Average	0.952 ± 0.052	0.945 ± 0.052
χ^2/d.o.f	19.1/31	19.1/31

Table 5.9: Ratios of LEP combined Z-pair cross-section measurements to the expectations according to ZZTO [104] and YFSZZ [103]. The results of the combined fits are given in the table together with the resulting χ^2. Both fits take into account inter-experiment as well as inter-energy correlations of systematic errors.

The measurements are shown in Figure 5.8 as a function of the LEP centre–of–mass energy, where they are compared to the YFSZZ [103] and ZZTO [104] predictions. Both these calculations have an estimated uncertainty of $\pm 2\%$ [72]. The data do not show any significant deviation from the theoretical expectations.

In analogy with the W-pair cross-section, a value for $\mathcal{R}_{ZZ}$ can also be determined: its definition and the procedure of the combination follows the one described for $\mathcal{R}_{WW}$. The data are compared with the YFSZZ and ZZTO predictions; Table 5.9 reports the numerical values of $\mathcal{R}_{ZZ}$ in energy and combined, whereas figure 5.9 show them in comparison to unity, where the $\pm 2\%$ error on the theoretical ZZ cross-section is shown as a yellow band. The experimental accuracy on the combined value of $\mathcal{R}_{ZZ}$ is about 5%.

The theory predictions, the details of the experimental inputs with the the breakdown of the error contributions and the LEP combined values of the total cross-sections and the ratios to theory are reported in Appendix A.

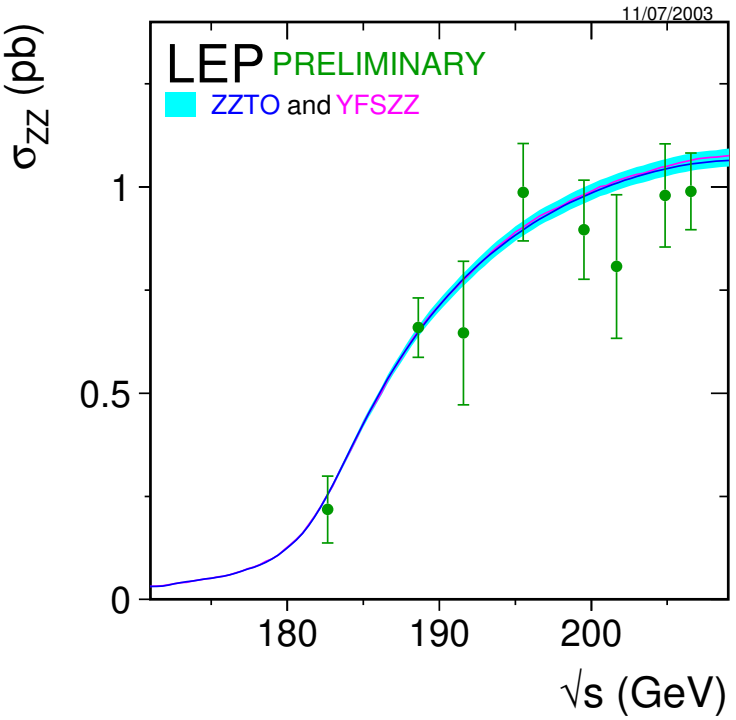

Figure 5.8: Measurements of the Z-pair production cross-section, compared to the predictions of YFSZZ [103] and ZZTO [104]. The shaded area represent the ±2% uncertainty on the predictions.

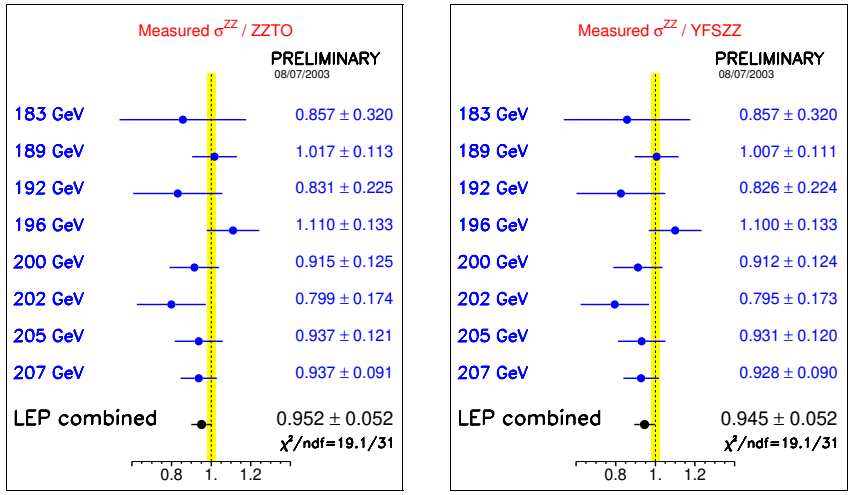

Figure 5.9: Ratios of LEP combined Z-pair cross-section measurements to the expectations according to ZZTO [104] and YFSZZ [103] The yellow bands represent constant relative errors of 2% on the two cross-section predictions.

5.7 Single-Z production cross-section

Single-Z production at LEP-II is studied considering only the $ee q\bar{q}$, $ee\mu\mu$ final states with the following phase space cuts and assuming one visible electron: $m_{q\bar{q}}(m_{\mu\mu}) > 60$ GeV/c^2, $\theta_{e+} < 12$ degrees, 12 degrees$< \theta_{e-} <$120 degrees and $E_{e-} >$3 GeV, with obvious notation and where the angle is defined with respect to the beam pipe, with the positron direction being along $+z$ and the electron direction being along $-z$. Corresponding cuts are imposed when the positron is visible: $\theta_{e-} > 168$ degrees, 60 degrees$< \theta_{e+} <$168 degrees and $E_{e+} >$3 GeV.

The LEP combination of the single-Z production cross-section uses final results by the ALEPH [105] and the L3 [106] Collaborations and has been updated with the final results by DELPHI [92].

The results concern the hadronic and the leptonic channel and all the centre–of–mass energies from 183 to 209 GeV.

$\sqrt{s}$	Single-Z hadronic cross-section (pb)					
(GeV)	ALEPH	DELPHI	L3	OPAL	LEP	χ^2/d.o.f.
182.7	$0.27\ ^{+\ 0.21\ *}_{-\ 0.16}$	$0.56\ ^{+\ 0.28\ *}_{-\ 0.23}$	$0.51\ ^{+\ 0.19\ *}_{-\ 0.16}$	—	0.45 ± 0.11	13.0/16
188.6	$0.42\ ^{+\ 0.14*}_{-\ 0.12}$	$0.64\ ^{+\ 0.16*}_{-\ 0.14}$	$0.55\ ^{+\ 0.11\ *}_{-\ 0.10}$	—	0.53 ± 0.07	
191.6	$0.61\ ^{+\ 0.39*}_{-\ 0.29}$	$0.63\ ^{+\ 0.40*}_{-\ 0.30}$	$0.60\ ^{+\ 0.26*}_{-\ 0.21}$	—	0.61 ± 0.15	
195.5	$0.72\ ^{+\ 0.24*}_{-\ 0.20}$	$0.66\ ^{+\ 0.22*}_{-\ 0.19}$	$0.40\ ^{+\ 0.13*}_{-\ 0.11}$	—	0.55 ± 0.10	
199.5	$0.60\ ^{+\ 0.21*}_{-\ 0.18}$	$0.57\ ^{+\ 0.20*}_{-\ 0.17}$	$0.33\ ^{+\ 0.13*}_{-\ 0.11}$	—	0.47 ± 0.10	
201.6	$0.89\ ^{+\ 0.35*}_{-\ 0.28}$	$0.19\ ^{+\ 0.21*}_{-\ 0.16}$	$0.81\ ^{+\ 0.27*}_{-\ 0.23}$	—	0.67 ± 0.13	
204.9	$0.42\ ^{+\ 0.17*}_{-\ 0.15}$	$0.37\ ^{+\ 0.18*}_{-\ 0.15}$	$0.56\ ^{+\ 0.16*}_{-\ 0.14}$	—	0.47 ± 0.10	
206.6	$0.70\ ^{+\ 0.17*}_{-\ 0.15}$	$0.69\ ^{+\ 0.16*}_{-\ 0.14}$	$0.59\ ^{+\ 0.12*}_{-\ 0.11}$	—	0.65 ± 0.08	

Table 5.10: Single-Z hadronic production cross-section from the four LEP experiments and combined values for the eight energies between 183 and 207 GeV. All results are preliminary with the exception of those indicated by *.

	Single-Z cross-section into muons(pb)				
	ALEPH	DELPHI	L3	OPAL	LEP
Av. $\sqrt{s}$(GeV)	196.67	197.10	196.60	—	196.79
$\sigma_{Zee\to\mu\mu ee}$	0.055 ± 0.016 *	$0.070\ ^{+\ 0.023}_{-\ 0.019}$	0.043 ± 0.013 *	—	0.057 ± 0.009

Table 5.11: Preliminary energy averaged single-Z production cross-section into muons from the four LEP experiments and combined values. The results indicated with * are final.

Tables 5.10 and 5.11 synthesize the inputs by the experiments and the corresponding LEP combinations in the hadronic and muon channel, respectively. The $ee\mu\mu$ cross-section is already combined in energy by the individual experiments to increase the statistics of the data. The combination accounts for energy and experiment correlation of the systematic errors. The results in the hadronic channel are compared with the WPHACT and `grc4f` predictions as a function of the centre–of–mass energy and shown in figure 5.10. Table 5.12 and figure 5.11 show the preliminary values of the ratio between measured and expected cross-sections at the various energy points and the combined value; the testing accuracy of the combined value is about 7% with three experiments contributing in the average.

The detailed breakdown of the inputs of the experiments with the split up of the systematic

contribution according to the correlations for the single-Z cross-section and its ratio to theory can be found in Appendix A.

$\sqrt{s}$(GeV)	$\mathcal{R}_{Zee}^{\texttt{grc4f}}$	$\mathcal{R}_{Zee}^{\text{WPHACT}}$
182.7	0.871 ± 0.219	0.876 ± 0.220
188.6	0.982 ± 0.126	0.990 ± 0.127
191.6	1.104 ± 0.275	1.112 ± 0.277
195.5	0.964 ± 0.167	0.972 ± 0.168
199.5	0.809 ± 0.165	0.816 ± 0.167
201.6	1.126 ± 0.222	1.135 ± 0.224
204.9	0.769 ± 0.160	0.776 ± 0.162
206.6	1.062 ± 0.124	1.067 ± 0.125
χ^2/d.o.f	13.0/16	13.0/16
Average	0.955 ± 0.065	0.962 ± 0.065
χ^2/d.o.f	17.1/23	17.0/23

Table 5.12: Ratios of LEP combined single-Z hadronic cross-section measurements to the expectations according to `grc4f` [95] and WPHACT [94]. The resulting averages over energies are also given. The averages take into account inter-experiment as well as inter-energy correlations of systematic errors.

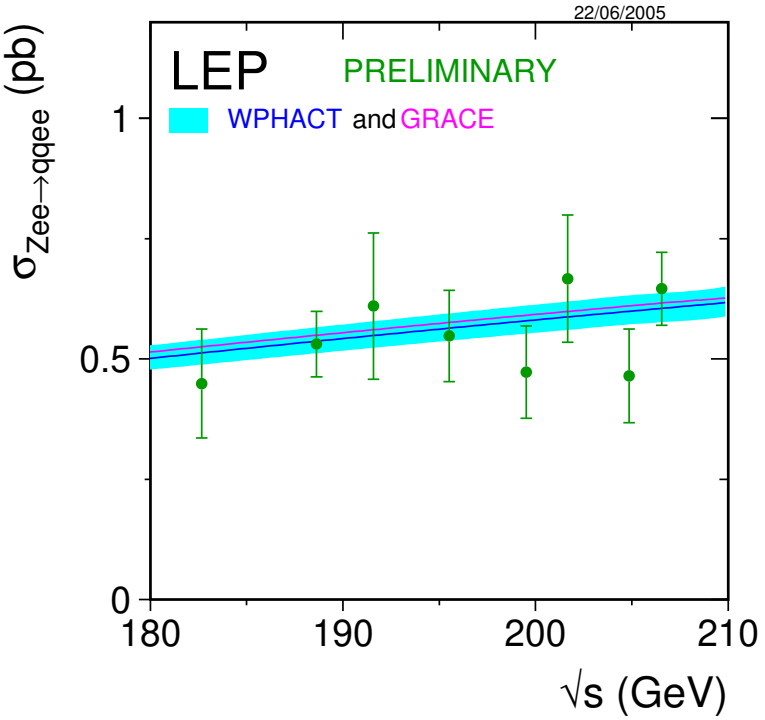

Figure 5.10: Measurements of the single-Z hadronic production cross-section, compared to the predictions of WPHACT and `grc4f`. The shaded area represents the ±5% uncertainty on the predictions.

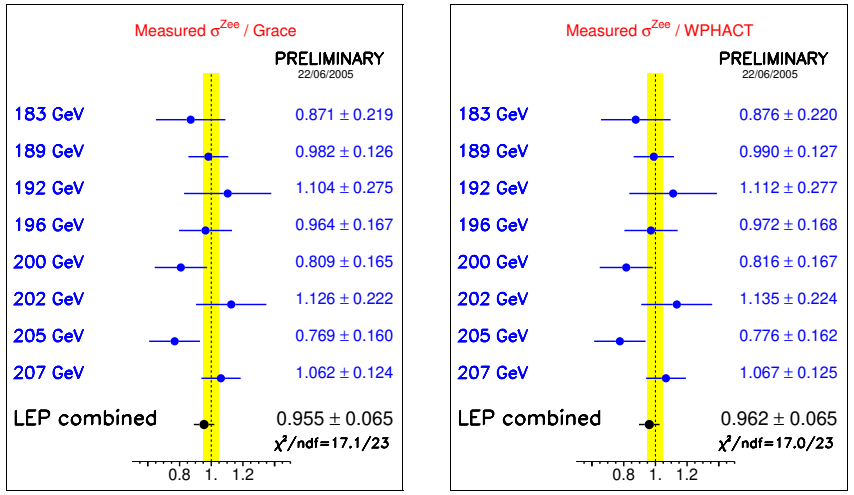

Figure 5.11: Ratios of LEP combined single-Z hadronic cross-section measurements to the expectations according to `grc4f` [95] and WPHACT [94]. The yellow bands represent constant relative errors of 5% on the two cross-section predictions.

5.8 Zγ^* production cross-section

The Zγ^* contribution to the four-fermion phase space is defined for the final states with two couples of same-kind, charge conjugate, leptons. It is required that one and only one of the invariant masses of the couples satisfies: $m_Z - 2\Gamma_Z < m_{ff'} < m_Z + 2\Gamma_Z$ with $m_{ff'}$ is the invariant mass of the two same-kind fermions. In case of four identical leptons all oppositely charged couples have to be considered. Moreover the following cuts, final state dependent, have been introduced:

- eeqq, $\mu\mu$qq: $|\cos\theta_\ell| < 0.95$, $m_{\ell\ell} > 5$GeV, $m_{qq} > 10$GeV, ℓ =e,μ
- $\nu\nu$qq: $m_{qq} > 10$GeV
- $\nu\nu\ell\ell$: $m_{\ell\ell} > 10$GeV, $m_{\ell\nu} > 90$GeV, $m_{\ell\nu} < 70$GeV, ℓ =e,μ
- $\ell_1\ell_1\ell_2\ell_2$: $|\cos\theta_{\ell_1\ell_2}| < 0.95$, $m_{\ell_1\ell_1} > 5$GeV, $m_{\ell_2\ell_2} > 5$GeV, ℓ =e,μ

The LEP collaborations did not provide a complete analysis of all possible Zγ^* final states. Indeed, the DELPHI collaboration provided preliminary results for the $\nu\nu$qq, $\ell\ell$qq final states [107], whereas the L3 collaboration provided final results for the $\nu\nu$qq, $\ell\ell$qq, $\ell\ell\nu\nu$, $\ell\ell\ell\ell$ channels [108]. Final states with only quarks or containing τs were not studied. ALEPH and OPAL did not present any result on Zγ^*.

To increase the statistics the cross-sections were determined using the full data sample at an average LEP-II centre-of-mass energy. Table 5.13 presents the measured cross-sections, where the expected statistical errors were used for the combination. The results agree well with the expectations.

channel	$\sqrt{s}$ (GeV)	Lumi (pb^{-1})	σ(pb)	$\delta\sigma_{\rm stat}$ (pb)	$\delta\sigma^{\rm unc}_{\rm syst}$ (pb)	$\delta\sigma^{\rm cor}_{\rm syst}$ (pb)	$\delta\sigma_{\rm MC}$ (pb)
DELPHI							
$\nu\nu$qq	197.1	666.7	0.042	$^{+0.022}_{-0.020}$	0.008	0.002	0.042
$\mu\mu$qq	197.1	666.7	0.031	$^{+0.013}_{-0.011}$	0.004	0.001	0.016
eeqq	197.1	666.7	0.063	$^{+0.018}_{-0.016}$	0.009	0.001	0.016
L3							
$\nu\nu$qq	196.7	679.4	0.072	$^{+0.047}_{-0.041}$	0.004	0.016	0.046
$\mu\mu$qq	196.7	681.9	0.040	$^{+0.018}_{-0.016}$	0.002	0.003	0.017
eeqq	196.7	681.9	0.100	$^{+0.024}_{-0.022}$	0.004	0.007	0.020
LEP combined							
channel	$\sqrt{s}$ (GeV)	Lumi (pb^{-1})	σ(pb)	$\delta\sigma_{\rm stat}$ (pb)	$\delta\sigma_{\rm syst}$ (pb)	$\delta\sigma_{\rm tot}$ (pb)	$\sigma_{\rm theory}$ (pb)
$\nu\nu$qq	196.9	679.4	0.055	0.031	0.008	0.032	0.083
$\mu\mu$qq	196.9	681.9	0.035	0.012	0.003	0.012	0.042
eeqq	196.9	681.9	0.079	0.012	0.005	0.013	0.059

Table 5.13: Zγ^* input by the experiments and combined LEP measurements. In the columns are reported, respectively, the channel, the luminosity weighted centre-of-mass energy, the luminosity, the cross-section value, the measured statistical error, the systematic contribution uncorrelated between experiments, the systematic contribution correlated between experiments and the expected statistical error from the simulation. All results are final. For the LEP combination the full systematic error and the total error are given and the last column presents the theory expectation with GRC4F.

5.9 WWγ production cross-section

A LEP combination of the WWγ production cross-section has been performed using final DELPHI [109], L3 [110] and OPAL [111] results available since the Summer 2003 Conferences. The signal is defined as the part of the WWγ process with the following cuts to the photon: $E_\gamma > 5$ GeV, $|\cos\theta_\gamma| < 0.95$, $|\cos\theta_{\gamma,f}| < 0.90$ and $m_W - 2\Gamma_W < m_{ff'} < m_W + 2\Gamma_W$ where $\theta_{\gamma,f}$ is the angle between the photon and the closest charged fermion and $m_{ff'}$ is the invariant mass of fermions from the Ws.

In order to increase the statistics the LEP combination is performed in energy intervals rather than at each energy point; they are defined according to the LEP-II running period where more statistics was accumulated. The luminosity weighted centre–of–mass per interval is determined in each experiment and then combined to obtain the corresponding value in the combination. Table 5.14 reports those energies and the cross-sections measured by the experiments, together with the combined LEP values.

$\sqrt{s}$	WWγ cross-section (pb)				
(GeV)	ALEPH	DELPHI	L3	OPAL	LEP
188.6	—	0.05 ± 0.08	0.20 ± 0.09	0.16 ± 0.04	0.15 ± 0.03
194.4	—	0.17 ± 0.12	0.17 ± 0.10	0.17 ± 0.06	0.17 ± 0.05
200.2	—	0.34 ± 0.12	0.43 ± 0.13	0.21 ± 0.06	0.27 ± 0.05
206.1	—	0.18 ± 0.08	0.13 ± 0.08	0.30 ± 0.05	0.24 ± 0.04

Table 5.14: WWγ production cross-section from the four LEP experiments and combined values for the four energy bins. All results are final.

Figure 5.12 shows the combined data points compared with the cross-section prediction by EEWWG [112] and by RACOONWW. The RACOONWW is shown in the figure without any theory error band.

5.10 Summary

The updated LEP combinations of the W-pair and single boson production cross-section, together with the W angular distributions, have been presented. A first combination of some of the $Z\gamma^*$ final states has also been performed. The combinations are based on data collected up to 209 GeV by the four LEP experiments.

All measurements agree with the expectations. In the fit to the W branching fractions without the assumption of lepton universality an excess of the W branching ratio into $\tau\nu_\tau$ with respect to the other lapton families is observed in the data. This excess is above two standard deviations from both the branching ratio into $e\nu_e$ and into $\mu\nu_\mu$.

This note still reflects a preliminary status of the analyses at the time of the Summer 2005 Conferences. A definitive statement on these results and the ones not updated for these Conferences must wait for publication by each collaboration.

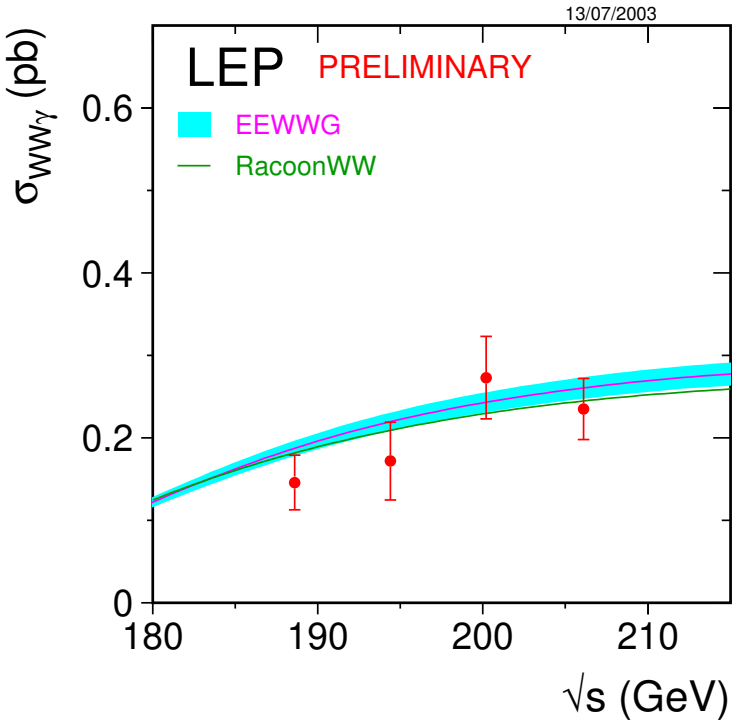

Figure 5.12: Measurements of the WWγ production cross-section, compared to the predictions of EEWWG [112] and RACOONWW [85]. The shaded area in the EEWWG curve represents the $\pm 5\%$ uncertainty on the predictions.

Chapter 6

Electroweak Gauge Boson Self Couplings

Updates with respect to summer 2005:
Unchanged w.r.t. summer 2003: Results are preliminary.
Note that some recent publications [99, 113–116] are not yet included in this combination.

6.1 Introduction

The measurement of gauge boson couplings and the search for possible anomalous contributions due to the effects of new physics beyond the Standard Model are among the principal physics aims at LEP-II [117]. Combined preliminary measurements of triple gauge boson couplings are presented here. Results from W-pair production are combined in single and two-parameter fits, including updated results from ALEPH, L3 and OPAL as well as an improved treatment of the main systematic effect in our previous combination, the uncertainty in the $O(\alpha_{em})$ correction. An updated combination of quartic gauge coupling (QGC) results for the ZZ$\gamma\gamma$ vertex is also presented, including data from ALEPH, L3 and OPAL. The combination of QGCs associated with the WW$\gamma\gamma$ vertex, including the sign convention as reported in [118, 119] and the reweighting based on [118] is foreseen for our next report. The combination of neutral TGCs measured in ZZ production (f-couplings) has been updated, including new results from L3 and OPAL. The combinations for neutral TGCs accessible through Zγ production (h-couplings) reported in 2001 still remain valid [120].

The W-pair production process, $e^+e^- \to W^+W^-$, involves charged triple gauge boson vertices between the W^+W^- and the Z or photon. During LEP-II operation, about 10,000 W-pair events were collected by each experiment. Single W (eνW) and single photon ($\nu\bar{\nu}\gamma$) production at LEP are also sensitive to the WWγ vertex. Results from these channels are also included in the combination for some experiments; the individual references should be consulted for details.

For the charged TGCs, Monte Carlo calculations (RacoonWW [121] and YFSWW [122]) incorporating an improved treatment of $O(\alpha_{em})$ corrections to the WW production have become our standard by now. The corrections affect the measurements of the charged TGCs in W-pair production. Results, some of them preliminary, including these $O(\alpha_{em})$ corrections have been submitted from all four LEP collaborations ALEPH [123], DELPHI [124], L3 [125] and OPAL [126]. LEP combinations are made for the charged TGC measurements in single- and two-parameter fits.

At centre-of-mass energies exceeding twice the Z boson mass, pair production of Z bosons is kinematically allowed. Here, one searches for the possible existence of triple vertices involving only

neutral electroweak gauge bosons. Such vertices could also contribute to Zγ production. In contrast to triple gauge boson vertices with two charged gauge bosons, purely neutral gauge boson vertices do not occur in the Standard Model of electroweak interactions.

Within the Standard Model, quartic electroweak gauge boson vertices with at least two charged gauge bosons exist. In e^+e^- collisions at LEP-II centre-of-mass energies, the WWZγ and WW$\gamma\gamma$ vertices contribute to WWγ and $\nu\bar{\nu}\gamma\gamma$ production in s-channel and t-channel, respectively. The effect of the Standard Model quartic electroweak vertices is below the sensitivity of LEP-II. Quartic gauge boson vertices with only neutral bosons, like the ZZ$\gamma\gamma$ vertex, do not exist in the Standard Model. However, anomalous QGCs associated with this vertex are studied at LEP.

Anomalous quartic vertices are searched for in the production of WWγ, $\nu\bar{\nu}\gamma\gamma$ and Z$\gamma\gamma$ final states. The couplings related to the ZZ$\gamma\gamma$ and WW$\gamma\gamma$ vertices are assumed to be different [127], and are therefore treated separately. In this report, we only combine the results for the anomalous couplings associated with the ZZ$\gamma\gamma$ vertex. The combination of the WW$\gamma\gamma$ vertex couplings is foreseen for the near future.

6.1.1 Charged Triple Gauge Boson Couplings

The parametrisation of the charged triple gauge boson vertices is described in References [117,128–133]. The most general Lorentz invariant Lagrangian which describes the triple gauge boson interaction has fourteen independent complex couplings, seven describing the WWγ vertex and seven describing the WWZ vertex. Assuming electromagnetic gauge invariance as well as C and P conservation, the number of independent TGCs reduces to five. A common set is $\{g_1^Z, \kappa_Z, \kappa_\gamma, \lambda_Z, \lambda_\gamma\}$ where $g_1^Z = \kappa_Z = \kappa_\gamma = 1$ and $\lambda_Z = \lambda_\gamma = 0$ in the SM. The parameters proposed in [117] and used by the LEP experiments are g_1^Z, λ_γ and κ_γ with the gauge constraints:

$$\kappa_Z = g_1^Z - (\kappa_\gamma - 1)\tan^2\theta_W\,, \tag{6.1}$$

$$\lambda_Z = \lambda_\gamma\,, \tag{6.2}$$

where θ_W is the weak mixing angle. The couplings are considered as real, with the imaginary parts fixed to zero. In contrast to previous LEP combinations [120, 134], we are quoting the measured coupling values themselves and not their deviation from the Standard Model.

Note that the photonic couplings λ_γ and κ_γ are related to the magnetic and electric properties of the W-boson. One can write the lowest order terms for a multipole expansion describing the W-γ interaction as a function of λ_γ and κ_γ. For the magnetic dipole moment μ_W and the electric quadrupole moment q_W one obtains $e(1+\kappa_\gamma+\lambda_\gamma)/2m_W$ and $-e(\kappa_\gamma-\lambda_\gamma)/m_W^2$, respectively.

The inclusion of $O(\alpha_{em})$ corrections in the Monte Carlo calculations has a considerable effect on the charged TGC measurement. Both the total cross-section and the differential distributions are affected. The cross-section is reduced by 1-2% (depending on the energy). Amongst the differential distributions, the effects are naturally more complex. The polar W^- production angle carries most of the information on the TGC parameters; its shape is modified to be more forwardly peaked. In a fit to data, the $O(\alpha_{em})$ effect manifests itself as a negative shift of the obtained TGC values with a magnitude of typically -0.015 for λ_γ and g_1^Z and -0.04 for κ_γ.

6.1.2 Neutral Triple Gauge Boson Couplings

There are two classes of Lorentz invariant structures associated with neutral TGC vertices which preserve $U(1)_{em}$ and Bose symmetry, as described in [129,135].

The first class refers to anomalous $Z\gamma\gamma^*$ and $Z\gamma Z^*$ couplings which are accessible at LEP in the process $e^+e^- \to Z\gamma$. The parametrisation contains eight couplings: h_i^V with $i = 1,...,4$ and $V = \gamma$,Z. The superscript γ refers to $Z\gamma\gamma^*$ couplings and superscript Z refers to $Z\gamma Z^*$ couplings. The photon and the Z boson in the final state are considered as on-shell particles, while the third boson at the vertex, the s-channel internal propagator, is off shell. The couplings h_1^V and h_2^V are CP-odd while h_3^V and h_4^V are CP-even.

The second class refers to anomalous $ZZ\gamma^*$ and ZZZ^* couplings which are accessible at LEP-II in the process $e^+e^- \to ZZ$. This anomalous vertex is parametrised in terms of four couplings: f_i^V with $i = 4,5$ and $V = \gamma$,Z. The superscript γ refers to $ZZ\gamma^*$ couplings and the superscript Z refers to ZZZ^* couplings, respectively. Both Z bosons in the final state are assumed to be on-shell, while the third boson at the triple vertex, the s-channel internal propagator, is off-shell. The couplings f_4^V are CP-odd whereas f_5^V are CP-even.

The h_i^V and f_i^V couplings are assumed to be real and they vanish at tree level in the Standard Model.

6.1.3 Quartic Gauge Boson Couplings

The couplings associated with the two QGC vertices $WW\gamma\gamma$ and $ZZ\gamma\gamma$ are assumed to be different, and are by convention treated as separate couplings at LEP. In this report, we only combine QGCs related to the $ZZ\gamma\gamma$ vertex. The contribution of such anomalous quartic gauge boson couplings is described by two coupling parameters a_c/Λ^2 and a_0/Λ^2, which are zero in the Standard Model [112, 136]. Events from $\nu\bar{\nu}\gamma\gamma$ and $Z\gamma\gamma$ final states can originate from the $ZZ\gamma\gamma$ vertex and are therefore used to study anomalous QGCs.

6.2 Measurements

The combined results presented here are obtained from charged and neutral electroweak gauge boson coupling measurements, and from quartic gauge boson couplings measurements as discussed above. The individual references should be consulted for details about the data samples used.

The charged TGC analyses of ALEPH, DELPHI, L3 and OPAL use data collected at LEP-II up to centre-of-mass energies of 209 GeV. These analyses use different channels, typically the semileptonic and fully hadronic W-pair decays [123–126]. The full data set is analysed by ALEPH, L3 and OPAL, whereas DELPHI presently uses all data at 189 GeV and above. Anomalous TGCs affect both the total production cross-section and the shape of the differential cross-section as a function of the polar W^- production angle. The relative contributions of each helicity state of the W bosons are also changed, which in turn affects the distributions of their decay products. The analyses presented by each experiment make use of different combinations of each of these quantities. In general, however, all analyses use at least the expected variations of the total production cross-section and the W^- production angle. Results from $e\nu W$ and $\nu\bar{\nu}\gamma$ production are included by some experiments. Single

W production is particularly sensitive to κ_γ, thus providing information complementary to that from W-pair production.

The h-coupling analyses of ALEPH, DELPHI and L3 use data collected up to centre-of-mass energies of 209 GeV. The OPAL measurements so far use the data at 189 GeV. The results of the f-couplings are obtained from the whole data set above the ZZ-production threshold by all of the experiments. The experiments already pre-combine different processes and final states for each of the couplings. For the neutral TGCs, the analyses use measurements of the total cross sections of $Z\gamma$ and ZZ production and the differential distributions: the h_i^V couplings [137–140] and the f_i^V couplings [137,138,141,142] are determined.

The combination of quartic gauge boson couplings associated with the $ZZ\gamma\gamma$ vertex is at present based on analyses of ALEPH [143], L3 [144] and OPAL [145]. The L3 analysis uses data from the $q\bar{q}\gamma\gamma$ final state all at centre-of-mass energies above the Z resonance, from 130 GeV to 207 GeV. Both ALEPH and OPAL analyse the $\nu\bar{\nu}\gamma\gamma$ final state, with ALEPH using data from centre-of-mass energies ranging from 183 GeV to 209 GeV, and OPAL from 189 GeV to 209 GeV.

6.3 Combination Procedure

The combination is based on the individual likelihood functions from the four LEP experiments. Each experiment provides the negative log likelihood, $\log\mathcal{L}$, as a function of the coupling parameters to be combined. The single-parameter analyses are performed fixing all other parameters to their Standard Model values. The two-parameter analyses are performed setting the remaining parameters to their Standard Model values. For the charged TGCs, the gauge constraints listed in Section 6.1.1 are always enforced.

The $\log\mathcal{L}$ functions from each experiment include statistical as well as those systematic uncertainties which are considered as uncorrelated between experiments. For both single- and multi-parameter combinations, the individual $\log\mathcal{L}$ functions are combined. It is necessary to use the $\log\mathcal{L}$ functions directly in the combination, since in some cases they are not parabolic, and hence it is not possible to properly combine the results by simply taking weighted averages of the measurements.

The main contributions to the systematic uncertainties that are uncorrelated between experiments arise from detector effects, background in the selected signal samples, limited Monte Carlo statistics and the fitting method. Their importance varies for each experiment and the individual references should be consulted for details.

In the neutral TGC sector, the systematic uncertainties arising from the theoretical cross section prediction in $Z\gamma$-production ($\simeq 1\%$ in the $q\bar{q}\gamma$- and $\simeq 2\%$ in the $\nu\bar{\nu}\gamma$ channel) are treated as correlated. For ZZ production, the uncertainty on the theoretical cross section prediction is small compared to the statistical accuracy and therefore is neglected. Smaller sources of correlated systematic uncertainties, such as those arising from the LEP beam energy, are for simplicity treated as uncorrelated.

The combination procedure for neutral TGCs, where the relative systematic uncertainties are small, is unchanged with respect to the previous LEP combinations of electroweak gauge boson couplings [120,134]. The correlated systematic uncertainties in the h-coupling analyses are taken into account by scaling the combined log-likelihood functions by the squared ratio of the sum of statistical and uncorrelated systematic uncertainty over the total uncertainty including all correlated uncertainties. For the general case of non-Gaussian probability density functions, this treatment of the

correlated errors is only an approximation; it also neglects correlations in the systematic uncertainties between the parameters in multi-parameter analyses.

In the charged TGC sector, systematic uncertainties considered correlated between the experiments are the theoretical cross section prediction (0.5% for W-pair production and 5% for single W production), hadronisation effects, the final state interactions, namely Bose-Einstein correlations and colour reconnection, and the uncertainty in the radiative corrections themselves. The latter was the dominant systematic error in our previous combination, where we used a conservative estimate, the full effect from applying the $O(\alpha_{em})$ corrections. New preliminary analyses on the subject are now available from several LEP experiments [123], based on comparisons of fully simulated events using two different leading-pole approximation schemes (LPA-A and LPA-B) [146]. In addition, the availability of comparisons of both generators incorporating $O(\alpha_{em})$ corrections (RacoonWW and YFSWW [121,122]) makes it now possible to perform a more realistic estimation of this effect. In general, the TGC shift measured in the comparison of the two generators is found to be larger than the effect from the different LPA schemes. This improved estimation, whilst still being conservative, reduces the systematic uncertainty from $O(\alpha_{em})$ corrections by about a third for g_1^Z and λ_γ and roughly halves it for κ_γ, compared to the full $O(\alpha_{em})$ correction applied previously. The application of this reduced systematic error renders the charged TGC measurements statistics dominated.

In case of the charged TGCs, the systematic uncertainties considered correlated between the experiments amount to 58% of the combined statistical and uncorrelated uncertainties for λ_γ and g_1^Z, while for κ_γ it is 68%. This means that the measurements of λ_γ, g_1^Z and κ_γ are now clearly limited by statistics. An improved combination procedure [147] is used for the charged TGCs. This procedure allows the combination of statistical and correlated systematic uncertainties, independently of the analysis method chosen by the individual experiments.

The combination of charged TGCs uses the likelihood curves and correlated systematic errors submitted by each of the four experiments. The procedure is based on the introduction of an additional free parameter to take into account the systematic uncertainties, which are treated as shifts on the fitted TGC value, and are assumed to have a Gaussian distribution. A simultaneous minimisation of both parameters (TGC and systematic error) is performed to the log-likelihood function.

In detail, the combination proceeds in the following way: the set of measurements from the LEP experiments ALEPH, DELPHI, OPAL and L3 is given with statistical plus uncorrelated systematic uncertainties in terms of likelihood curves: $-\log\mathcal{L}^A_{stat}(x)$, $-\log\mathcal{L}^D_{stat}(x)$ $-\log\mathcal{L}^L_{stat}(x)$ and $-\log\mathcal{L}^O_{stat}(x)$, respectively, where x is the coupling parameter in question. Also given are the shifts for each of the five totally correlated sources of uncertainty mentioned above; each source S is leading to systematic errors σ^S_A, σ^S_D, σ^S_L and σ^S_O.

Additional parameters Δ^S are included in order to take into account a Gaussian distribution for each of the systematic uncertainties. The procedure then consists in minimising the function:

$$-\log\mathcal{L}_{total} = \sum_{E=A,D,L,O} \log\mathcal{L}^E_{stat}(x - \sum_{S=DPA,\sigma_{WW},HAD,BE,CR}(\sigma^S_E\Delta^S)) + \sum_S \frac{(\Delta^S)^2}{2} \qquad (6.3)$$

where x and Δ_S are the free parameters, and the sums run over the four experiments and the five systematic errors. The resulting uncertainty on x will take into account all sources of uncertainty, yielding a measurement of the coupling with the error representing statistical and systematic sources. The projection of the minima of the log-likelihood as a function of x gives the combined log-likelihood curve including statistical and systematic uncertainties. The advantage over the scaling method used

previously is that it treats systematic uncertainties that are correlated between the experiments correctly, while not forcing the averaging of these systematic uncertainties into one global LEP systematics scaling factor. In other words, the (statistical) precision of each experiment now gets reduced by its own correlated systematic errors, instead of an averaged LEP systematic error. The method has been cross-checked against the scaling method, and was found to give comparable results. The inclusion of the systematic uncertainties lead to small differences as expected by the improved treatment of correlated systematic errors, a similar behaviour as seen in Monte Carlo comparisons of these two combinations methods [148]. Furthermore, it was shown that the minimisation-based combination method used for the charged TGCs agrees with the method based on optimal observables, where systematic effects are included directly in the mean values of the optimal observables (see [148]), for any realistic ratio of statistical and systematic uncertainties. Further details on the improved combination method can be found in [147].

In the combination of the QGCs, the influence of correlated systematic uncertainties is considered negligible compared to the statistical error, arising from the small number of selected events. Therefore, the QGCs are combined by adding the log-likelihood curves from the single experiments.

For all single- and multi-parameter results quoted in numerical form, the one standard deviation uncertainties (68% confidence level) are obtained by taking the coupling values for which $\Delta\log\mathcal{L} = +0.5$ above the minimum. The 95% confidence level (C.L.) limits are given by the coupling values for which $\Delta\log\mathcal{L} = +1.92$ above the minimum. Note that in the case of the neutral TGCs, double minima structures appear in the negative log-likelihood curves. For multi-parameter analyses, the two dimensional 68% C.L. contour curves for any pair of couplings are obtained by requiring $\Delta\log\mathcal{L} = +1.15$, while for the 95% C.L. contour curves $\Delta\log\mathcal{L} = +3.0$ is required. Since the results on the different parameters and parameter sets are obtained from the same data sets, they cannot be combined.

6.4 Results

We present results from the four LEP experiments on the various electroweak gauge boson couplings, and their combination. The charged TGC combination has been updated with the inclusion of recent results from ALEPH, L3 and OPAL. The neutral TGC results include an update of the f_i^V combinations, whilst the h_i^V combinations remain unchanged since our last note [120]. The results quoted for each individual experiment are calculated using the methods described in Section 6.3. Therefore they may differ slightly from those reported in the individual references, as the experiments in general use other methods to combine the data from different channels, and to include systematic uncertainties. In particular for the charged couplings, experiments using a combination method based on optimal observables (ALEPH, OPAL) obtain results with small differences compared to the values given by our combination technique. These small differences have been studied in Monte Carlo tests and are well understood [148]. For the h-coupling result from OPAL and DELPHI, a slightly modified estimate of the systematic uncertainty due to the theoretical cross section prediction is responsible for slightly different limits compared to the published results.

6.4.1 Charged Triple Gauge Boson Couplings

The individual analyses and results of the experiments for the charged couplings are described in [123–126].

Single-Parameter Analyses

The results of single-parameter fits from each experiment are shown in Table 6.1, where the errors include both statistical and systematic effects. The individual log $\mathcal{L}$ curves and their sum are shown in Figure 6.1. The results of the combination are given in Table 6.2. A list of the systematic errors treated as fully correlated between the LEP experiments, and their shift on the combined fit result are given in Table 6.3.

Two-Parameter Analyses

Contours at 68% and 95% confidence level for the combined two-parameter fits are shown in Figure 6.2. The numerical results of the combination are given in Table 6.4. The errors include both statistical and systematic effects.

Parameter	ALEPH	DELPHI	L3	OPAL
g_1^Z	$1.026^{+0.034}_{-0.033}$	$1.002^{+0.038}_{-0.040}$	$0.928^{+0.042}_{-0.041}$	$0.985^{+0.035}_{-0.034}$
κ_γ	$1.022^{+0.073}_{-0.072}$	$0.955^{+0.090}_{-0.086}$	$0.922^{+0.071}_{-0.069}$	$0.929^{+0.085}_{-0.081}$
λ_γ	$0.012^{+0.033}_{-0.032}$	$0.014^{+0.044}_{-0.042}$	$-0.058^{+0.047}_{-0.044}$	$-0.063^{+0.036}_{-0.036}$

Table 6.1: The measured central values and one standard deviation errors obtained by the four LEP experiments. In each case the parameter listed is varied while the remaining two are fixed to their Standard Model values. Both statistical and systematic errors are included. The values given here differ slightly from the ones quoted in the individual contributions from the four LEP experiments, as a different combination method is used. See text in section 6.3 for details.

Parameter	68% C.L.	95% C.L.
g_1^Z	$0.991^{+0.022}_{-0.021}$	[0.949, 1.034]
κ_γ	$0.984^{+0.042}_{-0.047}$	[0.895, 1.069]
λ_γ	$-0.016^{+0.021}_{-0.023}$	[−0.059, 0.026]

Table 6.2: The combined 68% C.L. errors and 95% C.L. intervals obtained combining the results from the four LEP experiments. In each case the parameter listed is varied while the other two are fixed to their Standard Model values. Both statistical and systematic errors are included.

Source	g_1^Z	λ_γ	κ_γ
$O(\alpha_{em})$ correction	0.010	0.010	0.020
σ_{WW} prediction	0.003	0.005	0.014
Hadronisation	0.004	0.002	0.004
Bose-Einstein Correlation	0.005	0.004	0.009
Colour Reconnection	0.005	0.004	0.010
$\sigma_{singleW}$ prediction	-	-	0.011

Table 6.3: The systematic uncertainties considered correlated between the LEP experiments in the charged TGC combination and their effect on the combined fit results.

Parameter	68% C.L.	95% C.L.	Correlations	
g_1^Z	$1.004^{+0.024}_{-0.025}$	[+0.954, +1.050]	1.00	+0.11
κ_γ	$0.984^{+0.049}_{-0.049}$	[+0.894, +1.084]	+0.11	1.00
g_1^Z	$1.024^{+0.029}_{-0.029}$	[+0.966, +1.081]	1.00	-0.40
λ_γ	$-0.036^{+0.029}_{-0.029}$	[−0.093, +0.022]	-0.40	1.00
κ_γ	$1.026^{+0.048}_{-0.051}$	[+0.928, +1.127]	1.00	+0.21
λ_γ	$-0.024^{+0.025}_{-0.021}$	[−0.068, +0.023]	+0.21	1.00

Table 6.4: The measured central values, one standard deviation errors and limits at 95% confidence level, obtained by combining the four LEP experiments for the two-parameter fits of the charged TGC parameters. Since the shape of the log-likelihood is not parabolic, there is some ambiguity in the definition of the correlation coefficients and the values quoted here are approximate. The listed parameters are varied while the remaining one is fixed to its Standard Model value. Both statistical and systematic errors are included.

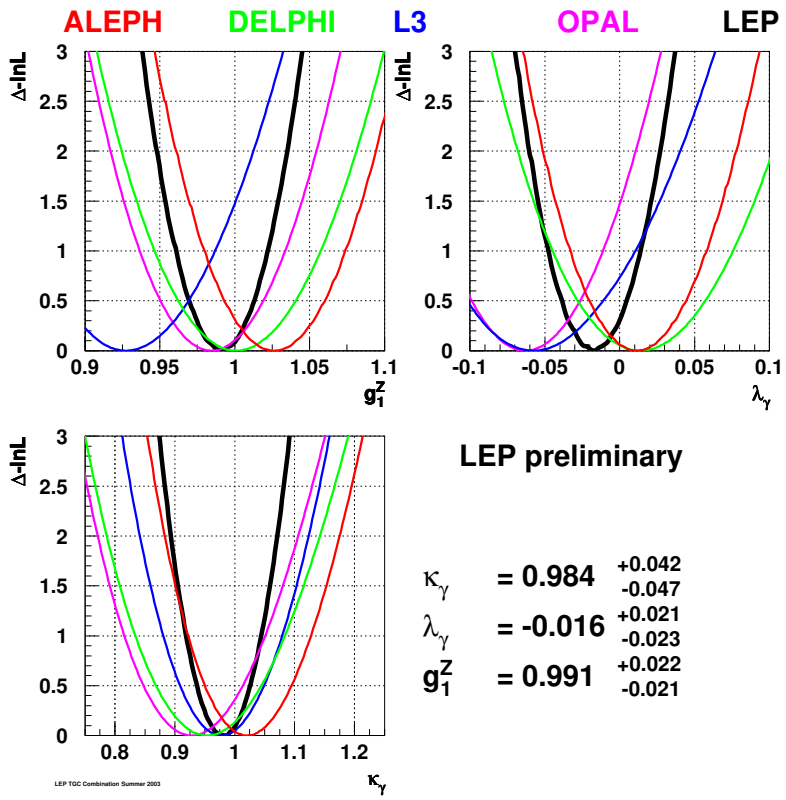

Figure 6.1: The log $\mathcal{L}$ curves of the four experiments (thin lines) and the LEP combined curve (thick line) for the three charged TGCs g_1^Z, κ_γ and λ_γ. In each case, the minimal value is subtracted.

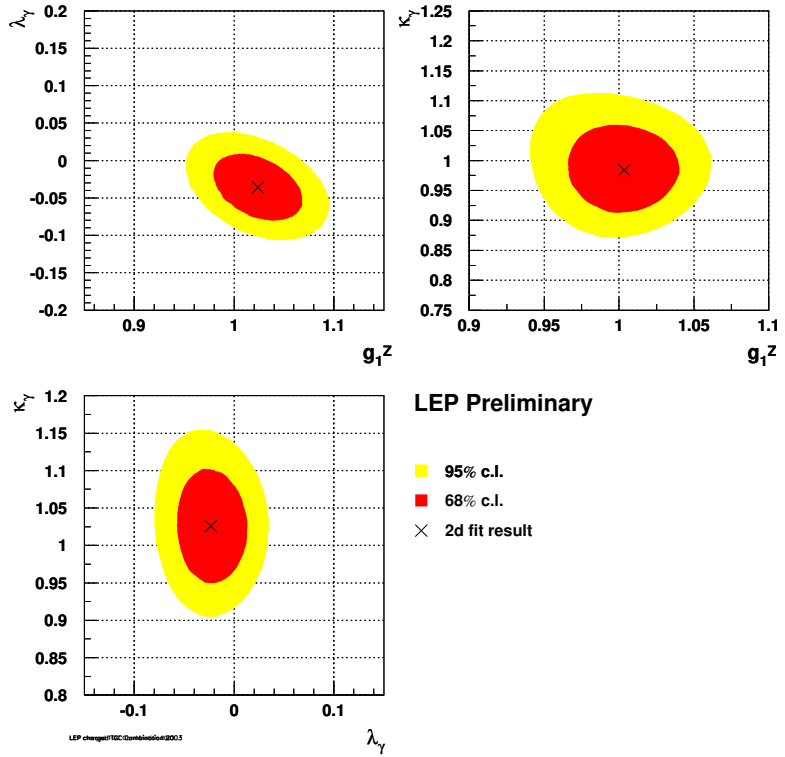

Figure 6.2: The 68% and 95% confidence level contours for the three two-parameter fits to the charged TGCs g_1^Z-λ_γ, g_1^Z-κ_γ and λ_γ-κ_γ. The fitted coupling value is indicated with a cross; the Standard Model value for each fit is in the centre of the grid. The contours include the contribution from systematic uncertainties.

6.4.2 Neutral Triple Gauge Boson Couplings in Zγ Production

The individual analyses and results of the experiments for the h-couplings are described in [137–140].

Single-Parameter Analyses

The results for each experiment are shown in Table 6.5, where the errors include both statistical and systematic uncertainties. The individual $\log \mathcal{L}$ curves and their sum are shown in Figures 6.3 and 6.4. The results of the combination are given in Table 6.6. From Figures 6.3 and 6.4 it is clear that the sensitivity of the L3 analysis [139] is the highest amongst the LEP experiments. This is partially due to the use of a larger phase space region, which increases the statistics by about a factor two, and partially due to additional information from using an optimal-observable technique.

Two-Parameter Analyses

The results for each experiment are shown in Table 6.7, where the errors include both statistical and systematic uncertainties. The 68% C.L. and 95% C.L. contour curves resulting from the combinations of the two-dimensional likelihood curves are shown in Figure 6.5. The LEP average values are given in Table 6.8.

Parameter	ALEPH	DELPHI	L3	OPAL
h_1^γ	$[-0.14, +0.14]$	$[-0.15, +0.15]$	$[-0.06, +0.06]$	$[-0.13, +0.13]$
h_2^γ	$[-0.07, +0.07]$	$[-0.09, +0.09]$	$[-0.053, +0.024]$	$[-0.089, +0.089]$
h_3^γ	$[-0.069, +0.037]$	$[-0.047, +0.047]$	$[-0.062, -0.014]$	$[-0.16, +0.00]$
h_4^γ	$[-0.020, +0.045]$	$[-0.032, +0.030]$	$[-0.004, +0.045]$	$[+0.01, +0.13]$
h_1^Z	$[-0.23, +0.23]$	$[-0.24, +0.25]$	$[-0.17, +0.16]$	$[-0.22, +0.22]$
h_2^Z	$[-0.12, +0.12]$	$[-0.14, +0.14]$	$[-0.10, +0.09]$	$[-0.15, +0.15]$
h_3^Z	$[-0.28, +0.19]$	$[-0.32, +0.18]$	$[-0.23, +0.11]$	$[-0.29, +0.14]$
h_4^Z	$[-0.10, +0.15]$	$[-0.12, +0.18]$	$[-0.08, +0.16]$	$[-0.09, +0.19]$

Table 6.5: The 95% C.L. intervals ($\Delta \log \mathcal{L} = 1.92$) measured by the ALEPH, DELPHI, L3 and OPAL. In each case the parameter listed is varied while the remaining ones are fixed to their Standard Model values. Both statistical and systematic uncertainties are included.

Parameter	95% C.L.
h_1^γ	$[-0.056, +0.055]$
h_2^γ	$[-0.045, +0.025]$
h_3^γ	$[-0.049, -0.008]$
h_4^γ	$[-0.002, +0.034]$
h_1^Z	$[-0.13, +0.13]$
h_2^Z	$[-0.078, +0.071]$
h_3^Z	$[-0.20, +0.07]$
h_4^Z	$[-0.05, +0.12]$

Table 6.6: The 95% C.L. intervals ($\Delta \log \mathcal{L} = 1.92$) obtained combining the results from the four experiments. In each case the parameter listed is varied while the remaining ones are fixed to their Standard Model values. Both statistical and systematic uncertainties are included.

Parameter	ALEPH	DELPHI	L3
h_1^γ	$[-0.32, +0.32]$	$[-0.28, +0.28]$	$[-0.17, +0.04]$
h_2^γ	$[-0.18, +0.18]$	$[-0.17, +0.18]$	$[-0.12, +0.02]$
h_3^γ	$[-0.17, +0.38]$	$[-0.48, +0.20]$	$[-0.09, +0.13]$
h_4^γ	$[-0.08, +0.29]$	$[-0.08, +0.15]$	$[-0.04, +0.11]$
h_1^Z	$[-0.54, +0.54]$	$[-0.45, +0.46]$	$[-0.48, +0.33]$
h_2^Z	$[-0.29, +0.30]$	$[-0.29, +0.29]$	$[-0.30, +0.22]$
h_3^Z	$[-0.58, +0.52]$	$[-0.57, +0.38]$	$[-0.43, +0.39]$
h_4^Z	$[-0.29, +0.31]$	$[-0.31, +0.28]$	$[-0.23, +0.28]$

Table 6.7: The 95% C.L. intervals ($\Delta \log \mathcal{L} = 1.92$) measured by ALEPH, DELPHI and L3. In each case the two parameters listed are varied while the remaining ones are fixed to their Standard Model values. Both statistical and systematic uncertainties are included.

Parameter	95% C.L.		Correlations	
h_1^γ	$[-0.16,$	$+0.05]$	1.00	$+0.79$
h_2^γ	$[-0.11,$	$+0.02]$	$+0.79$	1.00
h_3^γ	$[-0.08,$	$+0.14]$	1.00	$+0.97$
h_4^γ	$[-0.04,$	$+0.11]$	$+0.97$	1.00
h_1^Z	$[-0.35,$	$+0.28]$	1.00	$+0.77$
h_2^Z	$[-0.21,$	$+0.17]$	$+0.77$	1.00
h_3^Z	$[-0.37,$	$+0.29]$	1.00	$+0.76$
h_4^Z	$[-0.19,$	$+0.21]$	$+0.76$	1.00

Table 6.8: The 95% C.L. intervals ($\Delta \log \mathcal{L} = 1.92$) obtained combining the results from ALEPH, DELPHI and L3. In each case the two parameters listed are varied while the remaining ones are fixed to their Standard Model values. Both statistical and systematic uncertainties are included. Since the shape of the log-likelihood is not parabolic, there is some ambiguity in the definition of the correlation coefficients and the values quoted here are approximate.

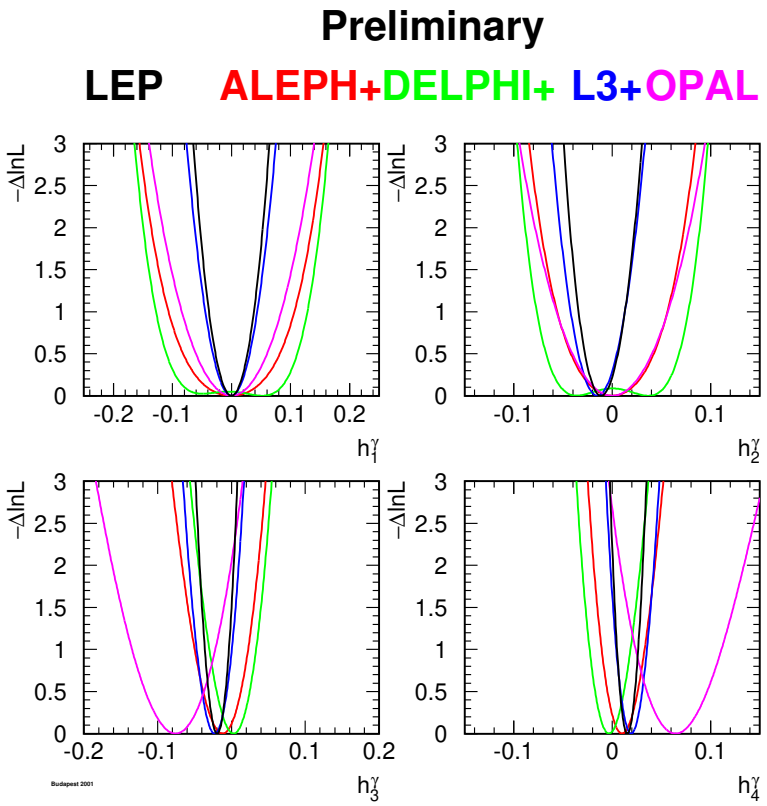

Figure 6.3: The $\log \mathcal{L}$ curves of the four experiments, and the LEP combined curve for the four neutral TGCs h_i^γ, $i = 1, 2, 3, 4$. In each case, the minimal value is subtracted.

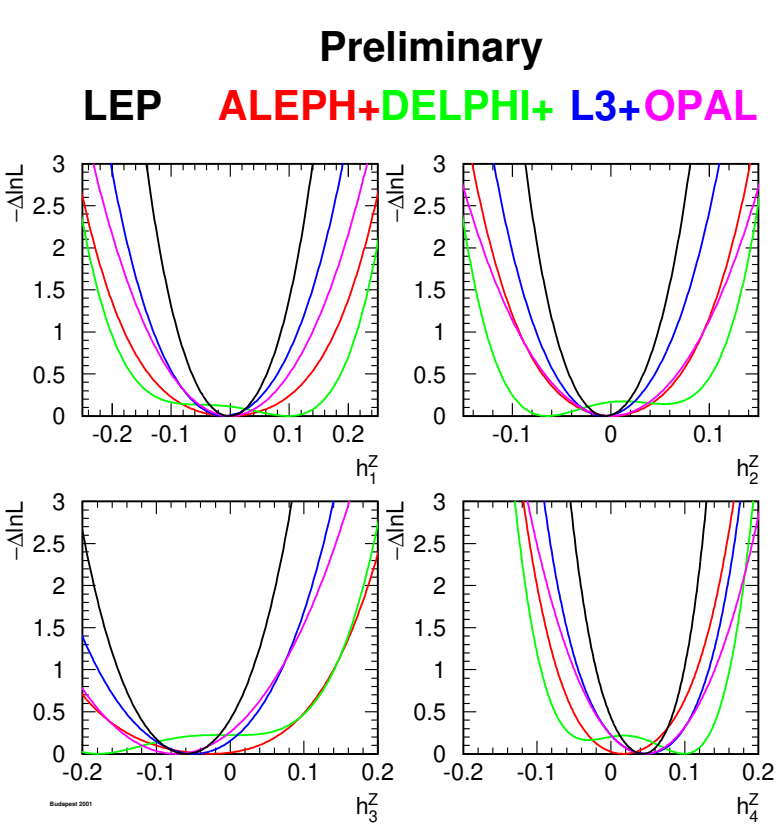

Figure 6.4: The log $\mathcal{L}$ curves of the four experiments, and the LEP combined curve for the four neutral TGCs h_i^Z, $i = 1,2,3,4$. In each case, the minimal value is subtracted.

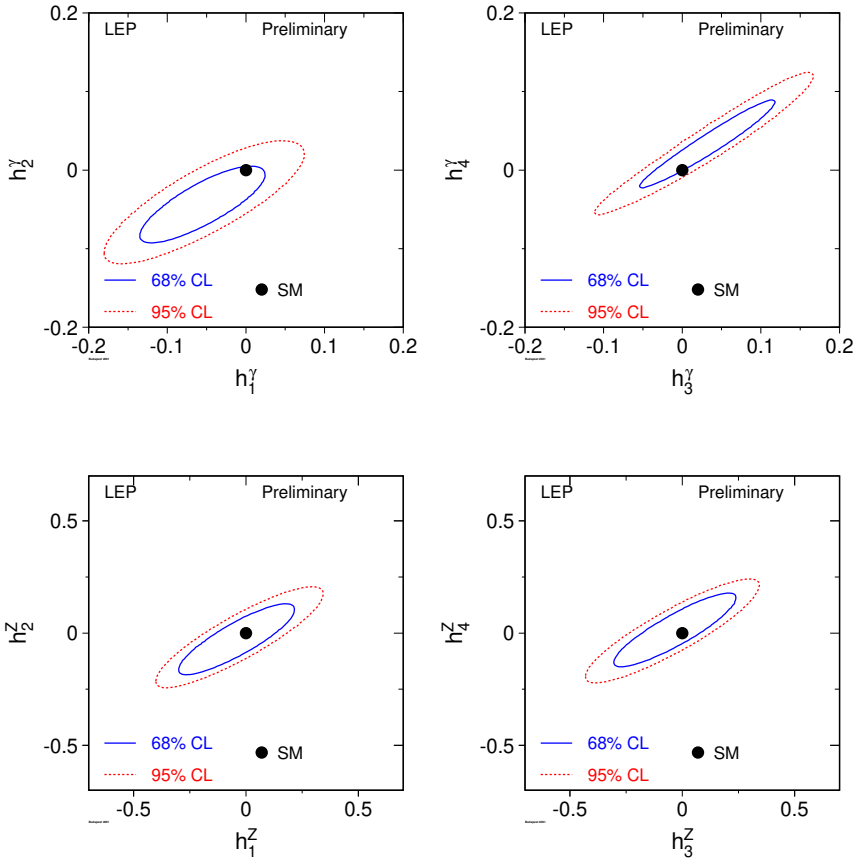

Figure 6.5: Contour curves of 68% C.L. and 95% C.L. in the planes (h_1^γ, h_2^γ), (h_3^γ, h_4^γ), (h_1^Z, h_2^Z) and (h_3^Z, h_4^Z) showing the LEP combined result.

6.4.3 Neutral Triple Gauge Boson Couplings in ZZ Production

The individual analyses and results of the experiments for the f-couplings are described in [137, 138, 141, 142].

Single-Parameter Analyses

The results for each experiment are shown in Table 6.9, where the errors include both statistical and systematic uncertainties. The individual $\log \mathcal{L}$ curves and their sum are shown in Figure 6.6. The results of the combination are given in Table 6.10.

Two-Parameter Analyses

The results from each experiment are shown in Table 6.11, where the errors include both statistical and systematic uncertainties. The 68% C.L. and 95% C.L. contour curves resulting from the combinations of the two-dimensional likelihood curves are shown in Figure 6.7. The LEP average values are given in Table 6.12.

Parameter	ALEPH	DELPHI	L3	OPAL
f_4^γ	$[-0.26, +0.26]$	$[-0.26, +0.28]$	$[-0.28, +0.28]$	$[-0.32, +0.33]$
f_4^Z	$[-0.44, +0.43]$	$[-0.49, +0.42]$	$[-0.48, +0.46]$	$[-0.45, +0.58]$
f_5^γ	$[-0.54, +0.56]$	$[-0.48, +0.61]$	$[-0.39, +0.47]$	$[-0.71, +0.59]$
f_5^Z	$[-0.73, +0.83]$	$[-0.42, +0.69]$	$[-0.35, +1.03]$	$[-0.94, +0.25]$

Table 6.9: The 95% C.L. intervals ($\Delta \log \mathcal{L} = 1.92$) measured by ALEPH, DELPHI, L3 and OPAL. In each case the parameter listed is varied while the remaining ones are fixed to their Standard Model values. Both statistical and systematic uncertainties are included.

Parameter	95% C.L.
f_4^γ	$[-0.17, +0.19]$
f_4^Z	$[-0.30, +0.30]$
f_5^γ	$[-0.32, +0.36]$
f_5^Z	$[-0.34, +0.38]$

Table 6.10: The 95% C.L. intervals ($\Delta \log \mathcal{L} = 1.92$) obtained combining the results from all four experiments. In each case the parameter listed is varied while the remaining ones are fixed to their Standard Model values. Both statistical and systematic uncertainties are included.

Parameter	ALEPH	DELPHI	L3	OPAL
f_4^γ	$[-0.26, +0.26]$	$[-0.26, +0.28]$	$[-0.28, +0.28]$	$[-0.32, +0.33]$
f_4^Z	$[-0.44, +0.43]$	$[-0.49, +0.42]$	$[-0.48, +0.46]$	$[-0.47, +0.58]$
f_5^γ	$[-0.52, +0.53]$	$[-0.52, +0.61]$	$[-0.52, +0.62]$	$[-0.67, +0.62]$
f_5^Z	$[-0.77, +0.86]$	$[-0.44, +0.69]$	$[-0.47, +1.39]$	$[-0.95, +0.33]$

Table 6.11: The 95% C.L. intervals ($\Delta \log \mathcal{L} = 1.92$) measured by ALEPH, DELPHI, L3 and OPAL. In each case the two parameters listed are varied while the remaining ones are fixed to their Standard Model values. Both statistical and systematic uncertainties are included.

Parameter	95% C.L.	Correlations	
f_4^γ	$[-0.17, +0.19]$	1.00	0.07
f_4^Z	$[-0.30, +0.29]$	0.07	1.00
f_5^γ	$[-0.34, +0.38]$	1.00	-0.17
f_5^Z	$[-0.38, +0.36]$	-0.17	1.00

Table 6.12: The 95% C.L. intervals ($\Delta \log \mathcal{L} = 1.92$) obtained combining the results from all four experiments. In each case the two parameters listed are varied while the remaining ones are fixed to their Standard Model values. Both statistical and systematic uncertainties are included. Since the shape of the log-likelihood is not parabolic, there is some ambiguity in the definition of the correlation coefficients and the values quoted here are approximate.

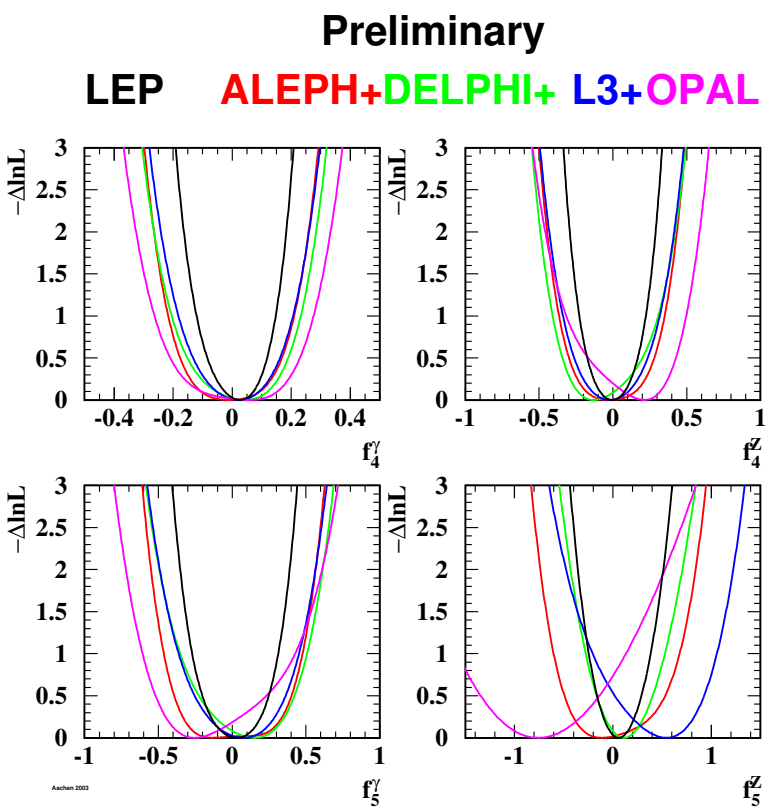

Figure 6.6: The log $\mathcal{L}$ curves of the four experiments, and the LEP combined curve for the four neutral TGCs f_i^V, $V = \gamma, Z$, $i = 4, 5$. In each case, the minimal value is subtracted.

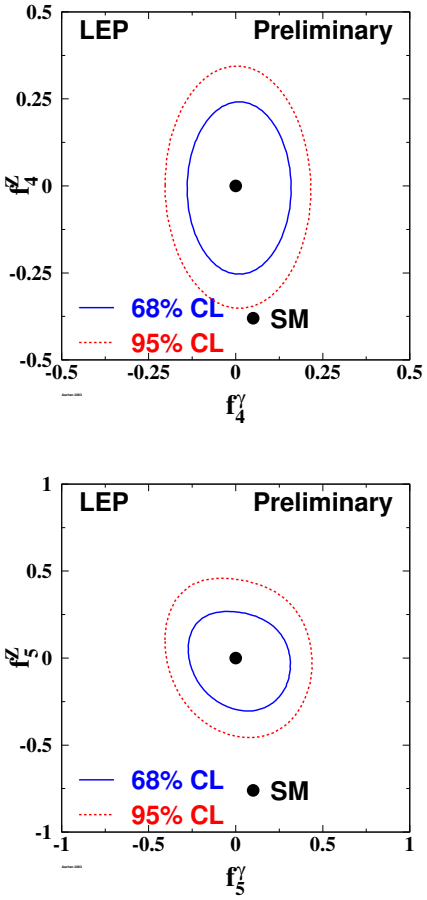

Figure 6.7: Contour curves of 68% C.L. and 95% C.L. in the plane (f_4^γ, f_4^Z) and (f_5^γ, f_5^Z) showing the LEP combined result.

6.4.4 Quartic Gauge Boson Couplings

The individual numerical results from the experiments participating in the combination, and the combined result are shown in Table 6.13. The corresponding $\log \mathcal{L}$ curves are shown in Figure 6.8. The errors include both statistical and systematic uncertainties.

Parameter	ALEPH	L3	OPAL	Combined
a_c/Λ^2	$[-0.041, +0.044]$	$[-0.037, +0.054]$	$[-0.045, +0.050]$	$[-0.029, +0.039]$
a_0/Λ^2	$[-0.012, +0.019]$	$[-0.014, +0.027]$	$[-0.012, +0.031]$	$[-0.008, +0.021]$

Table 6.13: The limits for the QGCs a_c/Λ^2 and a_0/Λ^2 associated with the ZZ$\gamma\gamma$ vertex at 95% confidence level for ALEPH, L3 and OPAL, and the LEP result obtained by combining them. Both statistical and systematic errors are included.

Conclusions

Combinations of charged and neutral triple gauge boson couplings, as well as quartic gauge boson couplings associated with the ZZ$\gamma\gamma$ vertex were made, based on results from the four LEP experiments ALEPH, DELPHI, L3 and OPAL. No significant deviation from the Standard Model prediction is seen for any of the electroweak gauge boson couplings studied. With the LEP-combined charged TGC results, the existence of triple gauge boson couplings among the electroweak gauge bosons is experimentally verified. As an example, these data allow the Kaluza-Klein theory [149], in which $\kappa_\gamma = -2$, to be excluded completely [150].

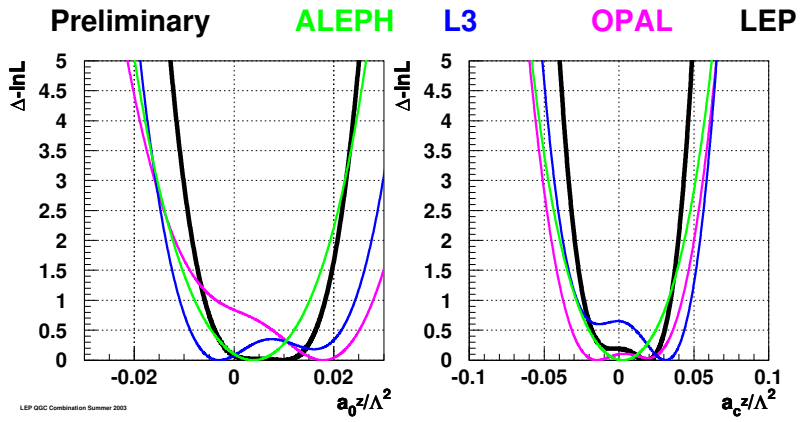

Figure 6.8: The $\log \mathcal{L}$ curves of L3 and OPAL (thin lines) and the combined curve (thick line) for the QGCs a_c/Λ^2 and a_0/Λ^2, associated with the ZZ$\gamma\gamma$ vertex. In each case, the minimal value is subtracted.

Chapter 7

Colour Reconnection in W-Pair Events

Updates with respect to summer 2005:
Unchanged w.r.t. summer 2002: Results are preliminary.
Note that some recent publications [151–153] are not yet included in this combination.

7.1 Introduction

In $W^+W^- \to q\bar{q}q\bar{q}$ events, the products of the two (colour singlet) W decays in general have a significant space-time overlap as the separation of their decay vertices, $\tau_W \sim 1/\Gamma_W \approx 0.1$ fm, is small compared to characteristic hadronic distance scales of ~ 1 fm. Colour reconnection, also known as colour rearrangement (CR), was first introduced in [154] and refers to a reorganisation of the colour flow between the two W bosons. A precedent is set for such effects by colour suppressed B meson decays, *e.g.* $B \to J/\psi K$, where there is "cross-talk" between the two original colour singlets, $\bar{c}$+s and c+spectator [154, 155].

QCD interference effects between the colour singlets in W^+W^- decays during the perturbative phase are expected to be small, affecting the W mass by $\sim (\frac{\alpha_S}{\pi N_{\text{colours}}})^2 \Gamma_W \sim \mathcal{O}(1\text{ MeV})$ [155]. In contrast, non-perturbative effects involving soft gluons with energies less than Γ_W may be significant, with effects on $m_W \sim \mathcal{O}(10\text{ MeV})$. To estimate the impact of this phenomenon a variety of phenomenological models have been developed [155–160], some of which are compared with data in this note.

Many observables have been considered in the search for an experimental signature of colour reconnection. The inclusive properties of events such as the mean charged particle multiplicity, distributions of thrust, rapidity, transverse momentum and $\ln(1/x_p)$ are found to have limited sensitivity [161–164]. The effects of CR are predicted to be numerically larger in these observables when only higher mass hadrons such as kaons and protons are considered [165]. However, experimental investigations [162,166] find no significant gain in sensitivity due to the low production rate of such species in W decays and the finite size of the data sample.

More recently, in analogy with the "string effect" analysis in 3-jet $e^+e^- \to q\bar{q}g$ events [167], the so-called "particle flow" method [168–170] has been investigated by all LEP collaborations [171–174]. In this, pairs of jets in $W^+W^- \to q\bar{q}q\bar{q}$ events are associated with the decay of a W, after which four jet-jet regions are chosen: two corresponding to jets sharing the same W parent (intra-W), and two

in which the parents differ (inter-W). As there is a two-fold ambiguity in the assignment of inter-W regions, the configuration having the smaller sum of inter-W angles is chosen.

Particles are projected onto the planes defined by these jet pairs and the particle density constructed as a function of ϕ, the projected angle relative to one jet in each plane. To account for the variation in the opening angles, ϕ_0, of the jet-jet pairs defining each plane, the particle densities in ϕ are constructed as functions of normalised angles, $\phi_r = \phi/\phi_0$, by a simple rescaling of the projected angles for each particle, event by event. Particles having projected angles ϕ smaller than ϕ_0 in at least one of the four planes are considered further. This gives particle densities, $\frac{1}{N_{\text{event}}}\frac{\mathrm{d}n}{\mathrm{d}\phi_r}$, in four regions with ϕ_r in the range 0–1, and where n and N_{event} are the number of particles and events, respectively.

As particle density reflects the colour flow in an event, CR models predict a change in the relative particle densities between inter-W and intra-W regions. On average, colour reconnection is expected to affect the particle densities of both inter-W regions in the same way and so they are added together, as are the two intra-W regions. The observable used to quantify such changes, R_N, is defined:

$$R_N = \frac{\frac{1}{N_{\text{event}}}\int_{0.2}^{0.8}\frac{\mathrm{d}n}{\mathrm{d}\phi_r}(\text{intra}-\text{W})\mathrm{d}\phi_r}{\frac{1}{N_{\text{event}}}\int_{0.2}^{0.8}\frac{\mathrm{d}n}{\mathrm{d}\phi_r}(\text{inter}-\text{W})\mathrm{d}\phi_r}\,. \tag{7.1}$$

As the effects of CR are expected to be enhanced for low momentum particles far from the jet axis, the range of integration excludes jet cores ($\phi_r \approx 0$ and $\phi_r \approx 1$). The precise upper and lower limits are optimised by model studies of predicted sensitivity.

Each LEP experiment has developed its own variation on this analysis, differing primarily in the selection of $W^+W^- \to q\bar{q}q\bar{q}$ events. In L3 [173] and DELPHI [172], events are selected in a very particular configuration ("topological selection") by imposing restrictions on the jet-jet angles and on the jet resolution parameter for the three- to four-jet transition (Durham or LUCLUS schemes). This selects events which are more planar than those in the inclusive $W^+W^- \to q\bar{q}q\bar{q}$ sample and the association between jet pairs and W's is given by the relative angular separation of the jets. The overall efficiency for selecting events is $\sim 15\%$. The ALEPH [171] and OPAL [174] event selections are based on their W mass analyses. Assignment of pairs of jets to W's also follows that used in measuring m_W, using either a 4-jet matrix element [175] or a multivariate algorithm [176]. These latter selections have much higher efficiencies, varying from 45% to 90%, but lead to samples of events having a less planar topology and hence a more complicated colour flow. ALEPH also uses the topological selection for consistency checks.

The data are corrected bin-by-bin for background contamination in the inter-W and intra-W regions separately. The possibility of CR effects existing in background processes, such as $ZZ \to q\bar{q}q\bar{q}$, is neglected. Since the data are not corrected for the effects of event selection, momentum resolution and finite acceptance, the values of R_N measured by the experiments cannot be compared directly with one another. However, it is possible to perform a relative comparison by using a common sample of Monte Carlo events, processed using the detector simulation program of each experiment.

7.2 Combination Procedure

The measured values of R_N can be compared after they have been normalised using a common sample of events, processed using the detector simulation and particle flow analysis of each experiment. A variable, r, is constructed:

$$r = \frac{R_N^{\text{data}}}{R_N^{\text{no-CR}}}\,, \tag{7.2}$$

where $R_N^{\rm data}$ and $R_N^{\rm no-CR}$ are the values of R_N measured by each experiment in data and in a common sample of events without CR. In the absence of CR, all experiments should find r consistent with unity. The default no-CR sample used for this normalisation consists of $e^+e^- \to W^+W^-$ events produced using the KORALW [177] event generator and hadronised using either the JETSET [178], ARIADNE [179] or HERWIG [157] model depending on the colour reconnection model being tested. Input from experiments used to perform the combination is given in terms of R_N and detailed in Appendix B.1.

7.2.1 Weights

The statistical precision of R_N measured by the experiments does not reflect directly the sensitivity to CR, for example the measurements of ALEPH and OPAL have efficiencies several times larger than the topological selections of L3 and DELPHI, yet only yield comparable sensitivity. The relative sensitivity of the experiments may also be model dependent. Therefore, results are averaged using model dependent weights, *i.e.*

$$w_i = \frac{(R_N^i - R_N^{i,\rm no-CR})^2}{\sigma^2_{R_N}(\text{stat.}) + \sigma^2_{R_N}(\text{syst.})}\,, \tag{7.3}$$

where R_N^i and $R_N^{i,\rm no-CR}$ represent the R_N values for CR model i and its corresponding no-CR scenario, and $\sigma^2_{R_N}$ are the total statistical and systematic uncertainties. To test models, R_N values using common samples are provided by experiments for each of the following models:

1. SK-I, 100% reconnected (KORALW + JETSET),
2. ARIADNE-II, inter-W reconnection rate about 22% (KORALW + ARIADNE),
3. HERWIG CR, reconnected fraction $\frac{1}{9}$ (KORALW + HERWIG).

Samples in parentheses are the corresponding no-CR scenarios used to define w_i. In each case, KORALW is used to generate the events at least up to the four-fermion level. These special Monte Carlo samples (called "Cetraro" samples) have been generated with the ALEPH tuned parameters, obtained with hadronic Z decays, and have been processed through the detector simulation of each experiment.

7.2.2 Combination of centre-of-mass energies

The common files required to perform the combination are only available at a single centre-of-mass energy ($E_{\rm cm}$) of 188.6 GeV. The data from the experiments can only therefore be combined at this energy. The procedure adopted to combine all LEP data is summarised below.

R_N is measured in each experiment at each centre-of-mass energy, in both data and Monte Carlo. The predicted variation of R_N with centre-of-mass energy is determined separately by each experiment using its own samples of simulated $e^+e^- \to W^+W^-$ events, with hadronisation performed using the no-CR JETSET model. This variation is parametrised by fitting a polynomial to these simulated R_N. The R_N measured in data are subsequently extrapolated to the reference energy of 189 GeV using this function, and the weighted average of the rescaled values in each experiment is used as input to the combination.

7.3 Systematics

The sources of potential systematic uncertainty identified are separated into those which are correlated between experiments and those which are not. For correlated sources, the component correlated between all experiments is assigned as the smallest uncertainty found in any single experiment, with the quadrature remainder treated as an uncorrelated contribution. Preliminary estimates of the dominant systematics on R_N are given in Appendix B.1 for each experiment, and described below.

7.3.1 Hadronisation

This is assigned by comparison of the single sample of W^+W^- events generated using KORALW, and hadronised with three different models, *i.e.* JETSET, HERWIG and ARIADNE. The systematic is assigned as the spread of the R_N values obtained when using the various models given in Appendix B.1. This is treated as a correlated uncertainty.

7.3.2 Bose-Einstein Correlations

Although a recent analysis by DELPHI reports the observation of inter-W Bose-Einstein correlation (BEC) in $W^+W^- \to q\bar{q}q\bar{q}$ events with a significance of 2.9 standard deviations for like-sign pairs and 1.9 standard deviations for unlike-sign pairs [180], analyses by other collaborations [181–183] find no significant evidence for such effects, see also chapter 8. Therefore, BEC effects are only considered within each W separately. The estimated uncertainty is assigned, using common MC samples, as the difference in R_N between an intra-W BEC sample and the corresponding no-BEC sample. This is treated as correlated between experiments.

7.3.3 Background

Background is dominated by the $e^+e^- \to q\bar{q}$ process, with a smaller contribution from $ZZ \to q\bar{q}q\bar{q}$ diagrams. As no common background samples exist, apart from dedicated ones for BEC analyses, experiment specific samples are used. The uncertainty is defined as the difference in the R_N value relative to that obtained using the default background model and assumed cross-sections in each experiment.

$e^+e^- \to q\bar{q}$

The systematic is separated into two components, one accounting for the shape of the background, the other for the uncertainty in the value of the background cross-section, $\sigma(e^+e^- \to q\bar{q})$.

Uncertainty in the shape is estimated by comparing hadronisation models. Experiments typically have large samples simulated using 2-fermion event generators hadronised with various models. This uncertainty is assigned as $\pm\frac{1}{2}$ of the largest difference between any pair of hadronisation models and treated as uncorrelated between experiments.

The second uncertainty arises due to the accuracy of the experimentally measured cross-sections. The systematic is assigned as the larger of the deviations in R_N caused when $\sigma(e^+e^- \to q\bar{q})$ is varied

by $\pm 10\%$ from its default value. This variation was based on the conclusions of a study comparing four-jet data with models [184], and is significantly larger than the $\sim 1\%$ uncertainty in the inclusive $e^+e^- \to q\bar{q}$ ($\sqrt{s'/s} > 0.85$) cross-section measured by the LEP-II 2-fermion group. It is treated as correlated between experiments.

$ZZ \to q\bar{q}q\bar{q}$

Similarly to the $e^+e^- \to q\bar{q}$ case, this background cross-section is varied by $\pm 15\%$. For comparison, the uncertainty on $\sigma(ZZ)$ measured by the LEP-II 4-fermion group is $\sim 11\%$ at $\sqrt{s} \simeq 189$ GeV. It is treated as correlated between experiments.

$W^+W^- \to q\bar{q}\ell\nu_\ell$

Semi-leptonic WW decays which are incorrectly identified as $W^+W^- \to q\bar{q}q\bar{q}$ events are the third main category of background, and its contribution is very small. The fraction of $W^+W^- \to q\bar{q}\ell\nu_\ell$ events present in the sample used for the particle flow analysis varies in the range 0.04–2.2% between the experiments. The uncertainty in this background consists of hadronisation effects and also uncertainty in the cross-section. As this source is a very small background relative to those discussed above, and the effect of either varying the cross-section by its measured uncertainty or of changing the hadronisation model do not change the measured R_N significantly, this source is neglected.

7.3.4 Detector Effects

The data are not corrected for the effects of finite resolution or acceptance. Various studies have been carried out, e.g. by analysing $W^+W^- \to q\bar{q}\ell\nu_\ell$ events in the same way as $W^+W^- \to q\bar{q}q\bar{q}$ events in order to validate the method and the choice of energy flow objects used to measure the particle yields between jets [173]. To take into account the effects of detector resolution and acceptance, ALEPH, L3 and OPAL have studied the impact of changing the object definition entering the particle flow distributions and have assigned a systematic error from the difference in the measured R_N.

7.3.5 Centre-of-mass energy dependence

As there may be model dependence in the parametrised energy dependence, the second order polynomial used to perform the extrapolation to the reference energy of 189 GeV is usually determined using several different models, with and without colour reconnection. DELPHI, L3 and OPAL use differences relative to the default no-CR model to assign a systematic uncertainty while ALEPH takes the spread of the results obtained with all the models with and without CR which have been used. This error is assumed to be uncorrelated between experiments.

7.3.6 Weighting function

The weighting function of Equation 7.3 could justifiably be modified such that only the uncorrelated components of the systematic uncertainty appear in the denominator. To accommodate this, the

average is performed using both variants of the weighting function. This has an insignificant effect on the consistency between data and model under test, e.g. for SK-I the result is changed by 0.02 standard deviations, and this effect is therefore neglected.

7.4 Combined Results

Experiments provide their results in the form of R_N (or changes to R_N) at a reference centre-of-mass energy of 189 GeV by scaling results obtained at various energies using the predicted energy dependence of their own no-CR MC samples. This avoids having to generate common samples at multiple centre-of-mass energies.

The detailed results from all experiments are included in Appendix B.1. These consist of preliminary results, taken from the publicly available notes [171–174], and additional information from analysis of Monte Carlo samples. The averaging procedure itself is carried out by each of the experiments and good agreement is obtained.

An example of this averaging to test an extreme scenario of the SK-I CR model (full reconnection) is given in Appendix B.2. The average obtained in this case is:

$$r(data) = 0.969 \pm 0.011(\text{stat.}) \pm 0.009(\text{syst. corr.}) \pm 0.006(\text{syst. uncorr.}), \quad (7.4)$$

$$r(\text{SK-I } 100\%) = 0.8909. \quad (7.5)$$

The measurements of each experiment and this combined result are shown in Figure 7.1. As the sensitivity of the analysis is different for each experiment, the value of r predicted by the SK-I model is indicated separately for each experiment by a dashed line in the figure. Thus the data disagree with the extreme scenario of this particular model at a level of 5.2 standard deviations. The data from the four experiments are consistent with each other and tend to prefer an intermediate colour reconnection scenario rather than the no colour reconnection one at the level of 2.2 standard deviations in the SK-I framework.

7.4.1 Parameter space in SK-I model

In the SK-I model, the reconnection probability is governed by an arbitrary, free parameter, k_I. By comparing the data with model predictions evaluated at a variety of k_I values, it is possible to determine the reconnection probability that is most consistent with data, which can in turn be used to estimate the corresponding bias in the measured m_W. By repeating the averaging procedure using model inputs for the set of k_I values given in Table B.2, including a re-evaluation of the weights for each value of k_I, it is found that the data prefer a value of $k_I = 1.18$ as shown in Figure 7.2. The 68% confidence level lower and upper limits are 0.39 and 2.13 respectively. The LEP averages in r obtained for the different k_I values are summarised in Table B.4. They correspond to a preferred reconnection probability of 49% in this model at 189 GeV as illustrated in Figure 7.3.

The small variations observed in the LEP average value of r and its corresponding error as a function of k_I (or P_{reco}) are essentially due to changes in the relative weighting of the experiments.

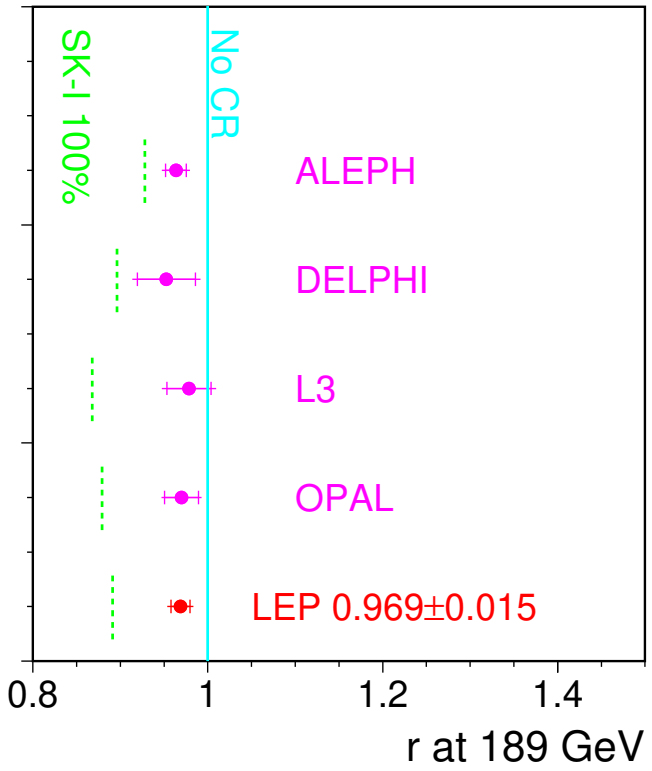

Figure 7.1: Preliminary particle flow results using all data, combined to test the limiting case of the SK-I model in which more than 99.9% of the events are colour reconnected. The error bars correspond to the total error with the inner part showing the statistical uncertainty. The predicted values of r for this CR model are indicated separately for the analysis of each experiment by dashed lines.

7.4.2 ARIADNE and HERWIG models

The combination procedure has been applied to common samples of ARIADNE and HERWIG Monte Carlo models. The R_N average values obtained with these models based on their respective predicted sensitivity are summarised in Table B.5. The four experiments have observed a weak sensitivity to these colour reconnected samples with the particle flow analysis, as can be seen from Figure 7.4.

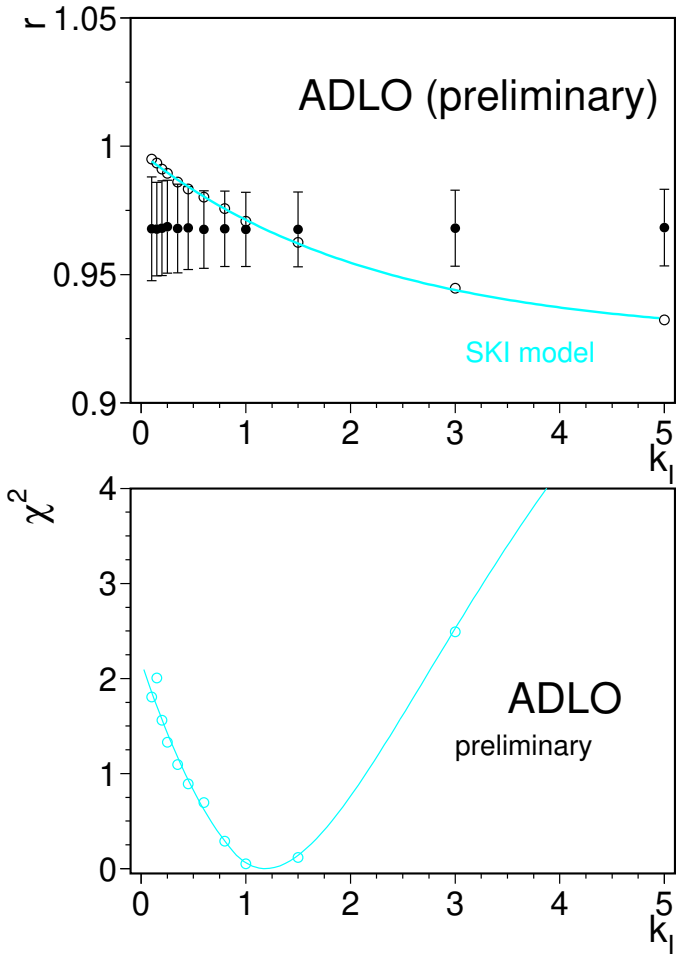

Figure 7.2: Comparison of the LEP average r values with the SK-I model prediction obtained as a function of the k_I parameter. The comparisons are performed after extrapolation of data to the reference centre-of-mass energy of 189 GeV. In the upper plot, the solid line is the result of fitting a function of the form $r(k_I) = p_1(1 - exp(-p_2 k_I)) + p_3$ to the MC predictions. The lower plot shows the corresponding χ^2 curve obtained from this comparison. The best agreement between the model and the data is obtained when $k_I = 1.18$.

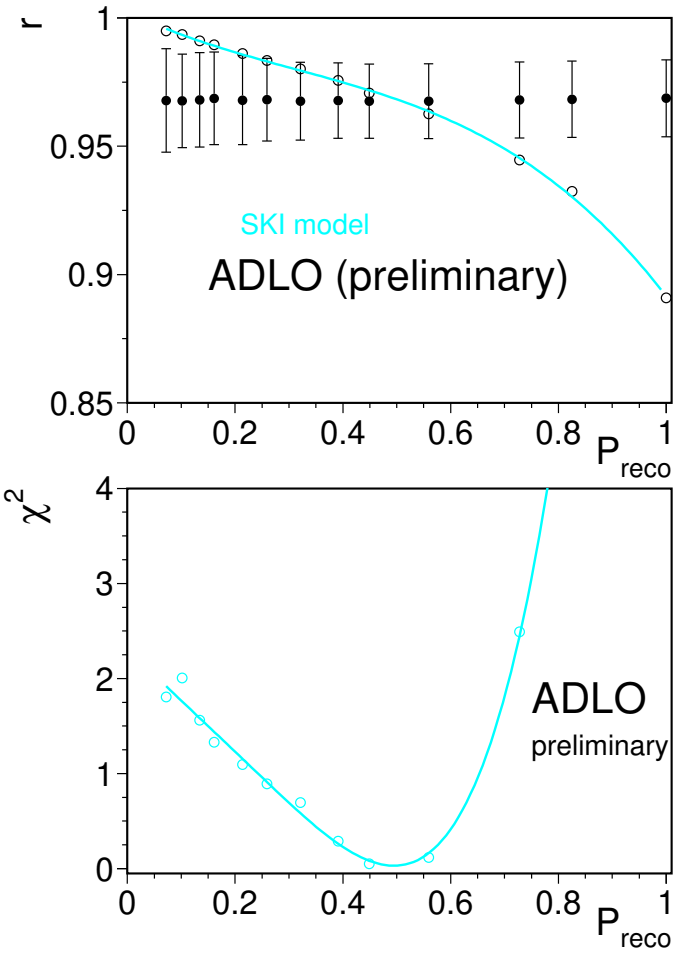

Figure 7.3: Comparison of the LEP average r values with the SK-I model prediction obtained as a function of the reconnection probability. In the upper plot, the solid line is the result of fitting a third order polynomial function to the MC predictions. The lower plot shows a χ^2 curve obtained from this comparison using all LEP data at the reference centre-of-mass energy of 189 GeV. The best agreement between the model and the data is obtained when 49% of events are reconnected in this model.

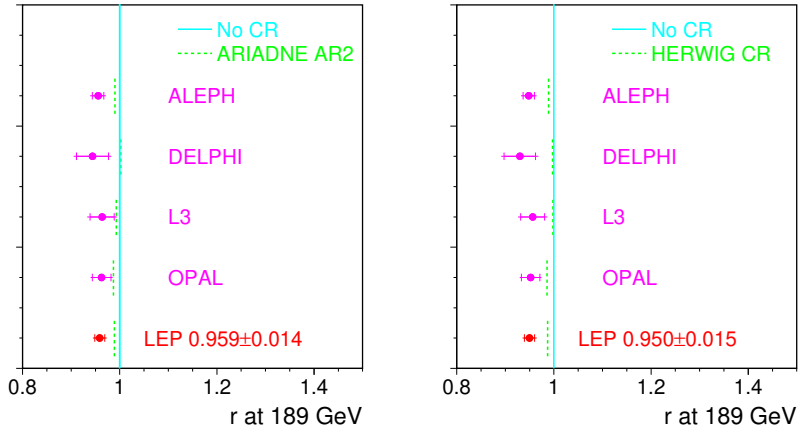

Figure 7.4: Preliminary particle flow results using all data, combined to test the ARIADNE and HERWIG colour reconnection models, based on the predicted sensitivity. The predicted values of r for this CR model are indicated separately for the analysis of each experiment by dashed lines.

7.5 Summary

A first, preliminary combination of the LEP particle flow results is presented, using the entire LEP-II data sample. The data disfavour by 5.2 standard deviations an extreme version of the SK-I model in which colour reconnection has been forced to occur in essentially all events. The combination procedure has been generalised to the SK-I model as a function of its variable reconnection probability. The combined data are described best by the model where 49% of events at 189 GeV are reconnected, corresponding to $k_I = 1.18$. The LEP data, averaged using weights corresponding to $k_I = 1.0$, *i.e.* closest to the optimal fit, do not exclude the no colour reconnection hypothesis, deviating from it by 2.2 standard deviations. A 68% confidence level range has been determined for k_I and corresponds to [0.39,2.13].

For both the ARIADNE and HERWIG models, which do not contain adjustable colour reconnection parameters, differences between the results of the colour reconnected and the no-CR scenarios are small and do not allow the particle flow analysis to discriminate between them. To test consistency between data and the no-CR models, the data are averaged using weights where the factor accounting for predicted sensitivity to a given CR model has been set to unity. The R_N values obtained with the no colour reconnection HERWIG and ARIADNE models, using the common Cetraro samples, differ from the measured data value by 3.7 and 3.1 standard deviations.

The observed deviations of the R_N values from all no colour reconnection models may indicate a possible systematic effect in the description of particle flow for 4-jet events. Independent studies of particle flow in WW semileptonic events as well as other CR-oriented analyses are required to investigate this.

Chapter 8

Bose-Einstein Correlations in W-Pair Events

Updates with respect to summer 2005:
Unchanged w.r.t. summer 2005: All results as well as the combinations are final.

8.1 Introduction

The LEP experiments have measured the strength of particle correlations between two hadronic systems obtained from W-pair decay occuring close in space-time at LEP-II. The work presented in this chapter is focused on so-called Bose-Einstein (BE) correlations, i.e., the enhanced probability of production of pairs (multiplets) of identical mesons close together in phase space. The effect is readily observed in particle physics, in particular in hadronic decays of the Z boson, and is qualitatively understood as a result of quantum-mechanical interference originating from the symmetry of the amplitude of the particle production process under exchange of identical mesons.

The presence of correlations between hadrons coming from the decay of a W^+W^- pair, in particular those between hadrons originating from different Ws, can affect the direct reconstruction of the mass of the initial W bosons. The measurement of the strength of these correlations can be used for the estimation of the systematic uncertainty of the W mass measurement.

8.2 Method

The principal method [185], called "mixing method", used in this measurement is based on the direct comparison of 2-particle spectra of genuine hadronic WW events $WW \to q\bar{q}q\bar{q}$ and of mixed WW events. The latter are constructed by mixing the hadronic parts of two semileptonic WW events $WW \to q\bar{q}\ell\nu$ (first used in [186]). Such a reference sample has the advantage of reproducing the correlations between particles belonging to the same W, while the particles from different Ws are uncorrelated by construction.

This method gives a model-independent estimate of the interplay between the two hadronic systems, for which BE correlations and also colour reconnection are considered as dominant sources. The possibility of establishing the strength of inter-W correlations in a model-independent way is rather unique; most correlations do carry an inherent model dependence on the reference sample. In the present measurement, the model dependence is limited to the background subtraction.

8.3 Distributions

The two-particle correlations are evaluated using two-particle densities defined in terms of the 4-momentum transfer $Q = \sqrt{-(p_1 - p_2)^2}$, where p_1, p_2 are the 4-momenta of the two particles:

$$\rho_2(Q) = \frac{1}{N_{ev}} \frac{dn_{pair\,s}}{dQ} \tag{8.1}$$

Here $n_{pair\,s}$ stands for the number of like-sign (unlike-sign) 2-particle permutations.[1] In the case of two stochastically independent hadronically decaying W bosons the two-particle inclusive density is given by:

$$\rho_2^{WW} = \rho_2^{W^+} + \rho_2^{W^-} + 2\rho_2^{mix}, \tag{8.2}$$

where ρ_2^{mix} can be expressed via the single-particle inclusive density $\rho_1(p)$ as:

$$\rho_2^{mix}(Q) = \int d^4p_1\, d^4p_2 \rho^{W^+}(p_1)\rho^{W^-}(p_2)\delta(Q^2 + (p_1 - p_2)^2)\delta(p_1^2 - m_\pi^2)\delta(p_2^2 - m_\pi^2). \tag{8.3}$$

Assuming further that:

$$\rho_2^{W^+}(Q) = \rho_2^{W^-}(Q) = \rho_2^{W}(Q), \tag{8.4}$$

we obtain for the case of two stochastically independent hadronically decaying W bosons:

$$\rho_2^{WW}(Q) = 2\rho_2^{W}(Q) + 2\rho_2^{mix}(Q). \tag{8.5}$$

In the mixing method, we obtain ρ_2^{mix} by combining two hadronic W systems from two different semileptonic WW events. The direct search for inter-W BE correlations is done using the difference of 2-particle densities:

$$\Delta\rho(Q) = \rho_2^{WW}(Q) - 2\rho_2^{W}(Q) - 2\rho_2^{mix}(Q), \tag{8.6}$$

or, alternatively, their ratio:

$$D(Q) = \frac{\rho_2^{WW}(Q)}{2\rho_2^{W}(Q) + 2\rho^{mix}(Q)} = 1 + \frac{\Delta\rho(Q)}{2\rho_2^{W}(Q) + 2\rho^{mix}(Q)}. \tag{8.7}$$

Given the definition of the genuine inter-W correlations function $\delta_I(Q)$ [187], it can be shown that

$$\delta_I(Q) = \frac{\Delta\rho(Q)}{2\rho_2^{mix}(Q)}. \tag{8.8}$$

To disentangle the BE correlation effects from other possible correlation sources (such as energy-momentum conservation or color reconnection), which are supposed to be the same for like-sign and unlike-sign charge pairs, we analyze the double difference,

$$\delta\rho(Q) = \Delta\rho^{like-sign}(Q) - \Delta\rho^{unlike-sign}(Q), \tag{8.9}$$

or the double ratio,

$$d(Q) = D^{like-sign}(Q)/D^{unlike-sign}(Q). \tag{8.10}$$

The event mixing procedure may introduce artificial distortions, or may not fully account for some detector effects or for correlations other than BE correlations. Most of these possible effects are

[1] For historical reasons, the number of particle permutations rather than combinations is used in formulas. For the same reason, a factor 2 appears in front of ρ_2^{mix} in Eq. 8.2. The experimental statistical errors are, however, based on the number of particle pairs, i.e., 2-particle combinations.

simulated in the Monte Carlo without inter-W BE correlations. Therefore they are reduced by using the double ratio or the double difference:

$$D'(Q) \;=\; \frac{D(Q)_{data}}{D(Q)_{MC,nointer}} \;, \qquad \Delta\rho'(Q) \;=\; \Delta\rho(Q)_{data} - \Delta\rho(Q)_{MC,nointer} \;, \tag{8.11}$$

where $D(Q)_{MC,nointer}$ and $\Delta\rho(Q)_{MC,nointer}$ are derived from a MC without inter-W BE correlations.

In addition to the mixing method, ALEPH [188] also uses the double ratio of like-sign pairs ($N_\pi^{++,--}(Q)$) and unlike-sign pairs $N_\pi^{+-}(Q)$ corrected with Monte-Carlo simulations not including BE effects:

$$R^*(Q) \;=\; \left(\frac{N_\pi^{++,--}(Q)}{N_\pi^{+-}(Q)}\right)^{data} \Bigg/ \left(\frac{N_\pi^{++,--}(Q)}{N_\pi^{+-}(Q)}\right)^{MC}_{noBE} . \tag{8.12}$$

In case of $\Delta\rho(Q)$, $\delta\rho(Q)$ or $\delta_I(Q)$, we look for a deviation from 0, while in case of $D(Q)$, $D'(Q)$, $d(Q)$ or $R^*(Q)$, inter-W BE correlations would manifest themselves by deviation from 1.

8.4 Results

The four LEP experiments have published results applying the mixing method to the full LEP-II data sample. As examples, the distributions of $\Delta\rho'$ measured by ALEPH [189], δ_I measured by DELPHI [190], D and D' measured by L3 [182] and D measured by OPAL [191] are shown in Figures 8.1, 8.2, 8.3 and 8.4, respectively. In addition ALEPH have published results using R^* variable [188]. The centre-of-mass energies, luminosities and the number of events collected by different measurements are shown in Table 8.1.

	$\sqrt{s}$	luminosity	number of events	
	[GeV]	[pb^{-1}]	WW $\to$ q$\bar{\text{q}}$q$\bar{\text{q}}$	WW $\to$ q$\bar{\text{q}}\ell\nu$
ALEPH	183-209	683	6155	4849
DELPHI	189-209	550	3252	2567
L3	189-209	629	5100	3800
OPAL	183-209	680	4470	4533
ALEPH R*	172-189	242	2021	-

Table 8.1: The centre-of-mass energies, luminosities and the number of events collected by different measurements.

A simple combination procedure is available through a χ^2 average of the numerical results of each experiment [182,188–191] with respect to a specific BE model under study, here based on comparisons with various tuned versions of the LUBOEI model [192,193]. The tuning is performed by adjusting the parameters of the model to reproduce correlations in samples of Z and semileptonic W decays, and applying identical parameters to the modelling of inter-W correlations (so-called "fullBE" scenario). In this way the tuning of each experiment takes into account detector systematics in the track measurements.

An important advantage of the combination procedure used here is that it allows the combination of results obtained using different analyses. The combination procedure assumes a linear dependence of the observed size of BE correlations on various estimators used to analyse the different distributions. It is also verified that there is a linear dependence between the measured W mass shift and the

	data–noBE	stat.	syst.	corr. syst.	fullBE–noBE	Ref.
ALEPH (fit to D')	**-0.004**	**0.011**	**0.014**	**0.003**	**0.081**	[189]
ALEPH (integral of $\Delta\rho$)	-0.127	0.143	0.199	0.044	0.699	[189]
ALEPH (fit to R^*)	-0.004	0.0062	0.0036	negligible	0.0177	[188]
DELPHI (fit to δ_I)	**$+0.72$**	**0.29**	**0.17**	**0.070**	**1.40**	[190]
L3 (fit to D')	**$+0.008$**	**0.018**	**0.012**	**0.0042**	**0.103**	[182]
L3 (integral of $\Delta\rho$)	$+0.03$	0.33	0.15	0.055	1.38	[182]
OPAL (integral of $\Delta\rho$)	-0.01	0.27	0.23	0.06	0.77	[191]
OPAL (fit to D)	**$+0.040$**	**0.038**	**0.038**	**0.017**	**0.120**	[191]
OPAL (fit to D')	$+0.042$	0.042	0.047	0.019	0.123	[191]
OPAL (fit to d)	-0.017	0.055	0.050	0.003	0.133	[191]

Table 8.2: An overview of the input values from different measurements: the difference between the measured correlations and the model without inter-W correlations (data–noBE), the corresponding statistical (stat.) and total systematic (syst.) errors, the correlated systematic error contribution (corr. syst.), and the difference between "fullBE" and "noBE" scenario. The measurements used in the combination are highlighted.

	fraction of the model	stat.	syst.
ALEPH (fit to D')	**-0.05**	**0.14**	**0.17**
ALEPH (integral of $\Delta\rho$)	-0.18	0.20	0.28
ALEPH (fit to R^*)	-0.23	0.35	0.20
DELPHI (fit to δ_I)	**$+0.51$**	**0.21**	**0.12**
L3 (fit to D')	**$+0.08$**	**0.17**	**0.12**
L3 (integral of $\Delta\rho$)	$+0.02$	0.24	0.11
OPAL (integral of $\Delta\rho$)	-0.01	0.35	0.30
OPAL (fit to D)	**$+0.33$**	**0.32**	**0.32**
OPAL (fit to D')	$+0.34$	0.34	0.38
OPAL (fit to d)	-0.13	0.41	0.38

Table 8.3: The measured size of correlations expressed as the relative fraction of the model with inter-W correlations (see Eq. 8.13 and Table 8.2). The measurements used in the combination are highlighted.

values of these estimators [194]. The estimators are: the integral of the $\Delta\rho(Q)$ distribution (ALEPH, L3, OPAL); the parameter Λ when fitting the function $N(1+\delta Q)(1+\Lambda\exp(-k^2Q^2))$ to the $D'(Q)$ distribution, with N fixed to unity (L3), or δ fixed to zero and k fixed to the value obtained from a fit to the full BE sample (ALEPH); the parameter Λ when fitting the function $N(1+\delta Q)(1+\Lambda\exp(-Q/R))$ to the $D(Q)$, $D(Q)'$ and d distributions, with R fixed to the value obtained from a fit to the full BE sample (OPAL); the parameter Λ when fitting the function $\Lambda\exp(-RQ)(1+\epsilon RQ)+\delta(1+\frac{\rho_2^W}{\rho_2^{mix}})$ to the δ_I distribution, with R and ϵ fixed to the value obtained from a fit to the full BE sample (DELPHI); and finally the integral of the term describing the BE correlation part, $\int\lambda\exp(-\sigma^2Q^2)$, when fitting the function $\kappa(1+\epsilon Q)(1+\lambda\exp(-\sigma^2Q^2))$ to the $R^*(Q)$ distribution (ALEPH).

The size of the correlations for like-sign pairs of particles measured in terms of these estimators is compared with the values expected in the model with and without inter-W correlations in Table 8.2. Table 8.3 summarizes the normalized fractions of the model seen. Note that DELPHI also finds a 1.4 standard deviation effect for pairs of unlike-sign particles from different W bosons [190], compatible with the prediction of the LUBOEI model with full strength correlations.

For the combination of the above measurements one has to take into account correlations between them. Correlations between results of the same experiment are strong and are not available. It is however found, for example, that taking reasonable value of these correlations and combining three ALEPH measurements, one obtains normalized fractions of the model seen very close to those of the most precise measurement. Therefore, for simplicity, the combination of the most precise measurements of each experiment is made here: D' from ALEPH, δ_I from DELPHI, D' from L3 and D from OPAL. In this combination only the uncertainties in the understanding of the background contribution in the data are treated as correlated between experiments (denoted as "corr. syst." in Table 8.2). The combination via a MINUIT fit gives:

$$\frac{\text{data} - \text{model(noBE)}}{\text{model(fullBE)} - \text{model(noBE)}} \;=\; 0.17 \pm 0.095(stat.) \pm 0.085(sys.) \;=\; 0.17 \pm 0.13 \;, \qquad (8.13)$$

where "noBE" includes correlations between decay products of each W, but not the ones between decay products of different Ws and "fullBE" includes all the correlations. A χ^2/dof=3.5/3 of the fit is observed. The measurements and their average are shown in Figure 8.5. The measurements used in the combination are marked with an arrow.

In conclusion, the results of LEP experiments are in good agreement (χ^2/dof=3.5/3). The LUBOEI model of BE correlations between pions from different W bosons is disfavoured. The 68% confidence level (CL) upper limit on these correlations is

$$0.17 \;+\; 0.13 \;=\; 0.30 \;. \qquad (8.14)$$

This result can be translated into a 68% CL upper limit on the shift of the W mass measurements due to the BE correlations between particles from different Ws, Δm_{W}, assuming a linear dependence of Δm_{W} on the size of the correlation. For the specific BE model investigated, LUBOEI, a typical shift of -35 MeV in the W mass is obtained at full BE correlation strength. Thus the 68% CL upper limit on the magnitude of the mass shift within the LUBOEI model is: $|\Delta m_{\mathrm{W}}| = 11$ MeV.

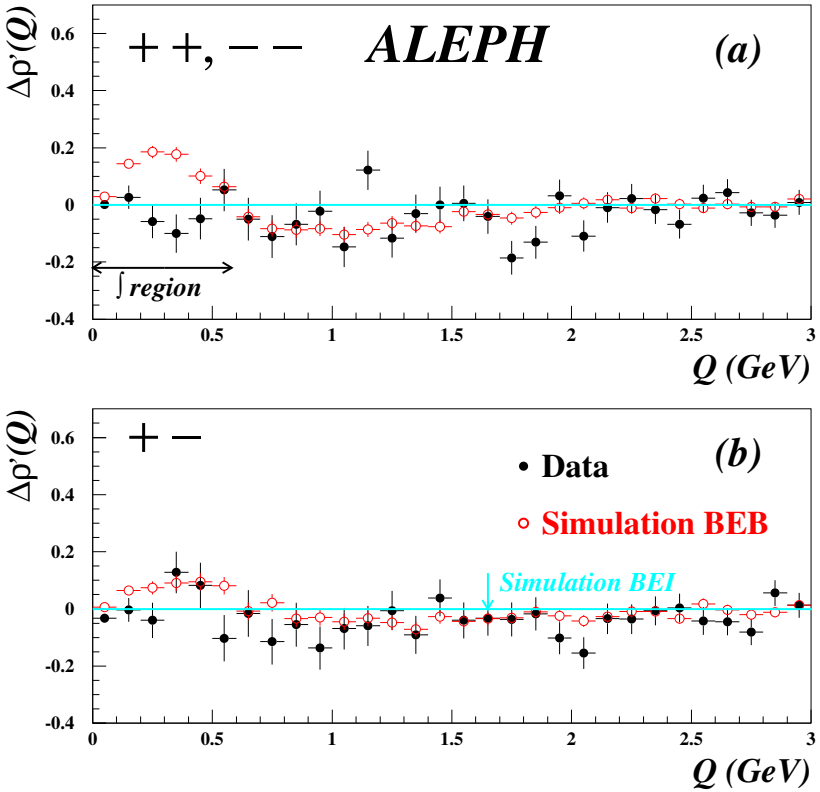

Figure 8.1: Distribution of the quantity $\Delta\rho'$ for like- and unlike-sign pairs as a function of Q as measured by the ALEPH collaboration [189]. BEI stands for the case in which Bose-Einstein correlations do not occur between decay products of different W bosons, and BEB if they do.

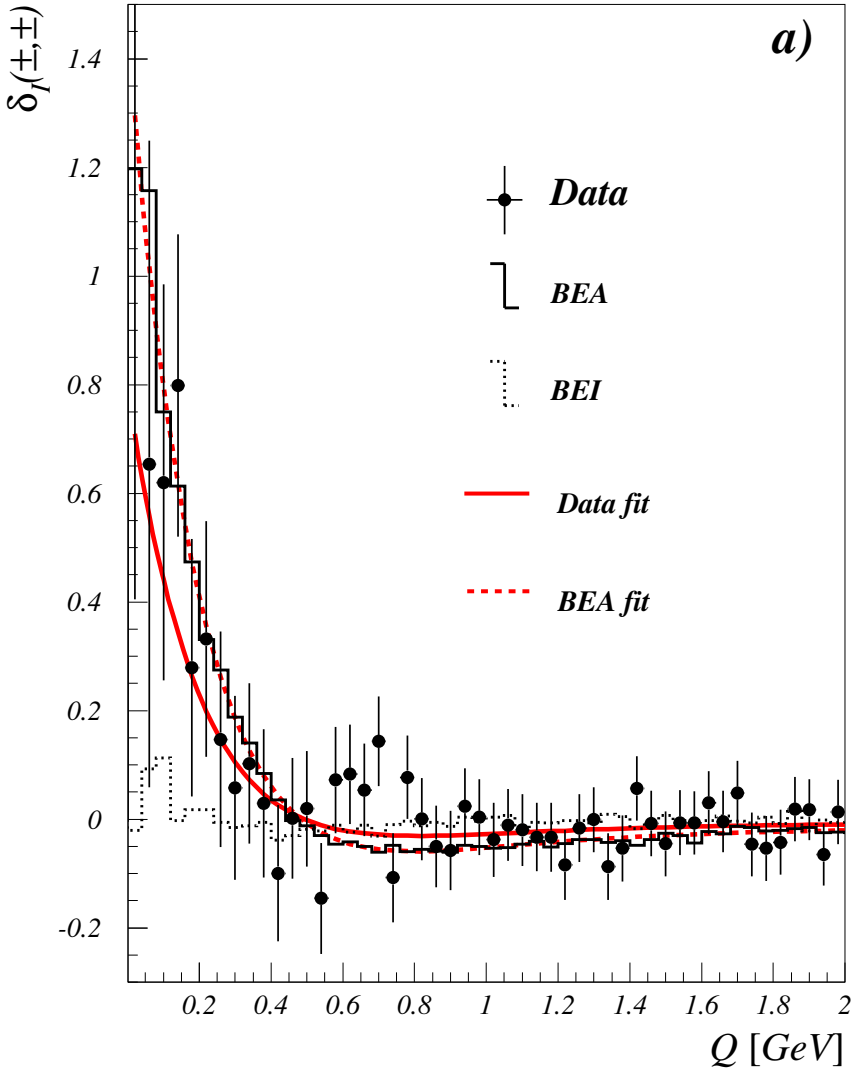

Figure 8.2: Distributions of the quantity δ_I for like-sign pairs as a function of Q as measured by the DELPHI collaboration [190]. The solid line shows the fit results. BEI stands for the case in which Bose-Einstein correlations do not occur between decay products of different W bosons, and BEA if they do.

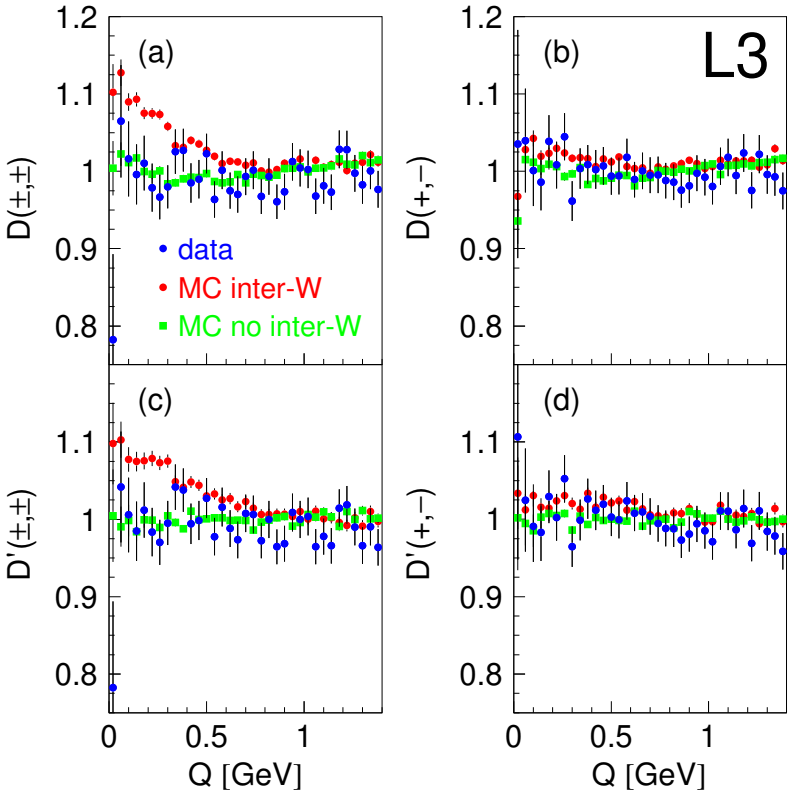

Figure 8.3: Distributions of the quantity D and D' for like- and unlike-sign pairs as a function of Q as measured by the L3 collaboration [182].

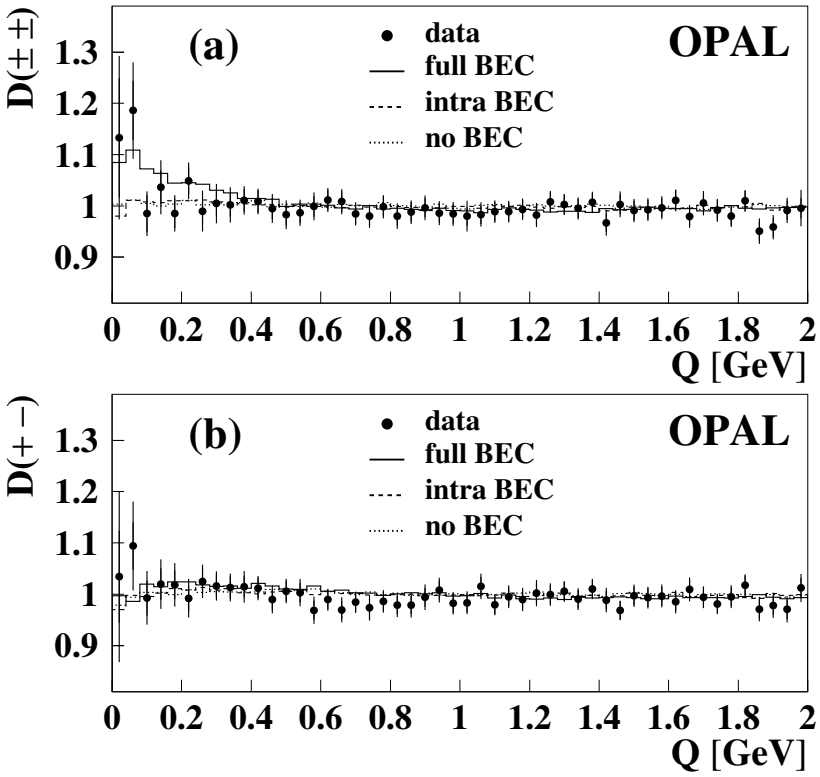

Figure 8.4: Distribution of the quantity D for like- and unlike-sign pairs as a function of Q as measured by the OPAL collaboration [191].

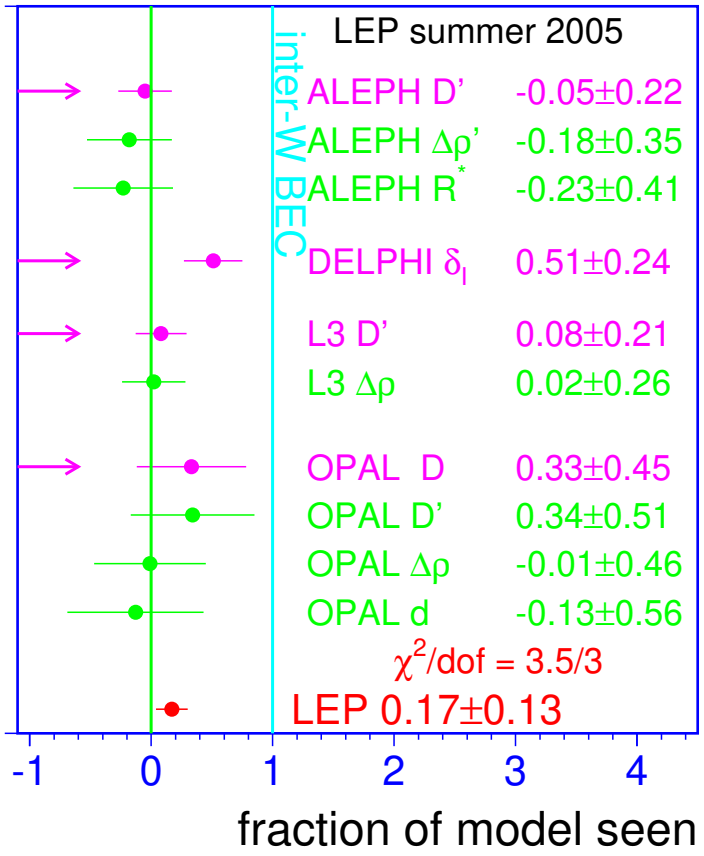

Figure 8.5: Correlations expressed as the relative fraction of the model with inter-W correlations. The arrows indicate the measurements used in the combination. The LEP combination is shown at the bottom.

Chapter 9

W-Boson Mass and Width at LEP-II

Updates with respect to summer 2005:
New combinations using the final results from ALEPH, DELPHI, L3 and OPAL are presented. While the results from all 4 experiments are now final, the combinations are still preliminary.

9.1 Introduction

The W boson mass and width results presented here are obtained from data recorded over a range of centre-of-mass energies, $\sqrt{s} = 161 - 209$ GeV, during the 1996-2000 operation of the LEP collider (LEPII), and correspond to a luminosity of about 700 pb^{-1} per experiment. In contrast to previous combinations [3], the results reported by all four LEP experiments, ALEPH, DELPHI, L3 and OPAL, are now final. However, the combination and its results are still preliminary. The final W mass results of the experiments in the $\mathrm{W^+W^-}\to\mathrm{q\bar{q}q\bar{q}}$ channel use an analysis trading statistical accuracy for reduced FSI systematic uncertainties in order to achieve a smaller total error.

The observables W mass, m_W, and total width, Γ_W, quoted here correspond to a definition based on a Breit-Wigner denominator with a mass-dependent width, $|(m^2 - m_\mathrm{W}^2) + im^2\Gamma_\mathrm{W}/m_\mathrm{W}|$.

9.2 W Mass Measurements

Since 1996 until 2000 the LEP $\mathrm{e^+e^-}$ collider operated above the threshold for $\mathrm{W^+W^-}$ pair production. Initially, 10 pb^{-1} of data were recorded close to the $\mathrm{W^+W^-}$ pair production threshold. At this energy the $\mathrm{W^+W^-}$ cross section is sensitive to the W boson mass. Table 9.1 summarises the W mass results from the four LEP collaborations based on these data [195].

Subsequently LEP operated at energies significantly above the $\mathrm{W^+W^-}$ threshold, where the $\mathrm{e^+e^-} \to \mathrm{W^+W^-}$ cross section has little sensitivity to m_W. For these higher energy data m_W is measured through the direct reconstruction of the W boson's invariant mass from the observed jets and leptons. Table 9.2 summarises the W mass results published by the four LEP experiments using the direct reconstruction method. The combined values of m_W from each collaboration take into account the correlated systematic uncertainties between the decay channels and between the different years of data taking. In addition to the combined numbers, each experiment presents mass measurements from $\mathrm{W^+W^-}\to\mathrm{q\bar{q}}\ell\overline{\nu}_\ell$ and $\mathrm{W^+W^-}\to\mathrm{q\bar{q}q\bar{q}}$ channels separately. The DELPHI and OPAL

THRESHOLD ANALYSIS [195]	
Experiment	m_W(threshold)/GeV
ALEPH	80.14 ± 0.35
DELPHI	80.40 ± 0.45
L3	$80.80^{+0.48}_{-0.42}$
OPAL	$80.40^{+0.46}_{-0.43}$

Table 9.1: W mass measurements from the $\mathrm{W^+W^-}$ threshold cross section at $\sqrt{s} = 161$ GeV. The errors include statistical and systematic contributions.

	DIRECT RECONSTRUCTION		
	$\mathrm{W^+W^-}\to\mathrm{q\bar{q}}\ell\overline{\nu}_\ell$	$\mathrm{W^+W^-}\to\mathrm{q\bar{q}q\bar{q}}$	Combined
Experiment	m_W/GeV	m_W/GeV	m_W/GeV
ALEPH [196]	80.429 ± 0.059	80.475 ± 0.081	80.444 ± 0.051
DELPHI [197]	80.339 ± 0.075	80.311 ± 0.137	80.336 ± 0.067
L3 [198]	80.212 ± 0.071	80.325 ± 0.080	80.270 ± 0.055
OPAL [199]	80.449 ± 0.063	80.353 ± 0.083	80.416 ± 0.053
ALEPH	80.429 ± 0.059	80.475 ± 0.082	80.444 ± 0.051
DELPHI	80.340 ± 0.076	80.310 ± 0.102	80.330 ± 0.064
L3	80.213 ± 0.071	80.323 ± 0.091	80.253 ± 0.058
OPAL	80.449 ± 0.062	80.353 ± 0.081	80.415 ± 0.052

Table 9.2: W mass measurements from direct reconstruction ($\sqrt{s} = 172 - 209$ GeV). Results are given for the semi-leptonic, fully-hadronic channels and the combined value. The top part of the table shows the results as published by the experiments, using their individual evaluations of FSI effects; these results are final. The bottom part of the table shows the results of the experiments when propagating the common LEP estimates of FSI effects to the mass (see text), affecting also the $\mathrm{W^+W^-}\to\mathrm{q\bar{q}}\ell\overline{\nu}_\ell$ results through correlations due to other systematic uncertainties; these results are preliminary. The $\mathrm{W^+W^-}\to\mathrm{q\bar{q}}\ell\overline{\nu}_\ell$ results from the OPAL collaboration include mass information from the $\mathrm{W^+W^-}\to\ell\overline{\nu}_\ell\ell\overline{\nu}_\ell$ channel.

collaborations provide results from independent fits to the data in the $\mathrm{q\bar{q}}\ell\overline{\nu}_\ell$ and $\mathrm{q\bar{q}q\bar{q}}$ decay channels separately and hence account for correlations between years but do not need to include correlations between the two channels. The $\mathrm{q\bar{q}}\ell\overline{\nu}_\ell$ and $\mathrm{q\bar{q}q\bar{q}}$ results quoted by the ALEPH and L3 collaborations are obtained from a simultaneous fit to all data which, in addition to other correlations, takes into account the correlated systematic uncertainties between the two channels.

The precision of the $\mathrm{q\bar{q}q\bar{q}}$ channel is limited by the Final State Interactions (FSI) systematic, namely Colour Reconnection (CR) and Bose-Einstein Correlation (BEC). Hence, the final LEP analyses remove low momentum particles from the jets as these particles are more sensitive to FSI effects. Removing low momentum particles from jets reduces the systematic uncertainties due to possible FSI effects in the $\mathrm{W^+W^-}\to\mathrm{q\bar{q}q\bar{q}}$. The systematic errors in the $\mathrm{W^+W^-}\to\mathrm{q\bar{q}}\ell\overline{\nu}_\ell$ channel are dominated by uncertainties from hadronisation.

9.3 Combination Procedure

A combined LEP W mass measurement is obtained from the results of the four experiments. In order to perform a reliable combination of the measurements, a more detailed input than that given in Table 9.2 is required. Each experiment provided a W mass measurement for both the $W^+W^- \to q\bar{q}\ell\bar{\nu}_\ell$ and $W^+W^- \to q\bar{q}q\bar{q}$ channels for each of the data taking years that it had analysed. In addition to the four threshold measurements a total of 38 direct reconstruction measurements are supplied: ALEPH provided 8 measurements (1997-2000), DELPHI provided 10 measurements (1996-2000), L3 gave 10 measurements (1996-2000), and OPAL gave 10 measurements (1996-2000). The $W^+W^- \to \ell\bar{\nu}_\ell\ell\bar{\nu}_\ell$ channel is also analysed by the OPAL (1996-2000) collaboration; the lower precision results obtained from this channel are combined with the mass determinations in the $W^+W^- \to q\bar{q}\ell\bar{\nu}_\ell$ channel.

Subdividing the results by data-taking years enables a proper treatment of the correlated systematic uncertainty from the LEP beam energy and other dependences on the centre-of-mass energy or data-taking period. A detailed breakdown of the sources of systematic uncertainty is provided for each result and the correlations specified. The inter-year, inter-channel and inter-experiment correlations are included in the combination. The main sources of correlated systematic errors are: Colour Reconnection, Bose-Einstein Correlations, hadronisation, the LEP beam energy, and uncertainties from initial and final state radiation. The full correlation matrix for the LEP beam energy is employed [200]. The combination is performed and the evaluation of the components of the total error assessed using the Best Linear Unbiased Estimate (BLUE) technique, see Reference 26.

FSI Effects

In the old mass analyses all experiments had the same sensitivity to FSI effects. The final LEP analyses have a different sensitivity to FSI, depending on the method and cuts employed to reduce this systematic. Hence, *in contrast to our old preliminary combinations we do NOT equalise the FSI systematic anymore*. Instead, we use as (energy dependent) uncertainty what the experiments find for exactly the same FSI models and parameter variations, as detailed in the following.

In the case of Bose-Einstein Correlations, the uncertainties are evaluated using the LUBOEI model with full BEC, with the effect rescaled to match the final LEP-2 combined one standard-deviation limit of 30 % of the full effect, see Chapter 8.

A preliminary study of Colour Reconnection has been made by the LEP experiments using the particle flow method [201] on a sample of fully-hadronic WW events, see Chapter 7. [1] The combined results are interpreted in terms of the reconnection parameter k_i of the SK-I model [203] and yield a 68% confidence level range of:

$$0.39 < k_i < 2.13\,. \tag{9.1}$$

The method was found to be insensitive to the HERWIG and ARIADNE-II models of Colour Reconnection.

As indicated above, the final LEP analyses have a reduced sensitivity to CR effects. Some analyses were optimised to give the smallest total error based on the experiment's own value of the SK-I model parameter k_i. For the combination, all CR errors have been re-evaluated for the common preliminary LEP-2 value of $k_i = 2.13$, without, however, reoptimising individual analyses for this k_i value. The mass results propagating the common LEP estimates of FSI effects are also shown in Table 9.2.

[1] This preliminary combination does not take into account the final particle flow and δM constraints on possible Colour Reconnection models, nor the final OPAL Colour-Reconnection analysis published recently [202]. We expect this to change once the final LEP combinations for CR effects will become available.

Early m_W combinations had relied upon theoretical expectations of Colour Reconnection effects, in which there is considerable uncertainty. This new data-driven approach achieves a more robust uncertainty estimate at the expense of a significantly increased Colour Reconnection uncertainty. The ARIADNE-II and HERWIG models of Colour Reconnection have also been studied and the W mass shift was found to be lower than that from SK-I with $k_i = 2.13$ used for the combination.

9.4 LEP Combined W Boson Mass

The combined LEP W mass from direct reconstruction alone is

$$m_W(\text{direct}) = 80.375 \pm 0.025(\text{stat.}) \pm 0.022(\text{syst.})\ \text{GeV}, \tag{9.2}$$

with a χ^2/d.o.f. of 47.7/37, corresponding to a χ^2 probability of 11.1%. The weight of the fully-hadronic channel in the combined fit, previously 0.16 [3] as a consequence of the relatively large size of the estimates for the systematic errors from CR and BEC, increased to 0.22 in this combination due to the experiments' final results with reduced FSI sensitivity.

Table 9.3 gives a breakdown of the contribution to the total error of the various sources of systematic errors. The largest contribution to the systematic error comes from hadronisation uncertainties, which are conservatively treated as correlated between the two channels, between experiments and between years. In the absence of systematic effects the current LEP statistical precision on m_W would be 20 MeV: the statistical error contribution in the LEP combination is larger than this (25 MeV) due to the reduced weight of the fully-hadronic channel. Compared to older combinations [1], the final LEP results lead to an increased statistical error in the $W^+W^- \to q\bar{q}q\bar{q}$ combination but reduced systematics due to CR and BEC, for an overall smaller total error.

In addition to the direct reconstruction results, the W boson mass is measured at LEP from the 10 pb^{-1} per experiment of data recorded at threshold for W pair production:

$$m_W(\text{threshold}) = 80.40 \pm 0.20(\text{stat.}) \pm 0.07(\text{syst.}) \pm 0.03(E_{\text{beam}})\ \text{GeV}. \tag{9.3}$$

When the threshold measurements are combined with the much more precise results obtained from direct reconstruction one achieves a W mass measurement of

$$m_W = 80.376 \pm 0.025(\text{stat.}) \pm 0.022(\text{syst.})\text{GeV}. \tag{9.4}$$

The LEP beam energy uncertainty is the only correlated systematic error source between the threshold and direct reconstruction measurements. The threshold measurements have a weight of only 0.02 in the combined fit. This LEP combined result is compared with the results (threshold and direct reconstruction combined) of the four LEP experiments in Figures 9.1 and 9.3.

9.5 Consistency Checks

The difference between the combined W boson mass measurements obtained from the fully-hadronic and semi-leptonic channels, $\Delta m_W(q\bar{q}q\bar{q} - q\bar{q}\ell\bar{\nu}_\ell)$, is determined:

$$\Delta m_W(q\bar{q}q\bar{q} - q\bar{q}\ell\bar{\nu}_\ell) = -12 \pm 45\ \text{MeV}. \tag{9.5}$$

Source	Systematic Error on m_W (MeV)		
	$q\bar{q}\ell\bar{\nu}_\ell$	$q\bar{q}q\bar{q}$	Combined
ISR/FSR	8	5	7
Hadronisation	13	19	14
Detector Systematics	10	8	10
LEP Beam Energy	9	9	9
Colour Reconnection	–	35	8
Bose-Einstein Correlations	–	7	2
Other	3	11	4
Total Systematic	21	44	22
Statistical	30	40	25
Total	36	59	33
Statistical in absence of Systematics	30	27	20

Table 9.3: Error decomposition for the combined LEP W mass results. Detector systematics include uncertainties in the jet and lepton energy scales and resolution. The 'Other' category refers to errors, all of which are uncorrelated between experiments, arising from: simulation statistics, background estimation, four-fermion treatment, fitting method and event selection. The error decomposition in the $q\bar{q}\ell\bar{\nu}_\ell$ and $q\bar{q}q\bar{q}$ channels refers to the independent fits to the results from the two channels separately.

A significant non-zero value for Δm_W could indicate that CR and BEC effects are biasing the value of m_W determined from $W^+W^-\to q\bar{q}q\bar{q}$ events. Since Δm_W is primarily of interest as a check of the possible effects of final state interactions, the errors from CR and BEC are set to zero in its determination. The above result on the mass difference is obtained from a fit where the imposed correlations are the same as those for the results given in the previous sections.

The masses from the two channels with all errors and correlations included are:

$$m_W(W^+W^-\to q\bar{q}\ell\bar{\nu}_\ell) = 80.372 \pm 0.030(\text{stat.}) \pm 0.020(\text{syst.})\ \text{GeV}, \quad (9.6)$$
$$m_W(W^+W^-\to q\bar{q}q\bar{q}) = 80.387 \pm 0.040(\text{stat.}) \pm 0.044(\text{syst.})\ \text{GeV}. \quad (9.7)$$

The two results are correlated with a correlation coefficient of 0.20. These results and the correlation between them can be used to combine the two measurements or to form the mass difference. The LEP combined results from the two channels are compared with those quoted by the individual experiments in Figures 9.2 and 9.4.

Experimentally, separate m_W measurements are obtained from the $q\bar{q}\ell\bar{\nu}_\ell$ and $q\bar{q}q\bar{q}$ channels for each of the years of data. The combination using only the $q\bar{q}\ell\bar{\nu}_\ell$ measurements yields:

$$M_W^{\text{indep}}(W^+W^-\to q\bar{q}\ell\bar{\nu}_\ell) = 80.374 \pm 0.030(\text{stat.}) \pm 0.021(\text{syst.})\ \text{GeV}.$$

The largest contribution to the systematic error arises from the hadronisation uncertainties, ± 13 MeV. The combination using only the $q\bar{q}q\bar{q}$ measurements gives:

$$m_W^{\text{indep}}(W^+W^-\to q\bar{q}q\bar{q}) = 80.389 \pm 0.040(\text{stat.}) \pm 0.044(\text{syst.})\ \text{GeV}.$$

where the dominant contributions to the systematic error are from CR (± 35 MeV) and hadronisation (± 19 MeV).

9.6 LEP Combined W Boson Width

The method of direct reconstruction is also well suited to the direct measurement of the total width of the W boson. The results of the four LEP experiments, as published and when propagating the common LEP estimates of FSI effects, are shown in Table 9.4 and in Figures 9.1 and 9.3.

Experiment	Γ_W (GeV)	Γ_W (GeV)
	published	common
ALEPH	2.14 ± 0.11	2.14 ± 0.11
DELPHI	2.40 ± 0.17	2.39 ± 0.17
L3	2.18 ± 0.14	2.24 ± 0.15
OPAL	2.00 ± 0.14	2.00 ± 0.14

Table 9.4: W width measurements ($\sqrt{s} = 172 - 209$ GeV) from the individual experiments. The column labelled "published" shows the results as published by the experiments, using their individual evaluations of FSI effects; these results are final. The column labelled "common" shows the results of the experiments when propagating the common LEP estimates of FSI effects to the width (see text); these results are preliminary.

Each experiment provided a W width measurement for both $W^+W^-\to q\bar{q}\ell\bar{\nu}_\ell$ and $W^+W^-\to q\bar{q}q\bar{q}$ channels for each of the data taking years (1996-2000) that it has analysed. A total of 34 measurements are supplied: ALEPH provided 8 results (1997-2000), DELPHI 8 measurements (1997-2000), L3 10 measurements (1996-2000), and OPAL provided 8 measurements (1997-2000).

The BEC and CR uncertainties supplied by the experiments were based on studies of phenomenological models of these effects, using the same estimates of FSI effects as for the mass (see text) and propagating them to the width. Note that the final W width results of the experiments do not use the techniques introduced to reduce sensitivity to FSI effects as used for the mass analysis.

A simultaneous fit to the results of the four LEP collaborations is performed in the same way as for the m_W measurement. Correlated systematic uncertainties are taken into account and the combination gives:

$$\Gamma_W = 2.196 \pm 0.063(\text{stat.}) \pm 0.055(\text{syst.})\ \text{GeV},$$

with a χ^2/d.o.f. of 37.4/33.

9.7 Summary

The results of the four LEP experiments on the mass and width of the W boson are combined taking into account correlated systematic uncertainties, giving:

$$m_W = 80.376 \pm 0.033\ \text{GeV},$$
$$\Gamma_W = 2.196 \pm 0.083\ \text{GeV}.$$

The statistical correlation between mass and width is small and neglected. Their correlation due to common systematic effects is under study.

ALEPH, DELPHI, L3, OPAL as published.

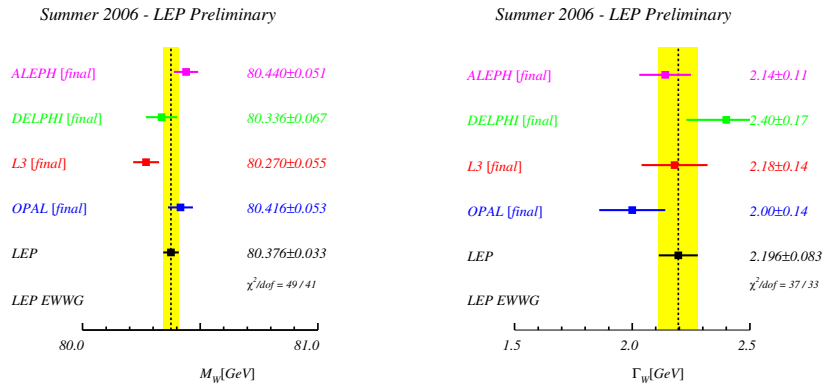

Figure 9.1: The combined results for the measurements of the W mass (left) and total W width (right) compared to the results obtained by the four LEP collaborations (as published). The combined values take into account correlations between experiments and years and hence, in general, do not give the same central value as a simple average. The individual and combined m_{W} results include the measurements from the threshold cross section.

ALEPH, DELPHI, L3, OPAL as published.

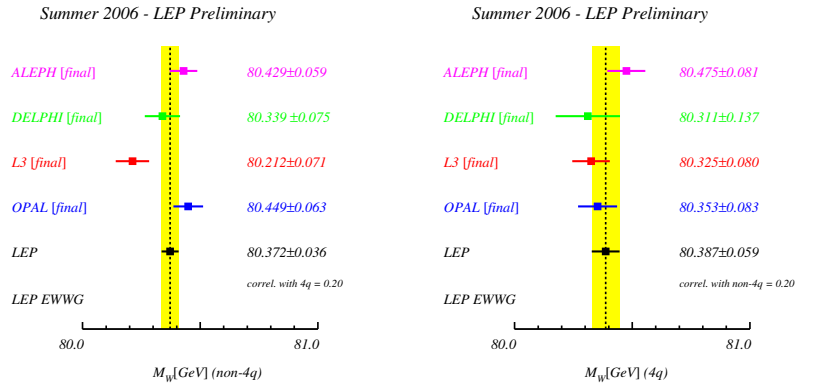

Figure 9.2: The W mass measurements from the $\mathrm{W^+W^-}\to\mathrm{q\overline{q}}\ell\overline{\nu}_\ell$ (left) and $\mathrm{W^+W^-}\to\mathrm{q\overline{q}q\overline{q}}$ (right) channels obtained by the four LEP collaborations (as published) compared to the combined value. The combined values take into account correlations between experiments, years and the two channels. The ALEPH and L3 $\mathrm{q\overline{q}}\ell\overline{\nu}_\ell$ and $\mathrm{q\overline{q}q\overline{q}}$ results are correlated since they are obtained from a fit to both channels taking into account inter-channel correlations.

ALEPH, DELPHI, L3, OPAL re-evaluated propagating the common LEP FSI estimates.

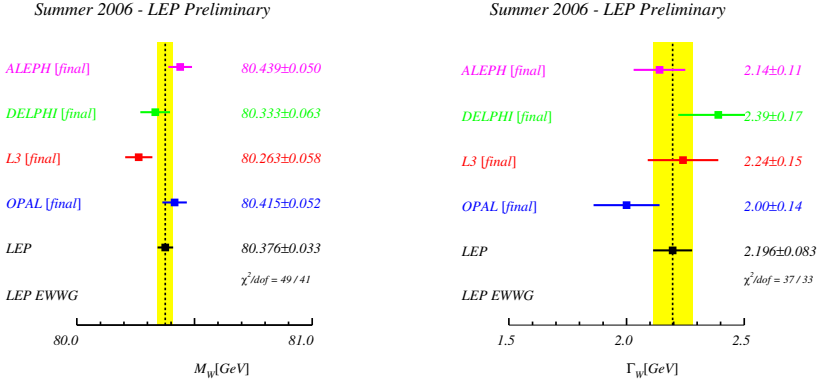

Figure 9.3: The combined results for the measurements of the W mass (left) and total W width (right) compared to the results obtained by the four LEP collaborations, propagating the common LEP estimates of FSI effects to mass and width (see text). The combined values take into account correlations between experiments and years and hence, in general, do not give the same central value as a simple average. The individual and combined m_{W} results include the measurements from the threshold cross section.

ALEPH, DELPHI, L3, OPAL re-evaluated propagating the common LEP FSI estimates.

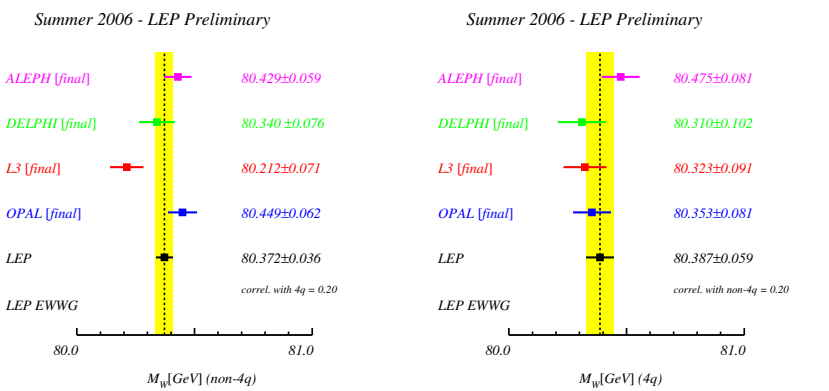

Figure 9.4: The W mass measurements from the $\mathrm{W^+W^-}\to\mathrm{q\overline{q}}\ell\overline{\nu}_\ell$ (left) and $\mathrm{W^+W^-}\to\mathrm{q\overline{q}q\overline{q}}$ (right) channels obtained by the four LEP collaborations, propagating the common LEP estimates of FSI effects to the mass. The combined values take into account correlations between experiments, years and the two channels. The $\mathrm{q\overline{q}}\ell\overline{\nu}_\ell$ and $\mathrm{q\overline{q}q\overline{q}}$ results are correlated since they are obtained from a fit to both channels taking into account inter-channel correlations.

Chapter 10

Constraints on the Standard Model

Updates with respect to summer 2005:
Updated preliminary and published measurements as discussed in the previous chapters are taken into account, including also the final and published Z-pole results [2] as well as new preliminary results on the mass of the top-quark obtained at the Tevatron. ZFITTER version 6.42 is used for the Standard Model analyses.

10.1 Introduction

The precise electroweak measurements performed at LEP-II and elsewhere (LEP-I, SLC, Tevatron, etc.) allow us to check the validity of the Standard Model (SM) and, within its framework, to infer valuable information about its fundamental parameters. The accuracy of the measurements makes them sensitive to the mass of the top quark $m_{\rm t}$, and to the mass of the Higgs boson $m_{\rm H}$ through loop corrections. While the leading $m_{\rm t}$ dependence is quadratic, the leading $m_{\rm H}$ dependence is logarithmic. Therefore, the inferred constraints on $m_{\rm t}$ are much stronger than those on $m_{\rm H}$.

10.2 Measurements

The measurements considered here are reported in Table 10.1. Also shown are the results of the SM fit to these combined high-Q^2 measurements. The measurements obtained at the Z pole by the LEP and SLC experiments ALEPH, DELPHI, L3, OPAL and SLD, and their combinations, reported in parts a), b) and c) of Table 10.1, are final and published [2].

The results on the W-boson mass by UA2 [204], CDF [205] and DØ [206] in Run-I, and the W-boson width by CDF [207] and DØ [208] in Run-I, are combined by the Tevatron Electroweak Working Group based on a detailed treatment of common systematic uncertainties. The results are [209]: $m_{\rm W} = 80452 \pm 59$ MeV, $\Gamma_{\rm W} = 2102 \pm 106$ MeV, with a correlation of -17.4%. Combining these results with the new preliminary LEP-II combination as presented in Chapter 9, the new preliminary world averages used here are:

$$m_{\rm W} = 80.392 \pm 0.029 \ {\rm GeV} \quad (10.1)$$
$$\Gamma_{\rm W} = 2.147 \pm 0.060 \ {\rm GeV}\,, \quad (10.2)$$

with a correlation of -7%.

For the mass of the top quark, $m_{\rm t}$, the published Run-I results from CDF [210] and DØ [211], also including recent preliminary results based on Run-II data, are combined by the Tevatron Electroweak Working Group with the result: $m_{\rm t} = 171.4 \pm 2.1$ GeV [212].

In addition, the following final results obtained in low-Q^2 interactions are considered: (i) the measurements of atomic parity violation in caesium [213,214], with the numerical result [215] taken from a recently published revised analysis of QED radiative corrections applied to the raw measurement; (ii) the result of the E-158 collaboration on the electroweak mixing angle[1] measured in Moller scattering [217]; and (iii) the final result of the NuTeV collaboration on neutrino-nucleon neutral to charged current cross section ratios [218].

Using both muon neutrino and muon anti-neutrino beams, the NuTeV collaboration has published by far the most precise result in neutrino-nucleon scattering [218], obtained at an average $Q^2 \simeq 20$ GeV^2. Based on an analysis mainly exploiting the Paschos-Wolfenstein quantity R_- [219], with $R_\pm \equiv (\sigma_{NC}(\nu) \pm \sigma_{NC}(\bar{\nu}))/(\sigma_{CC}(\nu) \pm \sigma_{CC}(\bar{\nu})) = g^2_{\nu{\rm Lud}} \pm g^2_{\nu{\rm Rud}}$, where $g^2_{\nu{\rm Lud}} = 4g^2_{{\rm L}\nu}(g^2_{\rm Lu} + g^2_{\rm Ld}) = [1/2 - \sin^4\theta_{\rm eff} + (5/9)\sin^4\theta_{\rm eff}]\rho_{\nu\nu}\rho_{\rm ud}$ and $g^2_{\nu{\rm Rud}} = 4g^2_{{\rm L}\nu}(g^2_{\rm Ru} + g^2_{\rm Rd}) = (5/9)\sin^4\theta_{\rm eff}\rho_{\nu\nu}\rho_{\rm ud}$, the NuTeV results for the effective couplings defined above are: $g^2_{\nu{\rm Lud}} = 0.30005 \pm 0.00137$ and $g^2_{\nu{\rm Rud}} = 0.03076 \pm 0.00110$, with a correlation of -0.017. While the result on $g_{\nu{\rm Rud}}$ agrees with the SM expectation, the result on $g_{\nu{\rm Lud}}$, measured nearly eight times more precisely, shows a deficit with respect to the expectation at the level of 3.0 standard deviations.

An additional input parameter, not shown in the table, is the Fermi constant G_F, determined from the μ lifetime, $G_F = 1.16637(1) \cdot 10^{-5}$ GeV^{-2} [220]. The relative error of G_F is comparable to that of $m_{\rm Z}$; both errors have negligible effects on the fit results.

10.3 Theoretical and Parametric Uncertainties

Detailed studies of the theoretical uncertainties in the SM predictions due to missing higher-order electroweak corrections and their interplay with QCD corrections had been carried out by the working group on 'Precision calculations for the Z resonance' [222], and later in [223,224]. Theoretical uncertainties are evaluated by comparing different but, within our present knowledge, equivalent treatments of aspects such as resummation techniques, momentum transfer scales for vertex corrections and factorisation schemes. The effects of these theoretical uncertainties are reduced by the inclusion of higher-order corrections [225,226] in the electroweak libraries TOPAZ0 [227] and ZFITTER [228].

The use of the QCD corrections [226] increases the value of $\alpha_{\rm S}(m^2_{\rm Z})$ by 0.001, as expected. The effects of missing higher-order QCD corrections on $\alpha_{\rm S}(m^2_{\rm Z})$ covers missing higher-order electroweak corrections and uncertainties in the interplay of electroweak and QCD corrections. A discussion of theoretical uncertainties in the determination of $\alpha_{\rm S}$ can be found in References 222 and 229, with a recent analysis in Reference 230 where the theoretical uncertainty is estimated to be about 0.001 for the analyses presented in the following.

Recently, the complete (fermionic and bosonic) two-loop corrections for the calculation of $m_{\rm W}$ [231], and the complete fermionic two-loop corrections for the calculation of $\sin^2\theta^{\rm lept}_{\rm eff}$ [232] have been calculated. Including three-loop top-quark contributions to the ρ parameter in the limit of large $m_{\rm t}$ [233],

[1] E-158 quotes in the MSbar scheme, evolved to $Q^2 = m^2_{\rm Z}$. We add 0.00029 to the quoted value in order to obtain the effective electroweak mixing angle [216].

		Measurement with Total Error	Systematic Error	Standard Model fit	Pull
	$\Delta\alpha^{(5)}_{\rm had}(m_{\rm Z}^2)$ [221]	0.02758 ± 0.00035	0.00034	0.02766	-0.2
a)	LEP-I				
	line-shape and				
	lepton asymmetries:				
	$m_{\rm Z}$ [GeV]	91.1875 ± 0.0021	[a] 0.0017	91.1875	0.0
	$\Gamma_{\rm Z}$ [GeV]	2.4952 ± 0.0023	[a] 0.0012	2.4957	-0.2
	$\sigma^0_{\rm had}$ [nb]	41.540 ± 0.037	[b] 0.028	41.477	1.7
	R^0_ℓ	20.767 ± 0.025	[b] 0.007	20.744	0.9
	$A^{0,\ell}_{\rm FB}$	0.0171 ± 0.0010	[b] 0.0003	0.0164	0.8
	+ correlation matrix [2]				
	τ polarisation:				
	$\mathcal{A}_\ell$ ($\mathcal{P}_\tau$)	0.1465 ± 0.0033	0.0016	0.1479	-0.4
	$q\overline{q}$ charge asymmetry:				
	$\sin^2\theta^{\rm lept}_{\rm eff}(Q^{\rm had}_{\rm FB})$	0.2324 ± 0.0012	0.0010	0.23141	0.8
b)	SLD				
	$\mathcal{A}_\ell$ (SLD)	0.1513 ± 0.0021	0.0010	0.1479	1.7
c)	LEP-I/SLD Heavy Flavour				
	$R^0_{\rm b}$	0.21629 ± 0.00066	0.00050	0.21585	0.7
	$R^0_{\rm c}$	0.1721 ± 0.0030	0.0019	0.1722	0.0
	$A^{0,{\rm b}}_{\rm FB}$	0.0992 ± 0.0016	0.0007	0.1037	-2.8
	$A^{0,{\rm c}}_{\rm FB}$	0.0707 ± 0.0035	0.0017	0.0741	-1.0
	$\mathcal{A}_{\rm b}$	0.923 ± 0.020	0.013	0.935	-0.6
	$\mathcal{A}_{\rm c}$	0.670 ± 0.027	0.015	0.668	0.1
	+ correlation matrix [2]				
d)	LEP-II and Tevatron				
	$m_{\rm W}$ [GeV] (LEP-II, Tevatron)	80.392 ± 0.029		80.372	0.7
	$\Gamma_{\rm W}$ [GeV] (LEP-II, Tevatron)	2.147 ± 0.060		2.091	0.9
	$m_{\rm t}$ [GeV] (Tevatron [212])	171.4 ± 2.1	1.8	171.7	-0.2

Table 10.1: Summary of high-Q^2 measurements included in the combined analysis of SM parameters. Section a) summarises LEP-I averages, Section b) SLD results ($\mathcal{A}_\ell$ includes $A_{\rm LR}$ and the polarised lepton asymmetries), Section c) the LEP-I and SLD heavy flavour results, and Section d) electroweak measurements from LEP-II and the Tevatron. The total errors in column 2 include the systematic errors listed in column 3. Although the systematic errors include both correlated and uncorrelated sources, the determination of the systematic part of each error is approximate. The SM results in column 4 and the pulls (difference between measurement and fit in units of the total measurement error) in column 5 are derived from the SM fit including all high-Q^2 data (Table 10.2, column 4).
[a] The systematic errors on $m_{\rm Z}$ and $\Gamma_{\rm Z}$ contain the errors arising from the uncertainties in the LEP-I beam energy only.
[b] Only common systematic errors are indicated.

efficient routines for evaluating these corrections have been implemented since version 6.40 in the semi-analytical program ZFITTER. The remaining theoretical uncertainties are estimated to be 4 MeV on $m_{\rm W}$ and 0.000049 on $\sin^2\theta^{\rm lept}_{\rm eff}$. The latter uncertainty dominates the theoretical uncertainty in SM fits and the extraction of constraints on the mass of the Higgs boson presented below. For a complete picture, the complete two-loop calculation for the partial Z decay widths should be calculated.

The determination of the size of remaining theoretical uncertainties is under continued study. The theoretical errors discussed above are not included in the results presented in Table 10.2. At present the impact of theoretical uncertainties on the determination of SM parameters from the precise electroweak measurements is small compared to the error due to the uncertainty in the value of $\alpha(m_{\rm Z}^2)$, which is included in the results.

The uncertainty in $\alpha(m_{\rm Z}^2)$ arises from the contribution of light quarks to the photon vacuum polarisation ($\Delta\alpha^{(5)}_{\rm had}(m_{\rm Z}^2)$):

$$\alpha(m_{\rm Z}^2) = \frac{\alpha(0)}{1 - \Delta\alpha_\ell(m_{\rm Z}^2) - \Delta\alpha^{(5)}_{\rm had}(m_{\rm Z}^2) - \Delta\alpha_{\rm top}(m_{\rm Z}^2)}\,, \tag{10.3}$$

where $\alpha(0) = 1/137.036$. The top contribution, $-0.00007(1)$, depends on the mass of the top quark, and is therefore determined inside the electroweak libraries TOPAZ0 and ZFITTER. The leptonic contribution is calculated to third order [234] to be 0.03150, with negligible uncertainty.

For the hadronic contribution, we no longer use the value 0.02804 ± 0.00065 [235,236], but rather the new evaluation 0.02758 ± 0.0035 [221] which takes into account published results on electron-positron annihilations into hadrons at low centre-of-mass energies by the BES collaboration [237], as well as the revised published results from CMD-2 [238] and new results from KLOE [239]. The reduced uncertainty still causes an error of 0.00013 on the SM prediction of $\sin^2\theta^{\rm lept}_{\rm eff}$, and errors of 0.2 GeV and 0.1 on the fitted values of $m_{\rm t}$ and $\log(m_{\rm H})$, included in the results presented below. The effect on the SM prediction for $\Gamma_{\ell\ell}$ is negligible. The $\alpha_{\rm S}(m_{\rm Z}^2)$ values for the SM fits presented here are stable against a variation of $\alpha(m_{\rm Z}^2)$ in the interval quoted.

There are also several evaluations of $\Delta\alpha^{(5)}_{\rm had}(m_{\rm Z}^2)$ [240–250] which are more theory-driven. The most recent of these (Reference 250) also includes the new results from BES, yielding 0.02749 ± 0.00012. To show the effects of the uncertainty of $\alpha(m_{\rm Z}^2)$, we also use this evaluation of the hadronic vacuum polarisation. Note that all these evaluations obtain values for $\Delta\alpha^{(5)}_{\rm had}(m_{\rm Z}^2)$ consistently lower than - but in agreement with - the old value of 0.02804 ± 0.00065.

10.4 Selected Results

Figure 10.1 shows a comparison of the leptonic partial width from LEP-I, $\Gamma_{\ell\ell} = 83.985 \pm 0.086$ MeV [2], and the effective electroweak mixing angle from asymmetries measured at LEP-I and SLD, $\sin^2\theta^{\rm lept}_{\rm eff} = 0.23153 \pm 0.00016$ [2], with the SM shown as a function of $m_{\rm t}$ and $m_{\rm H}$. Good agreement with the SM prediction using the most recent measurements of $m_{\rm t}$ and $m_{\rm W}$ is observed. The point with the arrow indicates the prediction if among the electroweak radiative corrections only the photon vacuum polarisation is included, which shows that the precision electroweak Z-pole data are sensitive to non-trivial electroweak corrections. Note that the error due to the uncertainty on $\alpha(m_{\rm Z}^2)$ (shown as the length of the arrow) is not much smaller than the experimental error on $\sin^2\theta^{\rm lept}_{\rm eff}$ from LEP-I and SLD. This underlines the continued importance of a precise measurement of $\sigma(e^+e^- \to \text{hadrons})$ at low centre-of-mass energies.

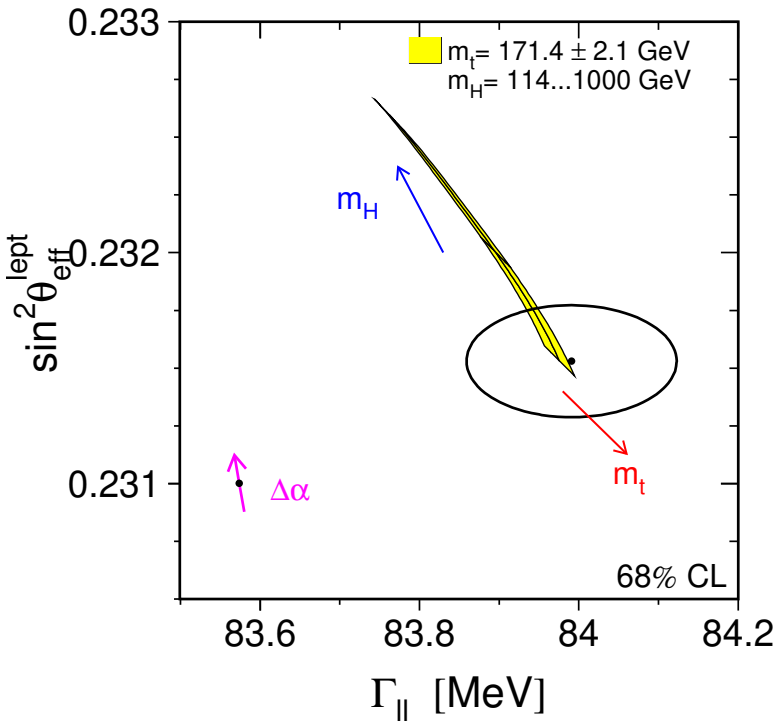

Figure 10.1: LEP-I+SLD measurements [2] of $\sin^2\theta^{\rm lept}_{\rm eff}$ and $\Gamma_{\ell\ell}$ and the SM prediction. The point shows the predictions if among the electroweak radiative corrections only the photon vacuum polarisation is included. The corresponding arrow shows variation of this prediction if $\alpha(m_{\rm Z}^2)$ is changed by one standard deviation. This variation gives an additional uncertainty to the SM prediction shown in the figure.

Of the measurements given in Table 10.1, R^0_ℓ is one of the most sensitive to QCD corrections. For $m_{\rm Z} = 91.1875$ GeV, and imposing $m_{\rm t} = 171.4 \pm 2.1$ GeV as a constraint, $\alpha_{\rm S} = 0.1222 \pm 0.0037$ is obtained. Alternatively, $\sigma^0_{\rm lep} \equiv \sigma^0_{\rm had}/Rl = 2.0003 \pm 0.027$ nb [2] which has higher sensitivity to QCD corrections and less dependence on $m_{\rm H}$ yields: $\alpha_{\rm S} = 0.1178 \pm 0.0030$. Typical errors arising from the variation of $m_{\rm H}$ between 100 GeV and 200 GeV are of the order of 0.001, somewhat smaller for $\sigma^0_{\rm lep}$. These results on $\alpha_{\rm S}$, as well as those reported in the next section, are in very good agreement with recently determined world averages ($\alpha_{\rm S}(m_{\rm Z}^2) = 0.118 \pm 0.002$ [251], or $\alpha_{\rm S}(m_{\rm Z}^2) = 0.1178 \pm 0.0033$ based solely on NNLO QCD results excluding the LEP-I lineshape results and accounting for correlated errors [252]).

10.5 Standard Model Analyses

In the following, several different SM fits reported in Table 10.2 are discussed. The χ^2 minimisation is performed with the program MINUIT [81], and the predictions are calculated with ZFITTER as a function of the five SM input parameters $\Delta\alpha^{(5)}_{\rm had}(m_{\rm Z}^2)$, $\alpha_{\rm S}(m_{\rm Z}^2)$, $m_{\rm Z}$, $m_{\rm t}$ and $\log_{10}(m_{\rm H}/{\rm GeV})$ which are varied simultaneously in the fits. The somewhat increased χ^2/d.o.f. for all of these fits is caused by the large dispersion in the values of the leptonic effective electroweak mixing angle measured through the various asymmetries at LEP-I and SLD [2]. Following [2] for the analyses presented here, this dispersion is interpreted as a fluctuation in one or more of the input measurements, and thus we neither modify nor exclude any of them. A further drastic increase in χ^2/d.o.f. is observed when the NuTeV results are included in the analysis.

To test the agreement between the Z-pole data [2] (LEP-I and SLD) and the SM, a fit to this data is performed. The result is shown in Table 10.2, column 1. The indirect constraints on $m_{\rm W}$ and $m_{\rm t}$ from this data sample are shown in Figure 10.2, compared with the direct measurements. Also shown are the SM predictions for Higgs masses between 114 and 1000 GeV. As can be seen in the figure, the indirect and direct measurements of $m_{\rm W}$ and $m_{\rm t}$ are in good agreement, and both sets prefer a low value of the Higgs mass.

For the fit shown in column 2 of Table 10.2, the direct $m_{\rm t}$ measurement is included to obtain the best indirect determination of $m_{\rm W}$. The result is also shown in Figure 10.3. Also in this case, the indirect determination of W boson mass, 80.361 ± 0.020 GeV, is in good agreement with the direct measurements from LEP-II and the Tevatron, $m_{\rm W} = 80.392 \pm 0.029$ GeV. For the fit shown in column 3 of Table 10.2 and Figure 10.4, the direct $m_{\rm W}$ and $\Gamma_{\rm W}$ measurements from LEP-II and the Tevatron are included instead of the direct $m_{\rm t}$ measurement in order to obtain the constraint $m_{\rm t} = 178^{+12}_{-9}$ GeV, in very good agreement with the direct measurement of $m_{\rm t} = 171.4 \pm 2.1$ GeV.

Finally, the best constraints on $m_{\rm H}$ are obtained when all high-Q^2 measurements are used in the fit. The results of this fit are shown in column 4 of Table 10.2. The predictions of this fit for observables measured in high-Q^2 and low-Q^2 reactions are listed in Tables 10.1 and 10.3, respectively. In Figure 10.5 the observed value of $\Delta\chi^2 \equiv \chi^2 - \chi^2_{\rm min}$ as a function of $m_{\rm H}$ is plotted for this fit including all high-Q^2 results. The solid curve is the result using ZFITTER, and corresponds to the last column of Table 10.2. The shaded band represents the uncertainty due to uncalculated higher-order corrections, as estimated by ZFITTER.

The 95% confidence level upper limit on $m_{\rm H}$ (taking the band into account) is 166 GeV. The 95% C.L. lower limit on $m_{\rm H}$ of 114.4 GeV obtained from direct searches [253] is not used in the determination of this limit. Including it increases the limit to 199 GeV. Also shown is the result (dashed curve) obtained when using $\Delta\alpha^{(5)}_{\rm had}(m_{\rm Z}^2)$ of Reference 250.

Given the constraints on the other four SM input parameters, each observable is equivalent to a constraint on the mass of the SM Higgs boson. The constraints on the mass of the SM Higgs boson resulting from each observable are compared in Figure 10.6. For very low Higgs-masses, these constraints are qualitative only as the effects of real Higgs-strahlung, neither included in the experimental analyses nor in the SM calculations of expectations, may then become sizeable [254]. Besides the measurement of the W mass, the most sensitive measurements are the asymmetries, *i.e.*, $\sin^2\theta^{\rm lept}_{\rm eff}$. A reduced uncertainty for the value of $\alpha(m_{\rm Z}^2)$ would therefore result in an improved constraint on $\log m_{\rm H}$ and thus $m_{\rm H}$, as already shown in Figures 10.1 and 10.5.

	- 1 - all Z-pole data	- 2 - all Z-pole data plus m_t	- 3 - all Z-pole data plus m_W, Γ_W	- 4 - all Z-pole data plus m_t, m_W, Γ_W
m_t [GeV]	173^{+13}_{-10}	$171.4^{+2.1}_{-2.1}$	178^{+12}_{-9}	$171.7^{+2.0}_{-2.0}$
m_H [GeV]	111^{+190}_{-60}	103^{+54}_{-37}	137^{+228}_{-76}	85^{+39}_{-28}
$\log(m_H/\mathrm{GeV})$	$2.05^{+0.43}_{-0.34}$	$2.01^{+0.18}_{-0.19}$	$2.14^{+0.43}_{-0.35}$	$1.93^{+0.16}_{-0.17}$
$\alpha_S(m_Z^2)$	0.1190 ± 0.0027	0.1190 ± 0.0027	0.1190 ± 0.0028	0.1186 ± 0.0027
χ^2/d.o.f. (P)	16.0/10 (9.9%)	16.0/11 (14%)	17.4/12 (14%)	17.8/13 (17%)
$\sin^2\theta_{\mathrm{eff}}^{\mathrm{lept}}$	0.23149	0.23149	0.23145	0.23141
	± 0.00016	± 0.00016	± 0.00014	± 0.00014
$\sin^2\theta_W$	0.22331	0.22336	0.22298	0.22316
	± 0.00062	± 0.00039	± 0.00041	± 0.00031
m_W [GeV]	80.363 ± 0.032	80.361 ± 0.020	80.380 ± 0.021	80.371 ± 0.016

Table 10.2: Results of the fits to: (1) all Z-pole data (LEP-I and SLD), (2) all Z-pole data plus direct m_t determination, (3) all Z-pole data plus direct m_W and Γ_W determinations, (4) all Z-pole data plus direct m_t, m_W, Γ_W determinations (i.e., all high-Q^2 results). As the sensitivity to m_H is logarithmic, both m_H as well as $\log(m_H/\mathrm{GeV})$ are quoted. The bottom part of the table lists derived results for $\sin^2\theta_{\mathrm{eff}}^{\mathrm{lept}}$, $\sin^2\theta_W$ and m_W. See text for a discussion of theoretical errors not included in the errors above.

	Measurement with Total Error	Standard Model High-Q^2 Fit	Pull
APV [215]			
Q_W(Cs)	-72.74 ± 0.46	-72.907 ± 0.033	0.4
Møller [217]			
$\sin^2\theta_{\overline{\mathrm{MS}}}(m_Z)$	0.2330 ± 0.0015	0.23112 ± 0.00013	1.3
νN [218]			
$g^2_{\nu\mathrm{Lud}}$	0.30005 ± 0.00137	0.30389 ± 0.00017	2.8
$g^2_{\nu\mathrm{Rud}}$	0.03076 ± 0.00110	0.03011 ± 0.00003	0.6

Table 10.3: Summary of measurements performed in low-Q^2 reactions, namely atomic parity violation, e^-e^- Moller scattering and neutrino-nucleon scattering. The SM results and the pulls (difference between measurement and fit in units of the total measurement error) are derived from the SM fit including all high-Q^2 data (Table 10.2, column 4) with the Higgs mass treated as a free parameter.

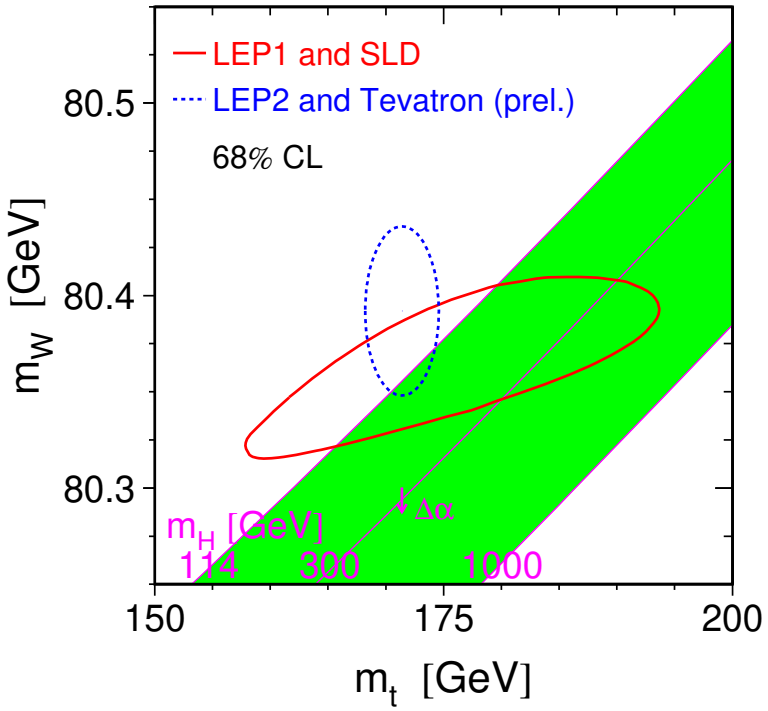

Figure 10.2: The comparison of the indirect measurements of m_W and m_t (LEP-I+ SLD data) (solid contour) and the direct measurements ($p\overline{p}$ colliders and LEP-II data) (dashed contour). In both cases the 68% CL contours are plotted. Also shown is the SM relationship for the masses as a function of the Higgs mass. The arrow labelled $\Delta\alpha$ shows the variation of this relation if $\alpha(m_Z^2)$ is changed by one standard deviation. This variation gives an additional uncertainty to the SM band shown in the figure.

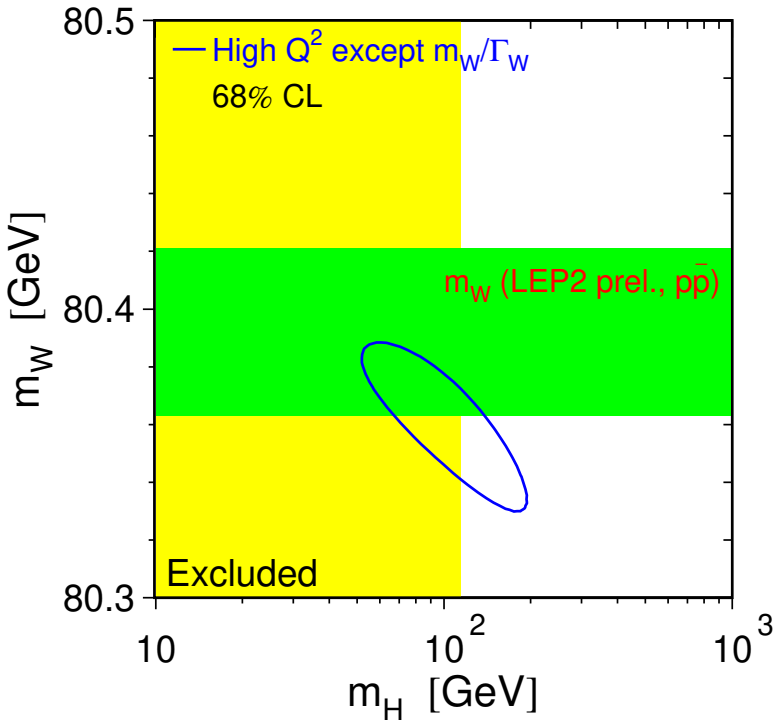

Figure 10.3: The 68% confidence level contour in m_{W} and m_{H} for the fit to all data except the direct measurement of m_{W}, indicated by the shaded horizontal band of ± 1 sigma width. The vertical band shows the 95% CL exclusion limit on m_{H} from the direct search.

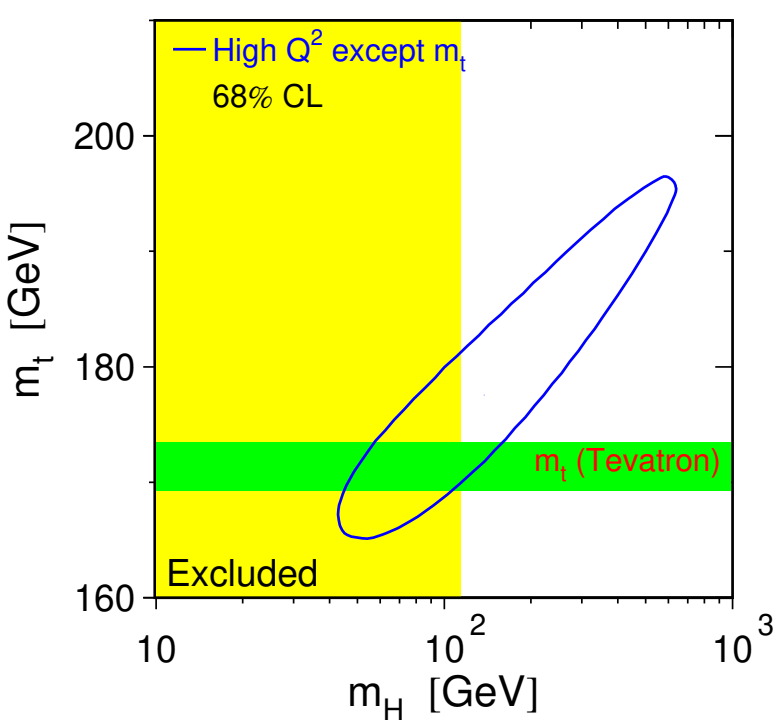

Figure 10.4: The 68% confidence level contour in m_{t} and m_{H} for the fit to all data except the direct measurement of m_{t}, indicated by the shaded horizontal band of ± 1 sigma width. The vertical band shows the 95% CL exclusion limit on m_{H} from the direct search.

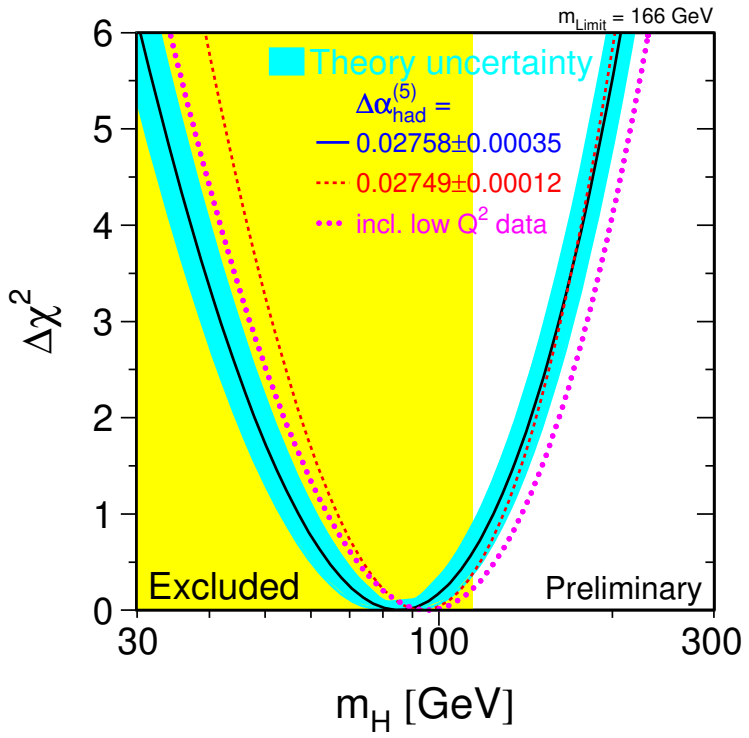

Figure 10.5: $\Delta\chi^2 = \chi^2 - \chi^2_{min}$ *vs.* $m_{\rm H}$ curve. The line is the result of the fit using all data (last column of Table 10.2); the band represents an estimate of the theoretical error due to missing higher order corrections. The vertical band shows the 95% CL exclusion limit on $m_{\rm H}$ from the direct search. The dashed curve is the result obtained using the evaluation of $\Delta\alpha^{(5)}_{\rm had}(m^2_{\rm Z})$ from Reference 250.

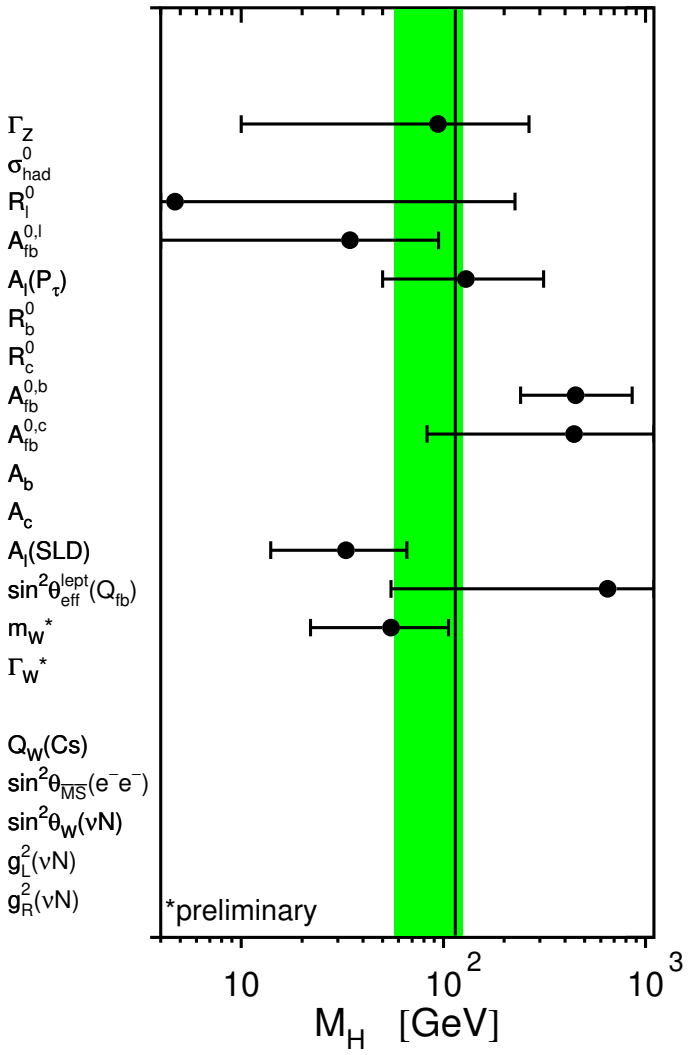

Figure 10.6: Constraints on the mass of the Higgs boson from each pseudo-observable. The Higgs-boson mass and its 68% CL uncertainty is obtained from a five-parameter SM fit to the observable, constraining $\Delta\alpha^{(5)}_{\rm had}(m^2_{\rm Z}) = 0.02761 \pm 0.00036$, $\alpha_{\rm S}(m^2_{\rm Z}) = 0.118 \pm 0.003$, $m_{\rm Z} = 91.1875 \pm 0.0021$ GeV and $m_{\rm t} = 171.4 \pm 2.1$ GeV. Because of these four common constraints the resulting Higgs-boson mass values are highly correlated. The shaded band denotes the overall constraint on the mass of the Higgs boson derived from all pseudo-observables including the above four SM parameters as reported in the last column of Table 10.2.

Chapter 11

Conclusions

A combination of many electroweak measurements in electron-positron collisions at centre-of-mass energies above the Z-pole is presented. The LEP experiments ALEPH, DELPHI, L3 and OPAL wish to stress that this report reflects for many of the results a preliminary status of their analyses at the time of the 2006 summer conferences. A definitive statement on the results must wait for publication by each collaboration. Note that in some cases some experiments have already published final results which are not yet included in the combinations presented in this paper.

The preliminary and published results from the LEP experiments and their combinations, test the Standard Model (SM) successfully at the highest interaction energies. The combination of the many precise electroweak results, including those obtained at the Z-pole [2], yields stringent constraints on the SM and its free parameters. Most measurements agree well with the predictions. The spread in values of the various determinations of the effective electroweak mixing angle in asymmetry measurements at the Z pole is somewhat larger than expected [2]. Within the SM analysis, this seems to be caused by the measurement of the forward-backward asymmetry in b-quark production, showing the largest pull of all Z-pole measurements w.r.t. the SM expectation. The final result of the NuTeV collaboration on the low-Q^2 left-handed couplings combination differs also by about 2.8 deviations from the SM expectation calculated based on the high-Q^2 precision electroweak measurements. Note, however, that these measurements pertain to different fermion flavours, are measured at very different Q^2 scales, and are of very different accuracy.

Prospects for the Future

The measurements from data taken at or near the Z resonance, both at LEP as well as at SLC, are final and published [2]. Improvements in accuracy will therefore take place in the high energy data (LEP-II), where each experiment has accumulated about 700 pb^{-1} of data. The measurements of m_{W} are likely to reach a precision not too far from the uncertainty on the prediction obtained via the radiative corrections of the Z-pole data, providing an important test of the Standard Model. In the measurement of the triple and quartic electroweak gauge boson self couplings, the analysis of the complete LEP-II statistics, together with the increased sensitivity at higher beam energies, will lead to an improvement in the current precision.

Acknowledgements

We would like to thank the CERN accelerator divisions for the efficient operation of the LEP accelerator, the precise information on the absolute energy scale and their close cooperation with the four experiments. We would also like to thank members of the SLD, CDF, DØ, E-158 and NuTeV collaborations for useful discussions concerning their results. Finally, the results of the section on Standard Model constraints would not be possible without the close collaboration of many theorists.

Appendix A

Detailed inputs and results on W-boson and four-fermion averages

Tables A.1 - A.18 give the details of the inputs and of the results for the calculation of LEP averages of the four-fermion cross-section and the corresponding cross-section ratios For both inputs and results, whenever relevant, the breakdown of the errors into their various components is given in the table.

For each measurement, the Collaborations have privately provided unpublished information which is necessary for the combination of LEP results, such as the expected statistical error or the split up of the systematic uncertainty into its correlated and uncorrelated components. Unless otherwise specified in the References, all other inputs are taken from published papers and public notes submitted to conferences.

$\sqrt{s}$ (GeV)	σ_{WW}	$\Delta\sigma^{\mathrm{stat}}_{\mathrm{WW}}$	(LCEC) $\Delta\sigma^{\mathrm{syst}}_{\mathrm{WW}}$	(LUEU) $\Delta\sigma^{\mathrm{syst}}_{\mathrm{WW}}$	(LUEC) $\Delta\sigma^{\mathrm{syst}}_{\mathrm{WW}}$	$\Delta\sigma^{\mathrm{syst}}_{\mathrm{WW}}$	$\Delta\sigma_{\mathrm{WW}}$	
ALEPH [75]								
182.7	15.86	±0.61	±0.08	±0.08	±0.09	±0.14	±0.63	
188.6	15.78	±0.34	±0.07	±0.05	±0.09	±0.12	±0.36	
191.6	17.10	±0.90	±0.07	±0.07	±0.09	±0.14	±0.90	
195.5	16.60	±0.52	±0.07	±0.06	±0.09	±0.12	±0.54	
199.5	16.93	±0.50	±0.07	±0.06	±0.09	±0.12	±0.52	
201.6	16.63	±0.70	±0.07	±0.07	±0.09	±0.13	±0.71	
204.9	16.84	±0.53	±0.07	±0.06	±0.09	±0.13	±0.54	
206.6	17.42	±0.41	±0.07	±0.06	±0.09	±0.13	±0.43	
DELPHI [76]								
182.7	16.07	±0.68	±0.09	±0.09	±0.08	±0.15	±0.70	
188.6	16.09	±0.39	±0.08	±0.09	±0.09	±0.15	±0.42	
191.6	16.64	±0.99	±0.09	±0.10	±0.09	±0.16	±1.00	
195.5	17.04	±0.58	±0.09	±0.10	±0.09	±0.16	±0.60	
199.5	17.39	±0.55	±0.09	±0.10	±0.09	±0.16	±0.57	
201.6	17.37	±0.80	±0.10	±0.10	±0.09	±0.17	±0.82	
204.9	17.56	±0.57	±0.10	±0.10	±0.09	±0.17	±0.59	
206.6	16.35	±0.44	±0.10	±0.10	±0.09	±0.17	±0.47	
L3 [77]								
182.7	16.53	±0.67	±0.19	±0.13	±0.12	±0.26	±0.72	
188.6	16.17	±0.37	±0.11	±0.06	±0.11	±0.17	±0.41	
191.6	16.11	±0.90	±0.11	±0.07	±0.11	±0.17	±0.92	
195.5	16.22	±0.54	±0.11	±0.06	±0.10	±0.16	±0.57	
199.5	16.49	±0.56	±0.11	±0.07	±0.11	±0.17	±0.58	
201.6	16.01	±0.82	±0.11	±0.06	±0.12	±0.17	±0.84	
204.9	17.00	±0.58	±0.12	±0.06	±0.11	±0.17	±0.60	
206.6	17.33	±0.44	±0.12	±0.04	±0.11	±0.17	±0.47	
OPAL [78,79]								
182.7	15.43	±0.61	±0.14	±0.00	±0.22	±0.26	±0.66	
188.6	16.30	±0.35	±0.11	±0.12	±0.07	±0.18	±0.39	
191.6	16.60	±0.90	±0.23	±0.32	±0.14	±0.42	±0.99	
195.5	18.59	±0.61	±0.23	±0.34	±0.14	±0.43	±0.75	
199.5	16.32	±0.55	±0.23	±0.26	±0.14	±0.37	±0.67	
201.6	18.48	±0.82	±0.23	±0.33	±0.14	±0.42	±0.92	
204.9	15.97	±0.52	±0.23	±0.26	±0.14	±0.37	±0.64	
206.6	17.77	±0.42	±0.23	±0.28	±0.14	±0.38	±0.57	
LEP Averages								χ^2/d.o.f.
182.7	15.88	±0.33	±0.10	±0.05	±0.06	±0.13	±0.35	
188.6	16.03	±0.18	±0.08	±0.04	±0.05	±0.10	±0.21	
191.6	16.56	±0.46	±0.10	±0.08	±0.05	±0.14	±0.48	
195.5	16.90	±0.29	±0.09	±0.06	±0.05	±0.12	±0.31	26.6/24
199.5	16.76	±0.27	±0.10	±0.06	±0.05	±0.13	±0.30	
201.6	16.99	±0.39	±0.10	±0.07	±0.05	±0.13	±0.41	
204.9	16.79	±0.28	±0.10	±0.07	±0.05	±0.13	±0.31	
206.6	17.15	±0.22	±0.10	±0.06	±0.05	±0.13	±0.25	

Table A.1: W-pair production cross-section (in pb) for different centre–of–mass energies. The first column contains the centre–of–mass energy and the second the measurements. Observed statistical uncertainties are used in the fit and are listed in the third column; when asymmetric errors are quoted by the Collaborations, the positive error is listed in the table and used in the fit. The fourth, fifth and sixth columns contain the components of the systematic errors, as subdivided by the Collaborations into LEP-correlated energy-correlated (LCEC), LEP-uncorrelated energy-uncorrelated (LUEU), LEP-uncorrelated energy-correlated (LUEC). The total systematic error is given in the seventh column, the total error in the eighth. For the LEP averages, the χ^2 of the fit is also given in the ninth column.

$\sqrt{s}$(GeV)	182.7	188.6	191.6	195.5	199.5	201.6	204.9	206.6
182.7	1.000	0.161	0.090	0.128	0.138	0.101	0.141	0.165
188.6	0.161	1.000	0.117	0.169	0.180	0.131	0.182	0.217
191.6	0.090	0.117	1.000	0.093	0.099	0.072	0.101	0.119
195.5	0.128	0.169	0.093	1.000	0.143	0.104	0.145	0.171
199.5	0.138	0.180	0.099	0.143	1.000	0.111	0.155	0.183
201.6	0.101	0.131	0.072	0.104	0.111	1.000	0.113	0.134
204.9	0.141	0.182	0.101	0.145	0.155	0.113	1.000	0.186
206.6	0.165	0.217	0.119	0.171	0.183	0.134	0.186	1.000

Table A.2: Correlation matrix for the LEP combined W-pair cross-sections listed at the bottom of Table A.1. Correlations are all positive and range from 9% to 22%.

$\sqrt{s}$	WW cross-section (pb)	
(GeV)	$\sigma_{\rm WW}^{\rm YFSWW}$	$\sigma_{\rm WW}^{\rm RACOONWW}$
182.7	15.361 ± 0.005	15.368 ± 0.008
188.6	16.266 ± 0.005	16.249 ± 0.011
191.6	16.568 ± 0.006	16.519 ± 0.009
195.5	16.841 ± 0.006	16.801 ± 0.009
199.5	17.017 ± 0.007	16.979 ± 0.009
201.6	17.076 ± 0.006	17.032 ± 0.009
204.9	17.128 ± 0.006	17.079 ± 0.009
206.6	17.145 ± 0.006	17.087 ± 0.009

Table A.3: W-pair cross-section predictions (in pb) for different centre–of–mass energies, according to YFSWW [84] and RACOONWW [85], for $m_{\rm W}$ = 80.35 GeV. The errors listed in the table are only the statistical errors from the numerical integration of the cross-section.

$\sqrt{s}$ (GeV)	$\mathcal{R}_{\rm WW}$	$\Delta\mathcal{R}_{\rm WW}^{\rm stat}$	(LCEU) $\Delta\mathcal{R}_{\rm WW}^{\rm syst}$	(LCEC) $\Delta\mathcal{R}_{\rm WW}^{\rm syst}$	(LUEU) $\Delta\mathcal{R}_{\rm WW}^{\rm syst}$	(LUEC) $\Delta\mathcal{R}_{\rm WW}^{\rm syst}$	$\Delta\mathcal{R}_{\rm WW}$	χ^2/d.o.f.
YFSWW [84]								
182.7	1.034	±0.021	±0.000	±0.006	±0.003	±0.004	±0.023	26.6/24
188.6	0.986	±0.011	±0.000	±0.005	±0.003	±0.003	±0.013	
191.6	1.000	±0.028	±0.000	±0.006	±0.005	±0.003	±0.029	
195.5	1.003	±0.017	±0.000	±0.006	±0.004	±0.003	±0.019	
199.5	0.985	±0.016	±0.000	±0.006	±0.004	±0.003	±0.018	
201.6	0.995	±0.023	±0.000	±0.006	±0.004	±0.003	±0.024	
204.9	0.980	±0.016	±0.000	±0.006	±0.004	±0.003	±0.018	
206.6	1.000	±0.013	±0.000	±0.006	±0.003	±0.003	±0.015	
Average	0.994	±0.006	±0.000	±0.005	±0.001	±0.003	±0.009	32.2/31
RACOONWW [85]								
182.7	1.033	±0.021	±0.001	±0.006	±0.003	±0.004	±0.023	26.6/24
188.6	0.987	±0.011	±0.001	±0.005	±0.003	±0.003	±0.013	
191.6	1.003	±0.028	±0.001	±0.006	±0.005	±0.003	±0.029	
195.5	1.006	±0.017	±0.001	±0.006	±0.004	±0.003	±0.019	
199.5	0.987	±0.016	±0.001	±0.006	±0.004	±0.003	±0.018	
201.6	0.998	±0.023	±0.001	±0.006	±0.004	±0.003	±0.024	
204.9	0.983	±0.016	±0.001	±0.006	±0.004	±0.003	±0.018	
206.6	1.004	±0.013	±0.001	±0.006	±0.003	±0.003	±0.015	
Average	0.996	±0.006	±0.000	±0.006	±0.001	±0.003	±0.009	32.0/31

Table A.4: Ratios of LEP combined W-pair cross-section measurements to the expectations of the considered theoretical models, for different centre–of–mass energies and for all energies combined. The first column contains the centre–of–mass energy, the second the combined ratios, the third the statistical errors. The fourth, fifth, sixth and seventh columns contain the sources of systematic errors that are considered as LEP-correlated energy-uncorrelated (LCEU), LEP-correlated energy-correlated (LCEC), LEP-uncorrelated energy-uncorrelated (LUEU), LEP-uncorrelated energy-correlated (LUEC). The total error is given in the eighth column. The only LCEU systematic sources considered are the statistical errors on the cross-section theoretical predictions, while the LCEC, LUEU and LUEC sources are those coming from the corresponding errors on the cross-section measurements. For the LEP averages, the χ^2 of the fit is also given in the ninth column.

Decay channel	$\mathcal{B}$	$\Delta\mathcal{B}^{\rm stat}$	$\Delta\mathcal{B}^{\rm syst}$ (unc)	$\Delta\mathcal{B}^{\rm syst}$ (cor)	$\Delta\mathcal{B}^{\rm syst}$	$\Delta\mathcal{B}$	3×3 correlation for $\Delta\mathcal{B}$		
ALEPH [75]									
$\mathcal{B}(W \to e\overline{\nu}_e)$	10.78	±0.27	±0.09	±0.04	±0.10	±0.29	1.000	-0.009	-0.332
$\mathcal{B}(W \to \mu\overline{\nu}_\mu)$	10.87	±0.25	±0.07	±0.04	±0.08	±0.26	-0.009	1.000	-0.268
$\mathcal{B}(W \to \tau\overline{\nu}_\tau)$	11.25	±0.32	±0.19	±0.05	±0.20	±0.38	-0.332	-0.268	1.000
DELPHI [76]									
$\mathcal{B}(W \to e\overline{\nu}_e)$	10.55	±0.31	±0.13	±0.05	±0.14	±0.34	1.000	0.030	-0.340
$\mathcal{B}(W \to \mu\overline{\nu}_\mu)$	10.65	±0.26	±0.06	±0.05	±0.08	±0.27	0.030	1.000	-0.170
$\mathcal{B}(W \to \tau\overline{\nu}_\tau)$	11.46	±0.39	±0.17	±0.09	±0.19	±0.43	-0.340	-0.170	1.000
L3 [77]									
$\mathcal{B}(W \to e\overline{\nu}_e)$	10.78	±0.29	±0.10	±0.08	±0.13	±0.32	1.000	-0.016	-0.279
$\mathcal{B}(W \to \mu\overline{\nu}_\mu)$	10.03	±0.29	±0.10	±0.07	±0.12	±0.31	-0.016	1.000	-0.295
$\mathcal{B}(W \to \tau\overline{\nu}_\tau)$	11.89	±0.40	±0.17	±0.11	±0.20	±0.45	-0.279	-0.295	1.000
OPAL [78,79]									
$\mathcal{B}(W \to e\overline{\nu}_e)$	10.40	±0.25	±0.24	±0.05	±0.25	±0.35	1.000	0.141	-0.179
$\mathcal{B}(W \to \mu\overline{\nu}_\mu)$	10.61	±0.25	±0.23	±0.06	±0.24	±0.35	0.141	1.000	-0.174
$\mathcal{B}(W \to \tau\overline{\nu}_\tau)$	11.18	±0.31	±0.37	±0.05	±0.37	±0.48	-0.179	-0.174	1.000
LEP Average (without lepton universality assumption)									
$\mathcal{B}(W \to e\overline{\nu}_e)$	10.65	±0.14	±0.07	±0.05	±0.09	±0.17	1.000	0.110	-0.195
$\mathcal{B}(W \to \mu\overline{\nu}_\mu)$	10.59	±0.13	±0.05	±0.05	±0.08	±0.15	0.110	1.000	-0.132
$\mathcal{B}(W \to \tau\overline{\nu}_\tau)$	11.44	±0.18	±0.11	±0.07	±0.13	±0.22	-0.195	-0.132	1.000
χ^2/d.o.f.	6.3/9								
LEP Average (with lepton universality assumption)									
$\mathcal{B}(W \to \ell\overline{\nu}_\ell)$	10.84	±0.06	±0.04	±0.06	±0.07	±0.09			
$\mathcal{B}(W \to$ had.)	67.48	±0.19	±0.12	±0.18	±0.21	±0.28			
χ^2/d.o.f.	15.4/11								

Table A.5: W branching fraction measurements (in %). The first column contains the decay channel, the second the measurements, the third the statistical uncertainty. The fourth and fifth column list the uncorrelated and correlated components of the systematic errors, as provided by the Collaborations. The total systematic error is given in the sixth column and the total error in the seventh. Correlation matrices for the three leptonic branching fractions are given in the last column.

ALEPH [75]

$\sqrt{s}$ interval (GeV)			Luminosity (pb^{-1})			Lumi weighted $\sqrt{s}$ (GeV)				
180-184			56.81			182.65				
cosθ_{W-} bin i	1	2	3	4	5	6	7	8	9	10
σ_i (pb)	0.216	0.498	0.696	1.568	1.293	1.954	2.486	2.228	4.536	6.088
$\delta\sigma_i$(stat) (pb)	0.053	0.137	0.185	0.517	0.319	0.481	0.552	0.363	0.785	0.874
$\delta\sigma_i$(stat,exp.) (pb)	0.263	0.276	0.309	0.341	0.376	0.415	0.459	0.523	0.597	0.714
$\delta\sigma_i$(syst,unc) (pb)	0.012	0.018	0.017	0.025	0.023	0.021	0.036	0.047	0.047	0.066
$\delta\sigma_i$(syst,cor) (pb)	0.004	0.003	0.003	0.003	0.003	0.004	0.004	0.003	0.004	0.006
$\sqrt{s}$ interval (GeV)			Luminosity (pb^{-1})			Lumi weighted $\sqrt{s}$ (GeV)				
184-194			203.14			189.05				
cosθ_{W-} bin i	1	2	3	4	5	6	7	8	9	10
σ_i (pb)	0.665	0.743	0.919	0.990	1.156	2.133	2.795	3.070	3.851	5.772
$\delta\sigma_i$(stat) (pb)	0.148	0.140	0.158	0.142	0.144	0.287	0.337	0.297	0.300	0.366
$\delta\sigma_i$(stat,exp.) (pb)	0.132	0.147	0.157	0.175	0.196	0.223	0.246	0.282	0.332	0.408
$\delta\sigma_i$(syst,unc) (pb)	0.010	0.016	0.015	0.024	0.021	0.020	0.035	0.047	0.049	0.075
$\delta\sigma_i$(syst,cor) (pb)	0.003	0.003	0.003	0.002	0.002	0.003	0.003	0.003	0.005	0.005
$\sqrt{s}$ interval (GeV)			Luminosity (pb^{-1})			Lumi weighted $\sqrt{s}$ (GeV)				
194-204			208.03			198.42				
cosθ_{W-} bin i	1	2	3	4	5	6	7	8	9	10
σ_i (pb)	0.802	0.475	0.886	0.972	1.325	1.889	2.229	3.581	4.428	6.380
$\delta\sigma_i$(stat) (pb)	0.225	0.082	0.162	0.147	0.186	0.248	0.245	0.363	0.343	0.368
$\delta\sigma_i$(stat,exp.) (pb)	0.124	0.134	0.149	0.167	0.188	0.214	0.241	0.281	0.338	0.433
$\delta\sigma_i$(syst,unc) (pb)	0.007	0.013	0.012	0.021	0.018	0.016	0.032	0.046	0.049	0.082
$\delta\sigma_i$(syst,cor) (pb)	0.003	0.002	0.002	0.002	0.002	0.002	0.002	0.003	0.003	0.004
$\sqrt{s}$ interval (GeV)			Luminosity (pb^{-1})			Lumi weighted $\sqrt{s}$ (GeV)				
204-210			214.62			205.90				
cosθ_{W-} bin i	1	2	3	4	5	6	7	8	9	10
σ_i (pb)	0.334	0.637	0.800	1.229	1.229	1.789	2.810	2.740	4.192	8.005
$\delta\sigma_i$(stat) (pb)	0.072	0.136	0.148	0.224	0.176	0.237	0.351	0.246	0.306	0.474
$\delta\sigma_i$(stat,exp.) (pb)	0.114	0.126	0.143	0.155	0.180	0.206	0.234	0.273	0.338	0.443
$\delta\sigma_i$(syst,unc) (pb)	0.008	0.013	0.013	0.020	0.018	0.017	0.033	0.046	0.052	0.089
$\delta\sigma_i$(syst,cor) (pb)	0.003	0.003	0.003	0.002	0.002	0.003	0.003	0.003	0.004	0.005

Table A.6: W^- differential angular cross-section in the 10 angular bins for the four chosen energy intervals for the ALEPH experiment. For each energy range, the measured integrated luminosity and the luminosity weighted centre-of-mass energy is reported. The results per angular bin in each of the energy interval are then presented: σ_i indicates the average of $d[\sigma_{WW}(BR_{e\nu}+BR_{\mu\nu})]/d\cos\theta_{W-}$ in the i-th bin of $\cos\theta_{W-}$ with width 0.2. The values, in each bin, of the measured and expected statistical error and of the systematic errors, LEP uncorrelated and correlated, are reported as well. All values are expressed in pb

DELPHI [76]

$\sqrt{s}$ interval (GeV)	Luminosity (pb^{-1})	Lumi weighted $\sqrt{s}$ (GeV)
180-184	51.63	182.65

$\cos\theta_{W-}$ bin i	1	2	3	4	5	6	7	8	9	10
σ_i (pb)	0.715	0.795	1.175	1.365	1.350	1.745	1.995	2.150	4.750	6.040
$\delta\sigma_i$(stat) (pb)	0.320	0.315	0.380	0.400	0.400	0.450	0.485	0.510	0.775	0.895
$\delta\sigma_i$(stat,exp.) (pb)	0.320	0.315	0.350	0.370	0.405	0.450	0.505	0.580	0.695	0.850
$\delta\sigma_i$(syst,unc) (pb)	0.020	0.025	0.035	0.035	0.040	0.085	0.050	0.065	0.095	0.075
$\delta\sigma_i$(syst,cor) (pb)	0.045	0.025	0.020	0.015	0.015	0.025	0.015	0.015	0.030	0.035

$\sqrt{s}$ interval (GeV)	Luminosity (pb^{-1})	Lumi weighted $\sqrt{s}$ (GeV)
184-194	178.32	189.03

$\cos\theta_{W-}$ bin i	1	2	3	4	5	6	7	8	9	10
σ_i (pb)	0.865	0.760	0.990	0.930	1.330	1.460	1.675	2.630	4.635	5.4000
$\delta\sigma_i$(stat) (pb)	0.180	0.170	0.185	0.180	0.215	0.225	0.240	0.300	0.405	0.4550
$\delta\sigma_i$(stat,exp.) (pb)	0.165	0.170	0.180	0.200	0.215	0.240	0.270	0.320	0.385	0.4900
$\delta\sigma_i$(syst,unc) (pb)	0.020	0.020	0.035	0.035	0.040	0.085	0.050	0.060	0.100	0.0850
$\delta\sigma_i$(syst,cor) (pb)	0.040	0.020	0.020	0.015	0.015	0.020	0.015	0.015	0.025	0.0350

$\sqrt{s}$ interval (GeV)	Luminosity (pb^{-1})	Lumi weighted $\sqrt{s}$ (GeV)
194-204	193.52	198.46

$\cos\theta_{W-}$ bin i	1	2	3	4	5	6	7	8	9	10
σ_i (pb)	0.600	0.675	1.510	1.150	1.055	1.635	2.115	3.175	4.470	7.1400
$\delta\sigma_i$(stat) (pb)	0.155	0.160	0.215	0.190	0.185	0.225	0.255	0.320	0.385	0.5000
$\delta\sigma_i$(stat,exp.) (pb)	0.150	0.160	0.170	0.180	0.200	0.230	0.260	0.310	0.380	0.5050
$\delta\sigma_i$(syst,unc) (pb)	0.015	0.020	0.030	0.035	0.035	0.085	0.045	0.055	0.105	0.1000
$\delta\sigma_i$(syst,cor) (pb)	0.025	0.015	0.015	0.015	0.015	0.015	0.010	0.015	0.025	0.0300

$\sqrt{s}$ interval (GeV)	Luminosity (pb^{-1})	Lumi weighted $\sqrt{s}$ (GeV)
204-210	198.59	205.91

$\cos\theta_{W-}$ bin i	1	2	3	4	5	6	7	8	9	10
σ_i (pb)	0.275	0.590	0.575	0.930	1.000	1.190	2.120	2.655	4.585	7.2900
$\delta\sigma_i$(stat) (pb)	0.120	0.145	0.140	0.170	0.175	0.195	0.255	0.290	0.385	0.5050
$\delta\sigma_i$(stat,exp.) (pb)	0.145	0.150	0.160	0.175	0.195	0.220	0.250	0.300	0.380	0.5200
$\delta\sigma_i$(syst,unc) (pb)	0.015	0.020	0.025	0.035	0.035	0.085	0.045	0.055	0.110	0.1100
$\delta\sigma_i$(syst,cor) (pb)	0.020	0.015	0.010	0.010	0.015	0.010	0.010	0.010	0.020	0.0300

Table A.7: W^- differential angular cross-section in the 10 angular bins for the four chosen energy intervals for the DELPHI experiment. For each energy range, the measured integrated luminosity and the luminosity weighted centre-of-mass energy is reported. The results per angular bin in each of the energy interval are then presented: σ_i indicates the average of $d[\sigma_{WW}(BR_{e\nu}+BR_{\mu\nu})]/d\cos\theta_{W-}$ in the i-th bin of $\cos\theta_{W-}$ with width 0.2. The values, in each bin, of the measured and expected statistical error and of the systematic errors, LEP uncorrelated and correlated, are reported as well. All values are expressed in pb

L3 [77]

$\sqrt{s}$ interval (GeV)	Luminosity (pb^{-1})	Lumi weighted $\sqrt{s}$ (GeV)
180-184	55.46	182.68

$\cos\theta_{W-}$ bin i	1	2	3	4	5	6	7	8	9	10
σ_i (pb)	0.691	0.646	0.508	0.919	1.477	2.587	3.541	3.167	3.879	4.467
$\delta\sigma_i$(stat) (pb)	0.270	0.265	0.243	0.322	0.407	0.539	0.640	0.619	0.708	0.801
$\delta\sigma_i$(stat,exp.) (pb)	0.269	0.290	0.329	0.364	0.404	0.453	0.508	0.591	0.704	0.877
$\delta\sigma_i$(syst,unc) (pb)	0.016	0.009	0.007	0.011	0.018	0.031	0.043	0.039	0.048	0.058
$\delta\sigma_i$(syst,cor) (pb)	0.002	0.002	0.002	0.003	0.005	0.009	0.012	0.011	0.013	0.015

$\sqrt{s}$ interval (GeV)	Luminosity (pb^{-1})	Lumi weighted $\sqrt{s}$ (GeV)
184-194	206.49	189.16

$\cos\theta_{W-}$ bin i	1	2	3	4	5	6	7	8	9	10
σ_i (pb)	0.759	0.902	1.125	1.320	1.472	1.544	2.085	2.870	4.144	6.022
$\delta\sigma_i$(stat) (pb)	0.128	0.151	0.173	0.190	0.209	0.213	0.254	0.303	0.370	0.459
$\delta\sigma_i$(stat,exp.) (pb)	0.115	0.137	0.160	0.180	0.205	0.223	0.262	0.304	0.367	0.461
$\delta\sigma_i$(syst,unc) (pb)	0.017	0.013	0.015	0.015	0.017	0.018	0.024	0.034	0.048	0.074
$\delta\sigma_i$(syst,cor) (pb)	0.003	0.003	0.004	0.005	0.005	0.005	0.007	0.010	0.014	0.021

$\sqrt{s}$ interval (GeV)	Luminosity (pb^{-1})	Lumi weighted $\sqrt{s}$ (GeV)
194-204	203.50	198.30

$\cos\theta_{W-}$ bin i	1	2	3	4	5	6	7	8	9	10
σ_i (pb)	0.652	0.709	0.880	0.859	1.140	1.295	2.114	2.334	3.395	5.773
$\delta\sigma_i$(stat) (pb)	0.105	0.123	0.146	0.155	0.179	0.192	0.255	0.264	0.333	0.442
$\delta\sigma_i$(stat,exp.) (pb)	0.092	0.117	0.140	0.164	0.184	0.209	0.245	0.288	0.354	0.459
$\delta\sigma_i$(syst,unc) (pb)	0.014	0.010	0.011	0.010	0.013	0.015	0.024	0.027	0.040	0.071
$\delta\sigma_i$(syst,cor) (pb)	0.002	0.002	0.003	0.003	0.004	0.004	0.007	0.008	0.012	0.020

$\sqrt{s}$ interval (GeV)	Luminosity (pb^{-1})	Lumi weighted $\sqrt{s}$ (GeV)
204-210	217.30	205.96

$\cos\theta_{W-}$ bin i	1	2	3	4	5	6	7	8	9	10
σ_i (pb)	0.678	0.578	0.768	1.052	1.620	1.734	1.873	2.903	4.638	7.886
$\delta\sigma_i$(stat) (pb)	0.111	0.114	0.140	0.168	0.212	0.226	0.238	0.302	0.394	0.534
$\delta\sigma_i$(stat,exp.) (pb)	0.089	0.117	0.141	0.164	0.186	0.216	0.251	0.303	0.387	0.528
$\delta\sigma_i$(syst,unc) (pb)	0.015	0.008	0.010	0.012	0.019	0.020	0.021	0.034	0.054	0.097
$\delta\sigma_i$(syst,cor) (pb)	0.002	0.002	0.003	0.004	0.006	0.006	0.006	0.010	0.016	0.027

Table A.8: W^- differential angular cross-section in the 10 angular bins for the four chosen energy intervals for the L3 experiment. For each energy range, the measured integrated luminosity and the luminosity weighted centre-of-mass energy is reported. The results per angular bin in each of the energy interval are then presented: σ_i indicates the average of $d[\sigma_{WW}(BR_{e\nu}+BR_{\mu\nu})]/d\cos\theta_{W-}$ in the i-th bin of $\cos\theta_{W-}$ with width 0.2. The values, in each bin, of the measured and expected statistical error and of the systematic errors, LEP uncorrelated and correlated, are reported as well. All values are expressed in pb

$\sqrt{s}$ (GeV)	$\sigma_{We\nu\ (tot)}$	$\Delta\sigma^{stat}_{We\nu\ (tot)}$	(LCEC) $\Delta\sigma^{syst}_{We\nu\ (tot)}$	(LUEU) $\Delta\sigma^{syst}_{We\nu\ (tot)}$	(LUEC) $\Delta\sigma^{syst}_{We\nu\ (tot)}$	$\Delta\sigma_{We\nu\ (tot)}$	$\Delta\sigma^{stat\ (exp)}_{We\nu\ (tot)}$
ALEPH [105]							
182.7	0.60	$^{+0.32}_{-0.26}$	±0.02	±0.01	±0.01	$^{+0.32}_{-0.26}$	±0.29
188.6	0.55	$^{+0.18}_{-0.16}$	±0.02	±0.01	±0.01	$^{+0.18}_{-0.16}$	±0.18
191.6	0.89	$^{+0.58}_{-0.44}$	±0.02	±0.01	±0.02	$^{+0.58}_{-0.44}$	±0.48
195.5	0.87	$^{+0.31}_{-0.27}$	±0.03	±0.01	±0.02	$^{+0.31}_{-0.27}$	±0.28
199.5	1.31	$^{+0.32}_{-0.29}$	±0.03	±0.01	±0.02	$^{+0.32}_{-0.29}$	±0.26
201.6	0.80	$^{+0.42}_{-0.35}$	±0.03	±0.01	±0.02	$^{+0.42}_{-0.35}$	±0.38
204.9	0.65	$^{+0.27}_{-0.23}$	±0.03	±0.02	±0.02	$^{+0.27}_{-0.23}$	±0.27
206.6	0.81	$^{+0.22}_{-0.20}$	±0.03	±0.02	±0.02	$^{+0.22}_{-0.20}$	±0.22
DELPHI [92,255]							
182.7	0.69	$^{+0.41}_{-0.23}$	±0.02	±0.04	±0.08	$^{+0.42}_{-0.25}$	±0.33
188.6	0.75	$^{+0.22}_{-0.20}$	±0.02	±0.04	±0.08	$^{+0.23}_{-0.22}$	±0.20
191.6	0.40	$^{+0.54}_{-0.31}$	±0.02	±0.03	±0.08	$^{+0.55}_{-0.33}$	±0.48
195.5	0.68	$^{+0.33}_{-0.28}$	±0.02	±0.03	±0.08	$^{+0.34}_{-0.38}$	±0.30
199.5	0.95	$^{+0.33}_{-0.29}$	±0.02	±0.03	±0.08	$^{+0.34}_{-0.30}$	±0.29
201.6	1.24	$^{+0.51}_{-0.42}$	±0.02	±0.04	±0.08	$^{+0.52}_{-0.43}$	±0.41
204.9	1.06	$^{+0.36}_{-0.30}$	±0.02	±0.05	±0.08	$^{+0.37}_{-0.32}$	±0.33
206.6	1.14	$^{+0.26}_{-0.23}$	±0.02	±0.04	±0.08	$^{+0.28}_{-0.25}$	±0.23
L3 [256,257]							
182.7	0.80	$^{+0.28}_{-0.25}$	±0.04	±0.04	±0.01	$^{+0.28}_{-0.25}$	±0.26
188.6	0.69	$^{+0.16}_{-0.14}$	±0.03	±0.03	±0.01	$^{+0.16}_{-0.15}$	±0.15
191.6	1.11	$^{+0.48}_{-0.41}$	±0.02	±0.04	±0.01	$^{+0.48}_{-0.41}$	±0.46
195.5	0.97	$^{+0.27}_{-0.25}$	±0.02	±0.02	±0.01	$^{+0.27}_{-0.25}$	±0.25
199.5	0.88	$^{+0.26}_{-0.24}$	±0.02	±0.03	±0.01	$^{+0.26}_{-0.24}$	±0.25
201.6	1.50	$^{+0.45}_{-0.40}$	±0.03	±0.04	±0.02	$^{+0.45}_{-0.40}$	±0.38
204.9	0.78	$^{+0.29}_{-0.25}$	±0.02	±0.03	±0.01	$^{+0.29}_{-0.25}$	±0.29
206.6	1.08	$^{+0.21}_{-0.20}$	±0.02	±0.03	±0.01	$^{+0.21}_{-0.20}$	±0.23
OPAL [258]							
188.6 GeV	0.67	$^{+0.16}_{-0.14}$	±0.04	±0.04	±0.00	$^{+0.17}_{-0.15}$	±0.16
LEP							χ^2/d.o.f.
182.7	0.70	±0.17	±0.03	±0.02	±0.02	±0.17	
188.6	0.66	±0.08	±0.03	±0.02	±0.01	±0.09	
191.6	0.81	±0.27	±0.02	±0.02	±0.02	±0.28	
195.5	0.85	±0.16	±0.02	±0.01	±0.02	±0.16	
199.5	1.05	±0.15	±0.02	±0.01	±0.02	±0.16	8.1/16
201.6	1.17	±0.23	±0.03	±0.02	±0.02	±0.23	
204.9	0.80	±0.17	±0.02	±0.02	±0.02	±0.17	
206.6	1.00	±0.13	±0.03	±0.02	±0.02	±0.14	

Table A.9: Single-W total production cross-section (in pb) at different energies. The first column contains the LEP centre–of–mass energy, and the second the measurements. The third column reports the statistical error, whereas in the fourth to the sixth columns the different systematic uncertainties are listed. The seventh column contains the total error and the eight lists, for the four LEP measurements, the symmetrized expected statistical error, and for the LEP combined value, the χ^2 of the fit.

$\sqrt{s}$ (GeV)	$\sigma_{We\nu\ (had)}$	$\Delta\sigma^{stat}_{We\nu\ (had)}$	(LCEC) $\Delta\sigma^{syst}_{We\nu\ (had)}$	(LUEU) $\Delta\sigma^{syst}_{We\nu\ (had)}$	(LUEC) $\Delta\sigma^{syst}_{We\nu\ (had)}$	$\Delta\sigma_{We\nu\ (had)}$	$\Delta\sigma^{stat\ (exp)}_{We\nu\ (had)}$
ALEPH [105]							
182.7	0.44	$^{+0.29}_{-0.24}$	±0.01	±0.01	±0.01	$^{+0.29}_{-0.24}$	±0.26
188.6	0.33	$^{+0.16}_{-0.14}$	±0.02	±0.01	±0.01	$^{+0.16}_{-0.15}$	±0.16
191.6	0.52	$^{+0.52}_{-0.40}$	±0.02	±0.01	±0.01	$^{+0.52}_{-0.40}$	±0.45
195.5	0.61	$^{+0.28}_{-0.25}$	±0.02	±0.01	±0.01	$^{+0.28}_{-0.25}$	±0.25
199.5	1.06	$^{+0.30}_{-0.27}$	±0.02	±0.01	±0.01	$^{+0.30}_{-0.27}$	±0.24
201.6	0.72	$^{+0.39}_{-0.33}$	±0.02	±0.01	±0.02	$^{+0.39}_{-0.33}$	±0.34
204.9	0.34	$^{+0.24}_{-0.21}$	±0.02	±0.01	±0.02	$^{+0.24}_{-0.21}$	±0.25
206.6	0.64	$^{+0.21}_{-0.19}$	±0.02	±0.01	±0.02	$^{+0.21}_{-0.19}$	±0.19
DELPHI [92,255]							
182.7	0.11	$^{+0.30}_{-0.11}$	±0.02	±0.03	±0.08	$^{+0.31}_{-0.14}$	±0.30
188.6	0.57	$^{+0.19}_{-0.18}$	±0.02	±0.04	±0.08	$^{+0.21}_{-0.20}$	±0.18
191.6	0.30	$^{+0.47}_{-0.30}$	±0.02	±0.03	±0.08	$^{+0.48}_{-0.31}$	±0.43
195.5	0.50	$^{+0.29}_{-0.26}$	±0.02	±0.03	±0.08	$^{+0.30}_{-0.27}$	±0.27
199.5	0.57	$^{+0.27}_{-0.25}$	±0.02	±0.02	±0.08	$^{+0.28}_{-0.26}$	±0.25
201.6	0.67	$^{+0.39}_{-0.35}$	±0.02	±0.03	±0.08	$^{+0.40}_{-0.36}$	±0.35
204.9	0.99	$^{+0.32}_{-0.30}$	±0.02	±0.05	±0.08	$^{+0.33}_{-0.31}$	±0.28
206.6	0.81	$^{+0.22}_{-0.20}$	±0.02	±0.04	±0.08	$^{+0.23}_{-0.22}$	±0.20
L3 [256,257]							
182.7	0.58	$^{+0.23}_{-0.20}$	±0.03	±0.03	±0.00	$^{+0.23}_{-0.20}$	±0.21
188.6	0.52	$^{+0.14}_{-0.13}$	±0.02	±0.02	±0.00	$^{+0.14}_{-0.13}$	±0.14
191.6	0.84	$^{+0.44}_{-0.37}$	±0.03	±0.03	±0.00	$^{+0.44}_{-0.37}$	±0.41
195.5	0.66	$^{+0.24}_{-0.22}$	±0.02	±0.03	±0.00	$^{+0.25}_{-0.23}$	±0.21
199.5	0.37	$^{+0.22}_{-0.20}$	±0.01	±0.02	±0.00	$^{+0.22}_{-0.20}$	±0.22
201.6	1.10	$^{+0.40}_{-0.35}$	±0.05	±0.05	±0.00	$^{+0.40}_{-0.35}$	±0.35
204.9	0.42	$^{+0.25}_{-0.21}$	±0.02	±0.03	±0.00	$^{+0.25}_{-0.21}$	±0.25
206.6	0.66	$^{+0.19}_{-0.17}$	±0.02	±0.03	±0.00	$^{+0.20}_{-0.18}$	±0.20
OPAL [258]							
188.6	0.53	$^{+0.13}_{-0.12}$	±0.04	±0.04	±0.00	$^{+0.14}_{-0.13}$	±0.14
LEP							χ^2/d.o.f.
182.7	0.42	±0.15	±0.02	±0.02	±0.01	±0.15	
188.6	0.48	±0.07	±0.02	±0.02	±0.01	±0.08	
191.6	0.56	±0.25	±0.02	±0.02	±0.02	±0.25	
195.5	0.60	±0.14	±0.02	±0.01	±0.02	±0.14	
199.5	0.65	±0.14	±0.02	±0.01	±0.02	±0.14	13.3/16
201.6	0.82	±0.20	±0.03	±0.02	±0.02	±0.20	
204.9	0.54	±0.15	±0.02	±0.02	±0.02	±0.15	
206.6	0.69	±0.11	±0.02	±0.02	±0.02	±0.12	

Table A.10: Single-W hadronic production cross-section (in pb) at different energies. The first column contains the LEP centre–of–mass energy, and the second the measurements. The third column reports the statistical error, whereas in the fourth to the sixth columns the different systematic uncertainties are listed. The seventh column contains the total error and the eight lists, for the four LEP measurements, the symmetrized expected statistical error, and for the LEP combined value, the χ^2 of the fit.

$\sqrt{s}$ (GeV)	Weν $\to$qqeν cross-section (pb)			Weν total cross-section (pb)	
	$\sigma^{\texttt{grc4f}}_{\mathrm{We}\nu\ (\mathrm{had})}$	$\sigma^{\mathrm{WPHACT}}_{\mathrm{We}\nu\ (\mathrm{had})}$	$\sigma^{\mathrm{WTO}}_{\mathrm{We}\nu\ (\mathrm{had})}$	$\sigma^{\texttt{grc4f}}_{\mathrm{We}\nu\ (\mathrm{tot})}$	$\sigma^{\mathrm{WPHACT}}_{\mathrm{We}\nu\ (\mathrm{tot})}$
182.7	0.4194[1]	0.4070[2]	0.40934[8]	0.6254[1]	0.6066[2]
188.6	0.4699[1]	0.4560[2]	0.45974[9]	0.6999[1]	0.6796[2]
191.6	0.4960[1]	0.4810[2]	0.4852[1]	0.7381[2]	0.7163[2]
195.5	0.5308[2]	0.5152[2]	0.5207[1]	0.7896[2]	0.7665[3]
199.5	0.5673[2]	0.5509[3]	0.5573[1]	0.8431[2]	0.8182[3]
201.6	0.5870[2]	0.5704[4]	0.5768[1]	0.8718[2]	0.8474[4]
204.9	0.6196[2]	0.6021[4]	0.6093[2]	0.9185[3]	0.8921[4]
206.6	0.6358[2]	0.6179[4]	0.6254[2]	0.9423[3]	0.9157[5]

Table A.11: Single-W hadronic and total cross-section predictions (in pb) interpolated at the data centre–of–mass energies, according to the `grc4f` [95], WPHACT [94] and WTO [93] predictions. The numbers in brackets are the errors on the last digit and are coming from the numerical integration of the cross-section only.

$\sqrt{s}$ (GeV)	$\mathcal{R}_{\mathrm{We}\nu}$	$\Delta\mathcal{R}^{\mathrm{stat}}_{\mathrm{We}\nu}$	(LCEU) $\Delta\mathcal{R}^{\mathrm{syst}}_{\mathrm{We}\nu}$	(LCEC) $\Delta\mathcal{R}^{\mathrm{syst}}_{\mathrm{We}\nu}$	(LUEU) $\Delta\mathcal{R}^{\mathrm{syst}}_{\mathrm{We}\nu}$	(LUEC) $\Delta\mathcal{R}^{\mathrm{syst}}_{\mathrm{We}\nu}$	$\Delta\mathcal{R}_{\mathrm{We}\nu}$	χ^2/d.o.f.
`grc4f` [95]								
182.7	1.122	$\pm$0.266	$\pm$0.001	$\pm$0.041	$\pm$0.029	$\pm$0.026	$\pm$0.272	8.1/16
188.6	0.942	$\pm$0.121	$\pm$0.001	$\pm$0.039	$\pm$0.023	$\pm$0.018	$\pm$0.130	
191.6	1.094	$\pm$0.370	$\pm$0.001	$\pm$0.030	$\pm$0.026	$\pm$0.028	$\pm$0.373	
195.5	1.081	$\pm$0.199	$\pm$0.001	$\pm$0.028	$\pm$0.017	$\pm$0.023	$\pm$0.203	
199.5	1.242	$\pm$0.183	$\pm$0.001	$\pm$0.028	$\pm$0.017	$\pm$0.022	$\pm$0.187	
201.6	1.340	$\pm$0.258	$\pm$0.001	$\pm$0.031	$\pm$0.021	$\pm$0.023	$\pm$0.261	
204.9	0.873	$\pm$0.185	$\pm$0.001	$\pm$0.025	$\pm$0.020	$\pm$0.020	$\pm$0.189	
206.6	1.058	$\pm$0.138	$\pm$0.001	$\pm$0.026	$\pm$0.019	$\pm$0.021	$\pm$0.143	
Average	1.051	$\pm$0.065	$\pm$0.000	$\pm$0.031	$\pm$0.009	$\pm$0.021	$\pm$0.076	12.2/24
WPHACT [94]								
182.7	1.157	$\pm$0.274	$\pm$0.001	$\pm$0.043	$\pm$0.030	$\pm$0.027	$\pm$0.281	8.1/16
188.6	0.971	$\pm$0.124	$\pm$0.001	$\pm$0.040	$\pm$0.023	$\pm$0.018	$\pm$0.134	
191.6	1.128	$\pm$0.382	$\pm$0.001	$\pm$0.031	$\pm$0.027	$\pm$0.029	$\pm$0.385	
195.5	1.115	$\pm$0.206	$\pm$0.001	$\pm$0.029	$\pm$0.017	$\pm$0.023	$\pm$0.210	
199.5	1.280	$\pm$0.188	$\pm$0.001	$\pm$0.029	$\pm$0.018	$\pm$0.022	$\pm$0.193	
201.6	1.380	$\pm$0.265	$\pm$0.001	$\pm$0.032	$\pm$0.022	$\pm$0.024	$\pm$0.269	
204.9	0.899	$\pm$0.191	$\pm$0.001	$\pm$0.026	$\pm$0.020	$\pm$0.020	$\pm$0.195	
206.6	1.089	$\pm$0.142	$\pm$0.001	$\pm$0.027	$\pm$0.020	$\pm$0.022	$\pm$0.148	
Average	1.083	$\pm$0.067	$\pm$0.000	$\pm$0.032	$\pm$0.009	$\pm$0.022	$\pm$0.078	12.2/24

Table A.12: Ratios of LEP combined total single-W cross-section measurements to the expectations, for different centre–of–mass energies and for all energies combined. The first column contains the centre–of–mass energy, the second the combined ratios, the third the statistical errors. The fourth, fifth, sixth and seventh columns contain the sources of systematic errors that are considered as LEP-correlated energy-uncorrelated (LCEU), LEP-correlated energy-correlated (LCEC), LEP-uncorrelated energy-uncorrelated (LUEU), LEP-uncorrelated energy-correlated (LUEC). The total error is given in the eighth column. The only LCEU systematic sources considered are the statistical errors on the cross-section theoretical predictions, while the LCEC, LUEU and LUEC sources are those coming from the corresponding errors on the cross-section measurements.

$\sqrt{s}$ (GeV)	σ_{ZZ}	$\Delta\sigma^{\mathrm{stat}}_{\mathrm{ZZ}}$	(LCEC) $\Delta\sigma^{\mathrm{syst}}_{\mathrm{ZZ}}$	(LUEU) $\Delta\sigma^{\mathrm{syst}}_{\mathrm{ZZ}}$	(LUEC) $\Delta\sigma^{\mathrm{syst}}_{\mathrm{ZZ}}$	$\Delta\sigma_{\mathrm{ZZ}}$	$\Delta\sigma^{\mathrm{stat\,(exp)}}_{\mathrm{ZZ}}$
ALEPH [101, 102]							
182.7	0.11	$^{+0.16}_{-0.11}$	$\pm$0.01	$\pm$0.03	$\pm$0.03	$^{+0.16}_{-0.12}$	$\pm$0.14
188.6	0.67	$^{+0.13}_{-0.12}$	$\pm$0.01	$\pm$0.03	$\pm$0.03	$^{+0.14}_{-0.13}$	$\pm$0.13
191.6	0.53	$^{+0.34}_{-0.27}$	$\pm$0.01	$\pm$0.01	$\pm$0.01	$^{+0.34}_{-0.27}$	$\pm$0.33
195.5	0.69	$^{+0.23}_{-0.20}$	$\pm$0.01	$\pm$0.02	$\pm$0.02	$^{+0.23}_{-0.20}$	$\pm$0.23
199.5	0.70	$^{+0.22}_{-0.20}$	$\pm$0.01	$\pm$0.02	$\pm$0.02	$^{+0.22}_{-0.20}$	$\pm$0.23
201.6	0.70	$^{+0.33}_{-0.28}$	$\pm$0.01	$\pm$0.01	$\pm$0.01	$^{+0.33}_{-0.28}$	$\pm$0.35
204.9	1.21	$^{+0.26}_{-0.23}$	$\pm$0.01	$\pm$0.02	$\pm$0.02	$^{+0.26}_{-0.23}$	$\pm$0.27
206.6	1.01	$^{+0.19}_{-0.17}$	$\pm$0.01	$\pm$0.01	$\pm$0.01	$^{+0.19}_{-0.17}$	$\pm$0.18
DELPHI [98]							
182.7	0.35	$^{+0.20}_{-0.15}$	$\pm$0.01	$\pm$0.00	$\pm$0.02	$^{+0.20}_{-0.15}$	$\pm$0.16
188.6	0.52	$^{+0.12}_{-0.11}$	$\pm$0.01	$\pm$0.00	$\pm$0.02	$^{+0.12}_{-0.11}$	$\pm$0.13
191.6	0.63	$^{+0.36}_{-0.30}$	$\pm$0.01	$\pm$0.01	$\pm$0.02	$^{+0.36}_{-0.30}$	$\pm$0.35
195.5	1.05	$^{+0.25}_{-0.22}$	$\pm$0.01	$\pm$0.01	$\pm$0.02	$^{+0.25}_{-0.22}$	$\pm$0.21
199.5	0.75	$^{+0.20}_{-0.18}$	$\pm$0.01	$\pm$0.01	$\pm$0.01	$^{+0.20}_{-0.18}$	$\pm$0.21
201.6	0.85	$^{+0.33}_{-0.28}$	$\pm$0.01	$\pm$0.01	$\pm$0.01	$^{+0.33}_{-0.28}$	$\pm$0.32
204.9	1.03	$^{+0.23}_{-0.20}$	$\pm$0.02	$\pm$0.01	$\pm$0.01	$^{+0.23}_{-0.20}$	$\pm$0.23
206.6	0.96	$^{+0.16}_{-0.15}$	$\pm$0.02	$\pm$0.01	$\pm$0.01	$^{+0.16}_{-0.15}$	$\pm$0.17
L3 [99]							
182.7	0.31	$\pm$0.16	$\pm$0.05	$\pm$0.00	$\pm$0.01	$\pm$0.17	$\pm$0.16
188.6	0.73	$\pm$0.15	$\pm$0.02	$\pm$0.02	$\pm$0.02	$\pm$0.15	$\pm$0.15
191.6	0.29	$\pm$0.22	$\pm$0.01	$\pm$0.01	$\pm$0.02	$\pm$0.22	$\pm$0.34
195.5	1.18	$\pm$0.24	$\pm$0.04	$\pm$0.05	$\pm$0.06	$\pm$0.26	$\pm$0.22
199.5	1.25	$\pm$0.25	$\pm$0.04	$\pm$0.05	$\pm$0.07	$\pm$0.27	$\pm$0.24
201.6	0.95	$\pm$0.38	$\pm$0.03	$\pm$0.04	$\pm$0.05	$\pm$0.39	$\pm$0.35
204.9	0.77	$^{+0.21}_{-0.19}$	$\pm$0.01	$\pm$0.01	$\pm$0.04	$^{+0.21}_{-0.19}$	$\pm$0.22
206.6	1.09	$^{+0.17}_{-0.16}$	$\pm$0.02	$\pm$0.02	$\pm$0.06	$^{+0.18}_{-0.17}$	$\pm$0.17
OPAL [100]							
182.7	0.12	$^{+0.20}_{-0.18}$	$\pm$0.00	$\pm$0.03	$\pm$0.00	$^{+0.20}_{-0.18}$	$\pm$0.19
188.6	0.80	$^{+0.14}_{-0.13}$	$\pm$0.01	$\pm$0.05	$\pm$0.03	$^{+0.15}_{-0.14}$	$\pm$0.14
191.6	1.29	$^{+0.47}_{-0.40}$	$\pm$0.02	$\pm$0.09	$\pm$0.05	$^{+0.48}_{-0.41}$	$\pm$0.36
195.5	1.13	$^{+0.26}_{-0.24}$	$\pm$0.02	$\pm$0.06	$\pm$0.05	$^{+0.27}_{-0.25}$	$\pm$0.25
199.5	1.05	$^{+0.25}_{-0.22}$	$\pm$0.02	$\pm$0.05	$\pm$0.04	$^{+0.26}_{-0.23}$	$\pm$0.25
201.6	0.79	$^{+0.35}_{-0.29}$	$\pm$0.02	$\pm$0.05	$\pm$0.03	$^{+0.36}_{-0.30}$	$\pm$0.37
204.9	1.07	$^{+0.27}_{-0.24}$	$\pm$0.02	$\pm$0.06	$\pm$0.04	$^{+0.28}_{-0.25}$	$\pm$0.26
206.6	0.97	$^{+0.19}_{-0.18}$	$\pm$0.02	$\pm$0.05	$\pm$0.04	$^{+0.20}_{-0.19}$	$\pm$0.20
LEP							χ^2/d.o.f.
182.7	0.22	$\pm$0.08	$\pm$0.02	$\pm$0.01	$\pm$0.01	$\pm$0.08	16.1/24
188.6	0.66	$\pm$0.07	$\pm$0.01	$\pm$0.01	$\pm$0.01	$\pm$0.07	
191.6	0.65	$\pm$0.17	$\pm$0.01	$\pm$0.02	$\pm$0.01	$\pm$0.17	
195.5	0.99	$\pm$0.11	$\pm$0.02	$\pm$0.02	$\pm$0.02	$\pm$0.12	
199.5	0.90	$\pm$0.12	$\pm$0.02	$\pm$0.02	$\pm$0.02	$\pm$0.12	
201.6	0.81	$\pm$0.17	$\pm$0.02	$\pm$0.02	$\pm$0.01	$\pm$0.17	
204.9	0.98	$\pm$0.12	$\pm$0.01	$\pm$0.01	$\pm$0.02	$\pm$0.13	
206.6	0.99	$\pm$0.09	$\pm$0.02	$\pm$0.01	$\pm$0.02	$\pm$0.09	

Table A.13: Z-pair production cross-section (in pb) at different energies. The first column contains the LEP centre–of–mass energy, the second the measurements and the third the statistical uncertainty. The fourth, the fifth and the sixth columns list the different components of the systematic errors, as provided by the Collaborations. The total error is given in the seventh column, whereas the eighth column lists, for the four LEP measurements, the symmetrized expected statistical error, and for the LEP combined value, the χ^2 of the fit.

$\sqrt{s}$ (GeV)	ZZ cross-section (pb)	
	σ_{ZZ}^{YFSZZ}	σ_{ZZ}^{ZZTO}
182.7	0.254[1]	0.25425[2]
188.6	0.655[2]	0.64823[1]
191.6	0.782[2]	0.77670[1]
195.5	0.897[3]	0.89622[1]
199.5	0.981[2]	0.97765[1]
201.6	1.015[1]	1.00937[1]
204.9	1.050[1]	1.04335[1]
206.6	1.066[1]	1.05535[1]

Table A.14: Z-pair cross-section predictions (in pb) interpolated at the data centre–of–mass energies,according to the YFSZZ [103] and ZZTO [104] predictions. The numbers in brackets are the errors on the last digit and are coming from the numerical integration of the cross-section only.

$\sqrt{s}$ (GeV)	$\mathcal{R}_{ZZ}$	$\Delta\mathcal{R}_{ZZ}^{stat}$	(LCEU) $\Delta\mathcal{R}_{ZZ}^{syst}$	(LCEC) $\Delta\mathcal{R}_{ZZ}^{syst}$	(LUEU) $\Delta\mathcal{R}_{ZZ}^{syst}$	(LUEC) $\Delta\mathcal{R}_{ZZ}^{syst}$	$\Delta\mathcal{R}_{ZZ}$	χ^2/d.o.f.
YFSZZ [103]								
182.7	0.857	±0.307	±0.018	±0.068	±0.041	±0.040	±0.320	16.1/24
188.6	1.007	±0.104	±0.020	±0.019	±0.022	±0.018	±0.111	
191.6	0.826	±0.220	±0.017	±0.014	±0.025	±0.017	±0.224	
195.5	1.100	±0.127	±0.022	±0.021	±0.019	±0.020	±0.133	
199.5	0.912	±0.119	±0.019	±0.018	±0.016	±0.017	±0.124	
201.6	0.795	±0.170	±0.016	±0.017	±0.015	±0.013	±0.173	
204.9	0.931	±0.116	±0.019	±0.014	±0.013	±0.014	±0.120	
206.6	0.928	±0.085	±0.019	±0.014	±0.010	±0.015	±0.090	
Average	0.945	±0.045	±0.008	±0.017	±0.006	±0.016	±0.052	19.1/31
ZZTO [104]								
182.7	0.857	±0.307	±0.018	±0.068	±0.041	±0.040	±0.320	16.1/24
188.6	1.017	±0.105	±0.021	±0.019	±0.022	±0.019	±0.113	
191.6	0.831	±0.222	±0.017	±0.014	±0.025	±0.017	±0.225	
195.5	1.100	±0.127	±0.022	±0.021	±0.019	±0.020	±0.133	
199.5	0.915	±0.120	±0.019	±0.018	±0.016	±0.017	±0.125	
201.6	0.799	±0.171	±0.016	±0.017	±0.015	±0.013	±0.174	
204.9	0.937	±0.117	±0.019	±0.014	±0.013	±0.014	±0.121	
206.6	0.937	±0.085	±0.019	±0.014	±0.011	±0.015	±0.091	
Average	0.952	±0.046	±0.008	±0.017	±0.006	±0.016	±0.052	19.1/31

Table A.15: Ratios of LEP combined Z-pair cross-section measurements to the expectations, for different centre–of–mass energies and for all energies combined. The first column contains the centre–of–mass energy, the second the combined ratios, the third the statistical errors. The fourth, fifth, sixth and seventh columns contain the sources of systematic errors that are considered as LEP-correlated energy-uncorrelated (LCEU), LEP-correlated energy-correlated (LCEC), LEP-uncorrelated energy-uncorrelated (LUEU), LEP-uncorrelated energy-correlated (LUEC). The total error is given in the eighth column. The only LCEU systematic sources considered are the statistical errors on the cross-section theoretical predictions, while the LCEC, LUEU and LUEC sources are those coming from the corresponding errors on the cross-section measurements. For the LEP averages, the χ^2 of the fit is also given in the ninth column.

$\sqrt{s}$ (GeV)	σ_{Zee}	$\Delta\sigma_{Zee}^{stat}$	(LCEC) $\Delta\sigma_{Zee}^{syst}$	(LUEU) $\Delta\sigma_{Zee}^{syst}$	(LUEC) $\Delta\sigma_{Zee}^{syst}$	$\Delta\sigma_{Zee}$	$\Delta\sigma_{Zee}^{stat\,(exp)}$
ALEPH [105]							
182.7	0.27	$^{+0.21}_{-0.16}$	±0.01	±0.02	±0.01	$^{+0.21}_{-0.16}$	±0.20
188.6	0.42	$^{+0.14}_{-0.12}$	±0.01	±0.03	±0.01	$^{+0.14}_{-0.12}$	±0.12
191.6	0.61	$^{+0.39}_{-0.29}$	±0.01	±0.03	±0.01	$^{+0.39}_{-0.29}$	±0.29
195.5	0.72	$^{+0.24}_{-0.20}$	±0.01	±0.03	±0.01	$^{+0.24}_{-0.20}$	±0.18
199.5	0.60	$^{+0.21}_{-0.18}$	±0.01	±0.03	±0.01	$^{+0.21}_{-0.18}$	±0.17
201.6	0.89	$^{+0.35}_{-0.28}$	±0.01	±0.03	±0.01	$^{+0.35}_{-0.28}$	±0.24
204.9	0.42	$^{+0.17}_{-0.14}$	±0.01	±0.03	±0.01	$^{+0.17}_{-0.15}$	±0.17
206.6	0.70	$^{+0.17}_{-0.15}$	±0.01	±0.03	±0.01	$^{+0.17}_{-0.15}$	±0.14
DELPHI [92]							
182.7	0.56	$^{+0.27}_{-0.22}$	±0.01	±0.06	±0.02	$^{+0.28}_{-0.23}$	±0.24
188.6	0.64	$^{+0.15}_{-0.14}$	±0.01	±0.03	±0.02	$^{+0.16}_{-0.14}$	±0.14
191.6	0.63	$^{+0.40}_{-0.30}$	±0.01	±0.03	±0.03	$^{+0.40}_{-0.30}$	±0.32
195.5	0.66	$^{+0.22}_{-0.18}$	±0.01	±0.02	±0.03	$^{+0.22}_{-0.19}$	±0.19
199.5	0.57	$^{+0.20}_{-0.17}$	±0.01	±0.02	±0.02	$^{+0.20}_{-0.17}$	±0.18
201.6	0.19	$^{+0.21}_{-0.16}$	±0.01	±0.02	±0.01	$^{+0.21}_{-0.16}$	±0.25
204.9	0.37	$^{+0.18}_{-0.15}$	±0.01	±0.02	±0.02	$^{+0.18}_{-0.15}$	±0.19
206.6	0.69	$^{+0.16}_{-0.14}$	±0.01	±0.01	±0.03	$^{+0.16}_{-0.14}$	±0.14
L3 [106]							
182.7	0.51	$^{+0.19}_{-0.16}$	±0.02	±0.01	±0.03	$^{+0.19}_{-0.16}$	±0.16
188.6	0.55	$^{+0.10}_{-0.09}$	±0.02	±0.01	±0.03	$^{+0.11}_{-0.10}$	±0.09
191.6	0.60	$^{+0.26}_{-0.21}$	±0.01	±0.01	±0.03	$^{+0.26}_{-0.21}$	±0.21
195.5	0.40	$^{+0.13}_{-0.11}$	±0.01	±0.01	±0.03	$^{+0.13}_{-0.11}$	±0.13
199.5	0.33	$^{+0.12}_{-0.10}$	±0.01	±0.01	±0.03	$^{+0.13}_{-0.11}$	±0.14
201.6	0.81	$^{+0.27}_{-0.23}$	±0.02	±0.02	±0.03	$^{+0.27}_{-0.23}$	±0.19
204.9	0.56	$^{+0.16}_{-0.14}$	±0.01	±0.01	±0.03	$^{+0.16}_{-0.14}$	±0.14
206.6	0.59	$^{+0.12}_{-0.10}$	±0.01	±0.01	±0.03	$^{+0.12}_{-0.11}$	±0.11
LEP							χ^2/d.o.f.
182.7	0.45	±0.11	±0.01	±0.02	±0.01	±0.11	13.0/16
188.6	0.53	±0.07	±0.01	±0.01	±0.01	±0.07	
191.6	0.61	±0.15	±0.01	±0.02	±0.01	±0.15	
195.5	0.55	±0.09	±0.01	±0.01	±0.01	±0.10	
199.5	0.47	±0.09	±0.01	±0.02	±0.01	±0.10	
201.6	0.67	±0.13	±0.01	±0.01	±0.01	±0.13	
204.9	0.47	±0.10	±0.01	±0.01	±0.01	±0.10	
206.6	0.65	±0.07	±0.01	±0.01	±0.01	±0.08	

Table A.16: Single-Z hadronic production cross-section (in pb) at different energies. The first column contains the LEP centre–of–mass energy, and the second the measurements. The third column reports the statistical error, whereas in the fourth to the sixth columns the different systematic uncertainties are listed. The seventh column contains the total error and the eight lists, for the four LEP measurements, the symmetrized expected statistical error, and for the LEP combined value, the χ^2 of the fit.

$\sqrt{s}$ (GeV)	Zee cross-section (pb)	
	$\sigma_{\mathrm{Zee}}^{\mathrm{WPHACT}}$	$\sigma_{\mathrm{Zee}}^{\texttt{grc4f}}$
182.7	0.51275[4]	0.51573[4]
188.6	0.53686[4]	0.54095[5]
191.6	0.54883[4]	0.55314[5]
195.5	0.56399[5]	0.56891[4]
199.5	0.57935[5]	0.58439[4]
201.6	0.58708[4]	0.59243[4]
204.9	0.59905[4]	0.60487[4]
206.6	0.61752[4]	0.60819[4]

Table A.17: Zee cross-section predictions (in pb) interpolated at the data centre–of–mass energies,according to the WPHACT [94] and `grc4f` [95] predictions. The numbers in brackets are the errors on the last digit and are coming from the numerical integration of the cross-section only.

$\sqrt{s}$ (GeV)	$\mathcal{R}_{\mathrm{Zee}}$	$\Delta\mathcal{R}_{\mathrm{Zee}}^{\mathrm{stat}}$	(LCEU) $\Delta\mathcal{R}_{\mathrm{Zee}}^{\mathrm{syst}}$	(LCEC) $\Delta\mathcal{R}_{\mathrm{Zee}}^{\mathrm{syst}}$	(LUEU) $\Delta\mathcal{R}_{\mathrm{Zee}}^{\mathrm{syst}}$	(LUEC) $\Delta\mathcal{R}_{\mathrm{Zee}}^{\mathrm{syst}}$	$\Delta\mathcal{R}_{\mathrm{Zee}}$	χ^2/d.o.f.
`grc4f` [95]								
182.7	0.871	±0.214	±0.000	±0.020	±0.035	±0.025	±0.219	13.0/16
188.6	0.982	±0.120	±0.000	±0.022	±0.023	±0.024	±0.126	
191.6	1.104	±0.272	±0.000	±0.019	±0.027	±0.025	±0.276	
195.5	0.964	±0.163	±0.000	±0.016	±0.024	±0.025	±0.167	
199.5	0.809	±0.160	±0.000	±0.018	±0.030	±0.023	±0.165	
201.6	1.126	±0.219	±0.000	±0.023	±0.024	±0.021	±0.222	
204.9	0.769	±0.157	±0.000	±0.019	±0.019	±0.021	±0.160	
206.6	1.062	±0.119	±0.000	±0.018	±0.018	±0.024	±0.124	
Average	0.955	±0.057	±0.000	±0.019	±0.009	±0.023	±0.065	17.1/23
WPHACT [94]								
182.7	0.876	±0.215	±0.000	±0.020	±0.035	±0.025	±0.220	13.0/16
188.6	0.990	±0.120	±0.000	±0.022	±0.023	±0.025	±0.127	
191.6	1.112	±0.274	±0.000	±0.020	±0.027	±0.026	±0.277	
195.5	0.972	±0.164	±0.000	±0.016	±0.025	±0.025	±0.168	
199.5	0.816	±0.161	±0.000	±0.019	±0.030	±0.023	±0.167	
201.6	1.135	±0.221	±0.000	±0.023	±0.024	±0.021	±0.224	
204.9	0.776	±0.158	±0.000	±0.019	±0.019	±0.021	±0.162	
206.6	1.067	±0.120	±0.000	±0.018	±0.018	±0.024	±0.125	
Average	0.962	±0.057	±0.000	±0.020	±0.009	±0.024	±0.065	17.0/23

Table A.18: Ratios of LEP combined single-Z cross-section measurements to the expectations, for different centre–of–mass energies and for all energies combined. The first column contains the centre–of–mass energy, the second the combined ratios, the third the statistical errors. The fourth, fifth, sixth and seventh columns contain the sources of systematic errors that are considered as LEP-correlated energy-uncorrelated (LCEU), LEP-correlated energy-correlated (LCEC), LEP-uncorrelated energy-uncorrelated (LUEU), LEP-uncorrelated energy-correlated (LUEC). The total error is given in the eighth column. The only LCEU systematic sources considered are the statistical errors on the cross-section theoretical predictions, while the LCEC, LUEU and LUEC sources are those coming from the corresponding errors on the cross-section measurements. For the LEP averages, the χ^2 of the fit is also given in the ninth column.

Appendix B

Colour Reconnection Combination

B.1 Inputs

R_N	Experiment			
	ALEPH	DELPHI	L3	OPAL
Data	1.0951 ± 0.0135	0.8996 ± 0.0314	0.8436 ± 0.0217	1.2570 ± 0.0251
SK-I (100%)	1.0548 ± 0.0012	0.8463 ± 0.0036	0.7482 ± 0.0033	1.1386 ± 0.0027
JETSET	1.1365 ± 0.0013	0.9444 ± 0.0039	0.8622 ± 0.0037	1.2958 ± 0.0028
AR-2	1.1341 ± 0.0013	0.9552 ± 0.0041	0.8696 ± 0.0037	1.2887 ± 0.0028
ARIADNE	1.1461 ± 0.0013	0.9530 ± 0.0039	0.8754 ± 0.0037	1.3057 ± 0.0028
HERWIG CR	1.1416 ± 0.0013	0.9649 ± 0.0039	0.8805 ± 0.0037	1.3016 ± 0.0029
HERWIG	1.1548 ± 0.0013	0.9675 ± 0.0040	0.8822 ± 0.0038	1.3204 ± 0.0029
Systematics				
Intra-W BEC	±0.0020	±0.0094	±0.0017	±0.0015
$e^+e^- \to q\bar{q}$ shape	±0.0012	±0.0013	±0.0086	±0.0035
±10% $\sigma(e^+e^- \to q\bar{q})$	±0.0036	±0.0042	±0.0071	±0.0040
±15% $\sigma(ZZ \to q\bar{q}q\bar{q})$	±0.0004	±0.0001	±0.0020	±0.0013
Detector effects	0.0040	–	±0.0016	±0.0072
E_{cm} dependence	±0.0062	±0.0012	±0.0020	±0.0030

Table B.1: Inputs provided by the experiments for the combination.

k_i	P_{reco} (%)	ALEPH	DELPHI	L3	OPAL
0.10	7.2	1.1357 ± 0.0057	0.9410 ± 0.0034	0.8613 ± 0.0037	1.2887 ± 0.0028
0.15	10.2	1.1341 ± 0.0057	0.9393 ± 0.0032	0.8598 ± 0.0037	1.2859 ± 0.0028
0.20	13.4	1.1336 ± 0.0057	0.9378 ± 0.0031	0.8585 ± 0.0037	1.2823 ± 0.0028
0.25	16.1	1.1336 ± 0.0057	0.9363 ± 0.0030	0.8561 ± 0.0037	1.2800 ± 0.0028
0.35	21.4	1.1303 ± 0.0057	0.9334 ± 0.0028	0.8551 ± 0.0037	1.2741 ± 0.0028
0.45	25.9	1.1269 ± 0.0057	0.9307 ± 0.0027	0.8509 ± 0.0036	1.2693 ± 0.0028
0.60	32.1	1.1216 ± 0.0057	0.9271 ± 0.0025	0.8482 ± 0.0036	1.2639 ± 0.0028
0.80	39.1	1.1166 ± 0.0056	0.9227 ± 0.0024	0.8414 ± 0.0037	1.2576 ± 0.0028
1.00	44.9	1.1109 ± 0.0056	0.9189 ± 0.0024	0.8381 ± 0.0036	1.2499 ± 0.0028
1.50	55.9	1.1048 ± 0.0056	0.9110 ± 0.0025	0.8318 ± 0.0036	1.2368 ± 0.0028
3.00	72.8	1.0929 ± 0.0056	0.8959 ± 0.0028	0.8135 ± 0.0036	1.2093 ± 0.0027
5.00	82.5	1.0852 ± 0.0056	0.8846 ± 0.0030	0.7989 ± 0.0035	1.1920 ± 0.0022

Table B.2: SK-I Model predictions for R_N obtained with the common LEP samples at 189 GeV. The second column gives the fraction of reconnected events in the common samples obtained for the different choice of k_I values.

B.2 Example Average

Model tested SK-I (100%)	Experiment ALEPH	DELPHI	L3	OPAL
R_N (no-CR)	1.1365 ± 0.0013	0.9444 ± 0.0039	0.8622 ± 0.0037	1.2958 ± 0.0028
R_N (with CR)	1.0548 ± 0.0012	0.8463 ± 0.0036	0.7482 ± 0.0033	1.1386 ± 0.0027
weight	19.688	7.054	18.250	28.202
r ($\equiv R_N(\text{data})/R_N^{\text{no-CR}}$)				
Data	0.9636	0.9526	0.9784	0.9701
Stat. error	0.0119	0.0332	0.0252	0.0194
Syst. error	0.0110	0.0206	0.0180	0.0121
Uncorrel. syst.				
Background	0.0013	0.0035	0.0128	0.0029
Hadronisation	0.0000	0.0094	0.0086	0.0051
Intra-W BEC	0.0013	0.0099	0.0016	0.0000
Detector effects	0.0035	–	0.0019	0.0056
E_{cm} dependence	0.0055	0.0123	0.0023	0.0023
Total uncorr. error	0.0068	0.0187	0.0158	0.0084
Correl. syst.				
Background	0.0031	0.0031	0.0031	0.0031
Hadronisation	0.0081	0.0081	0.0081	0.0081
Intra-W BEC	0.0012	0.0012	0.0012	0.0012
Total correl. error	0.0087	0.0087	0.0087	0.0087

Table B.3: Normalised results of particle flow analysis, based on the predicted SK-I 100% sensitivity.

k_i	P_{reco} (%)	$\langle r \rangle^{MC}$	$\langle r \rangle^{ADLO}$	data-MC (σ)
0.10	7.2	0.9950	$0.9679 \pm 0.0167 \pm 0.0087 \pm 0.0076$	-1.34
0.15	10.2	0.9935	$0.9677 \pm 0.0146 \pm 0.0087 \pm 0.0065$	-1.42
0.20	13.4	0.9911	$0.9681 \pm 0.0148 \pm 0.0087 \pm 0.0066$	-1.25
0.25	16.1	0.9895	$0.9687 \pm 0.0144 \pm 0.0087 \pm 0.0066$	-1.15
0.35	21.4	0.9861	$0.9680 \pm 0.0136 \pm 0.0087 \pm 0.0062$	-1.05
0.45	25.9	0.9834	$0.9681 \pm 0.0123 \pm 0.0087 \pm 0.0057$	-0.98
0.60	32.1	0.9802	$0.9676 \pm 0.0112 \pm 0.0087 \pm 0.0053$	-0.84
0.80	39.1	0.9757	$0.9678 \pm 0.0106 \pm 0.0087 \pm 0.0052$	-0.54
1.00	44.9	0.9708	$0.9676 \pm 0.0103 \pm 0.0087 \pm 0.0051$	-0.22
1.50	55.9	0.9626	$0.9676 \pm 0.0105 \pm 0.0087 \pm 0.0051$	+0.34
3.00	72.8	0.9447	$0.9680 \pm 0.0107 \pm 0.0087 \pm 0.0053$	+1.58
5.00	82.5	0.9324	$0.9683 \pm 0.0108 \pm 0.0087 \pm 0.0054$	+2.42
10000	100	0.8909	$0.9687 \pm 0.0108 \pm 0.0087 \pm 0.0057$	+5.20

Table B.4: LEP Average values of r in Monte Carlo, $\langle r \rangle^{MC}$ ($\equiv \langle R_N/R_N^{\text{no-CR}} \rangle^{MC}$), and data, $\langle r \rangle^{ADLO}$ ($\equiv \langle R_N/R_N^{\text{no-CR}} \rangle^{ADLO}$), for various k_I values in SK-I model. The first uncertainty is statistical, the second corresponds to the correlated systematic error and the third corresponds to the uncorrelated systematic error.

Model	$\langle r \rangle^{MC}$	$\langle r \rangle^{ADLO}$	data-MC (σ)
AR2	0.9888	$0.9589 \pm 0.0101 \pm 0.0086 \pm 0.0050$	-2.10
HERWIG CR	0.9874	$0.9498 \pm 0.0105 \pm 0.0086 \pm 0.0052$	-2.59

Table B.5: LEP Average values of r in Monte Carlo, $\langle r \rangle^{MC}$ ($\equiv \langle R_N / R_N^{\mathrm{no-CR}} \rangle^{MC}$), and data, $\langle r \rangle^{ADLO}$ ($\equiv \langle R_N / R_N^{\mathrm{no-CR}} \rangle^{ADLO}$), for ARIADNE and HERWIG models with colour reconnection. The first uncertainty is statistical, the second corresponds to the correlated systematic error and the third corresponds to the uncorrelated systematic error.

Bibliography

[1] The LEP Collaborations ALEPH, DELPHI, L3, OPAL, the LEP Electroweak Working Group, the SLD Electroweak and Heavy Flavour Groups, *A Combination of Preliminary Electroweak Measurements and Constraints on the Standard Model*, Eprint hep-ex/0412015, CERN, 2004.

[2] The ALEPH, DELPHI, L3, OPAL, SLD Collaborations, the LEP Electroweak Working Group, the SLD Electroweak and Heavy Flavour Groups, Phys. Rept. **427** (2006) 257.

[3] The LEP Collaborations ALEPH, DELPHI, L3, OPAL, and the LEP Electroweak Working Group, *A Combination of Preliminary Electroweak Measurements and Constraints on the Standard Model*, Eprint hep-ex/0511027, CERN, 2005.

[4] DELPHI Collaboration, J. Abdallah *et al.*, Eur. Phys. J. **C37** (2004) 405–419.

[5] W. Heitler, Quantum Theory of Radiation, (Oxford University Press, second edition, 1944), pages 204–207.

[6] F. A. Berends and R. Kleiss, Nucl. Phys. **B186** (1981) 22.

[7] ALEPH Collab., Eur. Phys. J., C 28 (2003) 1 and ref. therein;
DELPHI Collab., DELPHI 2001-093 CONF 521 and ref. therein;
L3 Collab., Phys. Lett. **B531** (2002) 28 and ref. therein;
OPAL Collab., Eur.Phys.J.C26 (2003) 331 and ref. therein.

[8] S. D. Drell, Ann. Phys. **4** (1958) 75.

[9] F. E. Low, Phys. Rev. Lett. **14** (() 1965) 238.

[10] O. J. P. Eboli, A. A. Natale, and S. F. Novaes, Phys. Lett. **B271** (1991) 274.

[11] P. Mery, M. Perrottet, and F. M. Renard, Z. Phys. **C38** (1988) 579.

[12] S. J. Brodsky and S. D. Drell, Phys. Rev. **D22** (1980) 2236.

[13] F. Boudjema, A. Djouadi, and J. L. Kneur, Z. Phys. **C57** (1993) 425–450.

[14] B. Vachon, *Excited electron contribution to the* $e^+e^- \to \gamma\gamma$ *cross-section*, hep-ph/0103132, 2001.

[15] K. Agashe and N. G. Deshpande, Phys. Lett. **B456** (1999) 60.

[16] OPAL Collaboration, G. Abbiendi *et al.*, Eur. Phys. J. **C33** (2004) 173–212.

[17] OPAL Collaboration, G. Abbiendi *et al.*, Phys. Lett. **B609** (2005) 212–225.

[18] L3 Collaboration, P. Achard *et al.*, *Measurement of Hadron and Lepton-Pair Production in* e^+e^- *Collisions at* $\sqrt{s} = 192 - 208$ *GeV at LEP*, Eprint hep-ex/0603022, 2006, (submitted to Eur. Phys. J.).

[19] DELPHI Collaboration, J. Abdallah *et al.*, Eur. Phys. J. **C45** (2006) 589–632.

[20] DELPHI Collaboration, J. Abdallah *et al.*, Eur. Phys. J. **C46** (2006) 295–305.

[21] The LEP Collaborations ALEPH, DELPHI, L3, OPAL, the LEP Electroweak Working Group, the SLD Electroweak and Heavy Flavour Groups, *A Combination of Preliminary Electroweak Measurements and Constraints on the Standard Model*, Eprint hep-ex/0212036, CERN, 2002.

[22] LEPEWWG $f\bar{f}$ subgroup: http://www.cern.ch/LEPEWWG/lep2/ .

[23] ALEPH Collaboration "Study of Fermion Pair Production in e^+e^- Collisions at 130-183 GeV", Eur. Phys. J. **C12** (2000) 183;
ALEPH Collaboration, "Fermion Pair Production in e^+e^- Collisions at 189 GeV and Kimits on Physics Beyond the Standard Model", ALEPH 99-018 CONF 99-013;
ALEPH Collaboration "Fermion Pair Production in e^+e^- Collisions from 192 to 202 GeV and Limits on Physics beyond the Standard Model", ALEPH 2000-047 CONF 2000-030;
ALEPH Collaboration "Fermion Pair Production in e^+e^- Collisions at high energy and Limits on Physics beyond the Standard Model", ALEPH 2002-032 CONF 2002-021;
ALEPH Collaboration, "Fermion Pair Production in e^+e^- Collisions at high energy and Limits on Physics beyond the Standard Model ", ALEPH 2001-019 CONF 2001-016;
DELPHI Collaboration,"Measurement and Interpretation of Fermion-Pair Production at LEP energies from 130 to 172 GeV", Eur. Phys. J. **C11** (1999), 383;
DELPHI Collaboration, "Measurement and Interpretation of Fermion-Pair Production at LEP Energies from 183 to 189 GeV", Phys.Lett. **B485** (2000), 45;
DELPHI Collaboration, "Results on Fermion-Pair Production at LEP running from 192 to 202 GeV", DELPHI 2000-128 OSAKA CONF 427;
DELPHI Collaboration, "Results on Fermion-Pair Production at LEP running in 2000", DELPHI 2001-094 CONF 522;
L3 Collaboration, "Measurement of Hadron and Lepton-Pair Production at 161 GeV $< \sqrt{s} <$ 172 GeV at LEP", Phys. Lett. **B407** (1997) 361;
L3 Collaboration, "Measurement of Hadron and Lepton-Pair Production at 130 GeV $< \sqrt{s} <$ 189 GeV at LEP", Phys. Lett. **B479** (2000), 101.
L3 Collaboration, "Preliminary L3 Results on Fermion-Pair Production in 1999", L3 note 2563;
L3 Collaboration,"Preliminary L3 Results on Fermion-Pair Production in 2000", L3 note 2648;
OPAL Collaboration, "Tests of the Standard Model and Constraints on New Physics from Measurements of Fermion Pair Production at 130 - 172 GeV at LEP", Euro. Phys. J. **C2** (1998) 441;
OPAL Collaboration, "Tests of the Standard Model and Constraints on New Physics from Measurements of Fermion Pair Production at 183 GeV at LEP", Euro. Phys. J. **C6** (1999) 1;
OPAL Collaboration, "Tests of the Standard Model and Constraints on New Physics from Measurements of Fermion Pair Production at 189 GeV at LEP", Euro. Phys. J. **C13** (2000) 553;
OPAL Collaboration, "Tests of the Standard Model and Constraints on New Physics from Measurements of Fermion Pair Production at 192-202 GeV at LEP", OPAL PN424 (2000);
OPAL Collaboration, "Measurement of Standard Model Processes in e+e- Collisions at sqrts 203-209 GeV", OPAL PN469 (2001).

[24] M. Kobel *et al.*, "Two-Fermion Production in Electron Positron Collisions" in S. Jadach *et al.* [eds] , "Reports of the Working Groups on Precision Calculations for LEP2 Physics: proceedings" CERN 2000-009, hep-ph/0007180.

[25] D. Bardin *et al.*, CERN-TH 6443/92; http://www.ifh.de/∼riemann/Zfitter/zf.html .
Predictions are from ZFITTER versions 6.04 or later.

Definition 1 corresponds to the ZFITTER flags FINR=0 and INTF=0; definition 2 corresponds to FINR=0 and INTF=1 for hadrons, FINR=1 and INTF=1 for leptons.

[26] L. Lyons *et al.*, NIM A270 (1988) 110; A. Valassi, NIM A500 (2003) 391.

[27] S. Jadach, W. Placzek and B.Ward, Phys. Lett. **B390** (1997) 298.

[28] LEPEWWG $f\bar{f}$ Subgroup, C. Geweniger *et. al.*, LEP2FF/00-03,ALEPH 2000-088 PHYSIC 2000-034, DELPHI 2000-168 PHYS 881, L3 note 2624, OPAL TN673.

[29] ALEPH Collaboration, Euro. Phys J. **C12** (2000) 183;
DELPHI Collaboration, P.Abreu *et al.*, Euro. Phys J. **C11**(1999);
L3 Collaboration, M.Acciarri *et al.*, Phys. Lett. **B485** (2000) 71;
OPAL Collaboration, G.Abbiendi *et al.*, Euro. Phys. J. **C16** (2000) 41.

[30] ALEPH Collaboration, ALEPH 99-018 CONF 99-013;
ALEPH Collaboration, ALEPH 2000-046 CONF 2000-029;
ALEPH Collaboration, ICHEP2002, ABS388;
DELPHI Collaboration, DELPHI 2001-095 CONF 523;
L3 Collaboration, L3 Internal note 2640, 1 March 2001.

[31] LEPEWWG Heavy Flavour at LEP2 Subgroup, "Combination of Heavy Flavour Measurements at LEP2", LEP2FF/00-02.

[32] ZFITTER V6.23 is used.
D. Bardin *et al.*, Preprint hep-ph/9908433.
Relevant ZFITTER settings used are FINR=0 and INTF=1.

[33] DELPHI Collaboration, P.Abreu *et al.*, Euro Phys J. **C10**(1999) 415.
The LEP collaborations *et al.*, CERN-EP/2000-016.

[34] E. Eichten, K. Lane, and M. Peskin, Phys. Rev. Lett. **50** (1983) 811.

[35] H. Kroha, Phys. Rev. **D46** (1992) 58.

[36] P. Langacker, R.W. Robinett and J.L. Rosner, Phys. Rev. **D30** (1984) 1470;
D. London and J.L. Rosner, Phys. Rev. **D34** (1986) 1530;
J.C. Pati and A. Salam, Phys. Rev. **D10** (1974) 275;
R.N. Mohapatra and J.C. Pati, Phys. Rev. **D11** (1975) 566.

[37] G. Altarelli *et al.*, Z. Phys. **C45** (1989) 109;
erratum Z. Phys. **C47** (1990) 676.

[38] DELPHI Collaboration, P. Abreu *et al.*, Zeit. Phys. **C65** (1995) 603.

[39] W. Buchmüller, R. Rückl, D. Wyler, Phys. Lett. **B191** (1987) 442; Erratum-ibid. **B448** (1999) 320.

[40] J. Kalinowski *et al.*, Z. Phys. **C74** (1997) 595.

[41] H1 Collab., C. Adloff *et al.*, Phys. Lett. **B523** (2001) 234.

[42] ZEUS Collaboration; J. Breitweg *et al.*, Phys. Rev. **D63** (2001) 052002.

[43] CDF Collab., F. Abe *et al.*, Phys. Rev. Lett. **79** (1997) 4327;
DØ Collab., B. Abbott *et al.*, Phys. Rev. Lett. **80** (1998) 2051.

[44] N. Arkani-Hamed, S. Dimopoulos and G. Dvali, Phys. Lett. **B429** (1998) 263.

[45] I. Antoniadis, N. Arkani-Hamed, S. Dimopoulos and G. Dvali, Phys. Lett. **B436** (1998) 257.

[46] N. Arkani-Hamed, S. Dimopoulos and G. Dvali, Phys. Rev. **D59** (1999) 086004.

[47] D. Cremades, L.E. Ibanez and F. Marchesano, Nucl. Phys. **B643** (2002) 93.

[48] C. Kokorelis, Nucl. Phys. **B677** (2004) 115.

[49] J. Hewett, Phys. Rev. Lett. **82** (1999) 4765.

[50] T. Rizzo, Phys. Rev. **D59** (1999) 115010.

[51] G. Giudice, R. Rattazi and J. Wells, Nucl. Phys. **B544** (1999) 3.

[52] T. Han, J.D. Lykken and R-J. Zhang, Phys. Rev. **D59** (1999) 105006.

[53] S. Nussinov and R. Shrock, Phys. Rev. **D59** (1999) 105002.

[54] D. Bourilkov, J. High Energy Phys. **08** (1999) 006.

[55] D. Bourilkov, Phys. Rev. **D62** (2000) 076005.

[56] D. Bourilkov, Phys. Rev. **D64** (2001) 071701.

[57] Lineshape subgroup of the LEP EWWG,"Combination procedure for the precise determination of Z boson parameters from results of the LEP experiments", CERN-EP/2000-153, hep-ex/0101027 (2000).

[58] S-Matrix subgroup of the LEP EWWG,"An investigation of the interference between photon and Z boson exchange", LEPEWWG/LS/97-02, ALEPH 97-92 PHYSICS 97-82, DELPHI 97-153 PHYS 732, L3 Note 2164, OPAL TN510 (1997).

[59] A. Borelli *et al.*, Nucl. Phys. **B333** (1990) 357; R. G. Stuart, Phys. Lett. **B272** (1991) 353; A. Leike, T. Riemann, and J. Rose, Phys. Lett. **B273** (1991) 513; T. Riemann, Phys. Lett. **B293** (1992) 451.

[60] S. Kirsch and T. Riemann, Comput. Phys. Commun. **88** (1995) 89.

[61] LEP EWWG "A combination of preliminary electroweak measurements and constriants on the Standard Model", CERN-EP/2001-098, hep-ex/0112021 (2001).

[62] "S-Matrix fits to cross-section and forward-backward asymmetry measurements at LEP 1 and 2", ALEPH 2000-042 PHYSICS 2000-015 (2002).

[63] DELPHI collaboration, "S-Matrix fits to LEP 1 and LEP 2 data", DELPHI 2002-04 CONF 545 (2002).

[64] L3 Collaboration, M. Acciarri *et al.*, Euro. Phys. J. **C16** (2000) 1.

[65] OPAL Collaboration, G. Abbiendi *et al.*, Euro. Phys. J. **C19** (2001) 587.

[66] L3 collaboration, "Preliminary results on fermion-pair production in 2000", L3 Note 2648 (2001).

[67] OPAL Collaboration, "Determination of S-Matrix parameters from fermion pair production at OPAL", OPAL PN474 (2001).

[68] VENUS Collaboration, K. Yusa *et al.*, Phys. Lett. **B447** (1999) 167.

[69] TOPAZ Collaboration, K. Miyabuyaski *et al.*, Phys. Lett. **B347** (1995) 171.

[70] DELPHI Collaboration, J. Abdallah *et al.*, Eur. Phys. J. **C45** (2006) 273–289.

[71] The LEP WW Working Group, hep-ex/0412015 prepared for the Summer 2004 conferences, `http://lepewwg.web.cern.ch/LEPEWWG/stanmod/`.

[72] M.W. Grünewald, G. Passarino *et al.*, *"Four fermion production in electron positron collisions"*, Four fermion working group report of the LEP2 Monte Carlo Workshop 1999/2000, in *"Reports of the working groups on precision calculations for LEP2 Physics"* CERN 2000–009, `http://arXiv.org/abs/hep-ph/0005309`.

[73] ALEPH Collaboration, Phys. Lett. **B401** (1997) 347.
DELPHI Collaboration, Phys. Lett. **B397** (1997) 158.
L3 Collaboration, Phys. Lett. **B398** (1997) 223.
OPAL Collaboration, Phys. Lett. **B389** (1996) 416.

[74] ALEPH Collaboration, Phys. Lett. **B415** (1997) 435.
DELPHI Collaboration, Eur. Phys. J. **C2** (1998) 581.
L3 Collaboration, Phys. Lett. **B407** (1997) 419;
OPAL Collaboration, Eur. Phys. J. **C1** (1998) 395.

[75] ALEPH Collaboration, Eur. Phys. Jour. **C38** (2004) 147.

[76] DELPHI Collaboration, Eur. Phys. Jour. **C34** (2004) 127.

[77] L3 Collaboration, Phys. Lett. **B600** (2004) 22.

[78] OPAL Collaboration, Phys. Lett. **B493** (2000) 249.

[79] OPAL Collaboration, OPAL Physics Note PN469, submitted to the Summer 2001 Conferences, and PN437 and PN420.

[80] A. Valassi, Nucl. Instrum. Meth. **A500** (2003) 391.

[81] F. James and M. Roos, Comput. Phys. Commun. **10** (1975) 343.

[82] The LEP Collaborations ALEPH, DELPHI, L3, OPAL, the LEP Electroweak Working Group and the SLD Heavy Flavour Working Group, *"A Combination of Preliminary Electroweak Measurements and Constraints on the Standard Model"*, CERN–PPE/97–154.

[83] The LEP Collaborations ALEPH, DELPHI, L3, OPAL, the LEP Electroweak Working Group and the SLD Heavy Flavour Working Group, *"A Combination of Preliminary Electroweak Measurements and Constraints on the Standard Model"*, CERN–EP/99–15.

[84] S. Jadach, W. Placzek, M. Skrzypek, B.F.L. Ward, Phys. Rev. **D54** (1996) 5434.
S. Jadach, W. Placzek, M. Skrzypek, B.F.L. Ward, Z. Wąs, Phys. Lett. **B417** (1998) 326.
S. Jadach, W. Placzek, M. Skrzypek, B.F.L. Ward, Z. Wąs, Phys. Rev. **D61** (2000) 113010; preprint CERN-TH-99-222, hep-ph/9907346.
S. Jadach, W. Placzek, M. Skrzypek, B.F.L. Ward, Z. Wąs, preprint CERN-TH/2000-337, hep-ph/0007012; submitted to Phys. Lett. B.
S. Jadach, W. Placzek, M. Skrzypek, B.F.L. Ward, Z. Wąs, *The Monte Carlo Event Generator* `YFSWW3` *version* `1.16` *for W-Pair Production and Decay at LEP2/LC Energies*, preprint CERN-TH/2001-017, UTHEP-01-0101, hep-ph/0103163, accepted for publication by Comput. Phys. Commun.
The YFSWW cross-sections at 155–215 GeV have been kindly provided by the authors.

[85] A. Denner, S. Dittmaier, M. Roth and D. Wackeroth, Nucl. Phys. **B560** (1999) 33.
A. Denner, S. Dittmaier, M. Roth and D. Wackeroth, Nucl. Phys. **B587** (2000) 67.
A. Denner, S. Dittmaier, M. Roth and D. Wackeroth, Phys. Lett. **B475** (2000) 127.
A. Denner, S. Dittmaier, M. Roth and D. Wackeroth, hep-ph/0101257.
The RACOONWW cross-sections at 155–215 GeV have been kindly provided by the authors.

[86] See [72] and references therein for a discussion of complete $\mathcal{O}(\alpha)$ radiative corrections to W-pair production in the LPA/DPA approximations.

[87] The theoretical uncertainty $\Delta\sigma/\sigma$ on the W-pair production cross section calculated in the LPA/DPA above 170 GeV can be parametrised as $\Delta\sigma/\sigma = 0.4 \oplus 0.072 \cdot t_1 \cdot t_2$, where $t_1 = (200 - 2 \cdot m_{\mathrm{W}})/(\sqrt{s} - 2 \cdot m_{\mathrm{W}})$ and $t_2 = (1 - (\frac{2 \cdot M_{\mathrm{W}}}{200})^2)/(1 - (\frac{2 \cdot M_{\mathrm{W}}}{\sqrt{s}})^2)$. In the threshold region, a 2% uncertainty is assigned..

[88] D. Bardin, J. Biebel, D. Lehner, A. Leike, A. Olchevski and T. Riemann, Comp. Phys. Comm. **104** (1997) 161. See also [72].
The GENTLE cross-sections at 155–215 GeV have been kindly provided by Eric Lançon and Anne Ealet.

[89] M. Skrzypek, S. Jadach, M. Martinez, W. Płaczek, Z. Wąs, Phys. Lett. **B372** (1996) 289.
S. Jadach, W. Płaczek, M. Skrzypek, Z. Wąs, Comput. Phys. Commun. **94** (1996) 216.
S. Jadach, W. Płaczek, M. Skrzypek, B.F.L. Ward, Z. Wąs, Comput. Phys. Commun. **119** (1999) 272.
S. Jadach, W. Płaczek, M. Skrzypek, B.F.L. Ward, Z. Wąs, preprint hep-ph/0104049, submitted to Comput. Phys. Commun.
The "KORALW" cross-sections at 155–215 GeV have been kindly provided by the authors. They have actually been computed using YFSWW [84], switching off non-leading $\mathcal{O}(\alpha)$ radiative corrections and the screening of the Coulomb correction, to reproduce the calculation from KORALW.

[90] K. Hagiwara et al., Phys. Rev. **D66**, (2002) 010001.

[91] S. Jadach, W. Płaczek, M. Skrzypek, B.F.L. Ward, Z. Wąs, Comput. Phys. Commun. **140** (2001) 475.

[92] DELPHI Collaboration, DELPHI 2005-005 CONF 725, EPS 2005 abstract 1-84.

[93] G. Passarino, Nucl. Phys. **B578** (2000) 3.
G. Passarino, Nucl. Phys. **B574** (2000) 451.
The WTO cross-sections at 160–210 GeV have been kindly provided by the author.

[94] E. Accomando and A. Ballestrero, Comp. Phys. Comm. **99** (1997) 270.
E. Accomando, A. Ballestrero and E. Maina, Comp. Phys. Comm. **150** (2003) 166.
The WPHACT cross-sections at 160–210 GeV have been kindly provided by A. Ballestrero.

[95] J. Fujimoto *et al.*, Comp. Phys. Comm. **100** (1997) 74.
Y. Kurihara *et al.*, Prog. Theor. Phys. **103** (2000) 1199.
The `grc4f` cross-sections at 160–210 GeV have been kindly computed by R. Tanaka.

[96] The LEP WW Working Group, LEPEWWG/XSEC/2000-01, note prepared for the summer 2000 conferences, `http://lepewwg.web.cern.ch/LEPEWWG/lepww/4f/Summer00`.

[97] G. Montagna *et al.*, *"Higher–order QED corrections to single W production in electron–positron collisions"*, FNT/T–2000/08, `http://arXiv.org/abs/hep-ph/0006307`.

[98] DELPHI Collaboration, Eur. Phys. J **C30** (2003) 447.

[99] L3 Collaboration, Phys. Lett. **B572** (2003) 133.

[100] OPAL Collaboration, Eur. Phys. J **C32** (2004) 303.

[101] ALEPH Collaboration, Phys. Lett. **B469** (1999) 287.

[102] ALEPH Collaboration, ALEPH 2001–006 CONF 2001–003, submitted to the Winter 2001 Conferences.

[103] S. Jadach, W. Placzek, B.F.L. Ward, Phys. Rev. **D56** (1997) 6939.

[104] G. Passarino, in [72].

[105] ALEPH Collaboration, CERN-PH-EP/2004-034, submitted to Phys. Lett. B..

[106] L3 Collaboration, Phys. Lett. **B561** (2003) 73.

[107] DELPHI Collaboration, DELPHI 2004-019 CONF 694, contributed to Summert 2004 conferences.

[108] L3 Collaboration, Phys. Lett. **B616** (2005) 159.

[109] DELPHI Collaboration, Eur. Phys. Jour. **C31** (2003) 139.

[110] L3 Collaboration, Phys. Lett. **B527** (2002) 39.

[111] OPAL Collaboration, Phys. Lett. **B580** (2004) 17.

[112] J. W. Stirling and A. Werthenbach, Eur. Phys. J. **C14** (2000) 103.

[113] ALEPH Collaboration, A. Heister *et al.*, Phys. Lett. **B602** (2004) 31–40.

[114] L3 Collaboration, P. Achard *et al.*, Phys. Lett. **B586** (2004) 151–166.

[115] L3 Collaboration, P. Achard *et al.*, Phys. Lett. **B597** (2004) 119–130.

[116] OPAL Collaboration, G. Abbiendi *et al.*, Phys. Rev. **D70** (2004) 032005.

[117] G. Gounaris *et al.*, in *Physics at LEP 2*, Report CERN 96-01 (1996), eds G. Altarelli, T. Sjöstrand, F. Zwirner, Vol. 1, p. 525.

[118] G. Montagna *et al.*, Phys. Lett. **B515** (2001) 197–205.

[119] A. Denner *et al.*, Eur. Phys. J. **C 20** (2001) 201.

[120] The LEP-TGC combination group, LEPEWWG/TGC/2001-03, September 2001.

[121] A. Denner, S. Dittmaier, M. Roth and D. Wackeroth, Nucl. Phys. **B560** (1999) 33.
A. Denner, S. Dittmaier, M. Roth and D. Wackeroth, Nucl. Phys. **B587** (2000) 67.
A. Denner, S. Dittmaier, M. Roth and D. Wackeroth, Phys. Lett. **B475** (2000) 127.
A. Denner, S. Dittmaier, M. Roth and D. Wackeroth, hep-ph/0101257.
The RACOONWW cross-sections at 155–215 GeV have been kindly provided by the authors.

[122] S. Jadach, W. Placzek, M. Skrzypek, B.F.L. Ward, Phys. Rev. **D54** (1996) 5434.
S. Jadach, W. Placzek, M. Skrzypek, B.F.L. Ward, Z. Wąs, Phys. Lett. **B417** (1998) 326.
S. Jadach, W. Placzek, M. Skrzypek, B.F.L. Ward, Z. Wąs, Phys. Rev. **D61** (2000) 113010.
S. Jadach, W. Placzek, M. Skrzypek, B.F.L. Ward, Z. Wąs, preprint CERN-TH/2000-337, hep-ph/0007012; submitted to Phys. Lett. B.
S. Jadach, W. Placzek, M. Skrzypek, B.F.L. Ward, Z. Wąs, Comput. Phys. Commun. **140** (2001) 432.
The YFSWW cross-sections at 155–215 GeV have been kindly provided by the authors.

[123] ALEPH Collaboration, *Measurement of Triple Gauge-Boson Couplings in e^+e^- collisions from 183 to 209GeV*, ALEPH 2003-015 CONF 2003-011.

[124] DELPHI Collaboration, *Measurement of Charged Trilinear Gauge Boson Couplings* , DELPHI 2003-051 (July 2003) CONF-671.

[125] L3 Collaboration, *Preliminary Results on the Measurement of Triple-Gauge-Boson Couplings of the W Boson at LEP*, L3 Note 2820 (September 2003).

[126] OPAL Collaboration, *Measurement of charged current triple gauge boson couplings using W pairs at LEP*, submitted to Eur. Phys. J. C., CERN-EP 2003-042, hep-ex/0308067.

[127] G. Bélanger *et al.*, Eur. Phys. J. **C 13** (2000) 283.

[128] K. Gaemers and G. Gounaris, Z. Phys. **C 1** (1979) 259.

[129] K. Hagiwara *et al.*, Nucl. Phys. **B282** (1987) 253.

[130] K. Hagiwara, S. Ishihara, R. Szalapski, and D. Zeppenfeld, Phys. Lett. **B 283** (1992) 353;
K. Hagiwara, S. Ishihara, R. Szalapski, and D. Zeppenfeld, Phys. Rev. **D 48** (1993) 2182;
K. Hagiwara, T. Hatsukano, S. Ishihara and R. Szalapski, Nucl. Phys. **B 496** (1997) 66.

[131] M. Bilenky, J.L. Kneur, F.M. Renard and D. Schildknecht, Nucl. Phys. **B 409** (1993) 22;
M. Bilenky, J.L. Kneur, F.M. Renard and D. Schildknecht, Nucl. Phys. **B 419** (1994) 240.

[132] I. Kuss and D. Schildknecht, Phys. Lett. **B 383** (1996) 470.

[133] G. Gounaris and C.G. Papadopoulos, DEMO-HEP-96/04, THES-TP 96/11, hep-ph/9612378.

[134] The LEP-TGC combination group, LEPEWWG/TGC/2001-01, March 2001.

[135] G. J. Gounaris, J. Layssac, and F. M. Renard, Phys. Rev. **D62** (2000) 073013.

[136] G. Bélanger and F. Boudjema, Phys. Lett. **B 288** (1992) 201.

[137] ALEPH Collaboration, *Limits on anomalous neutral gauge couplings using data from ZZ and $Z\gamma$ production between 183-208 GeV*, ALEPH 2001-061 (July 2001) CONF 2001-041.

[138] DELPHI Collaboration, *Study of Trilinear Gauge Boson Couplings ZZZ, $ZZ\gamma$ and $Z\gamma\gamma$*, DELPHI 2001-097 (July 2001) CONF 525.

[139] L3 Collaboration, M. Acciarri *et al.*, Phys. Lett. **B 436** (1999) 187;
L3 Collaboration, M. Acciarri *et al.*, Phys. Lett. **B 489** (2000) 55;
L3 Collaboration, *Search for anomalous ZZg and Zgg couplings in the process ee→Zg at LEP*, L3 Note 2672 (July 2001).

[140] OPAL Collaboration, G. Abbiendi *et al.*, Eur. Phys. J. **C 17** (2000) 13.

[141] L3 Collaboration, M. Acciarri *et al.*, Phys. Lett. **B450** (1999) 281. The Z-pair cross-section at 183 GeV therein follows the L3 definition: the corresponding NC02 cross-section is given in L3 Collaboration, L3 Note 2366, submitted to the Winter 1999 Conferences.
L3 Collaboration, M. Acciarri *et al.*, Phys. Lett. **B465** (1999) 363.
L3 Collaboration, L3 Note 2805, EPS 2003 abstract 228.

[142] See OPAL Collaboration, G. Abbiendi *et al.*, Phys. Lett. **B476** (2000) 256 and reference [100].

[143] ALEPH Collaboration, *Constraints on Anomalous Quartic Gauge Boson Couplings*, ALEPH 2003-009 CONF 2003-006.

[144] L3 Collaboration, *The $e^+e^- \to Z\gamma\gamma \to q\bar{q}\gamma\gamma$ Reaction at LEP and Constraints on Anomalous Quartic Gauge Boson Couplings*, Phys. Lett. **B 540** (2002) 43.

[145] OPAL Collaboration, *Constraints on Anomalous Quartic Gauge Boson Couplings using Acoplanar Photon Pairs et LEP-2*, OPAL Physics Note PN510.

[146] R. Brunelière *et al.*, Phys. Lett. **B 533** (2002) 75 and references therein.

[147] J. Alcaraz, *A proposal for the combination of TGC measurements*, L3 Note 2718.

[148] R. Brunelière, *Tests on the LEP TGC combination procedures*, ALEPH 2002-008 PHYS-2002-007 (2002).

[149] O.Klein, *On the Theory of Charged Fields*, New Theories in Physics, Proceedings, Warsaw, 1938; reprinted in: Surveys of High Energ. Phys. **5** (1986) 269.

[150] L.Maiani and P.M.Zerwas, *W Static ELM Parameters*, Memorandum to the TGC Combination Group (1998).

[151] L3 Collaboration, P. Achard *et al.*, Phys. Lett. **B561** (2003) 202–212.

[152] OPAL Collaboration, G. Abbiendi *et al.*, *Colour reconnection in $e^+e^- \to W^+W^-$ at $\sqrt{s} = 189$ GeV to 209 GeV*, Eprint hep-ex/0508062, 2005.

[153] ALEPH Collaboration, S. Schael *et al.*, *Test of colour reconnection models using three-jet events in hadronic Z decays*, Eprint hep-ex/0604042, 2006.

[154] G. Gustafson, U. Pettersson, and P. M. Zerwas, Phys. Lett. **B209** (1988) 90.

[155] T. Sjöstrand and V. A. Khoze, Z. Phys. **C62** (1994) 281–310.

[156] L. Lönnblad, Z. Phys. **C70** (1996) 107–114.

[157] G. Corcella *et al.*, JHEP **01** (2001) 010.

[158] G. Gustafson and J. Hakkinen, Z. Phys. **C64** (1994) 659–664.

[159] J. R. Ellis and K. Geiger, Phys. Rev. **D54** (1996) 1967–1990.

[160] J. Rathsman, Phys. Lett. **B452** (1999) 364–371.

[161] OPAL Collaboration, *Colour Reconnection Studies in* $e^+e^- \to W^+W^-$ *at* $\sqrt{s}$ *=189 GeV*, OPAL PN417.

[162] DELPHI Collaboration, P. Abreu *et al.*, Eur. Phys. J. **C18** (2000) 203–228.

[163] ALEPH Collaboration, *Preliminary Charged Particle Multiplicity in* $e^+e^- \to$ *W-pairs*, ALEPH 2000-058 CONF 2000-038.

[164] L3 Collaboration, *Search for Colour Reconnection Effects in* $e^+e^- \to W^+W^- \to$ *hadrons*, L3 Note 2560.

[165] V. A. Khoze and T. Sjöstrand, Eur. Phys. J. **C6** (1999) 271–284.

[166] OPAL Collaboration, *Investigation of Colour Reconnection via Heavy Particle Production in* $e^+e^- \to W^+W^-$, OPAL PN412.

[167] JADE Collaboration, W. Bartel *et al.*, Phys. Lett. **B101** (1981) 129; JADE Collaboration, W. Bartel *et al.*, Z. Phys. **C21** (1983) 37; JADE Collaboration, W. Bartel *et al.*, Phys. Lett. **B134** (1984) 275; JADE Collaboration, W. Bartel *et al.*, Phys. Lett. **B157** (1985) 340; TPC/Two Gamma Collaboration, H. Aihara *et al.*, Z. Phys. **C28** (1985) 31; TPC/Two Gamma Collaboration, H. Aihara *et al.*, Phys. Rev. Lett. **57** (1986) 945; TASSO Collaboration, M. Althoff *et al.*, Z. Phys. **C29** (1985) 29.

[168] L3 Collaboration, *Colour Reconnection Studies in* $e^+e^- \to W^+W^-$ *Events at* $\sqrt{s} = 189$ *GeV*, L3 Note 2406.

[169] D. Duchesneau, *New Method Based on Energy and Particle Flow in* $e^+e^- \to W^+W^- \to$ *hadron Events for Colour Reconnection Studies*, LAPP-EXP-2000-02.

[170] A. Ballestrero *et al.*, J. Phys. **G24** (1998) 365–403.

[171] ALEPH Collaboration, *Colour Reconnection Studies Using Particle Flow Between W Bosons at* $\sqrt{s}$ *=189–208 GeV*, ALEPH 2002-020 CONF 2002-009.

[172] DELPHI Collaboration, *Update of the Investigation of Colour Reconnection in WW Pairs Using Particle Flow*, DELPHI 2002-047 CONF 581.

[173] L3 Collaboration, *Search for Colour Reconnection Effects in* $e^+e^- \to W^+W^- \to$ *hadrons Through Particle-Flow Studies at* $\sqrt{s}$ *=189–208 GeV*, L3 Note 2748.

[174] OPAL Collaboration, *Colour Reconnection Studies in* $e^+e^- \to W^+W^-$ *at* $\sqrt{s}$ *=189–208 GeV Using Particle Flow*, OPAL PN506.

[175] ALEPH Collaboration, R. Barate *et al.*, Eur. Phys. J. **C17** (2000) 241–261.

[176] OPAL Collaboration, G. Abbiendi *et al.*, Phys. Lett. **B507** (2001) 29–46.

[177] S. Jadach *et al.*, Comput. Phys. Commun. **140** (2001) 475–512.

[178] T. Sjöstrand, Comput. Phys. Commun. **82** (1994) 74–90, (JETSET).

[179] L. Lönnblad, Comp. Phys. Comm. **71** (1992) 15.

[180] DELPHI 2003-020-CONF-640 .

[181] ALEPH Collaboration, *Further Studies on Bose-Einstein Correlations in W-pair Decays*, ALEPH 2001-064 CONF 2001-044.

[182] L3 Coll., *Measurement of Bose-Einstein Correlations in* $e^+e^- \to W^+W^-$ *Events at LEP*, Phys. Lett. B547 (2002) 139.

[183] OPAL Collaboration, *Bose-Einstein Correlations in* $e^+e^- \to W^+W^-$ *Events at 172, 183 and 189 GeV*, OPAL PN393.

[184] A. Ballestrero *et al.*, hep-ph/0006259 (2000).

[185] S.V. Chekanov, E.A. De Wolf, W. Kittel, Eur. Phys. J. C6 (1999) 403.

[186] DELPHI Coll., P. Abreu et al., Phys. Lett. B401 (1997) 181.

[187] E.A. De Wolf, *Correlations in* $e^+e^- \to W^+W^-$ *hadronic decays*, hep-ph/0101243.

[188] ALEPH Coll., *Bose-Einstein Correlations in W-pair decays*, Phys. Lett. B478 (2000) 50.

[189] ALEPH Coll., *Bose-Einstein correlations in W-pair decays with an event-mixing technique*, Phys. Lett. B606 (2005) 265.

[190] DELPHI Coll., *Bose-Einstein Correlations in* W^+W^- *events at LEP2*, Eur. Phys. J. C44 (2005) 161.

[191] OPAL Coll., *Study of Bose-Einstein Correlations in* $e^+e^- \to W^+W^-$ *Events at LEP*, Eur. Phys. J. C36 (2004) 297.

[192] T. Sjöstrand: PYTHIA 5.7 and JETSET 7.4, Computer Physics Commun. 82 (1994) 74.

[193] L. Lönnblad and T. Sjöstrand, Eur. Phys. J. **C2** (1998) 165.

[194] LEPWW FSI group http://lepewwg.web.cern.ch/LEPEWWG/lepww/fsi.html.

[195] ALEPH Collaboration, R. Barate *et al.*, Phys. Lett. **B401** (1997) 347.
DELPHI Collaboration, P. Abreu *et al.*, Phys. Lett. **B397** (1997) 158.
L3 Collaboration, M. Acciarri *et al.*, Phys. Lett. **B398** (1997) 223.
OPAL Collaboration, K. Ackerstaff *et al.*, Phys. Lett. **B389** (1996) 416.

[196] ALEPH Collaboration, S. Schael *et al.*, (2006).

[197] DELPHI Collaboration, J. Abdallah *et al.*, (2006).

[198] L3 Collaboration, M. Acciarri *et al.*, Euro. Phys. C **45** (2006) 569.

[199] OPAL Collaboration, G. Abbiendi, hep-ex/0508060 (2005).

[200] LEP Energy Working Group, LEPEWG 01/01, March 2001.

[201] LEP W Working Group, LEPEWWG/FSI/2002-01, July 2002.

[202] OPAL Collaboration, G. Abbiendi, (2005).

[203] T. Sjöstrand and V. A. Khoze, Z. Phys. **C62** (1994) 281–310.

[204] UA2 Collaboration, J. Alitti *et al.*, Phys. Lett. **B276** (1992) 354–364.

[205] CDF Collaboration, F. Abe *et al.*, Phys. Rev. Lett. **65** (1990) 2243–2246; CDF Collaboration, F. Abe *et al.*, Phys. Rev. **D43** (1991) 2070–2093; CDF Collaboration, F. Abe *et al.*, Phys. Rev. Lett. **75** (1995) 11–16; CDF Collaboration, F. Abe *et al.*, Phys. Rev. **D52** (1995) 4784–4827; CDF Collaboration, T. Affolder *et al.*, Phys. Rev. **D64** (2001) 052001.

[206] DØ Collaboration, B. Abbott *et al.*, Phys. Rev. Lett. **80** (1998) 3008; DØ Collaboration, B. Abbott *et al.*, Phys. Rev. Lett. **84** (2000) 222–227; DØ Collaboration, V. M. Abazov *et al.*, Phys. Rev. **D66** (2002) 012001; DØ Collaboration, B. Abbott *et al.*, Phys. Rev. **D62** (2000) 092006.

[207] CDF Collaboration, T. Affolder *et al.*, Phys. Rev. Lett. **85** (2000) 3347–3352.

[208] DØ Collaboration, V. M. Abazov *et al.*, Phys. Rev. **D66** (2002) 032008.

[209] The CDF Collaboration, the DØ Collaboration, and the Tevatron Electroweak Working Group, Phys. Rev. **D70** (2004) 092008.

[210] CDF Collaboration, F. Abe *et al.*, Phys. Rev. Lett. **80** (1998) 2779–2784; CDF Collaboration, F. Abe *et al.*, Phys. Rev. Lett. **82** (1999) 271–276; CDF Collaboration, F. Abe *et al.*, Erratum: Phys. Rev. Lett. **82** (1999) 2808–2809; CDF Collaboration, F. Abe *et al.*, Phys. Rev. Lett. **80** (1998) 2767–2772; CDF Collaboration, T. Affolder *et al.*, Phys. Rev. **D63** (2001) 032003; CDF Collaboration, F. Abe *et al.*, Phys. Rev. Lett. **79** (1997) 1992–1997.

[211] DØ Collaboration, B. Abbott *et al.*, Phys. Rev. Lett. **80** (1998) 2063–2068; DØ Collaboration, B. Abbott *et al.*, Phys. Rev. **D60** (1999) 052001; DØ Collaboration, S. Abachi *et al.*, Phys. Rev. Lett. **79** (1997) 1197–1202; DØ Collaboration, B. Abbott *et al.*, Phys. Rev. **D58** (1998) 052001; DØ Collaboration, V. M. Abazov *et al.*, Nature **429** (2004) 638–642; DØ Collaboration, V. M. Abazov *et al.*, *New measurement of the top quark mass in lepton + jets t anti-t events at DØ*, Eprint hep-ex/0407005, 2004; DØ Collaboration, V. M. Abazov *et al.*, Phys. Lett. **B606** (2005) 25–33.

[212] The Tevatron Electroweak Working Group, for the CDF and DØ Collaborations, *Combination of CDF and DØ Results on the Mass of the Top Quark*, Eprint hep-ex/0608032, Fermilab, 2006.

[213] C. S. Wood *et al.*, Science **275** (1997) 1759.

[214] S. C. Bennett and C. E. Wieman, Phys. Rev. Lett. **82** (1999) 2484–2487.

[215] J. S. M. Ginges and V. V. Flambaum, Phys. Rept. **397** (2004) 63–154.

[216] Particle Data Group Collaboration, S. Eidelman *et al.*, Phys. Lett. **B592** (2004) 1.

[217] SLAC E158 Collaboration, P. Anthony *et al.*, Phys. Rev. Lett. **92** (2004) 181602; SLAC E158 Collaboration, P. L. Anthony *et al.*, Phys. Rev. Lett. **95** (2005) 081601.

[218] NuTeV Collaboration, G. P. Zeller *et al.*, Phys. Rev. Lett. **88** (2002) 091802, erratum: 90 (2003) 239902.

[219] E. A. Paschos and L. Wolfenstein, Phys. Rev. **D7** (1973) 91–95.

[220] T. van Ritbergen and R. G. Stuart, Phys. Rev. Lett. **82** (1999) 488–491; T. van Ritbergen and R. G. Stuart, Nucl. Phys. **B564** (2000) 343–390; M. Steinhauser and T. Seidensticker, Phys. Lett. **B467** (1999) 271–278.

[221] H. Burkhardt and B. Pietrzyk, Phys. Rev. **D72** (2005) 057501.

[222] D. Bardin *et al.*, in *Reports of the working group on precision calculations for the Z resonance*, CERN 95-03, ed. D. Bardin, W. Hollik, and G. Passarino, (CERN, Geneva, Switzerland, 1995), pp. 7–162.

[223] D. Y. Bardin and G. Passarino, *Upgrading of precision calculations for electroweak observables*, Eprint hep-ph/9803425, 1998.

[224] D. Y. Bardin, M. Grünewald, and G. Passarino, *Precision calculation project report*, Eprint hep-ph/9902452, 1999.

[225] G. Degrassi, S. Fanchiotti and A. Sirlin, Nucl. Phys. **B351** (1991) 49;
G. Degrassi and A. Sirlin, Nucl. Phys. **B352** (1991) 342;
G. Degrassi, P. Gambino and A. Vicini, Phys. Lett. **B383** (1996) 219;
G. Degrassi, P. Gambino and A. Sirlin, Phys. Lett. **B394** (1997) 188;
G. Degrassi and P. Gambino, Nucl. Phys. **B567** (2000) 3.

[226] A. Czarnecki and J. Kühn, Phys. Rev. Lett. **77** (1996) 3955;
R. Harlander, T. Seidensticker and M. Steinhauser, Phys. Lett. **B426** (1998) 125.

[227] G. Montagna *et al.*, Nucl. Phys. **B401** (1993) 3–66; G. Montagna *et al.*, Comput. Phys. Commun. **76** (1993) 328–360; G. Montagna *et al.*, Comput. Phys. Commun. **93** (1996) 120–126; G. Montagna *et al.*, Comput. Phys. Commun. **117** (1999) 278–289, updated to include initial state pair radiation (G. Passarino, priv. comm.).

[228] D. Y. Bardin *et al.*, Z. Phys. **C44** (1989) 493; D. Y. Bardin *et al.*, Comput. Phys. Commun. **59** (1990) 303–312; D. Y. Bardin *et al.*, Nucl. Phys. **B351** (1991) 1–48; D. Y. Bardin *et al.*, Phys. Lett. **B255** (1991) 290–296; D. Y. Bardin *et al.*, *ZFITTER: An Analytical program for fermion pair production in* e^+e^- *annihilation*, Eprint arXiv:hep-ph/9412201, 1992; D. Y. Bardin *et al.*, Comput. Phys. Commun. **133** (2001) 229–395, updated with results from [259]; Two Fermion Working Group Collaboration, M. Kobel *et al.*, *Two-fermion production in electron positron collisions*, Eprint hep-ph/0007180, 2000; A. B. Arbuzov *et al.*, *ZFITTER: a semi-analytical program for fermion pair production in e+e- annihilation, from version 6.21 to version 6.42*, Eprint hep-ph/0507146, 2005.

[229] T. Hebbeker, M. Martinez, G. Passarino and G. Quast, Phys. Lett. **B331** (1994) 165;
P.A. Raczka and A. Szymacha, Phys. Rev. **D54** (1996) 3073;
D.E. Soper and L.R. Surguladze, Phys. Rev. **D54** (1996) 4566.

[230] H. Stenzel, JHEP **07** (2005) 0132.

[231] M. Awramik *et al.*, Phys. Rev. **D69** (2004) 053006.

[232] M. Awramik *et al.*, Phys. Rev. Lett. **93** (2004) 201805.

[233] M. Faisst *et al.*, Nucl. Phys. **B665** (2003) 649–662.

[234] M. Steinhauser, Phys. Lett. **B429** (1998) 158–161.

[235] S. Eidelman and F. Jegerlehner, Z. Phys. **C67** (1995) 585–602.

[236] H. Burkhardt and B. Pietrzyk, Phys. Lett. **B356** (1995) 398–403.

[237] BES Collaboration, J. Z. Bai *et al.*, Phys. Rev. Lett. **88** (2002) 101802.

[238] CMD-2 Collaboration, R. R. Akhmetshin *et al.*, Phys. Lett. **B578** (2004) 285–289.

[239] KLOE Collaboration, A. Aloisio *et al.*, Phys. Lett. **B606** (2005) 12–24.

[240] M. L. Swartz, Phys. Rev. **D53** (1996) 5268–5282.

[241] A. D. Martin and D. Zeppenfeld, Phys. Lett. **B345** (1995) 558–563.

[242] R. Alemany, M. Davier, and A. Hocker, Eur. Phys. J. **C2** (1998) 123–135.

[243] M. Davier and A. Hocker, Phys. Lett. **B419** (1998) 419–431.

[244] J. H. Kuhn and M. Steinhauser, Phys. Lett. **B437** (1998) 425–431.

[245] F. Jegerlehner, in Proceedings, 4th International Symposium, RADCOR'98, ed. J. Sola, (World Scientific, Singapore, Sep 1999), p. 75.

[246] J. Erler, Phys. Rev. **D59** (1999) 054008.

[247] A. D. Martin, J. Outhwaite, and M. G. Ryskin, Phys. Lett. **B492** (2000) 69–73.

[248] J. F. de Troconiz and F. J. Yndurain, Phys. Rev. **D65** (2002) 093002.

[249] K. Hagiwara *et al.*, Phys. Rev. **D69** (2004) 093003.

[250] J. F. de Troconiz and F. J. Yndurain, Phys. Rev. **D71** (2005) 073008.

[251] Particle Data Group, D.E. Groom *et al.*, Euro. Phys. J. 15 (2000) 1.

[252] S. Bethke, J. Phys. **G26** (2000) R27; S. Bethke, Nucl. Phys. Proc. Suppl. **135** (2004) 345–352.

[253] ALEPH, DELPHI, L3, and OPAL Collaboration, Phys. Lett. **B565** (2003) 61–75.

[254] T. Kawamoto and R. G. Kellogg, Phys. Rev. **D69** (2004) 113008.

[255] DELPHI Collaboration, Phys. Lett. **B515** (2001) 238.

[256] L3 Collaboration, Phys. Lett. **B436** (1998) 417;
L3 Collaboration, Phys. Lett. **B487** (2000) 229.

[257] L3 Collaboration, Phys. Lett. **B547** (2002) 151.

[258] OPAL Collaboration, OPAL Physics Note PN427, March 2000.

[259] A. B. Arbuzov, *Light pair corrections to electron positron annihilation at LEP/SLC*, Eprint arXiv:hep-ph/9907500, Turin U. and INFN, Turin, 1999.

Links to LEP results on the World Wide Web

The physics notes describing the preliminary results of the four LEP experiments submitted to the 2006 summer conferences, as well as additional documentation from the LEP electroweak working group are available on the World Wide Web at:

ALEPH:	`http://aleph.web.cern.ch/aleph/alpub/oldconf/conferences.html`
DELPHI:	`http://delphiwww.cern.ch/pubxx/conferences/summer06/`
L3:	`http://l3.web.cern.ch/l3/conferences/Moscow2006/`
OPAL:	`http://opal.web.cern.ch/Opal/pubs/ichep2006/abstr.html`
LEP-EWWG:	`http://www.cern.ch/LEPEWWG/`